

**Crystal Structures and Spectral Aspects of Mixed  
Ligand Transition Metal Chelates Derived  
from Aldehyde based ONS Donor  
Thiosemicarbazones**

*Thesis submitted to  
Cochin University of Science and Technology  
in partial fulfillment of the requirements  
for the award of the degree of*

**DOCTOR OF PHILOSOPHY**

*Under the Faculty of Science*

*by*

**JINSA MARY JACOB**



**Department of Applied Chemistry  
Cochin University of Science and Technology  
Kochi 682 022**

*September 2013*

**Crystal Structures and Spectral Aspects of Mixed Ligand Transition Metal Chelates  
Derived from Aldehyde based ONS Donor Thiosemicarbazones**

Ph. D. Thesis under the Faculty of Science

*Author:*

**Jinsa Mary Jacob**

Research Fellow, Department of Applied Chemistry  
Cochin University of Science and Technology  
Kochi 682 022  
India  
Email: jinsamaryjacob@gmail.com

*Research Advisor:*

**Dr. M.R. Prathapachandra Kurup**

Professor  
Department of Applied Chemistry  
Cochin University of Science and Technology  
Kochi 682 022  
India  
Email: mrp@cusat.ac.in

Department of Applied Chemistry  
Cochin University of Science and Technology  
Kochi 682 022  
India

September 2013

Front cover: Intra and intermolecular hydrogen bonding interactions of 5-bromo-3-methoxysalicylaldehyde-N(4)-phenylthiosemicarbazone ( $H_2L^1$ ).

Back cover: Coordination polyhedra of  $[MoO_2L^1DMF] \cdot DMF$  (**34**) in a super cell.

*"I love you, Lord, my strength..*

*You are my rock, my fortress and my deliverer.."*

**(Psalms 18:1,2)**

---

\*\*\*\* *To my beloved*

*Appa & Amma\*\*\*\**

---

Phone Off. 0484-2862423  
Phone Res. 0484-2576904  
Telex: 885-5019 CUIIN  
Fax: 0484-2577595  
Email: mrp@cusat.ac.in  
mrp\_k@yahoo.com



**Department of Applied Chemistry**  
**Cochin University of Science and Technology**  
Kochi 682 022, India

---

**Dr. M.R. Prathapachandra Kurup**  
Professor

24<sup>th</sup> September 2013

## **Certificate**

*This is to certify that the thesis entitled "Crystal Structures and Spectral Aspects of Mixed Ligand Transition Metal Chelates Derived from Aldehyde based ONS Donor Thiosemicarbazones" submitted by Ms. Jinsa Mary Jacob, in partial fulfillment of the requirements for the degree of Doctor of Philosophy, to the Cochin University of Science and Technology, Kochi-22, is an authentic record of the original research work carried out by her under my guidance and supervision. The results embodied in this thesis, in full or in part, have not been submitted for the award of any other degree.*

**M.R. Prathapachandra Kurup**  
(Supervisor)

## **Declaration**

I hereby declare that the work presented in this thesis entitled **“Crystal Structures and Spectral Aspects of Mixed Ligand Transition Metal Chelates Derived from Aldehyde based ONS Donor Thiosemicarbazones”** is entirely original and was carried out independently under the supervision of **Prof. M.R. Prathapachandra Kurup**, Department of Applied Chemistry, Cochin University of Science and Technology and has not been included in any other thesis submitted previously for the award of any other degree.

24-09-2013

Kochi-22

**Jinsa Mary Jacob**

## *Acknowledgement*

---

*This doctoral thesis has been seen through to completion only because of the support and encouragement of numerous people. It is a pleasure to express my sincere gratitude to all those who helped me in many ways for the success of this study and made it an unforgettable experience for me.*

*First and foremost, I thank, and honour Jesus Christ for guiding and strengthening me throughout my research work. Dear Jesus, I would not have made it without you.*

*Next, I express my heart-felt gratitude to my supervising guide Prof. M.R. Prathapachandra Kurup for his valuable guidance, support and encouragement. Without his constructive criticisms, valuable suggestions and corrections, I would not have been able to successfully complete my work.*

*I express my sincere thanks to former Heads, Prof. K. Girish Kumar who is my doctoral committee member and Prof. K. Sreekumar for their encouragement and support. I am very much thankful to Dr. N. Manoj, Head, Department of Applied Chemistry, CUSAT for the support and cooperation during the period of this work. I am thankful for the support received from all the teaching and non-teaching staff of the Department of Applied Chemistry, CUSAT.*

*I sincerely thank the Council of Scientific and Industrial Research, New Delhi, India for financial support offered. I deeply acknowledge the heads of the institutions of SAIIF Kochi, IIT Madras and IIT Bombay for the services rendered in sample analyses. I express my thanks to Dr. Shibu Eapen, Sophisticated Testing and Instrumentation Centre, SAIIF, Kochi for doing single crystal XRD studies of the compounds.*

*I remember all my seniors, Dr. Seena E.B., Dr. Sheeja S.R., Dr. Reena T.A., Dr. Neema Ani Mangalam and Dr. Renjusha S., who helped me a lot in the beginning years of my research. I thank from the depth of my heart the teacher fellows Dr. Jessy Emmanuel, Dr. Annie C.F., Dr. K. Jayakumar and Dr. Laly K, for their valuable care, help and attention. My thanks are due to Roji sir and Dr. M. Sithambaresan for their valuable advices and extensive discussions around my work. Dear Bibitha chechi and Nisha chechi, the moments spent with you are so special and will remain in my heart forever. Thank you so much for your love, care and advices. I will surely cherish the beautiful moments spent with my hostel mates, Reshma and Vineetha. My special thanks to my junior labmates, Ambili, Aishwarya, Mridula, Sreejith, Nithya, Sajitha chechi, Anila and Fousia for their support and for creating many fun filled moments in the lab. I am also indebted to Asokan sir and Yamuna miss for their encouragement and support.*

*I thank my parents for being with me through all the good and hard times during these four years. Dear appa and amma, your prayers, care and support meant a lot for me. I am grateful to my sisters and their families for their encouragement and valuable prayers.*

*Janina Mary Jacob*

## *Preface*

.....❧.....

Thiosemicarbazones have emerged as an important class of ligands over a period of time, for a variety of reasons, such as variable donor properties, structural diversity and biological applications. Interesting as the coordination chemistry may be, the driving force for the study of these ligands has undoubtedly been their biological properties and the majority of the 3000 or so publications on thiosemicarbazones since 2000 have alluded to this feature. Thiosemicarbazones with potential donor atoms in their structural skeleton fascinate coordination chemists with their versatile chelating behavior. The thiosemicarbazones of aromatic aldehydes and ketones form stable chelates with transition metal cations by utilizing both their sulfur and azomethine nitrogen as donor atoms. They have been shown to possess a diverse range of biological activities including anticancer, antitumor, antibacterial, antiviral, antimalarial and antifungal properties owing to their ability to diffuse through the semipermeable membrane of the cell lines. The enhanced effect may be attributed to the increased lipophilicity of the metal complexes compared to the ligand alone.

In order to pursue the interesting coordinating properties of thiosemicarbazones, complexes with different types of ligand environments are essential. So in the present work we chose two different ONS donor thiosemicarbazones as principal ligands. Introduction of heterocyclic bases like 1,10-phenanthroline, 2,2'-bipyridine, 4,4'-dimethyl-2,2'-bipyridine and 5,5'-dimethyl-2,2'-bipyridine, the classical N,N donor ligands leads to the

syntheses of mixed ligand complexes which can cause different bonding, spectral properties and geometries in coordination compounds. The molecular structures of these thiosemicarbazones were established by single crystal X-ray diffraction studies. The metals selected for the preparation of the complexes are vanadium, nickel, copper, zinc, cadmium and molybdenum. The crystal structures of four of the complexes were studied through single crystal XRD.

The thesis is divided into eight chapters. Chapter 1 involves a brief prologue to thiosemicarbazones and their metal complexes, bonding and coordination strategy of thiosemicarbazones and their various applications. The objectives of the present work and the various physicochemical methods adopted for the characterization of the thiosemicarbazones and their complexes are also discussed in this chapter. Chapter 2 describes the syntheses of two new aldehyde based ONS donor thiosemicarbazones and their characterization by elemental analyses, mass, FTIR, UV-vis and <sup>1</sup>H NMR spectral studies. X-ray quality single crystals of these two ligands were grown and their molecular structures were established by single crystal X-ray diffraction studies. Chapters 3-8 discuss the syntheses and characterization of oxidovanadium(IV), nickel(II), copper(II), zinc(II), cadmium(II) and molybdenum(VI) complexes derived from the thiosemicarbazones under study. A brief summary and conclusion of the work is also included in the last part of the thesis.

## *Abbreviations*

H <sub>2</sub> L <sup>1</sup>	5-bromo-3-methoxysalicylaldehyde-N(4)-phenylthiosemicarbazone
H <sub>2</sub> L <sup>2</sup>	5-bromo-3-methoxysalicylaldehyde-N(4)-cyclohexylthiosemicarbazone
phen	1,10-phenanthroline
bipy	2,2'-bipyridine
4,4'-dmbipy	4,4'-dimethyl-2,2'-bipyridine
5,5'-dmbipy	5,5'-dimethyl-2,2'-bipyridine
Complex 1	[VOL <sup>1</sup> phen]
Complex 2	[VOL <sup>1</sup> bipy]
Complex 3	[(NiL <sup>1</sup> ) <sub>2</sub> ]
Complex 4	[NiL <sup>1</sup> phen]
Complex 5	[NiL <sup>1</sup> (5,5'-dmbipy)]
Complex 6	[(NiL <sup>2</sup> ) <sub>2</sub> ]
Complex 7	[NiL <sup>2</sup> bipy]
Complex 8	[(CuL <sup>1</sup> ) <sub>2</sub> ]
Complex 9	[CuL <sup>1</sup> phen]
Complex 10	[CuL <sup>1</sup> bipy]
Complex 11	[CuL <sup>1</sup> (4,4'-dmbipy)]
Complex 12	[CuL <sup>1</sup> (5,5'-dmbipy)]·DMF
Complex 13	[(CuL <sup>2</sup> ) <sub>2</sub> ]
Complex 14	[CuL <sup>2</sup> phen]
Complex 15	[CuL <sup>2</sup> bipy]
Complex 16	[CuL <sup>2</sup> (4,4'-dmbipy)]
Complex 17	[CuL <sup>2</sup> (5,5'-dmbipy)]
Complex 18	[(ZnL <sup>1</sup> ) <sub>2</sub> ]
Complex 19	[ZnL <sup>1</sup> phen]
Complex 20	[ZnL <sup>1</sup> bipy]
Complex 21	[ZnL <sup>1</sup> (4,4'-dmbipy)]·DMF
Complex 22	[ZnL <sup>1</sup> (5,5'-dmbipy)]
Complex 23	[(ZnL <sup>2</sup> ) <sub>2</sub> ]
Complex 24	[ZnL <sup>2</sup> phen]
Complex 25	[ZnL <sup>2</sup> bipy]
Complex 26	[(CdL <sup>1</sup> ) <sub>2</sub> ]

Complex 27	[CdL <sup>1</sup> phen]
Complex 28	[CdL <sup>1</sup> bipy]
Complex 29	[CdL <sup>1</sup> (4,4'-dmbipy)]
Complex 30	[CdL <sup>1</sup> (5,5'-dmbipy)]
Complex 31	[(CdL <sup>2</sup> ) <sub>2</sub> ]
Complex 32	[CdL <sup>2</sup> phen]
Complex 33	[CdL <sup>2</sup> bipy]
Complex 34	[MoO <sub>2</sub> L <sup>1</sup> DMF]·DMF

# *Contents*

.....\*

## *Chapter* **1**

<b>A BRIEF PROLOGUE TO THIOSEMICARBAZONES AND THEIR TRANSITION METAL COMPLEXES.....</b>	<b>1-22</b>
1.1 Introduction.....	1
1.2 Thiosemicarbazones.....	3
1.3 Bonding and coordination strategy of thiosemicarbazones.....	4
1.3.1 Bonding modes in neutral form.....	5
1.3.2 Bonding modes in anionic form.....	6
1.4 Importance of thiosemicarbazones .....	7
1.4.1 Biological.....	8
1.4.1a Antifungal and antibacterial properties.....	8
1.4.1b Anticancer properties .....	9
1.4.2 Analytical.....	9
1.5 Objectives of the present work.....	10
1.6 Physical measurements.....	12
1.6.1 Elemental analyses.....	12
1.6.2 Conductivity measurements.....	13
1.6.3 Magnetic susceptibility measurements.....	13
1.6.4 Infrared spectroscopy.....	13
1.6.5 Ultraviolet-visible spectroscopy .....	14
1.6.6 Mass spectroscopy .....	14
1.6.7 NMR spectroscopy.....	15
1.6.8 EPR spectroscopy .....	15
1.6.9 Single crystal X-ray diffraction studies.....	15
<b>References .....</b>	<b>16</b>

**Chapter 2**

**SYNTHESES, CRYSTAL STRUCTURES AND SPECTRAL ASPECTS  
OF ONS DONOR THIOSEMICARBAZONES.....23-56**

2.1	Introduction .....	23
2.2	5-Bromo-3-methoxysalicylaldehyde- N(4)-phenylthiosemicarbazone ( $H_2L^1$ ).....	25
2.2.1	Experimental.....	25
2.2.1.1	Materials.....	25
2.2.1.2	Synthesis .....	25
2.2.2	Characterization of 5-bromo-3-methoxysalicylaldehyde- N(4)- phenylthiosemicarbazone ( $H_2L^1$ ).....	26
2.2.2.1	Elemental analysis .....	26
2.2.2.2	Mass spectrum .....	26
2.2.2.3	Infrared spectrum.....	27
2.2.2.4	Electronic spectrum.....	28
2.2.2.5	NMR spectral studies .....	28
2.2.2.5a	$^1H$ NMR spectrum.....	28
2.2.2.5b	$^{13}C$ NMR spectrum .....	30
2.2.2.6	Crystal structure .....	32
2.3	5-Bromo-3-methoxysalicylaldehyde-N(4)- cyclohexylthiosemicarbazone ( $H_2L^2$ ).....	39
2.3.1	Experimental.....	39
2.3.1.1	Materials.....	39
2.3.1.2	Synthesis.....	39
2.3.2	Characterization of 5-bromo-3-methoxysalicylaldehyde- N(4)-cyclohexylthiosemicarbazone ( $H_2L^2$ ).....	41
2.3.2.1	Elemental analysis.....	41
2.3.2.2	Mass spectrum.....	41
2.3.2.3	Infrared spectrum.....	42
2.3.2.4	Electronic spectrum.....	43
2.3.2.5	NMR spectral studies .....	43
2.3.2.5a	$^1H$ NMR spectrum.....	43
2.3.2.5b	$^{13}C$ NMR spectrum.....	45
2.3.2.6	Crystal structure .....	47
	References .....	55

## *Chapter* **3**

### **SYNTHESES AND SPECTRAL ASPECTS OF OXIDOVANADIUM(IV) CHELATES DERIVED FROM ONS DONOR THIOSEMICARBAZONES.....57-73**

3.1	Introduction.....	57
3.2	Experimental.....	59
3.2.1	Materials.....	59
3.2.2	Synthesis of the thiosemicarbazone.....	59
3.2.3	Syntheses of the complexes.....	59
3.3	Results and discussion.....	60
3.3.1	Elemental analyses.....	61
3.3.2	Molar conductivity and magnetic susceptibility measurements ..	61
3.3.3	Infrared spectra.....	61
3.3.4	Electronic spectra.....	64
3.3.5	EPR spectra.....	67
	<b>References.....</b>	<b>71</b>

## *Chapter* **4**

### **SYNTHESES AND SPECTRAL ASPECTS OF NICKEL(II) CHELATES DERIVED FROM ONS DONOR THIOSEMICARBAZONES.....74-87**

4.1	Introduction.....	74
4.2	Experimental.....	76
4.2.1	Materials.....	76
4.2.2	Syntheses of the thiosemicarbazones.....	76
4.2.3	Syntheses of the complexes.....	76
4.3	Results and discussion.....	78
4.3.1	Elemental analyses.....	78
4.3.2	Molar conductivity and magnetic susceptibility measurements..	79
4.3.3	Infrared spectra.....	79
4.3.4	Electronic spectra.....	83
	<b>References.....</b>	<b>86</b>

## Chapter 5

### SYNTHESES, CRYSTAL STRUCTURES AND SPECTRAL ASPECTS OF COPPER(II) CHELATES DERIVED FROM ONS DONOR THIOSEMICARBAZONES.....88-138

5.1	Introduction.....	88
5.2	Experimental.....	90
5.2.1	Materials.....	90
5.2.2	Syntheses of the thiosemicarbazones.....	90
5.2.3	Syntheses of the complexes.....	90
5.3	Results and discussion.....	94
5.3.1	Elemental analyses.....	95
5.3.2	Molar conductivity and magnetic susceptibility measurements ..	95
5.3.3	Infrared spectra.....	96
5.3.4	Electronic spectra.....	102
5.3.5	EPR spectra.....	106
5.3.6	X-ray crystallography.....	119
	5.3.6a Crystal structure of the compound [CuL <sup>1</sup> bipy] ( <b>10</b> )...	121
	5.3.6b Crystal structure of the compound [CuL <sup>1</sup> (5,5'-dmbipy)]·DMF( <b>12</b> ).....	127
	References.....	134

## Chapter 6

### SYNTHESES, CRYSTAL STRUCTURES AND SPECTRAL ASPECTS OF ZINC(II) CHELATES DERIVED FROM ONS DONOR THIOSEMICARBAZONES.... 139-160

6.1	Introduction.....	139
6.2	Experimental.....	141
6.2.1	Materials.....	141
6.2.2	Syntheses of the thiosemicarbazones.....	141
6.2.3	Syntheses of the complexes.....	141
6.3	Results and discussion.....	144
6.3.1	Elemental analyses.....	144
6.3.2	Molar conductivity.....	145
6.3.3	Infrared spectra.....	145
6.3.4	Electronic spectra.....	150
6.3.5	X-ray crystallography.....	151
	6.3.5a Crystal structure of the compound [ZnL <sup>1</sup> (4,4'-dmbipy)]·DMF( <b>21</b> ).....	151
	References.....	158

## Chapter 7

### **SYNTHESES AND SPECTRAL ASPECTS OF CADMIUM(II) CHELATES DERIVED FROM ONS DONOR THIOSEMICARBAZONES.....161-174**

7.1	Introduction.....	161
7.2	Experimental.....	162
7.2.1	Materials.....	162
7.2.2	Syntheses of the thiosemicarbazones.....	163
7.2.3	Syntheses of the complexes.....	163
7.3	Results and discussion.....	166
7.3.1	Elemental analyses.....	166
7.3.2	Molar conductivity.....	166
7.3.3	Infrared spectra.....	167
7.3.4	Electronic spectra.....	171
	References.....	173

## Chapter 8

### **SYNTHESIS, CRYSTAL STRUCTURE AND SPECTRAL ASPECTS OF A DIOXIDOMOLYBDENUM(VI) CHELATE DERIVED FROM ONS DONOR THIOSEMICARBAZONE.....175-191**

8.1	Introduction.....	175
8.2	Experimental.....	177
8.2.1	Materials.....	177
8.2.2	Synthesis of the thiosemicarbazone $H_2L^1$ .....	177
8.2.3	Synthesis of the complex $[MoO_2L^1DMF] \cdot DMF$ ( <b>34</b> ).....	178
8.3	Results and discussion.....	178
8.3.1	Elemental analysis.....	178
8.3.2	Molar conductivity and magnetic susceptibility measurements ..	179
8.3.3	Infrared spectrum.....	179
8.3.4	Electronic spectrum.....	180
8.3.5	X-ray crystallography.....	182
	References.....	189

### **SUMMARY AND CONCLUSION.....192-198**

## A BRIEF PROLOGUE TO THIOSEMICARBAZONES AND THEIR METAL COMPLEXES

- 1.1 Introduction
- 1.2 Thiosemicarbazones
- 1.3 Bonding and coordination strategy of thiosemicarbazones
- 1.4 Importance of thiosemicarbazones
- 1.5 Objectives of the present work
- 1.6 Physical measurements
- References**

### 1.1. Introduction

Inorganic chemistry has considerable impact on our everyday lives and on other scientific disciplines. It is essential to the formulation and improvement of modern materials such as catalysts, semiconductors, optical devices, superconductors and advanced ceramic materials. The environmental and biological impact of inorganic chemistry is also huge. Coordination compounds are the backbone of modern inorganic and bio-inorganic chemistry and chemical industry. The chemistry of coordination compounds is an important and challenging area of modern inorganic chemistry. During the last fifty years, advances in this area have provided development of new concepts and models of bonding and molecular structure and novel breakthroughs in chemical industry. Coordination compounds are of great importance since they provide critical insights into the functioning and structures of vital components of biological systems.

They also find extensive applications in metallurgical processes, analytical and medicinal chemistry.

Coordination compounds are of importance in medical diagnosis and therapy. They act as contrast agents for magnetic resonance imaging (MRI) and are the active compounds in chemotherapy and photodynamic therapy for the treatment of cancer. Coordination compounds include such substances as vitamin B<sub>12</sub>, hemoglobin, chlorophyll, dyes, pigments and catalysts used in preparing organic substances. The origin of coordination chemistry as a distinct branch of chemistry dates back to the beginning of the 20<sup>th</sup> century and is marked by the award of a Nobel Prize to Alfred Werner in 1913 [1]. Among other achievements, Werner established the structure of the compound now known as cisplatin which is used in cancer therapy.

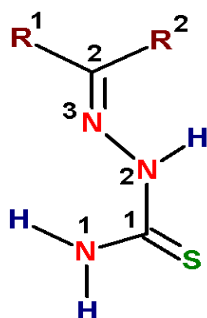
The architectural beauty of coordination compounds is due to the interesting ligand systems containing different donor sites say ONO, NNO, NO and NNS. It provides many new directions in research such as, in molecular magnetism, supramolecular chemistry, non-silicon-based devices, precursors for vapor phase deposition and single molecule-based photonic devices and sensors [2].

The thiosemicarbazones of aromatic aldehydes and ketones form stable chelates with transition metal cations by utilizing both their sulfur and azomethine nitrogen as donor atoms. They have been shown to possess a diverse range of biological activities including anticancer [3], antitumor [4], antibacterial [5,6], antiviral [7,8], antimalarial [9] and

antifungal [10] properties owing to their ability to diffuse through the semipermeable membrane of the cell lines. The enhanced effect may be attributed to the increased lipophilicity of the metal complexes compared to the ligand alone. The presence of coordination sites in the complexes enhances their activity. The inhibitory effect occurs by action of the complexes on the proliferation and differentiation of the cell lines. These complexes can further find their use in the treatment of other incurable diseases such as hepatitis, AIDS etc. [11] and catalytic activity [12]. Hence the structural and chemical properties of thiosemicarbazones and their metal complexes have attained considerable attention. They have been investigated intensively since they hold good promises in various fields of medicine. The pharmacological activity of thiosemicarbazones of *o*-hydroxy aromatic aldehydes is correlated to their ability to form chelates with biologically important metal ions by bonding through O, N and S atoms [13-17] and reductive capacity. It is observed that biological activity depends on the parent aldehyde or ketone [18-20] and increases remarkably when bulky groups are present at N<sup>4</sup> position [21]. Metal complexes of thiosemicarbazones often display enhanced activities when compared to the uncomplexed thiosemicarbazones.

## **1.2. Thiosemicarbazones**

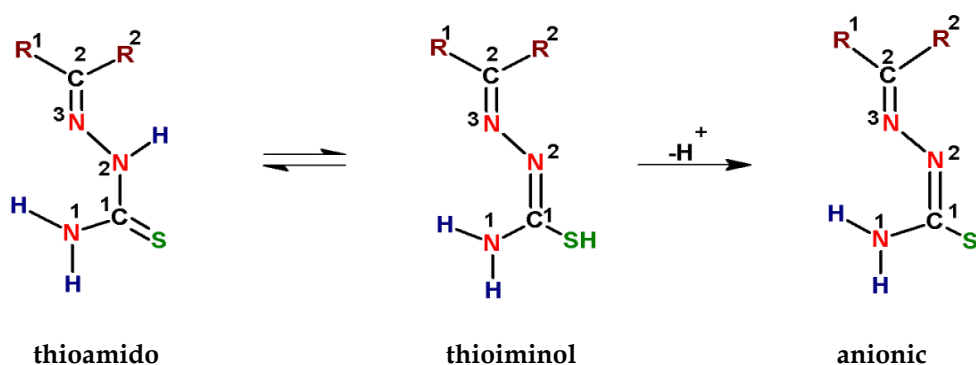
Thiosemicarbazones are thiourea derivatives and are prepared by the condensation of thiosemicarbazides with aldehydes or ketones in acidic medium [22]. They are represented by the general formula given below.



They are extensively delocalized systems, especially when aromatic radicals are bound to the azomethine carbon atom. Thiosemicarbazones with additional donor groups at the substituent  $R^1$  or  $R^2$  are of special interest since they can coordinate in a tridentate fashion which results in significant increase of the stability of the complexes.

### 1.3. Bonding and coordination strategy of thiosemicarbazones

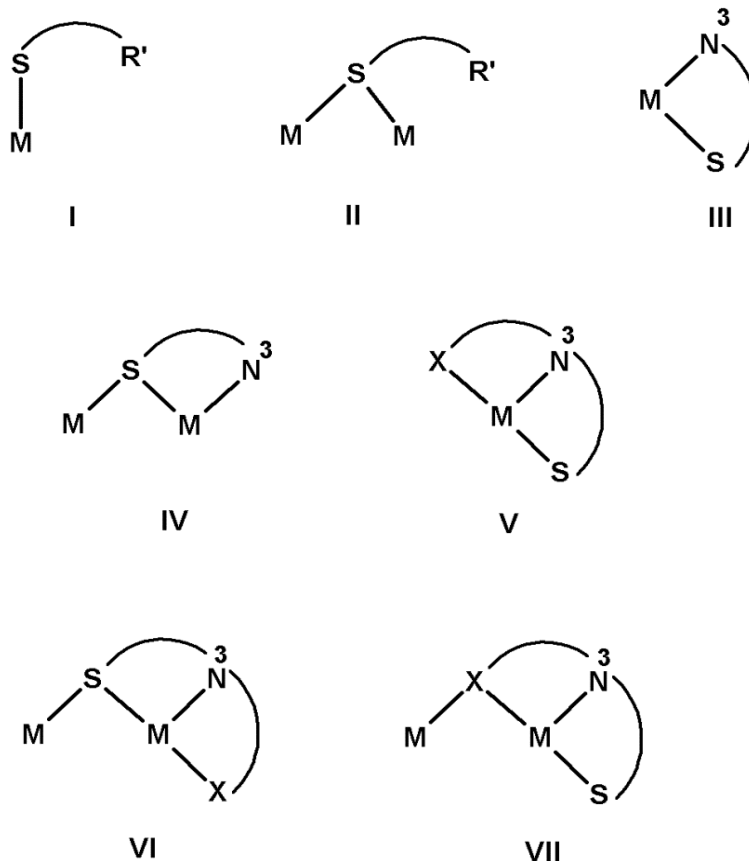
Thiosemicarbazones generally exist in the thioamido form in the solid state but in solution, they tend to exist as an equilibrium mixture of thioamido and thioiminol forms. The thioamido-thioiminol equilibrium depends on the pH of the medium used for reaction. Thiosemicarbazones can bind to a metal center in the neutral or the anionic forms. The anionic form is generated after loss of  $-N^2H$  or  $-SH$  hydrogen ions.



A number of bonding modes have been observed for the thiosemicarbazones in their neutral or anionic forms.

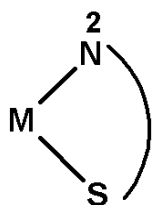
### 1.3.1. Bonding modes in neutral form

In neutral form, the binding occurs *via* only S atom in  $\eta^1$ -S (I),  $\mu^2$ -S (II),  $\eta^2$ -N<sup>3</sup>, S-chelation (III),  $\eta^2$ -N<sup>3</sup>, S-chelation and S-bridging (IV) modes. However, if the substituent at C<sup>2</sup> has a donor atom, and engages in bonding, the additional bonding modes observed are,  $\eta^3$ -X, N<sup>3</sup>, S-chelation (V),  $\eta^3$ -X, N<sup>3</sup>, S-chelation and S-bridging (VI) and  $\eta^3$ -X, N<sup>3</sup>, S-chelation and X-bridging (VII) (eg. X = N, O) [23-32].

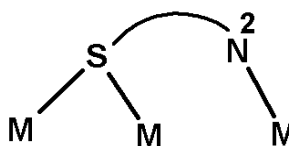


### 1.3.2. Bonding modes in anionic form

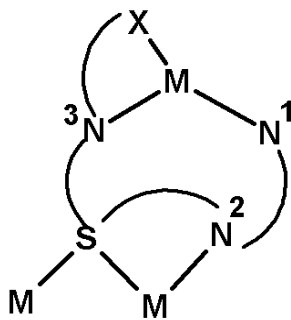
The modes (I-VII) shown by the neutral ligands are also exhibited by the anionic ligands, *viz.*  $\eta^1\text{-S}$ ,  $\mu^2\text{-S}$ ,  $\eta^2\text{-N}^3$ , S-chelation,  $\eta^2\text{-N}^3$ , S-chelation and S-bridging,  $\eta^3\text{-X}$ ,  $\text{N}^3$ , S-chelation,  $\eta^3\text{-X}$ ,  $\text{N}^3$ , S-chelation-cum-S-bridging and  $\eta^3\text{-X}$ ,  $\text{N}^3$ , S-chelation and X-bridging [33-39]. In addition,  $\eta^2\text{-N}^2$ , S (VIII) and  $\eta^2\text{-N}^2$ , S-bridging (IX) modes are identified [40,41]. A rare example of pentacoordination (X) by a thiosemicarbazone ligand has also been reported [42].



VIII



IX



X

The potential of thiosemicarbazones as ligands for a wide range of metals was realised and Jensen established the basis of their coordination chemistry in seminal papers in the 1930s [43,44]. He proposed that

coordination occurred *via* the sulfur and the azomethine nitrogen with the formation of a five membered ring (Fig. 1A). In the presence of base, loss of one of the ligand protons occurred, giving the ligand a uninegative charge. Without the advantage of X-ray structures he suggested that it was the exocyclic nitrogen that was deprotonated (Fig. 1B) whereas we now know that it is in fact a hydrazinic proton that is lost (Fig. 1C). These ligands can therefore provide a non-reducing source of anionic sulfur and also due to residual multiple bonding between C and S, the tendency for sulfur atom to bridge metal ions is substantially less compared to thiolate. The ability of this class of ligands to act as a source of ‘masked thiolate’ is one of the contributing factors to their ability to act as highly versatile donors towards a range of metal ions.

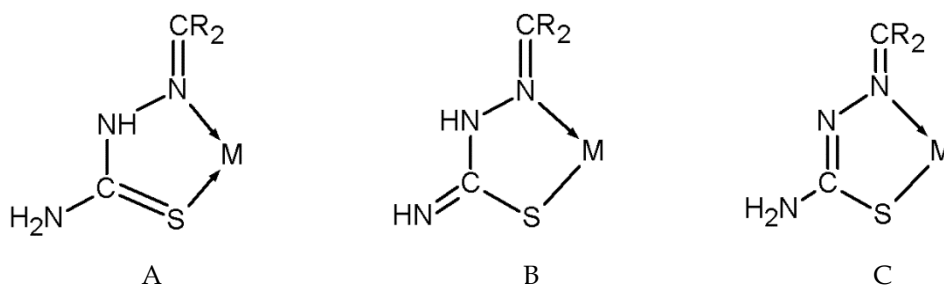


**Fig. 1. Jensen models for the coordination of thiosemicarbazones in neutral (A) and anionic (B) forms. Currently accepted structure representation for anionic binding (C).**

#### **1.4. Importance of thiosemicarbazones**

Thiosemicarbazones and their metal complexes show significant biological activity, suggesting accessibility of coordination site which is a fundamental requirement for biological activity by the complexes [45].

### 1.4.1. Biological applications

#### 1.4.1a. Antifungal and antibacterial properties

2-Benzoylpyridine thiosemicarbazone and its copper(II) complexes show antifungal activity against various strains of the pathogenic fungi. The activity varied with the nature of the substituent at the amino nitrogen of thiosemicarbazone. 2-Benzoylpyridine-N(4)-isopropyl thiosemicarbazone as well as its square pyramidal complex,  $[\text{Cu}(\text{HL})\text{Cl}_2]$  [46] were fungitoxic against the human pathogenic fungi, *A. niger* and *P. variotti*. 2-Benzoylpyridine thiosemicarbazone with N(4) phenyl substituent was most active against *S. aureus* while its dimeric complex  $[\text{Cu}_2\text{L}_2\text{X}_2]$  ( $\text{X}=\text{Cl}, \text{NCS}$ ) [47] was inactive against this strain. They, however, exhibited activity against other strains, *S. paratyphi* and *V. cholerae*, while thiosemicarbazones with bulkier hexamethyleneiminyl group at the amino nitrogen were more active both as free ligand as well as in the form of a copper(II) complex  $[\text{CuLCl}]$  [46]. Owing to the lower solubility of complexes in the non-aqueous solvents compared with the free ligand,  $[\text{CuL}(\text{NO}_3)(\text{H}_2\text{O})]\cdot\text{H}_2\text{O}$  showed a lower fungitoxic activity against phytopathogenic fungi, *A. alternata*, *F. phaseoline* and *F. equiseti* [48]. Square pyramidal Zn(II) complexes of N(4) substituted 2-acetylpyridine thiosemicarbazones *viz.*  $[\text{Zn}(\text{HL})\text{Cl}_2]$  and  $[\text{Zn}(\text{HL})(\text{H}_2\text{O})\text{SO}_4]$  display activities against four strains of bacteria (*B. subtilis*, *S. aureus*, *E. coli*, *P. aeruginosa*), two yeasts (*C. albicans*, *S. cerevisiae*) and two molds (*A. niger*, *P. citrinum*) [49].

#### **1.4.1b. Anticancer properties**

Thiosemicarbazones as well as their complexes are well known for their anticancer properties. They act by inducing apoptosis in the cancerous cell lines. Some anticancer drugs act by inducing apoptosis by activating the endonucleotidase leading to the DNA fragmentation [50]. The presence of a metal ion almost systematically increases the activity or contributes to mitigate the side effects of the organic parent compounds. The anti-leukemic effect of 2-formylpyridine thiosemicarbazone was first reported by Brockman *et al.* [51] in 1956. Sartorelli *et al.* [52] observed that these compounds repressed the incorporation of  $^3\text{H}$  thymidine into the DNA and first proposed the inhibition of ribonucleotide reductase as the mechanism through which these molecules work [53,54]. Ribonucleotide reductase is an iron-dependent enzyme that promotes the reduction of ribose to deoxyribose through a free radical mechanism that is triggered by a tyrosyl radical. Inhibition of this enzyme leads to a block in the synthesis phase of the cell cycle and eventually to cell death by apoptosis. They also indirectly demonstrated that the active species was the iron(II) complex of 1-formylisoquinoline thiosemicarbazone. In fact, it was later discovered that iron and copper complexes are by far more active than the free ligands [55].

#### **1.4.2. Analytical applications**

Due to the tendency of thiosemicarbazones to form complexes with metals, analytical applications have also been observed. Thiosemicarbazones are used in the determination of the trace metals in the biological and the pharmaceutical samples, in the extraction of metals, for the inhibition of corrosion etc. Basic mode of action is the formation of colored chelates with the metal ions which can be extracted into suitable solvents [10].

Trace amounts of Cu<sup>II</sup> were determined with cyclopentanone thiosemicarbazone by using stripping voltammetry (detection limits,  $1.57 \times 10^{-9}$  M) [56]. N-Ethyl-3-carbazolecarboxaldehyde thiosemicarbazone was used for spectrophotometric determination of Cu<sup>II</sup> in the environmental and pharmaceutical samples, by forming a green complex (pH 3.0), which can be extracted into *n*-butanol [57]. The low cost of thiosemicarbazones as well as their easy preparative methods could provide a major attraction for the development of analytical reagents for a range of applications in future.

### 1.5. Objectives of the present work

Thiosemicarbazones have emerged as an important class of ligands over a period of time, for a variety of reasons, such as variable donor properties, structural diversity and biological applications. Interesting as the coordination chemistry may be, the driving force for the study of these ligands has undoubtedly been their biological properties and the majority of the 3000 or so publications on thiosemicarbazones since 2000 have alluded to this feature. Some valuable reviews have appeared in this period on the structural features, biological activities and analytical applications of thiosemicarbazone complexes [10], the chemistry of copper complexes of thiosemicarbazones [58], structure activity relationships of metal complexes of thiosemicarbazones [59] and applications of metal complexes of thiosemicarbazones for imaging and therapy [60]. The potent biological activity of tridentate thiosemicarbazones and their metal complexes has been recognised for over 50 years [51,61]. Thiosemicarbazones have been investigated for their Topoisomerase II inhibition by a number of groups. An intriguing recent application of copper bis(thiosemicarbazone)

complexes has been in the potential clinical treatment of Alzheimer's Disease (AD) reported by Donnelly *et al.* This is based on the fact that increased intracellular concentrations of copper can activate Akt (protein kinase B) signalling and thereby inhibit glycogen synthase kinase 3 $\beta$  (GSK3 $\beta$ ) which regulates the accumulation of amyloid- $\beta$  aggregates [62].

In order to pursue the interesting coordinating properties of thiosemicarbazones, complexes with different types of ligand environments are essential. So in the present work we chose two different ONS donor thiosemicarbazones as principal ligands. Introduction of heterocyclic bases like 1,10-phenanthroline, 2,2'-bipyridine, 4,4'-dimethyl-2,2'-bipyridine and 5,5'-dimethyl-2,2'-bipyridine, the classical N,N donor ligands leads to the syntheses of mixed ligand complexes which can cause different bonding, spectral properties and geometries in coordination compounds. All the above said facts stimulated our interest in the study of transition metal complexes with ONS donor thiosemicarbazones and we undertook the present work with the following objectives.

- To synthesize some ONS donor thiosemicarbazones by the condensation of 5-bromo-3-methoxysalicylaldehyde with N(4)-phenylthiosemicarbazide and N(4)-cyclohexylthiosemicarbazide.
- To characterize the synthesized thiosemicarbazones by different physicochemical techniques.
- To synthesize different transition metal complexes using the synthesized thiosemicarbazones as principal ligands and some heterocyclic bases as coligands.

- To study the coordination modes of different thiosemicarbazones in metal complexes by using different physicochemical methods like partial elemental analysis and by different spectroscopic techniques.
- To establish the structure of the compounds by isolating single crystals of the compounds and by collecting and refining single crystal X-ray diffraction data.

In the present work two different thiosemicarbazones were synthesized and characterized. The molecular structures of these thiosemicarbazones were established by single crystal X-ray diffraction studies. The metals selected for the preparation of the complexes are vanadium, nickel, copper, zinc, cadmium and molybdenum. The crystal structures of four of the complexes were studied through single crystal XRD.

## 1.6. Physical measurements

The physicochemical methods adopted during the present study are discussed below.

### 1.6.1. Elemental analyses

Elemental analysis is a process where a sample of a chemical compound is analyzed for its elemental and sometimes isotopic composition. Elemental analysis can be qualitative (determining what elements are present) and it can be quantitative (determining how much of each is present). This information is important to help to determine the purity of a synthesized compound. Elemental analyses of C, H, N and S present in all the compounds were done on a Vario EL III CHNS elemental

analyzer at the Sophisticated Analytical Instrument Facility, Cochin University of Science and Technology, Kochi-22, Kerala, India.

### **1.6.2. Conductivity measurements**

The conductivity (or specific conductance) of an electrolyte solution is a measure of its ability to conduct electricity. The SI unit of conductivity is siemens per meter (S/m). Conductivity measurements are used as a fast, inexpensive and reliable way of measuring the ionic content in a solution. The molar conductivities of the complexes in DMF solutions ( $10^{-3}$  M) at room temperature were measured using a Systronic model 303 direct reading conductivity meter at the Department of Applied Chemistry, CUSAT, Kochi, India.

### **1.6.3. Magnetic susceptibility measurements**

In electromagnetism, the magnetic susceptibility is a dimensionless proportionality constant that indicates the degree of magnetization of a material in response to an applied magnetic field. Magnetic susceptibility measurements of the complexes were carried out on a Vibrating Sample Magnetometer using  $\text{Hg}[\text{Co}(\text{SCN})_4]$  as a calibrant at the SAIF, Indian Institute of Technology, Madras.

### **1.6.4. Infrared spectroscopy**

Infrared (IR) spectroscopy is one of the most common spectroscopic techniques used by inorganic chemists. The main goal of IR spectroscopic analysis is to determine the chemical functional groups in the sample. Different functional groups absorb characteristic frequencies of IR radiation. Thus, IR spectroscopy is an important and popular tool for

structural elucidation and compound identification. Infrared spectra of some of the complexes were recorded on a JASCO FT-IR-5300 Spectrometer in the range 4000-400  $\text{cm}^{-1}$  using KBr pellets at the Department of Applied Chemistry, CUSAT, Kochi, India.

#### 1.6.5. Ultraviolet-visible spectroscopy

Ultraviolet-visible spectroscopy is a technique in which intensity of light passing through a sample ( $I$ ) is measured and is compared to the intensity of light before it passes through the sample ( $I_0$ ). The ratio ( $I/I_0$ ) is called the transmittance and is usually expressed as a percentage (%T). The electronic spectra of the compounds were taken on a Spectro UV-vis Double Beam UVD-3500 spectrometer in the 200-900 nm range at the Department of Applied Chemistry, CUSAT, Kochi, India.

#### 1.6.6. Mass spectroscopy

Mass spectrometry (MS) is an analytical technique that measures the mass-to-charge ratio of charged particles. It is used for determining masses of particles, for determining the elemental composition of a sample or molecule and for elucidating the chemical structures of molecules. MS works by ionizing chemical compounds to generate charged molecules or molecular fragments and measuring their mass-to-charge ratios. Mass spectra of the thiosemicarbazones were recorded by direct injection on WATERS 3100 Mass Detector using Electron Spray Ionization (ESI) technique designed for routine HPLC-MS analyses at the Department of Applied Chemistry, CUSAT, Kochi, India.

### **1.6.7. NMR spectroscopy**

Nuclear magnetic resonance spectroscopy, most commonly known as NMR spectroscopy, is a research technique that exploits the magnetic properties of certain atomic nuclei to determine physical and chemical properties of atoms or the molecules in which they are contained. It relies on the phenomenon of nuclear magnetic resonance and can provide detailed information about the structure, dynamics, reaction state and chemical environment of molecules.  $^1\text{H}$  NMR spectra of thiosemicarbazones were recorded using Bruker AMX 400 FT-NMR Spectrometer with deuterated DMSO as the solvent and TMS as internal standard at the Sophisticated Analytical Instrument Facility, CUSAT, Kochi, India.

### **1.6.8. EPR spectroscopy**

Electron paramagnetic resonance (EPR) or electron spin resonance (ESR) spectroscopy is a technique for studying materials with unpaired electrons. The basic concepts of EPR are analogous to those of nuclear magnetic resonance (NMR), but it is electron spins that are excited instead of the spins of atomic nuclei. Because most stable molecules have all their electrons paired, the EPR technique is less widely used than NMR. The EPR spectra of the complexes in the solid state at 298 K and in DMF/DMSO at 77 K were recorded on a Varian E-112 spectrometer using TCNE as the standard, with 100 kHz modulation frequency, 2 G modulation amplitude and 9.1 GHz microwave frequency at SAIF, IIT Bombay, India.

### **1.6.9. Single crystal X-ray diffraction studies**

Single crystal X-ray diffraction is a non-destructive analytical technique which provides detailed information about the internal lattice of

crystalline substances, including unit cell dimensions, bond lengths, bond angles and details of site-ordering. Ideal crystals should be between 150-250 microns in size. Samples are mounted on the tip of a thin glass fiber using an epoxy or cement. This fiber is attached to a brass mounting pin, usually by the use of modeling clay and the pin is then inserted into the goniometer head. The goniometer head and sample are then affixed to the diffractometer. Then data is collected and phase problem is solved to find the unique set of phases that can be combined with the structure factors to determine the electron density and therefore, the crystal structure. The trial structure is then solved and refined.

Single crystal X-ray diffraction studies of the compounds were carried out using a Bruker SMART APEXII CCD diffractometer at SAIF, Cochin University of Science and Technology, Kochi-22, Kerala, India. Bruker SMART software was used for data acquisition and Bruker SAINT software for data integration [63]. Absorption corrections were carried out using SADABS based on Laue symmetry using equivalent reflections [64]. The structure was solved by direct methods using SHELXS97 [65] and refined by full-matrix least-squares refinement on  $F^2$  using SHELXL97 [66]. The graphics tool used was DIAMOND version 3.2g [67].

## References

- [1] J.E. Huheey, E.A. Keiter, R.L. Keiter, *Inorganic Chemistry, Principles of Structure and Reactivity*, 4<sup>th</sup> ed., Harper Collins College Publishers, New York, 1993.
- [2] A.B.P. Lever, *Comprehensive Coordination Chemistry II* (1987).

- [3] U. Kulandaivelu, V.G. Padmini, K. Suneetha, B. Shireesha, J.V. Vidyasagar, T.R. Rao, K.N. Jayaveera, A. Basu, V. Jayaprakash, *Arch Pharm (Weinheim)* 344 (2011) 84.
- [4] W. Hernández, J. Paz, A. Vaisberg, E. Spodine, R. Richter, L. Beyer, *Bioinorg. Chem. Appl.* (2008) 1.
- [5] B. Prathima, Y.S. Rao, S.A. Reddy, Y.P. Reddy, A.V. Reddy, *Spectrochim. Acta Part A: Mol. Biomol. Spectrosc.* 77 (2010) 248.
- [6] P. Kalaivani, R. Prabhakaran, F. Dallemer, P. Poornima, E. Vaishnavi, E. Ramachandran, V. Vijaya Padma, R. Renganathan, K. Natarajan, *Metallomics* 4 (2012) 101.
- [7] A.J. Kesel, *Eur. J. Med. Chem.* 46 (2011) 1656.
- [8] E.F. Castro, L.E. Fabian, M.E. Caputto, D. Gagey, L.M. Finkielsztejn, G.Y. Moltrasio, A.G. Moglioni, R.H. Campos, L.V. Cavallaro, *J. Virol.* 85 (2011) 5436.
- [9] D.L. Klayman, J.F. Bartosevich, T.S. Griffin, C.J. Mason, J.P. Scovill, *J. Med. Chem.* 22 (1979) 855.
- [10] G.L. Parrilha, J.G. Da Silva, L.F. Gouveia, A.K. Gasparoto, R.P. Dias, W.R. Rocha, D.A. Santos, N.L. Speziali, H. Beraldo, *Eur. J. Med. Chem.* 46 (2011) 1473.
- [11] T.S. Lobana, R. Sharma, G. Bawa, S. Khanna, *Coord. Chem. Rev.* 253 (2009) 977.
- [12] D.E. Barber, Z. Lu, T. Richardson, R.H. Crabtree, *Inorg. Chem.* 31 (1992) 4709.

- [13] R.P. John, A. Sreekanth, V. Rajakannan, T.A. Ajith, M.R.P. Kurup, *Polyhedron* 23 (2004) 2549.
- [14] P. Bindu, M.R.P. Kurup, *Transit. Met. Chem.* 22 (1997) 578.
- [15] P. Bindu, M.R.P. Kurup, T.R. Satyakeerthy, *Polyhedron* 18 (1999) 321.
- [16] Z. Lu, C. White, A.L. Rheingold, R.H. Crabtree, *Inorg. Chem.* 32 (1993) 3991.
- [17] S.K. Dutta, D.B. McConville, W.J. Youngs, M. Chaudhury, *Inorg. Chem.* 36 (1997) 2517.
- [18] S. Padhye, G.B. Kauffman, *Coord. Chem. Rev.* 63 (1985) 127.
- [19] A.E. Liberta, D.X. West, *Biometals* 5 (1992) 121.
- [20] E. Lukevics, D. Jansone, K. Rubina, E. Abele, S. Germane, L. Leite, M. Shymaska, J. Popelis, *Eur. J. Med. Chem.* 30 (1995) 983.
- [21] N.N. Durham, R.W. Chesnut, D.F. Haslam, K.D. Berlin, D.E. Kiser, *Mol. Pathol. Dis.* 4 (1974) 77.
- [22] R.B. Singh, B.S. Garg, R.P. Singh, *Talanta* 25 (1978) 619.
- [23] T.S. Lobana, Rekha, R.J. Butcher, *Transit. Met. Chem.* 29 (2004) 291.
- [24] T.S. Lobana, Rekha, R.J. Butcher, A. Castineiras, E. Bermejo, P.V. Bharatam, *Inorg. Chem.* 45 (2006) 1535.
- [25] T.S. Lobana, S. Khanna, R.J. Butcher, A.D. Hunter, M. Zeller, *Inorg. Chem.* 46 (2007) 5826.
- [26] T.S. Lobana, S. Khanna, R.J. Butcher, *Z. Anorg. Allg. Chem.* 633 (2007) 1820.
- [27] T.S. Lobana, P. Kumari, R.J. Butcher, *Inorg. Chem. Commun.* 11 (2008) 11.

- [28] E.M. Jouad, A. Riou, M. Allain, M.A. Khan, G.M. Bouet, *Polyhedron* 20 (2001) 67.
- [29] S. Lhuachan, S. Siripaisarnpipat, N. Chaichit, *Eur. J. Inorg. Chem.* (2003) 263.
- [30] E. Bermejo, R. Carballo, A. Castineiras, R. Dominguez, C. Maichle-Mossmer, J. Strahle, D.X. West, *Polyhedron* 18 (1999) 3695.
- [31] P. Gomez-Saiz, J. Garcia-Tojal, M.A. Maestro, J. Mahia, F.J. Arniaz, L. Lezama, T. Rojo, *Eur. J. Inorg. Chem.* (2003) 2639.
- [32] E. Labisbal, K.D. Haslow, A. Sousa-Pedrares, J. Valdes-Martinez, S. Hernandez-Ortega, D.X. West, *Polyhedron* 22 (2003) 2831.
- [33] D. Kovala-Demertzi, A. Domopoulou, M.A. Demertzis, J. Valdes-Martinez, S. Hernandez-Ortega, G. Espinosa-Perez, D.X. West, M.M. Salberg, G.A. Bain, P.D. Bloom, *Polyhedron* 15 (1996) 2587.
- [34] J.S. Casas, E.E. Castellano, M.C. Rodriguez-Arguellas, A. Sanchez, J. Sordo, J. Zukerman-Schpector, *Inorg. Chim. Acta* 260 (1997) 183.
- [35] J. Garcia-Tojal, J.L. Pizarro, A. Garcia-Orad, A.R. Perez-Sanz, M. Ugalde, A.A. Diaz, J.L. Serra, M.I. Arriortua, T. Rojo, *J. Inorg. Biochem.* 86 (2001) 627.
- [36] J.S. Casas, M.V. Castano, M.C. Cifuentes, A. Sanchez, J. Sordo, *Polyhedron* 21 (2002) 1651.
- [37] T.S. Lobana, G. Bawa, A. Castineiras, R.J. Butcher, *Inorg. Chem. Comm.* 10 (2007) 505.
- [38] S. Halder, S.-M. Peng, G.-H. Lee, T. Chatterjee, A. Mukherjee, S. Dutta, U. Sanyal, S. Bhattacharya, *New J. Chem.* 32 (2008) 105.

- [39] D. Kovala-Demertzi, N. Kourkoumelis, M.A. Demertzis, J.R. Miller, C.S. Frampton, J.K. Swearingen, D.X. West, *Eur. J. Inorg. Chem.* (2000) 727.
- [40] T.S. Lobana, G. Bawa, R.J. Butcher, B.-J. Liaw, C.W. Liu, *Polyhedron* 25 (2006) 2897.
- [41] L.J. Ashfield, A.R. Cowley, J.R. Dilworth, P.S. Donnelly, *Inorg. Chem.* 43 (2004) 4121.
- [42] I. Pal, F. Basuli, T.C.W. Mak, S. Bhattacharya, *Angew. Chem. Int. Ed.* 40 (2001) 2923.
- [43] K.A. Jensen, *Z. Anorg. Allg. Chem.* 221 (1934) 11.
- [44] K.A. Jensen, *Z. Anorg. Allg. Chem.* 221 (1934) 6.
- [45] H. Beraldo, D. Gambino, *Min. Rev. Med. Chem.* 4 (2004) 31.
- [46] D.X. West, J.S. Ives, J. Krejci, M.M. Salberg, T.L. Zumbahlen, G.A. Bain, A.E. Liberta, J. Valdes-Martinez, S. Hernandez-Ortiz, R.A. Toscano, *Polyhedron* 14 (1995) 2189.
- [47] M. Joseph, M. Kuriakose, M.R.P. Kurup, E. Suresh, A. Kishore, S.G. Bhat, *Polyhedron* 25 (2006) 61.
- [48] M.A. Ali, A.H. Mirza, A.M.S. Hossain, M. Nazimuddin, *Polyhedron* 20 (2001) 1045.
- [49] N.C. Kasuga, K. Sekino, M. Ishikawa, A. Honda, M. Yokoyama, S. Nakano, N. Shimada, C. Koumu, K. Nomiya, *J. Inorg. Biochem.* 96 (2003) 298.
- [50] M.B. Ferrari, F. Bisceglie, G.G. Fava, G. Pelosi, P. Tarasconi, R. Albertini, S. Pinelli, *J. Inorg. Biochem.* 89 (2002) 36.

- [51] R.W. Brockman, J.R. Thomson, M.J. Bell, H.E. Skipper, *Cancer Res.* 16 (1956) 167.
- [52] A.C. Sartorelli, K.C. Agrawal, E.C. Moore, *Biochem. Pharmacol.* 20 (1971) 3119.
- [53] R.W. Brockman, R.W. Sidwell, G. Arnett, S. Shaddix, *Proc. Soc. Exp. Biol. Med.* 133 (1970) 609.
- [54] A.C. Sartorelli, K.C. Agrawal, A.S. Tsiftoglou, E.C. Moore, *Adv. Enzyme Regul.* 15 (1977) 117.
- [55] W.E. Antholine, J.M. Knight, D.H. Petering, *J. Med. Chem.* 19 (1976) 339.
- [56] R.K. Mahajan, T.P.S. Walia, Sumanjit, T.S. Lobana, *Anal. Sci.* 22 (2006) 389.
- [57] K.J. Reddy, J.R. Kumar, C. Ramachandraiah, T. Thriveni, A.V. Reddy, *Food. Chem.* 101 (2007) 585.
- [58] P.S. Donnelly, *Dalton Trans.* 40 (2011) 999.
- [59] G. Pelosi, *The Open Crystallography Journal* 3 (2010) 16.
- [60] J.R. Dilworth, R. Hueting, *Inorg. Chim. Acta* 389 (2012) 3.
- [61] R. Brockman, J. Thomson, H. Skipper, *Canc. Res.* 2 (1955) 7.
- [62] P.J. Crouch, L.W. Hung, P.A. Adlard, M. Cortes, V. Lal, G. Filiz, K.A. Perez, M. Nurjono, A. Cragounis, T. Du, K. Laughton, I. Volitakis, A. Bush, Q.-X. Li, C.L. Masters, R. Cappai, R.A. Cherny, P.S. Donnelly, A.R. White, K.J. Barnham, *Proc. Natl. Acad. Sci. USA, Early Ed.* (2009) 1.

- [63] SMART and SAINT, Area Detector Software Package and SAX Area Detector Integration Program, Bruker Analytical X-ray; Madison, WI, USA, 1997.
- [64] SADABS, Area Detector Absorption Correction Program; Bruker Analytical X-ray; Madison, WI, 1997.
- [65] G.M. Sheldrick, Acta Crystallogr., Sect. A 46 (1990) 467.
- [66] G.M. Sheldrick, SHELXL97 and SHELXS97, University of Göttingen, Germany, 1997.
- [67] K. Brandenburg, Diamond Version 3.2g, Crystal Impact GbR, Bonn, Germany, 2010.

\*\*\*ORO\*\*\*

**SYNTHESES, CRYSTAL STRUCTURES AND SPECTRAL ASPECTS OF ONS DONOR THIOSEMICARBAZONES**

- 2.1 Introduction
  - 2.2 5-Bromo-3-methoxysalicylaldehyde-N(4)-phenylthiosemicarbazone ( $H_2L^1$ )
  - 2.3 5-Bromo-3-methoxysalicylaldehyde-N(4)-cyclohexylthiosemicarbazone ( $H_2L^2$ )
- References**

**2.1. Introduction**

Thiosemicarbazones with potential donor atoms in their structural skeleton fascinate coordination chemists with their versatile chelating behavior. The coordinating ability of thiosemicarbazones to both transition and main group metallic cations is attributed to the extended delocalization of electron density over  $-NH-C(S)-NH-N=$  system which is enhanced by substitution at the N(4) position. They have been studied for a considerable period of time for their biological properties. The first reports on their medical applications as drugs against tuberculosis and leprosy [1,2] began to appear in the fifties. Their antiviral properties were discovered in the sixties and a huge amount of research was carried out that eventually led to the commercialization of methisazone, Marboran, to treat smallpox [3]. One of the first antitumor activity results was published in this period [4] and recently Triapine (3-aminopyridine-2-carboxaldehyde thiosemicarbazone) has been developed as an anticancer drug and has reached

clinical phase II on several cancer types [5,6]. Recently a particularly attracting new line of action is being developed as inhibitors of multidrug resistance proteins. This target is of enormous interest since it could allow a systematic method to circumvent antibiotics or anticancer drug resistance.

We have synthesized the following two new ligands using 5-bromo-3-methoxysalicylaldehyde, N(4)-phenylthiosemicarbazide and N(4)-cyclohexylthiosemicarbazide. Their structures are given in Fig. 2.1.

- 5-bromo-3-methoxysalicylaldehyde-N(4)-phenylthiosemicarbazone ( $H_2L^1$ )
- 5-bromo-3-methoxysalicylaldehyde-N(4)-cyclohexylthiosemicarbazone ( $H_2L^2$ )

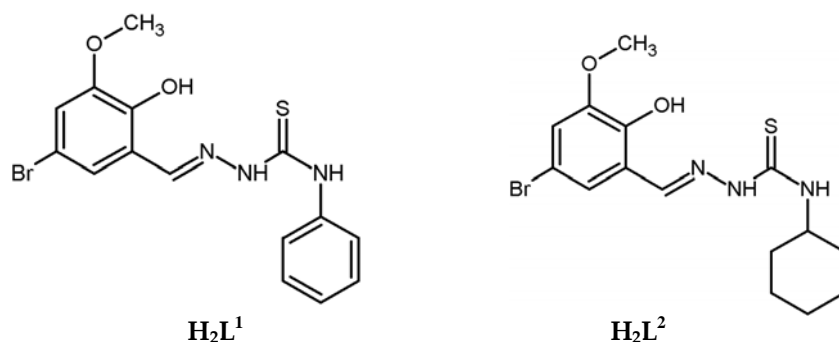


Fig. 2.1. Structures of the thiosemicarbazones.

This chapter discusses the syntheses, crystal structures and spectral aspects of these two thiosemicarbazones. They were synthesized by adapting the reported procedure of Klayman *et. al.* [7] and also others [8,9].

## 2.2. 5-Bromo-3-methoxysalicylaldehyde-N(4)-phenylthiosemicarbazone (H<sub>2</sub>L<sup>1</sup>)

### 2.2.1. Experimental

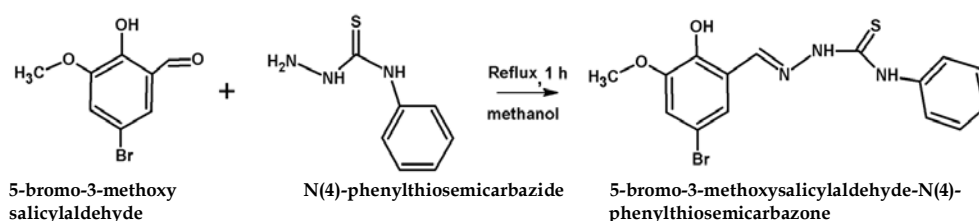
#### 2.2.1.1. Materials

5-Bromo-3-methoxysalicylaldehyde (Sigma-Aldrich) and N(4)-phenylthiosemicarbazide (Sigma-Aldrich) were of Analar grade and were used as received. The solvent methanol (Merck) was used without further purification.

#### 2.2.1.2. Synthesis

5-Bromo-3-methoxysalicylaldehyde-N(4)-phenylthiosemicarbazone was prepared by the condensation of 5-bromo-3-methoxysalicylaldehyde and N(4)-phenylthiosemicarbazide in acid medium (Scheme 2.1). A methanolic solution (20 ml) of N(4)-phenylthiosemicarbazide (0.167 g, 1 mmol) was added to a solution of 5-bromo-3-methoxysalicylaldehyde (0.231 g, 1 mmol) in 20 ml methanol and the reaction mixture was refluxed for 1 h after adding a drop of conc. HCl. The product formed was filtered, washed with methanol and dried. Yield: 88%

Elemental Anal. Found (calcd) %: C, 47.24 (47.38); H, 3.63 (3.71); N, 11.06 (11.05); S, 8.25 (8.43)



## 2.2.2. Characterization of 5-bromo-3-methoxysalicylaldehyde-N(4)-phenylthiosemicarbazone ( $H_2L^1$ )

### 2.2.2.1. Elemental analysis

C, H, N and S analysis results of  $H_2L^1$  are given in Section 2.2.1.2 which shows that it is analytically pure.

### 2.2.2.2. Mass spectrum

The electron spray ionization (ESI) technique was used to measure the mass to charge ( $m/z$ ) ratio of charged particles. The organic molecules are bombarded with high energy electrons and the result is quantitatively recorded as a spectrum of positive ion fragments. The most abundant ion formed in the ionization chamber gives rise to the tallest peak in the spectrum called the base peak. The spectral intensities are normalized by setting the base peak to relative abundance 100 and the rest of the ions are recorded as percentages of the base peak intensity. Mass spectrum is a plot of  $m/z$  of positive ion fragments versus their relative abundance. Here for the ligand  $H_2L^1$ , the molecular ion ( $M^+$ ) peak at 380.1 amu (Fig. 2.2) confirms the expected molecular weight.

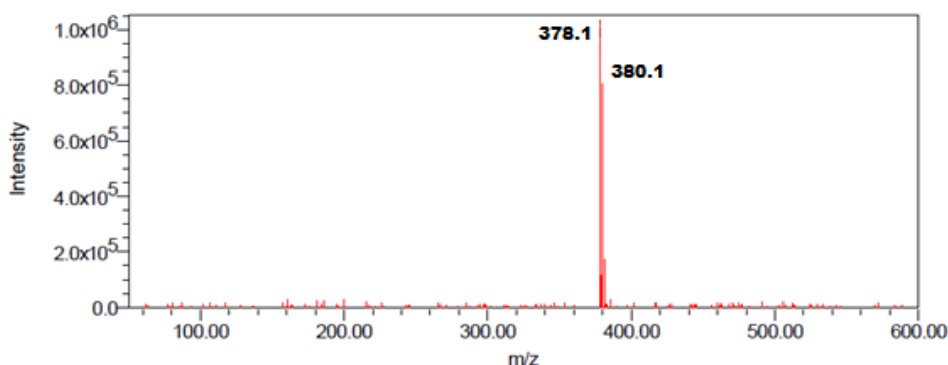


Fig. 2.2. Mass spectrum of  $H_2L^1$  showing molecular ion ( $M^+$ ) peak.

### 2.2.2.3. Infrared spectrum

The characteristic IR bands of the thiosemicarbazone provide significant information regarding the various functional groups present in it. A prominent band at  $1540\text{ cm}^{-1}$  due to azomethine  $\nu(\text{C}=\text{N})$  linkage is observed in the spectrum indicating the condensation of phenylthiosemicarbazide and the aldehyde moiety. The absence of  $\nu(\text{S}-\text{H})$  band at  $\sim 2600\text{ cm}^{-1}$  indicates that the thiosemicarbazone exists in thioamido form in the solid state and the crystal structure confirms this assignment. This is further supported by a band at  $3305\text{ cm}^{-1}$ , indicative of  $\nu(\text{N}-\text{H})$  vibration. The IR spectral band observed at  $1333\text{ cm}^{-1}$  corresponds to  $\nu(\text{C}=\text{S})$ . Another band at  $3441\text{ cm}^{-1}$  is due to O-H stretching vibration. The IR spectrum is shown in Fig. 2.3.

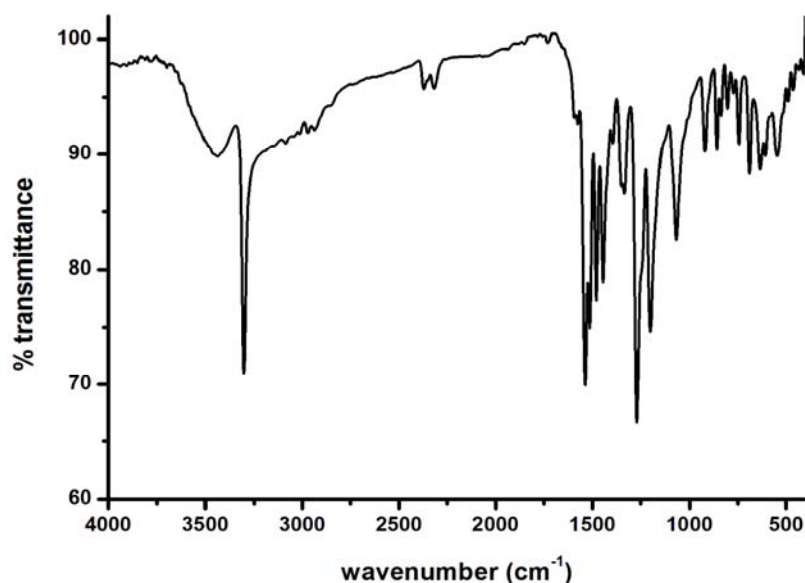


Fig. 2.3. IR spectrum of  $\text{H}_2\text{L}^1$ .

#### 2.2.2.4. Electronic spectrum

The electronic spectrum of the thiosemicarbazone was taken in DMF. Bands in the range 28770-30490  $\text{cm}^{-1}$  can be assigned to  $n \rightarrow \pi^*$  and  $\pi \rightarrow \pi^*$  transitions. This may be due to benzene ring, imine and thiocarbonyl groups present in the compound. Fig. 2.4. represents the electronic spectrum of  $\text{H}_2\text{L}^1$ .

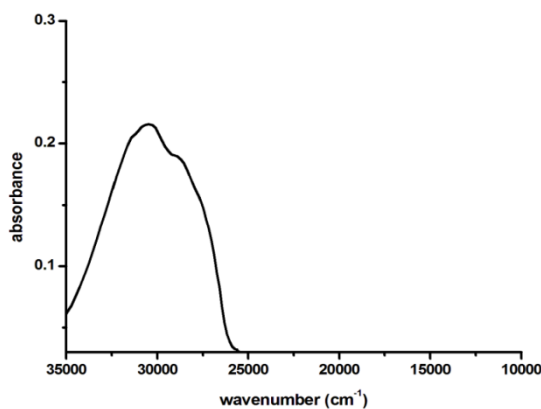


Fig. 2.4. Electronic spectrum of  $\text{H}_2\text{L}^1$ .

#### 2.2.2.5. NMR spectral studies

The NMR spectral assignments were done on the basis of  $^1\text{H}$  NMR,  $^{13}\text{C}$  NMR and DEPT-135.

##### 2.2.2.5a. $^1\text{H}$ NMR spectrum

The  $^1\text{H}$  NMR spectrum of the compound was recorded with deuterated dimethylsulphoxide ( $\text{DMSO-d}_6$ ) as solvent and trimethylsilane (TMS) as the internal standard. It is shown in Fig. 2.5.

A sharp singlet, which integrates as one hydrogen at  $\delta=11.80$  ppm is assigned to the  $-\text{OH}$  proton, while another similar singlet at  $\delta=10.15$  ppm

is assigned to the N2 proton. The downfield shift of these protons are assigned to their hydrogen bonding interactions which is evident from the crystal structure. Hydrogen bonding decreases the electron density around the proton and thus moves the proton absorption to a lower field. Absence of any coupling interactions by OH and N2 protons due to the lack of availability of protons on neighboring atoms render singlet peaks for them. These peaks are found to disappear in the  $H_2L^1$ -D<sub>2</sub>O <sup>1</sup>H NMR spectrum, since those protons exchange with the deuterium in the D<sub>2</sub>O (Fig. 2.6). The low field position of N3 proton ( $\delta$  =9.54 ppm) is attributed to the deshielding caused by the phenyl group and the adjacent thiosemicarbazone moiety. The singlet at  $\delta$  =8.46 ppm is assigned to C7 proton. Aromatic protons appear as multiplets at  $\delta$  =7.96-7.12 ppm range. The singlet at 3.84 ppm which integrates as three hydrogens is assigned for -OCH<sub>3</sub> protons.

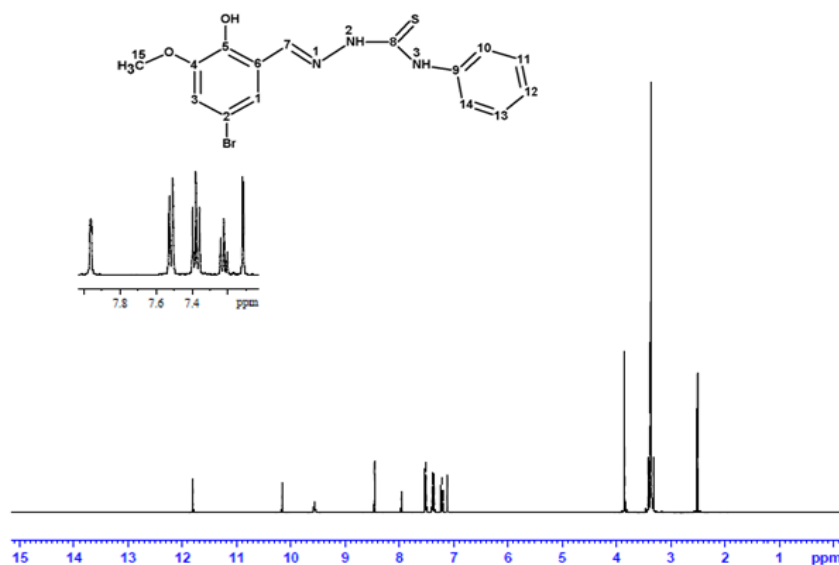


**Fig. 2.5.** <sup>1</sup>H NMR spectrum of  $H_2L^1$ .

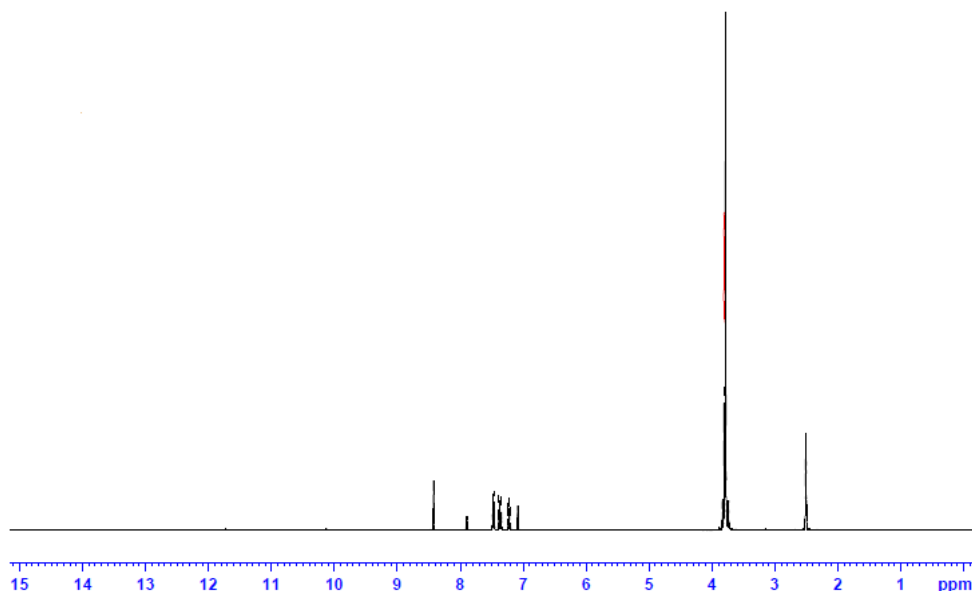
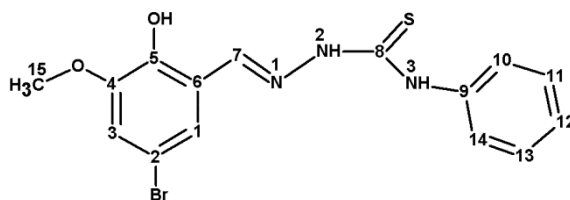


Fig. 2.6.  $^1\text{H}$  NMR spectrum of  $\text{H}_2\text{L}^1\text{-D}_2\text{O}$ .

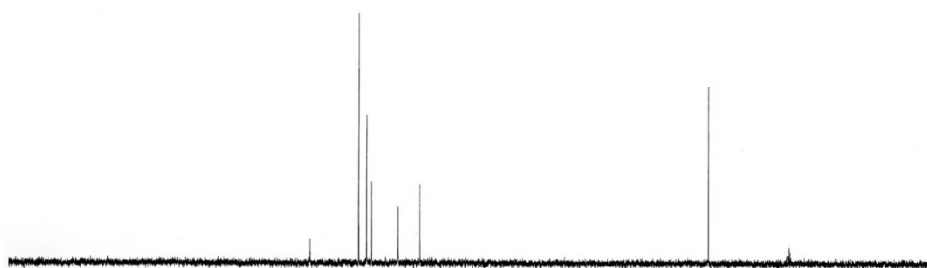
#### 2.2.2.5b. $^{13}\text{C}$ NMR spectrum

The proton decoupled  $^{13}\text{C}$  NMR spectrum provides direct information about the carbon skeleton of the molecule. The  $^{13}\text{C}$  NMR spectrum of the compound (Fig. 2.7) shows carbon signals supporting the  $^1\text{H}$  NMR assignments. There are 13 unique carbon atoms in the molecule which give a total of 13 different peaks in the spectrum. The non-protonated carbon atom C8 is shifted farthest downfield in the spectrum ( $\delta = 176.03$  ppm) due to the conjugative effect of the -N1-N2-C(S)-N3-thiosemicarbazone skeleton. The peak at  $\delta = 137.98$  ppm is assigned to the azomethine carbon C7. C4 and C5 carbon atoms also resonate at lower field values (C4, 145.43 ppm; C5, 148.88 ppm) due to a decreased electron density around carbon atoms resulting from the presence of electronegative oxygen atoms and  $\pi$  electron delocalization in the magnetic environment. The three different types of aromatic carbons on the N-substituted phenyl

ring are clearly distinguishable in the  $^{13}\text{C}$  NMR spectrum. The peaks corresponding to the ortho positioned carbon atoms [C10 and C14] are observed rather downfield when compared to its meta [C11 and C13] and para [C12] counter parts. The phenyl resonances are: C10 and C14, 127.92 ppm; C11 and C13, 126.27 ppm; C12, 115.41 ppm. The other  $^{13}\text{C}$  peaks can be assigned as follows: C9, 139.08 ppm; C1, 125.33 ppm; C2, 122.30; C3, 120.00 ppm; C6, 110.67 ppm; C15, 56.22 ppm.



DEPT-135



C-13

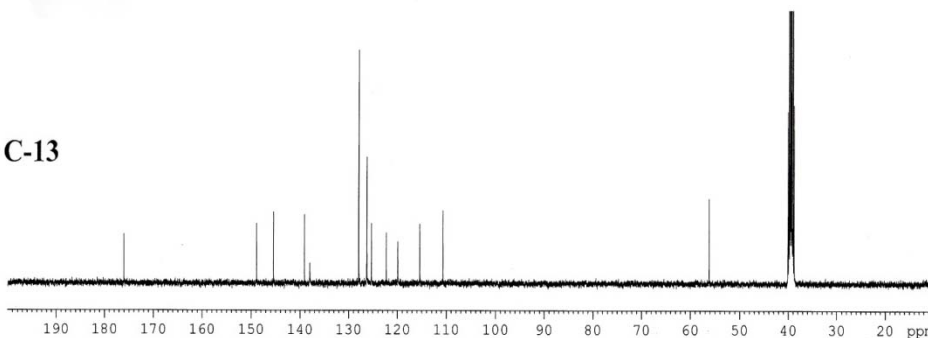


Fig. 2.7.  $^{13}\text{C}$  NMR spectrum of  $\text{H}_2\text{L}^1$  with DEPT.

In the DEPT-135 spectrum, the signals due to C2, C4, C5, C6, C8 and C9 disappear whereas C1, C3, C7, C10, C11, C12, C13, C14 and C15 are retained positive. This shows that C1, C3, C7, C10, C11, C12, C13, C14 and C15 have odd number of hydrogens whereas the other carbons are without hydrogens. Since none of the signals is inverted, it indicates the absence of carbons with even number of hydrogen atoms.

#### 2.2.2.6. Crystal structure

Yellow block shaped crystals of 5-bromo-3-methoxysalicylaldehyde-N(4)-phenylthiosemicarbazone suitable for single crystal X-ray diffraction analysis were obtained by slow evaporation of its solution in 1:1 (v/v) mixture of DMF and methanol over 3 days. A single crystal with approximate dimensions of  $0.35 \times 0.30 \times 0.25 \text{ mm}^3$  was selected for collecting the data. The data were collected using Bruker Kappa APEXII CCD diffractometer equipped with graphite monochromated Mo K $\alpha$  ( $\lambda = 0.71073 \text{ \AA}$ ) radiation at the Sophisticated Analytical Instruments Facility, Cochin University of Science and Technology, Kochi-22, India. The intensity data were collected at 296 K and absorption corrections were carried out using SADABS based on Laue symmetry using equivalent reflections [10]. The cell refinement was done using APEX2 and SAINT [10]. The data was reduced using SAINT and XPREP and the structure was solved by direct methods using SHELXS97 [11] and full-matrix least squares refinement using SHELXL97 [12] package. The graphics tool used was DIAMOND version 3.2g [13]. All H atoms on C were placed in calculated positions, guided by difference maps, with C-H bond distances 0.93–0.96 Å. H atoms were assigned as  $U_{\text{iso}}=1.2U_{\text{eq}}$  (1.5 for Me). N2-H2,

N3–H3' and O2–H2' H atoms were located from difference maps and their distances were restrained using DFIX instructions. The molecular structure of H<sub>2</sub>L<sup>1</sup> is given in Fig. 2.8.

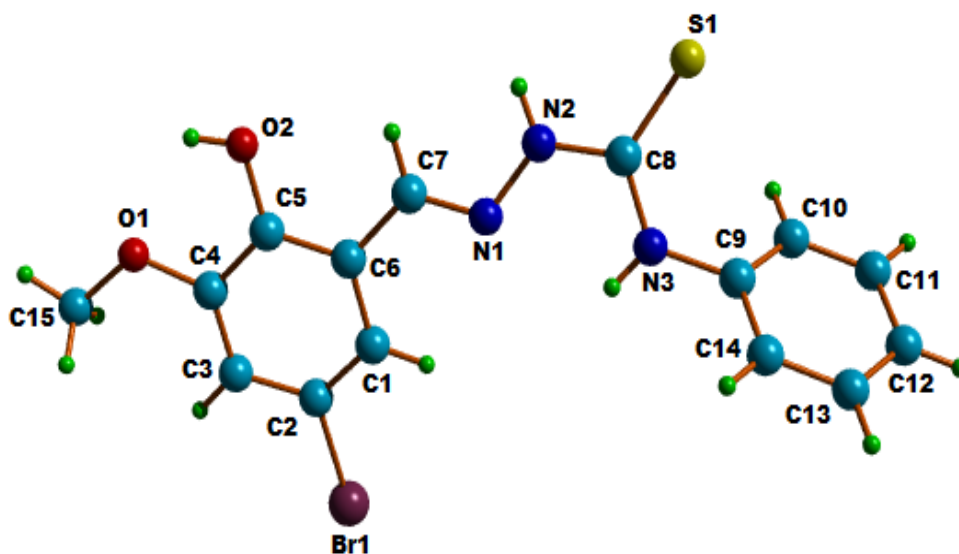


Fig. 2.8. Structure and labeling diagram for H<sub>2</sub>L<sup>1</sup>.

The crystallographic data and structure refinement parameters of the compound are given in Table 2.1 and the selected bond lengths and angles are given in Table 2.2 and torsional angles in Table 2.3.

Table 2.1. Crystal data and structure refinement parameters for H<sub>2</sub>L<sup>1</sup>

Parameters	H <sub>2</sub> L <sup>1</sup>
Empirical formula	C <sub>15</sub> H <sub>14</sub> BrN <sub>3</sub> O <sub>2</sub> S
Formula weight	380.26
Temperature	296 K
Wavelength	0.71073 Å
Crystal system	Triclinic
Space group	$P\bar{1}$
Unit cell dimensions	$a = 6.1046(5) \text{ \AA}$ $b = 11.0329(8) \text{ \AA}$ $c = 12.4303(9) \text{ \AA}$ $\alpha = 101.175(3)^\circ$ $\beta = 91.323(2)^\circ$ $\gamma = 104.759(2)^\circ$
Volume	791.91(10) Å <sup>3</sup>
Z	2
Density (calculated)	1.595 Mg/m <sup>3</sup>
Absorption coefficient	2.740 mm <sup>-1</sup>
$F(000)$	384
Crystal size	0.35 x 0.30 x 0.25 mm <sup>3</sup>
$\theta$ range for data collection	2.82 to 25.00°
Limiting indices	$-7 \leq h \leq 7$ $-13 \leq k \leq 13$ $-14 \leq l \leq 14$
Reflections collected	11624
Unique reflections	2774 [R(int) = 0.039]
Refinement method	Full-matrix least-squares on F <sup>2</sup>
Data / restraints / parameters	2774 / 3 / 212
Goodness-of-fit on F <sup>2</sup>	1.007
Final R indices [I > 2sigma(I)]	R <sub>1</sub> = 0.0285, wR <sub>2</sub> = 0.0640
R indices (all data)	R <sub>1</sub> = 0.0390, wR <sub>2</sub> = 0.0684
Largest diff. peak and hole	0.40 and -0.44 e Å <sup>-3</sup>

$$R_1 = \frac{\sum ||F_o| - |F_c||}{\sum |F_o|}$$

$$wR_2 = [\sum w(F_o^2 - F_c^2)^2 / \sum w(F_o^2)^2]^{1/2}$$

**Table 2.2. Selected bond lengths [Å] and angles [°] for H<sub>2</sub>L<sup>1</sup>**

Bond lengths		Bond angles	
N(1)–C(7)	1.270(3)	C(7)–N(1)–N(2)	114.91(19)
S(1)–C(8)	1.682(2)	C(8)–N(2)–N(1)	122.0(2)
O(1)–C(4)	1.361(3)	C(8)–N(3)–C(9)	126.3(2)
N(1)–N(2)	1.376(3)	N(3)–C(8)–N(2)	115.7(2)
O(2)–C(5)	1.358(3)	N(3)–C(8)–S(1)	125.34(18)
N(2)–C(8)	1.342(3)	N(2)–C(8)–S(1)	118.95(18)
N(3)–C(8)	1.337(3)		
N(3)–C(9)	1.427(3)		

**Table 2.3. Selected torsion angles [°] for H<sub>2</sub>L<sup>1</sup>**

Torsion angles	
O(1)–C(4)–C(5)–O(2)	-1.6(3)
N(2)–N(1)–C(7)–C(6)	174.8(2)
N(1)–N(2)–C(8)–N(3)	-5.9(4)
N(1)–N(2)–C(8)–S(1)	176.19(18)

The compound crystallized into a triclinic space group  $P\bar{1}$ . According to the molecular structure, the compound adopts an *E* configuration with respect to the azomethine bond [N(2)–N(1)–C(7)–C(6) = 174.8(2)°] [14]. Also *E* configuration is perceived about C(8)–N(2) bond similar to H<sub>2</sub>L<sup>2</sup> [15] but in contrast to 2-hydroxyacetophenone-N(4)-phenylthiosemicarbazone [16], where a *Z* configuration exists. This is confirmed by the N(1)–N(2)–C(8)–S(1) torsion angle of 176.19(18)°. Atom O(1) lies *cis* to O(2), with an O(1)–C(4)–C(5)–O(2) torsion angle of -1.6(3)° and atom N(1) lies *cis* to N(3), with an N(1)–N(2)–C(8)–N(3) torsion angle of -5.9(4)°. This favors the intramolecular hydrogen bonding interactions O(2)–H(2')···O(1) and N(3)–H(3')···N(1).

The C(8)–S(1) bond distance [1.682(2) Å] is closer to that expected for C=S bond length [1.60 Å] [17] which confirms the existence of the compound in the thioamido form in solid state. Also the C(7)–N(1) bond distance [1.270(3) Å] is appreciably close to that of a C=N bond [1.28 Å] [17], confirming the azomethine bond formation. The shorter length of C(7)–N(1) and longer length of C(8)–S(1) indicate the extended conjugation in the molecule similar to other thiosemicarbazones.

The mean plane deviation calculations show that the molecule as a whole is non-planar. But the central thiosemicarbazone moiety (C7/N1/N2/C8/S1/N3) is almost planar with a maximum deviation from the mean plane of 0.035(2) Å for atom N(2). This is similar to that observed in salicylaldehyde–N(4)–phenylthiosemicarbazone [18]. The planarity of thiosemicarbazone moiety allows delocalization of the  $\pi$  electrons throughout the C7/N1/N2/C8/S1/N3 group. The ring Cg(1) (comprising of atoms C1–C6, with a maximum deviation of -0.011(2) Å for C2) makes a dihedral angle of 14.80(10)° with thiosemicarbazone moiety while the two rings in the molecule are twisted away from each other by a dihedral angle of 69.13(13)°.

Fig. 2.9 shows the packing diagram of the compound. The crystal packing involves two types of intramolecular hydrogen bonding interactions (Table 2.4), O(2)–H(2') $\cdots$ O(1) and N(3)–H(3') $\cdots$ N(1) leading to the formation of five membered rings comprising of atoms C(4), C(5), O(2), H(2') and O(1) and N(2), C(8), N(3), H(3') and N(1) respectively. The intermolecular hydrogen bonds N(2)–H(2) $\cdots$ O(2) and O(2)–H(2') $\cdots$ S(1) cause the pairing of molecules leading to the formation of centrosymmetric

dimers in the crystal lattice (Fig. 2.10). These dimers are stacked along the 'a' axis (Fig. 2.11).

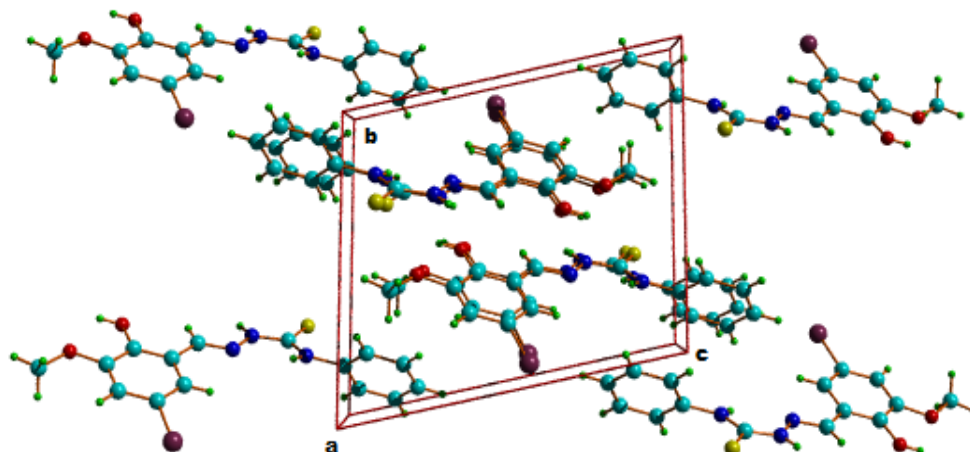


Fig. 2.9. Packing diagram of H<sub>2</sub>L<sup>1</sup> viewed along 'a' axis.

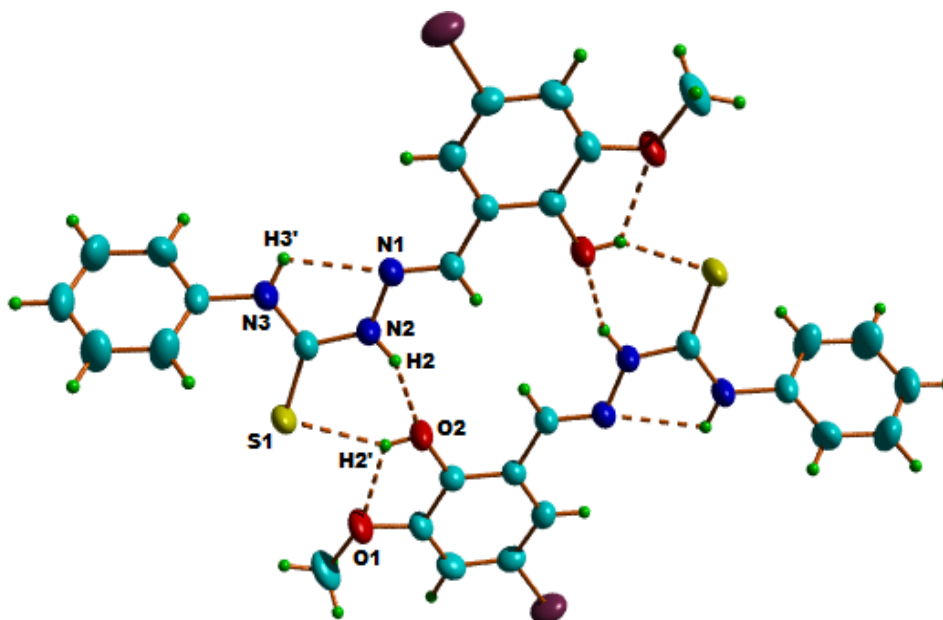


Fig. 2.10. Intra and intermolecular hydrogen bonding interactions of H<sub>2</sub>L<sup>1</sup>.

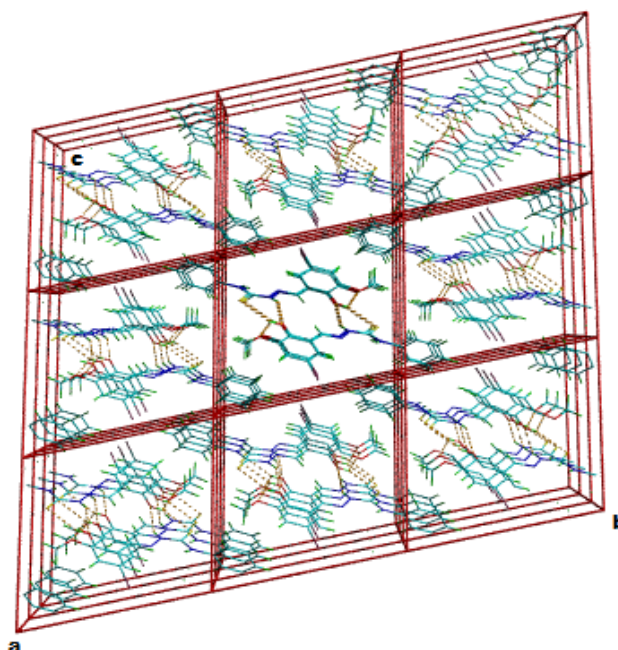


Fig 2.11. Super cell packing diagram of H<sub>2</sub>L<sup>1</sup> showing the stacking of centrosymmetric dimers along 'a' axis.

Further stabilization is provided by non-classical C(7)-H(7)⋯O(2) and C(15)-H(15A)⋯Cg(2) interactions (Fig. 2.12). The interaction parameters are shown in Table 2.4.

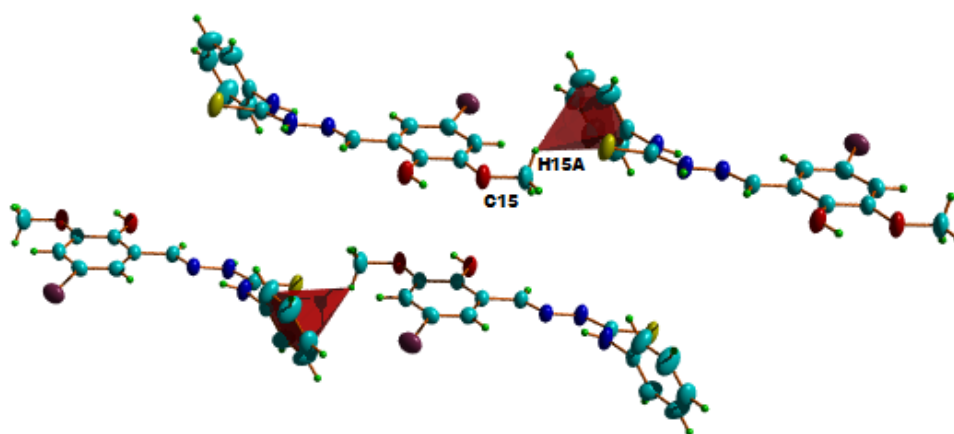


Fig. 2.12. C-H⋯π interactions in H<sub>2</sub>L<sup>1</sup>.

**Table 2.4. Interaction parameters of H<sub>2</sub>L<sup>1</sup>**

Hydrogen bonding				
D–H···A	D–H (Å)	H···A (Å)	D···A (Å)	∠D–H···A(°)
N(3)–H(3')···N(1)	0.83(2)	2.25(3)	2.654(3)	110(2)
N(2)–H(2)···O(2) <sup>a</sup>	0.84(2)	2.23(2)	2.983(3)	149(2)
O(2)–H(2')···O(1)	0.82(2)	2.20(3)	2.631(2)	113(3)
O(2)–H(2')···S(1) <sup>a</sup>	0.82(2)	2.44(2)	3.154(18)	146(3)
C–H···π Interactions				
C–H···Cg	C–H (Å)	H···Cg (Å)	C···Cg (Å)	∠C–H···Cg(°)
C(15)–H(15A)···Cg(2) <sup>b</sup>	0.96	2.90	3.649(3)	135

Equivalent position codes: a = -x+1, -y+1, -z+1; b = x+1, y, z+1

Cg2 = C9, C10, C11, C12, C13, C14

D = Donor, A = acceptor, Cg = Centroid

### 2.3. 5-Bromo-3-methoxysalicylaldehyde-N(4)-cyclohexylthiosemicarbazone(H<sub>2</sub>L<sup>2</sup>)

#### 2.3.1. Experimental

##### 2.3.1.1. Materials

5-Bromo-3-methoxysalicylaldehyde (Sigma-Aldrich), hydrazine hydrate (Lancaster) and cyclohexyl isothiocyanate (Fluka) were of Analar grade and were used as received. The solvent methanol (Merck) was used without further purification.

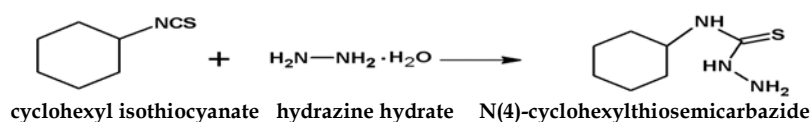
##### 2.3.1.2. Synthesis

The preparation of this compound involves a two step process [7].

## Step-1

## Preparation of N(4)-cyclohexylthiosemicarbazide

In the first step, cyclohexyl isothiocyanate (2 ml, 15 mmol) in 15 ml methanol and hydrazine hydrate (4.3 ml, 90 mmol) in 15 ml methanol were mixed and the resulting solution was stirred for an hour (Scheme 2.2). The white product, N(4)-cyclohexylthiosemicarbazide formed was filtered, washed with methanol and dried *in vacuo*.

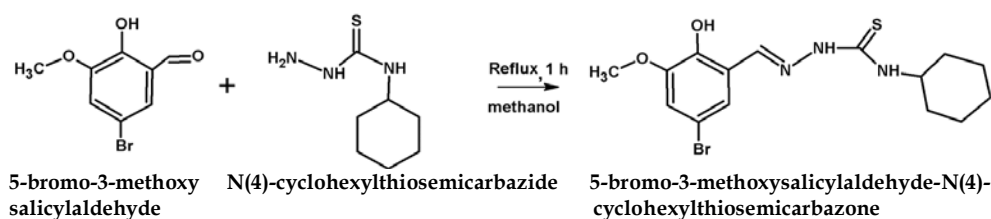


Scheme 2.2

## Step-2

Synthesis of 5-bromo-3-methoxysalicylaldehyde-N(4)-cyclohexylthiosemicarbazone (H<sub>2</sub>L<sup>2</sup>)

In the second step, a methanolic (20 ml) solution of N(4)-cyclohexylthiosemicarbazide (0.173 g, 1 mmol) was added to a solution of 5-bromo-3-methoxysalicylaldehyde (0.231 g, 1 mmol) in 15 ml methanol and the reaction mixture was refluxed for 1 h after adding a drop of conc. HCl (Scheme 2.3). The product formed was filtered, washed with methanol and dried *in vacuo*. Yield: 82%



Scheme 2.3

Elemental Anal. Found (calcd) %: C, 46.34 (46.64); H, 5.10 (5.22); N, 10.77 (10.88); S, 8.15 (8.30)

### 2.3.2. Characterization of 5-bromo-3-methoxysalicylaldehyde-N(4)-cyclohexylthiosemicarbazone ( $H_2L^2$ )

#### 2.3.2.1. Elemental analysis

C, H, N and S analysis results of  $H_2L^2$  are given in Section 2.3.1.2 which shows that it is analytically pure.

#### 2.3.2.2. Mass spectrum

Mass spectrum is a plot of mass to charge ratio ( $m/z$ ) of positive ion fragments versus their relative abundance. The electron spray ionization (ESI) technique was used to measure the mass to charge ( $m/z$ ) ratio of charged particles. The most abundant ion formed in the ionization chamber gives rise to the tallest peak in the spectrum called the base peak. The spectral intensities are normalized by setting the base peak to relative abundance 100 and the rest of the ions are recorded as percentages of the base peak intensity. Here for the ligand  $H_2L^2$ , the (M+1) peak at 387.2 amu (Fig. 2.13) confirms the expected molecular weight.

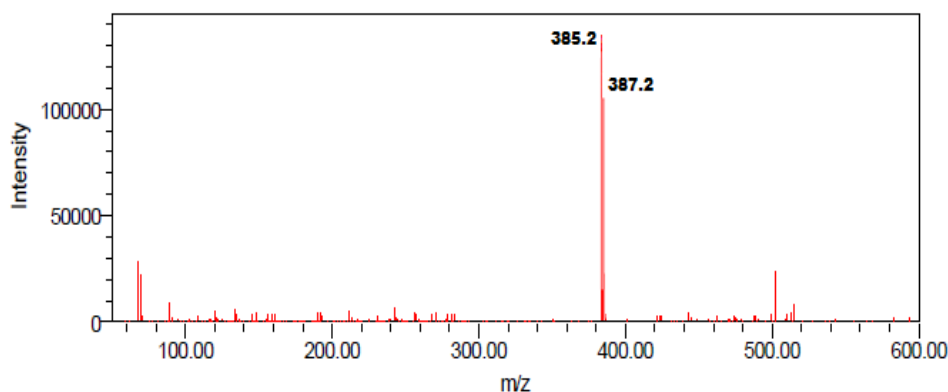


**Fig. 2.13. Mass spectrum of  $H_2L^2$  showing (M+1) peak.**

### 2.3.2.3. Infrared spectrum

The compound reveals well-defined molecular vibrations in the IR region. The absence of  $\nu(\text{S-H})$  band at  $\sim 2600\text{ cm}^{-1}$  suggests the existence of the thiosemicarbazone in the thioamido form in the solid state and the crystal structure confirms this assignment. This is further supported by a band at  $3309\text{ cm}^{-1}$ , indicative of  $\nu(\text{N-H})$  vibration. A prominent band at  $1539\text{ cm}^{-1}$  due to azomethine  $\nu(\text{C=N})$  linkage is observed in the spectrum indicating the condensation of cyclohexylthiosemicarbazide and the aldehyde moiety. The IR spectral band observed at  $1342\text{ cm}^{-1}$  corresponds to  $\nu(\text{C=S})$ . The  $-\text{OH}$  stretching vibration is perceived as a distinct peak at  $3454\text{ cm}^{-1}$ . The  $-\text{CH}$  stretching vibrations of the cyclohexyl moiety are observed as sharp peaks at  $2925$  and  $2854\text{ cm}^{-1}$ . The IR spectrum is shown in Fig. 2.14.

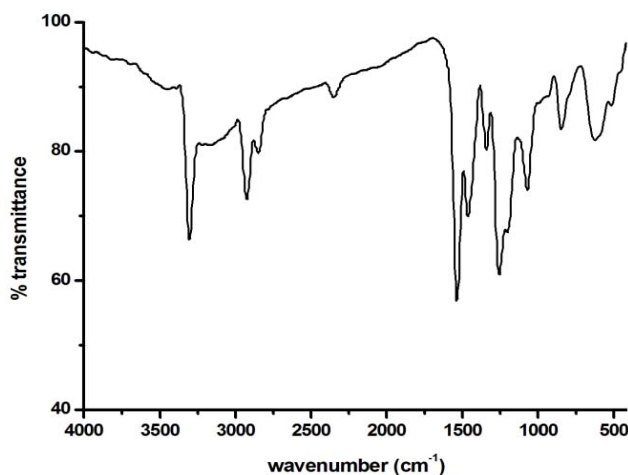


Fig. 2.14. IR spectrum of  $\text{H}_2\text{L}^2$ .

#### 2.3.2.4. Electronic spectrum

The electronic spectrum of the thiosemicarbazone was taken in DMF. Bands at 30490 and 29300  $\text{cm}^{-1}$  are due to  $\pi \rightarrow \pi^*$  and  $n \rightarrow \pi^*$  transitions. This may be due to benzene ring, imine and thiocarbonyl groups present in the compound. Fig. 2.15. represents the electronic spectrum of  $\text{H}_2\text{L}^2$ .

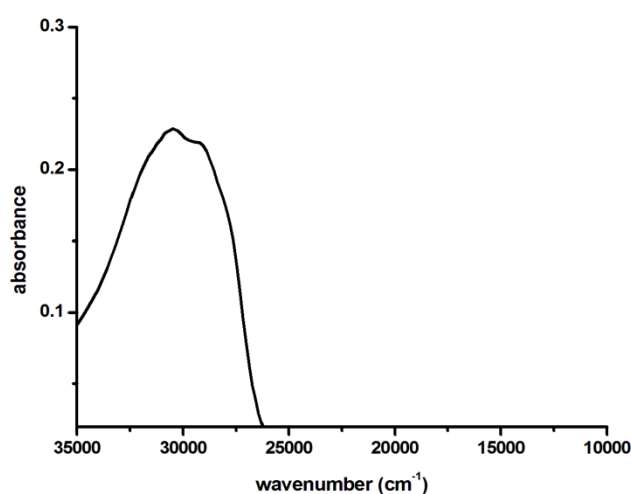


Fig. 2.15. Electronic spectrum of  $\text{H}_2\text{L}^2$ .

#### 2.3.2.5. NMR spectral studies

The NMR spectral assignments were done on the basis of  $^1\text{H}$  NMR,  $^{13}\text{C}$  NMR and DEPT-135.

##### 2.3.2.5a. $^1\text{H}$ NMR spectrum

The  $^1\text{H}$  NMR spectrum of the compound was recorded with deuterated dimethylsulphoxide ( $\text{DMSO-d}_6$ ) as solvent and TMS as the internal standard (Fig. 2.16). A sharp singlet, which integrates as one hydrogen at  $\delta = 11.37$  ppm is assigned to the  $-\text{OH}$  proton, while another similar singlet at  $\delta = 9.52$  ppm is assigned to the  $\text{N}(2)\text{H}$  proton. The

downfield shift of these protons are assigned to their hydrogen bonding interactions which is evident from the crystal structure. Hydrogen bonding decreases the electron density around the proton and thus moves the proton absorption to a lower field. Absence of any coupling interactions by OH and N(2)H protons due to the lack of availability of protons on neighboring atoms render singlet peaks for them. These peaks are found to disappear in the  $\text{H}_2\text{L}^2\text{-D}_2\text{O}$   $^1\text{H}$  NMR spectrum, since those protons exchange with the deuterium in the  $\text{D}_2\text{O}$  (Fig 2.17). The singlet at  $\delta = 8.36$  ppm is assigned to C(7)H proton and that at  $\delta = 8.05$  ppm is assigned to N(3)H proton. Also the singlet at 3.84 ppm is assigned for  $-\text{OCH}_3$  protons. Cyclohexyl protons appear as a multiplet in the range 1.40-1.89 ppm.

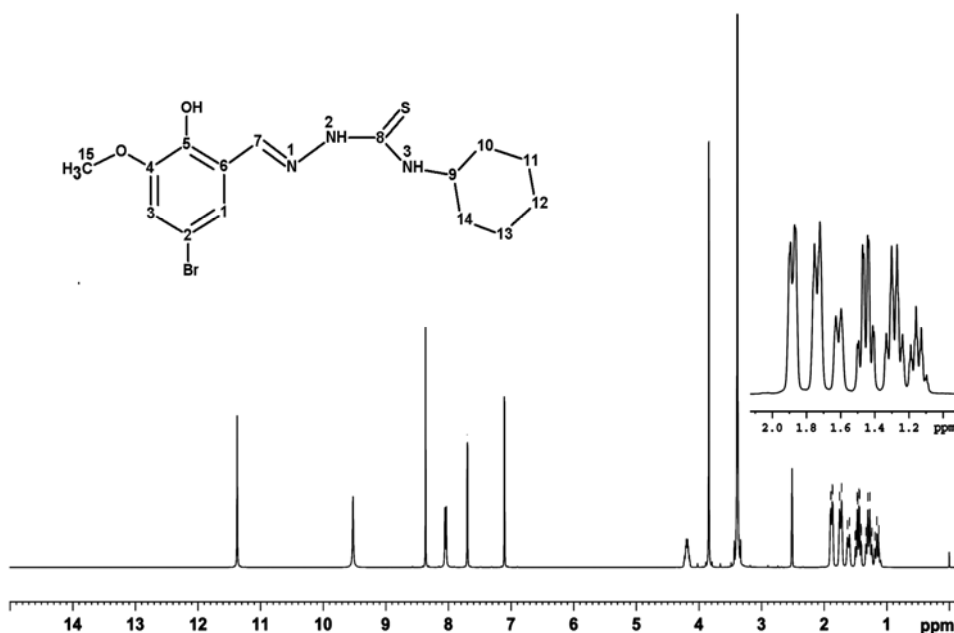


Fig. 2.16.  $^1\text{H}$  NMR spectrum of  $\text{H}_2\text{L}^2$ .

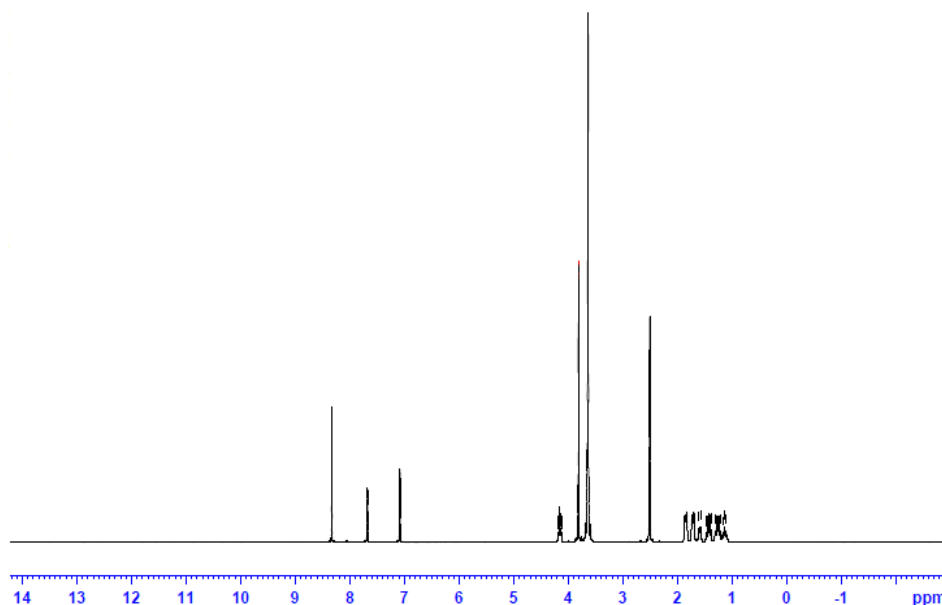


Fig. 2.17.  $^1\text{H}$  NMR spectrum of  $\text{H}_2\text{L}^2$ - $\text{D}_2\text{O}$  exchange.

#### 2.3.2.5b. $^{13}\text{C}$ NMR spectrum

In  $^{13}\text{C}$  NMR, the most significant factors affecting the chemical shifts are the electronegativity of the groups attached to the C and hybridization of carbon. The  $^{13}\text{C}$  NMR spectrum of  $\text{H}_2\text{L}^2$  (Fig. 2.18) gave a total of 13 peaks corresponding to 13 unique carbon atoms in the molecule. The non-protonated carbon atom C8 is shifted farthest downfield in the spectrum ( $\delta=175.71$  ppm) due to the conjugative effect of the -N1-N2-C(S)-N3-thiosemicarbazone skeleton. The peak at  $\delta = 137.64$  ppm is assigned to the azomethine carbon C7. C4 and C5 carbon atoms also resonate at lower field values (C4, 145.36 ppm; C5, 149.01 ppm) due to a decreased electron density around carbon atoms resulting from the presence of electronegative oxygen atoms and  $\pi$  electron delocalization in the magnetic environment. The other  $^{13}\text{C}$  peaks can be assigned as follows: C9, 139.08 ppm; C1, 125.33

ppm; C2, 122.30 ppm; C3, 120.00 ppm; C6, 110.67 ppm; C15, 56.22 ppm, C9, 52.79 ppm; C10, C14, 31.73 ppm; C12, 25.00 ppm; C11, C13, 24.93 ppm.

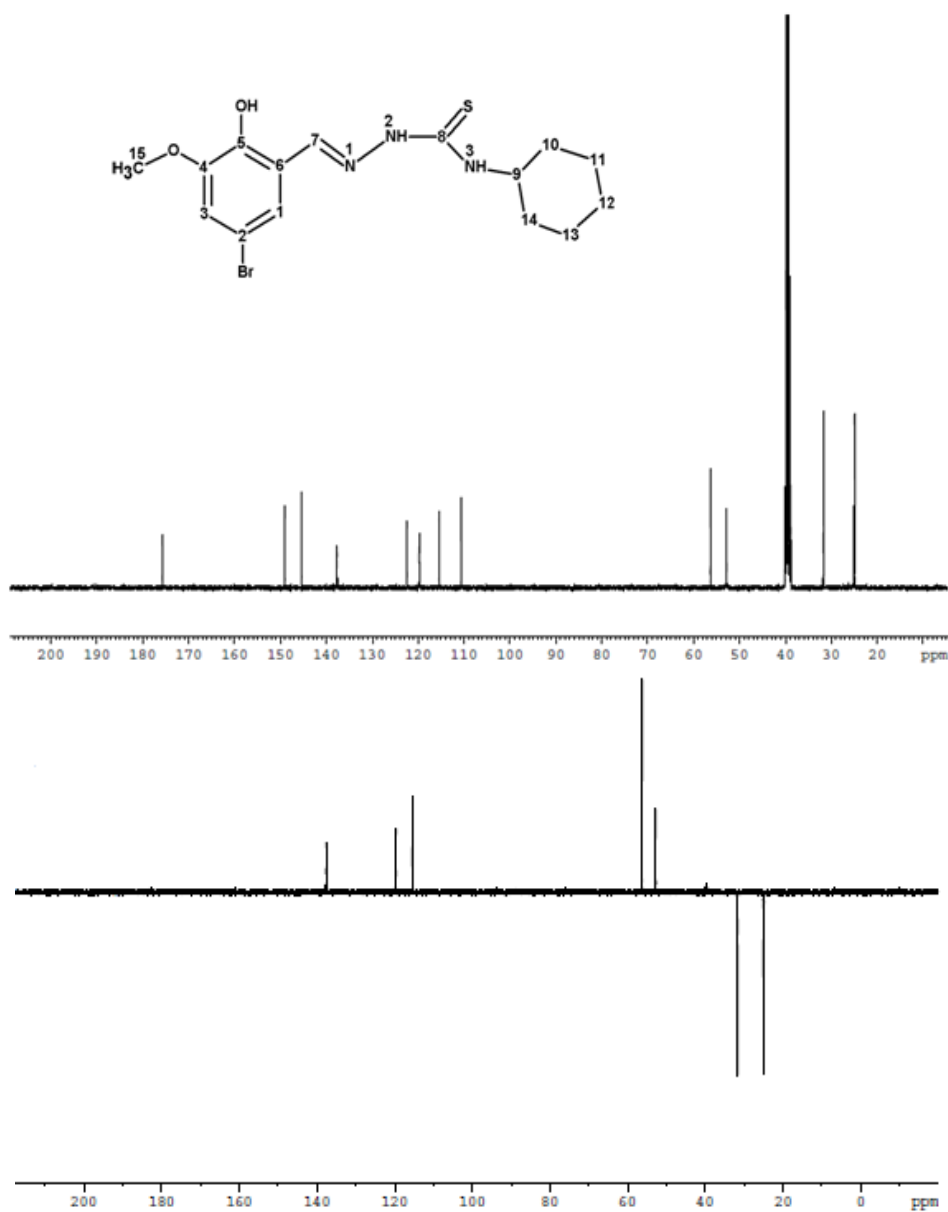


Fig. 2.18.  $^{13}C$  NMR spectrum of  $H_2L^2$  with DEPT.

In DEPT experiment, a sequence of pulses with various delay times are used to create the DEPT spectra where  $-\text{CH}_3$  and CH peaks appear as normal,  $-\text{CH}_2-$  peaks appear inverted and carbons with no protons disappear. In the DEPT-135 spectrum of  $\text{H}_2\text{L}^2$ , the signals due to C2, C4, C5, C6 and C8 disappear, C1, C3, C7, C9 and C15 are retained positive and C10, C11, C12, C13 and C14 have a negative phase. This shows that C1, C3, C7, C9 and C15 have odd number of hydrogens, C10, C11, C12, C13 and C14 have even number of hydrogens whereas the other carbons are without hydrogens.

#### **2.3.2.6. Crystal structure**

Colorless block shaped crystals of 5-bromo-3-methoxysalicylaldehyde-N(4)-cyclohexylthiosemicarbazone suitable for single crystal X-ray diffraction analysis were obtained by slow evaporation of its solution in 1:1 (v/v) mixture of DMF and methanol over 2 days. A single crystal with approximate dimensions of  $0.30 \times 0.25 \times 0.25 \text{ mm}^3$  was selected for collecting the data. The data were collected using Bruker Kappa APEXII CCD diffractometer equipped with graphite monochromated Mo K $\alpha$  ( $\lambda = 0.71073 \text{ \AA}$ ) radiation at the Sophisticated Analytical Instruments Facility, Cochin University of Science and Technology, Kochi-22, India. The intensity data were collected at 296 K and absorption corrections were carried out using SADABS based on Laue symmetry using equivalent reflections [10]. The cell refinement was done using APEX2 and SAINT [10]. The data was reduced using SAINT and XPREP and the structure was solved by direct methods using SHELXS97 [11] and full-matrix least squares refinement using SHELXL97 [12] package. The graphics tool used

was DIAMOND version 3.2g [13]. All H atoms on C were placed in calculated positions, guided by difference maps, with C-H bond distances 0.93–0.97 Å. H atoms were assigned as  $U_{\text{iso}}=1.2U_{\text{eq}}$  (1.5 for Me). N2-H2, N3-H3' and O2-H2' H atoms were located from difference maps and their distances were restrained using DFIX instructions. The molecular structure of  $\text{H}_2\text{L}^2$  is given in Fig. 2.19.

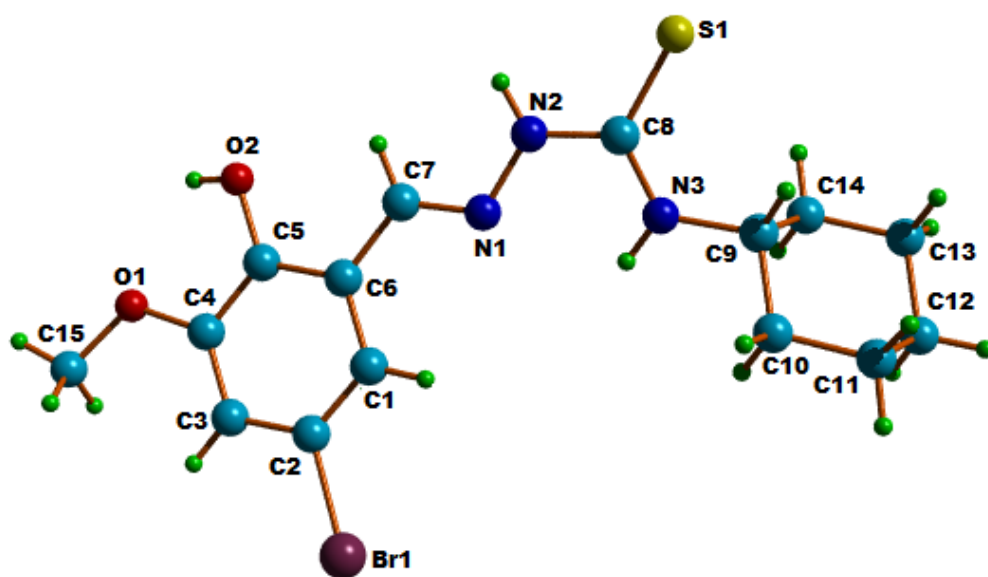


Fig. 2.19. Structure and labeling diagram for  $\text{H}_2\text{L}^2$ .

The crystallographic data and structure refinement parameters of the compound are given in Table 2.5 and the selected bond lengths and angles are given in Table 2.6 and torsional angles in Table 2.7.

**Table 2.5. Crystal data and structure refinement for H<sub>2</sub>L<sup>2</sup>**

Parameters	H <sub>2</sub> L <sup>2</sup>
Empirical formula	C <sub>15</sub> H <sub>20</sub> BrN <sub>3</sub> O <sub>2</sub> S
Formula weight	386.31
Temperature	296 K
Wavelength	0.71073 Å
Crystal system	Triclinic
Space group	$P\bar{1}$
Unit cell dimensions	$a = 5.788(4)$ Å $b = 11.412(1)$ Å $c = 13.131(12)$ Å $\alpha = 75.194(4)^\circ$ $\beta = 86.493(3)^\circ$ $\gamma = 83.489(3)^\circ$
Volume	832.72(12) Å <sup>3</sup>
Z	2
Density (calculated)	1.541 Mg/m <sup>3</sup>
Absorption coefficient	2.60 mm <sup>-1</sup>
<i>F</i> (000)	396
Crystal size	0.30 x 0.25 x 0.25 mm <sup>3</sup>
$\theta$ range for data collection	2.7-25.0°
Limiting indices	-6 ≤ <i>h</i> ≤ 6 -13 ≤ <i>k</i> ≤ 13 -15 ≤ <i>l</i> ≤ 15
Reflections collected	12149
Unique reflections	2923 [R(int) = 0.07]
Refinement method	Full-matrix least-squares on F <sup>2</sup>
Data / restraints / parameters	2923 / 3 / 213
Goodness-of-fit on F <sup>2</sup>	1.119
Final R indices [ <i>I</i> > 2σ( <i>I</i> )]	R <sub>1</sub> = 0.0347, wR <sub>2</sub> = 0.0929
R indices (all data)	R <sub>1</sub> = 0.0418, wR <sub>2</sub> = 0.0980
Extinction coefficient	0.0142(18)
Largest diff. peak and hole	0.27 and -0.41 e Å <sup>-3</sup>

$$R_1 = \frac{\sum ||F_o| - |F_c||}{\sum |F_o|}$$

$$wR_2 = [\sum w(F_o^2 - F_c^2)^2 / \sum w(F_o^2)^2]^{1/2}$$

Table 2.6. Selected bond lengths [Å] and angles [°] for H<sub>2</sub>L<sup>2</sup>

Bond lengths		Bond angles	
N(1)–C(7)	1.267(4)	C(7)–N(1)–N(2)	115.6(3)
S(1)–C(8)	1.685(3)	C(8)–N(2)–N(1)	120.9(2)
O(1)–C(4)	1.352(4)	C(8)–N(3)–C(9)	125.6(2)
N(1)–N(2)	1.363(3)	N(3)–C(8)–N(2)	116.6(3)
O(2)–C(5)	1.351(4)	N(3)–C(8)–S(1)	124.5(2)
N(2)–C(8)	1.342(4)	N(2)–C(8)–S(1)	118.8(2)
N(3)–C(8)	1.308(4)		
N(3)–C(9)	1.454(4)		

Table 2.7. Selected torsion angles [°] for H<sub>2</sub>L<sup>2</sup>

Torsion angles	
O(1)–C(4)–C(5)–O(2)	0.7(4)
N(2)–N(1)–C(7)–C(6)	-175.5(3)
N(1)–N(2)–C(8)–N(3)	4.1(4)
N(1)–N(2)–C(8)–S(1)	-175.9(2)

The compound crystallized into a triclinic space group  $P\bar{1}$ . According to the molecular structure, the compound adopts an *E* configuration with respect to the C(8)–N(2) bond similar to H<sub>2</sub>L<sup>1</sup> [18] and salicylaldehyde-N(4)-phenylthiosemicarbazone [19] but in contrast to 2-hydroxyacetophenone-N(4)-phenylthiosemicarbazone [16], where a *Z* configuration exists. This is confirmed by the N(1)–N(2)–C(8)–S(1) torsion angle of -175.9(2)°. Also *E* configuration is perceived about the azomethine bond [N(2)–N(1)–C(7)–C(6) = -175.5(3)°] [13]. Atom O(1) lies *cis* to O(2), with an O(1)–C(4)–C(5)–O(2) torsion angle of 0.7(4)°. This favors the intramolecular hydrogen bonding interaction between O(1) and H attached to O(2) atom. The C(8)–S(1) bond distance [1.685(3) Å] is closer to C=S bond length [1.60 Å] than to C–S bond length [1.81 Å] [20] which confirms the existence of the

compound in the thioamido form in solid state. Also the C(7)–N(1) bond distance [1.267(4) Å] is appreciably close to that of a C=N double bond [1.28 Å], confirming the azomethine bond formation [21].

The mean plane deviation calculations show that the molecule as a whole is non-planar. But the central thiosemicarbazone moiety (C7/N1/N2/C8/S1/N3/C9) is almost planar with a maximum deviation from the mean plane of -0.054(2) Å for atom N(1). This is similar to that observed in salicylaldehyde-N(4)-phenylthiosemicarbazone [16]. The ring Cg(1) (comprising atoms C1–C6, with a maximum deviation of 0.005(3) Å for C3) makes a dihedral angle of 18.90(12)° with the thiosemicarbazone moiety. Ring puckering analysis and least square plane calculations show that the cyclohexyl ring adopts a chair conformation ( $Q_T = 0.568(4)$  Å) with the equatorial substitution at C(9) for N(3) [22]. Fig. 2.20 shows the packing diagram of the compound.

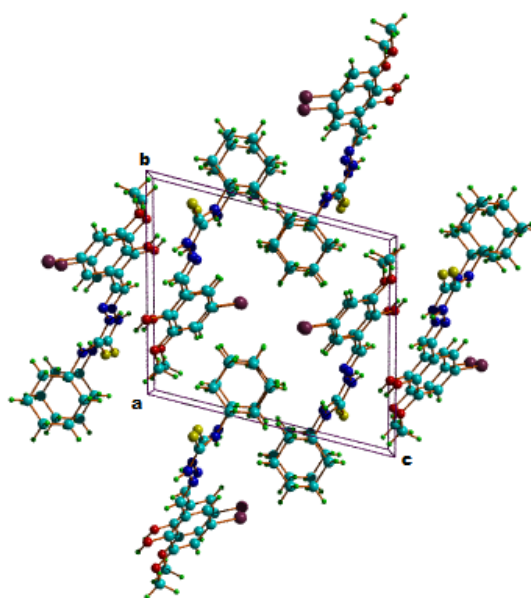


**Fig. 2.20.** Packing diagram of H<sub>2</sub>L<sup>2</sup> viewed along 'a' axis.

The crystal packing involves one intramolecular and three intermolecular hydrogen bonds (Table 2.8). The intramolecular hydrogen bonding interaction, O(2)–H(2')···O(1) leads to the formation of a five membered ring comprising of atoms C(4), C(5), O(2), H(2') and O(1) and facilitates almost planar geometry in part of the molecule. The intermolecular hydrogen bonds N(2)–H(2)···O(2) and O(2)–H(2')···S(1) cause the pairing of molecules leading to the formation of centrosymmetric dimers in the crystal lattice (Fig. 2.21). These dimers are stacked along the 'a' axis (Fig. 2.22) and are interconnected through a third intermolecular hydrogen bond N(3)–H(3')···S(1) to produce independent polymeric chains in the packing (Fig. 2.23). Further stabilization is provided by C(13)–H(13A)···Cg(1) interaction (Fig. 2.24).

**Table 2.8. Interaction parameters of H<sub>2</sub>L<sup>2</sup>**

<b>Hydrogen bonding</b>				
<b>D–H···A</b>	<b>D–H (Å)</b>	<b>H···A (Å)</b>	<b>D···A (Å)</b>	<b>∠D–H···A(°)</b>
O(2)–H(2')···O(1)	0.83(2)	2.21(3)	2.616(3)	110(3)
O(2)–H(2')···S(1) <sup>a</sup>	0.83(2)	2.43(3)	3.142(2)	145(3)
N(2)–H(2)···O(2) <sup>a</sup>	0.84(2)	2.25(2)	2.959(3)	142(3)
N(3)–H(3')···S(1) <sup>b</sup>	0.84(2)	2.81(3)	3.483(3)	138(3)
<b>C–H···π Interactions</b>				
<b>C–H···Cg</b>	<b>C–H (Å)</b>	<b>H···Cg (Å)</b>	<b>C···Cg (Å)</b>	<b>∠C–H···Cg(°)</b>
C(13)–H(13A)···Cg(1) <sup>c</sup>	0.97	2.71	3.664(4)	168

Equivalent position codes: a = -x+1, -y+1, -z+2; b = x-1, y, z; c = x, y+1, z

Cg(1) = C1, C2, C3, C4, C5, C6

D = Donor, A = acceptor, Cg = Centroid

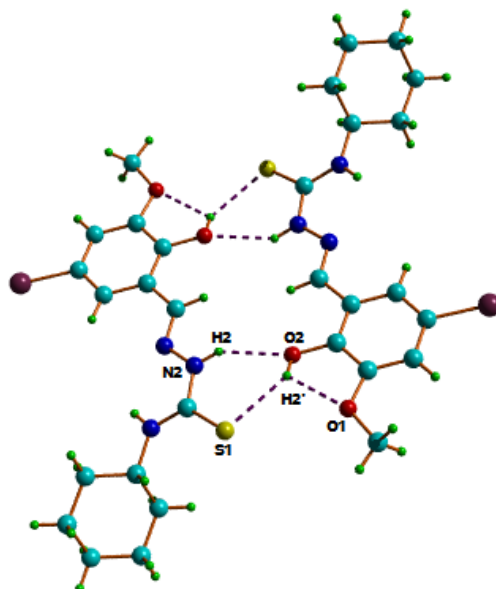


Fig. 2.21. Intra and intermolecular hydrogen bonding interactions of  $H_2L^2$ .

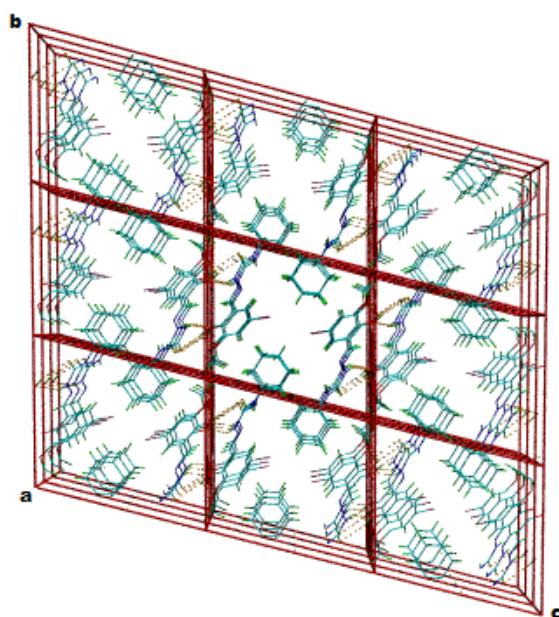


Fig. 2.22. Super cell packing diagram of  $H_2L^2$  showing the stacking of centrosymmetric dimers along 'a' axis.

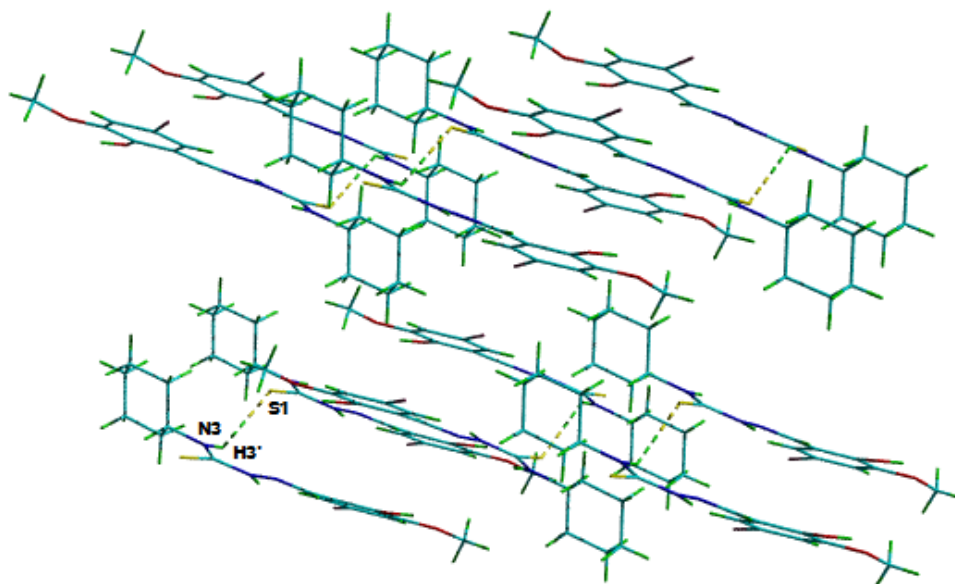


Fig. 2.23. Polymeric chain generated by N3-H3'...S1 hydrogen bonds.

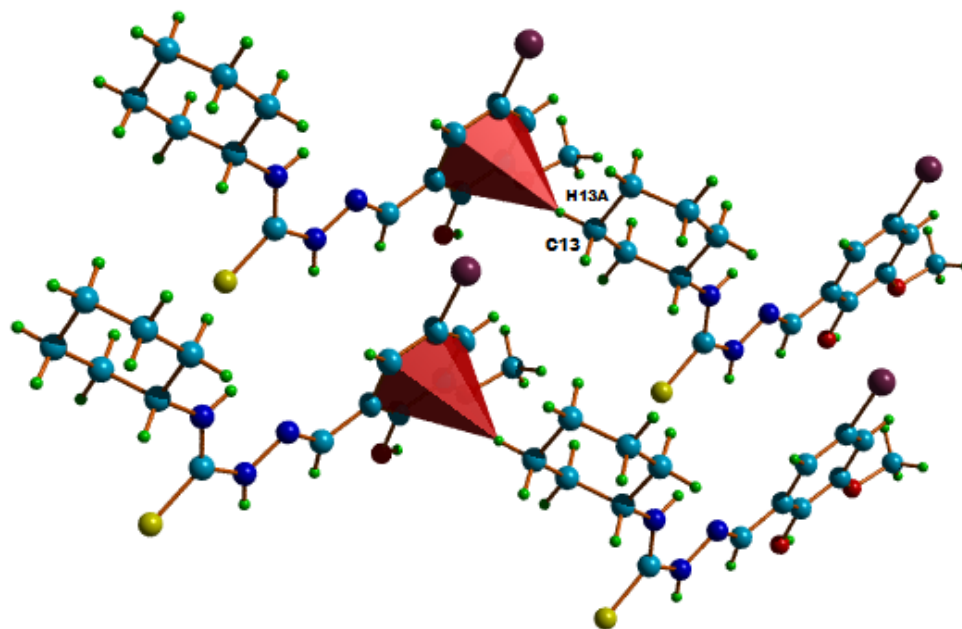


Fig. 2.24. C-H... $\pi$  interactions in  $H_2L^2$ .

## References

- [1] E.M. Bavin, R.J.W. Rees, J.M. Robson, M. Seiler, D.E. Seymour, D. Suddaby, *J. Pharm. Pharmacol.* 2 (1950) 764.
- [2] O. Koch, *G. Stuttgen, Naunyn. Schmiedebergs. Arch. Exp. Pathol. Pharmacol.* 210 (1950) 409.
- [3] G.A. Kune, *Br. Med. J.* 2 (1964) 621.
- [4] A.C. Sartorelli, B.A. Booth, *Cancer Res.* 27 (1967) 1614.
- [5] C.M. Nutting, C.M.L. van Herpen, A.B. Miah, *Ann. Oncol.* 20 (2009) 1275.
- [6] B. Ma, B.C. Goh, E.H. Tan, K.C. Lam, R. Soo, S.S. Leong, L.Z. Wang, F. Mo, A.T. Chan, B. Zee, T. Mok, *Invest New Drugs* 26 (2008) 169.
- [7] D.L. Klayman, J.F. Bartosevich, T.S. Griffin, C.J. Mason, J.P. Scovill, *J. Med. Chem.* 22 (1979) 855.
- [8] P. Bindu, M.R.P. Kurup, *Transit. Met. Chem.* 22 (1997) 578.
- [9] G.F. de Sousa, R.H.P. Francisco, M.T.P. Gambardella, R.H. de A. Santos, A. Abras, *J. Braz. Chem. Soc.* 12 (2001) 722.
- [10] Bruker, *SADABS, APEX2, XPREP and SAINT*, Bruker AXS Inc., Madison, Wisconsin, USA, 2004.
- [11] G.M. Sheldrick, *SHELXL97 and SHELXS97*, University of Göttingen, Germany, 1997.
- [12] G.M. Sheldrick, *Acta. Cryst. A*64 (2008) 112.
- [13] K. Brandenburg, *Diamond Version 3.2g*, Crystal Impact GbR, Bonn, Germany, 2010.

- [14] K. Nisha, M. Sithambaresan, M.R.P. Kurup, *Acta Cryst.* E67 (2011) o3420.
- [15] J.M. Jacob, M.R.P. Kurup, *Acta Cryst.* E68 (2012) o836.
- [16] E.B. Seena, M.R.P. Kurup, E. Suresh, *J. Chem. Crystallogr.* 36 (2006) 189.
- [17] F.H. Allen, O. Kennard, D.G. Watson, L. Brammer, A.G. Orpen, R. Taylor, *J. Chem. Soc., Perkin Trans. 2*, (1987) pp. S1-19.
- [18] J.M. Jacob, M. Sithambaresan, M.R.P. Kurup, *Acta Cryst.* E68 (2012) o1871.
- [19] E.B. Seena, M.R.P. Kurup, E. Suresh, *J. Chem. Crystallogr.* 38 (2008) 93.
- [20] J.E. Huheey, E.A. Keiter, R.L. Keiter, *Inorganic Chemistry, Principles of Structure and Reactivity*, 4<sup>th</sup> ed. New York: Harper Collins College Publishers, 1993.
- [21] J. March, *Advanced Organic Chemistry, Reactions, Mechanisms and Structure*, 4<sup>th</sup> ed. New York: Wiley, 1992.
- [22] D. Cremer, J.A. Pople, *J. Am. Chem. Soc.* 97 (1975) 1354.

\*\*\*RSC\*\*\*

## SYNTHESES AND SPECTRAL ASPECTS OF OXIDOVANADIUM(IV) CHELATES DERIVED FROM ONS DONOR THIOSEMICARBAZONES

3.1 Introduction
3.2 Experimental
3.3 Results and discussion
References

### 3.1. Introduction

Vanadium is a hard, silvery gray, ductile and malleable transition metal. It has good corrosion resistance to alkalis, sulfuric acid, hydrochloric acid and salt waters. Vanadium resists corrosion due to a protective film of oxide on the surface. Common oxidation states of vanadium include +2, +3, +4 and +5. Andrés Manuel del Río discovered vanadium in 1801 by analyzing a new lead-bearing mineral called "brown lead" and named the new element *erythronium* (Greek for "red") since, upon heating, most of its salts turned from their initial color to red. The element was rediscovered in 1831 by Nils Gabriel Sefström, who named it vanadium after the German goddess of beauty and fertility, Vanadís.

Vanadium occurs naturally in about 65 different minerals among which are patronite, vanadinite, carnotite and bauxite and in fossil fuel deposits. The metal oxidizes readily above 660 °C to form vanadium pentoxide ( $V_2O_5$ ), the most important industrial vanadium compound, which is used as a catalyst for the production of sulfuric acid and maleic

anhydride and in making ceramics. It is added to glass to produce green or blue tint.

In biology, vanadium is an essential component of some enzymes, particularly the vanadium nitrogenase used by some nitrogen-fixing microorganisms. It is used by some life forms as an active center of enzymes, such as the vanadium bromoperoxidase of some ocean algae. Vanadium is probably a micronutrient in mammals, including humans, but its precise role in this regard is unknown.

Since the recent discovery of the presence of trivalent vanadium in several biological systems, the interest for vanadium(III) chemistry has considerably grown [1]. The trivalent state is indeed one of its unstable oxidation states and can be easily oxidized to vanadium(IV) or vanadium(V) especially in solution where these reactions can be very fast. The chemistry of oxidovanadium(IV) has received considerable attention as the  $VO^{2+}$  unit can readily bond to four and five donor atoms to form  $VO_4$  and  $VO_5$  complexes respectively. Additional interest has been generated in the coordination chemistry of oxidovanadium(IV), oxidovanadium(V) and dioxidovanadium(V) complexes, as they model vanadium containing enzymes and serve as good oxidation catalysts. Oxidovanadium(IV) complexes find use in chemical reactivity studies either as models for V-O bond reactivity [2] or as potential free radicals.

Among the biological activities of vanadium, an interesting mimetic antidiabetic effect is the most striking, the effect being provided by the oxidation states of vanadic(III), vanadyl(IV) and vanadate(V) [3]. Medicinal applications of vanadium compounds have focussed on their *in vitro* and *in vivo* activity in the treatment of insulin deficiency, type I

diabetes and insulin tolerance, type II diabetes which is by far the more common form frequently found with elderly people and increasingly also a problem for obese young people [4]. In addition to the therapeutic effect of vanadium ion and vanadium complexes, they have a preventive effect also [3]. Dioxidovanadium(V), oxidovanadium(IV) or vanadium(III) complexes [5-9] with thiosemicarbazones are interesting because of their significant pharmacological activities and catalytic roles in many biological systems and industrial processes [10-13]. Having all these facts in mind, it was thought worthwhile to study the coordination chemistry of oxidovanadium(IV) complexes derived from 5-bromo-3-methoxysalicylaldehyde-N(4)-phenyl thiosemicarbazone ( $H_2L^1$ ).

## **3.2. Experimental**

### **3.2.1. Materials**

Vanadyl sulfate monohydrate (Sigma-Aldrich), 1,10-phenanthroline (phen) and 2,2'-bipyridine (bipy) were of Analar grade and were used as received. Solvents used were methanol and DMF.

### **3.2.2. Synthesis of the thiosemicarbazone**

The synthesis of thiosemicarbazone  $H_2L^1$  is already discussed in Chapter 2.

### **3.2.3. Syntheses of the complexes**

#### **3.2.3.1. [VOL<sup>1</sup>phen] (1)**

Aqueous solution of vanadyl sulfate monohydrate (0.081 g, 0.5 mmol) was added to a stirred mixture of  $H_2L^1$  (0.190 g, 0.5 mmol) in DMF and

methanol (1:1 v/v) and 1,10-phenanthroline (0.099 g, 0.5 mmol) in methanol. The resultant solution was refluxed for three hours. The brown product obtained was filtered, washed with methanol and dried *in vacuo*.

Elemental Anal. Found (Calcd.) (%) : C, 51.45 (51.85); H, 2.67 (3.22); N, 11.07 (11.20); S, 5.11 (5.13). Yield: 77%

### 3.2.3.2. [VOL<sup>1</sup>bipy] (2)

To a stirred mixture of H<sub>2</sub>L<sup>1</sup> (0.190 g, 0.5 mmol) in DMF and methanol (1:1 v/v) and 2,2'-bipyridine (0.078 g, 0.5 mmol) in methanol, aqueous solution of vanadyl sulphate monohydrate (0.081 g, 0.5 mmol) was added. The resultant solution was refluxed for 3 hours and the brown product separated out was filtered, washed with methanol and dried *in vacuo*.

Elemental Anal. Found (Calcd.) (%) : C, 49.41 (49.93); H, 3.66 (3.35); N, 11.18 (11.65); S, 5.77 (5.33). Yield: 72%

## 3.3. Results and discussion

Two oxidovanadium complexes of the thiosemicarbazone were synthesized. They were synthesized by refluxing metal salt, corresponding heterocyclic bases and thiosemicarbazone in 1:1:1 ratio. Both of the complexes are brown in colour and are soluble in solvents like DMF and DMSO. In both the complexes, the thiosemicarbazone exists in the thioiminolate form and act as dideprotonated tridentate ligands coordinating through phenolic oxygen, thioiminolate sulfur and azomethine nitrogen. Both of the complexes are monomeric mixed ligand metal chelates. They are characterized by the following physico-chemical methods.

### 3.3.1. Elemental analyses

The analytical data indicate that the complexes are analytically pure. The elemental analyses data are consistent with the general formula [VOL<sup>1</sup>B], where L<sup>1</sup> is the doubly deprotonated thiosemicarbazone ligand and B is the bidentate heterocyclic bases *viz.* phen, bipy. However we could not isolate single crystals of suitable quality for XRD studies for any of these complexes.

### 3.3.2. Molar conductivity and magnetic susceptibility measurements

The conductivity measurements were made in DMF (10<sup>-3</sup> M) and all the complexes were found to be non-electrolytes [14]. The room temperature magnetic moments of the complexes **1** and **2** in the polycrystalline state are 1.51 and 1.62 B.M. respectively, which are very close to the spin-only value for a *d*<sup>1</sup> system (1.73 B.M.) [15]. Both the complexes are EPR active due to this unpaired electron.

**Table 3.1. Molar conductivity and magnetic moments of V(IV) complexes**

Compound	$\lambda_m^a$	$\mu_{\text{eff}}$ (B.M.)
[VOL <sup>1</sup> phen] ( <b>1</b> )	18.6	1.51
[VOL <sup>1</sup> bipy] ( <b>2</b> )	29.0	1.62

<sup>a</sup> = mho cm<sup>2</sup> mol<sup>-1</sup>

### 3.3.3. Infrared spectra

A comparison of the IR spectra of H<sub>2</sub>L<sup>1</sup> and the metal complexes shows that significant variations have occurred in the characteristic frequencies upon complexation. The tentative IR spectral assignments of

the complexes are listed in Table 3.2. In all the complexes, the bands due to O-H and  $^2\text{N-H}$  stretching vibrations are absent which is a clear evidence for the coordination of the thiosemicarbazone in the dideprotonated form. The band corresponding to azomethine bond,  $\nu(\text{C=N})$ , shifts to higher energy on coordination due to the combination of  $\nu(\text{C=N})$  with the newly formed C=N bond which results from the loss of the thioamide hydrogen from the thiosemicarbazone moiety [16-20]. The band at  $1333\text{ cm}^{-1}$  present in  $\text{H}_2\text{L}^1$  shifts to lower wavenumbers in both the complexes and this can be assigned to the  $\nu(\text{C-S})$  vibration suggesting the change of bond order and strong electron-delocalization upon chelation. This shows that the H-N-C=S in the ligand has transformed to N=C-S-H thereby coordinating to vanadium in the thioiminolate form. Coordination *via* thioiminolate sulfur is also indicated by the negative shift of the band assigned to  $\delta(\text{C=S})$  vibration in the thiosemicarbazone [21]. The bands in the range  $439\text{-}455\text{ cm}^{-1}$  indicates the coordination of azomethine nitrogen to vanadium centre. The increase in frequency of  $\nu(\text{N-N})$  bands in complexes, due to the increase in double bond character is another proof for the coordination of the thiosemicarbazone through the azomethine nitrogen [22]. The broad absorption band at  $3441\text{ cm}^{-1}$  assigned to phenolic -OH of  $\text{H}_2\text{L}^1$  has disappeared in the complexes which indicate the coordination of the phenolic oxygen to the vanadium atom. The IR spectra of these complexes display bands characteristic of coordinated heterocyclic bases [23]. Further, the intense bands observed at  $964\text{ cm}^{-1}$  for complex **1** and  $954\text{ cm}^{-1}$  for complex **2** correspond to the terminal V=O stretching band [24]. Figs. 3.1 and 3.2 depict the infrared spectra of these complexes.

In both the complexes, the thiosemicarbazone  $H_2L^1$  acts as a dianionic tridentate ligand coordinating to vanadium through O, N and S atoms and the two nitrogen atoms of heterocyclic bases occupy the fourth and fifth coordination positions of vanadium.

**Table 3.2. IR spectral assignments ( $cm^{-1}$ ) of thiosemicarbazone and its oxidovanadium(IV) complexes**

Compound	$\nu(O-H)$	$\nu(C=N)$	$\nu(C=N)^a$	$\nu(N-N)$	$\nu(C=S)/\nu(C-S),$ $\delta(C=S)/\delta(C-S)$	$\nu(C-O)$	$\nu(V-O)$	$\nu(V-N)$
$H_2L^1$	3441	1540	----	1071	1333, 857	1267	----	----
[VOL <sup>1</sup> phen] (1)	----	1588	1539	1100	1295, 845	1237	502	455
[VOL <sup>1</sup> bipy] (2)	----	1588	1544	1110	1306, 846	1228	474	439

<sup>a</sup> = newly formed C=N bond

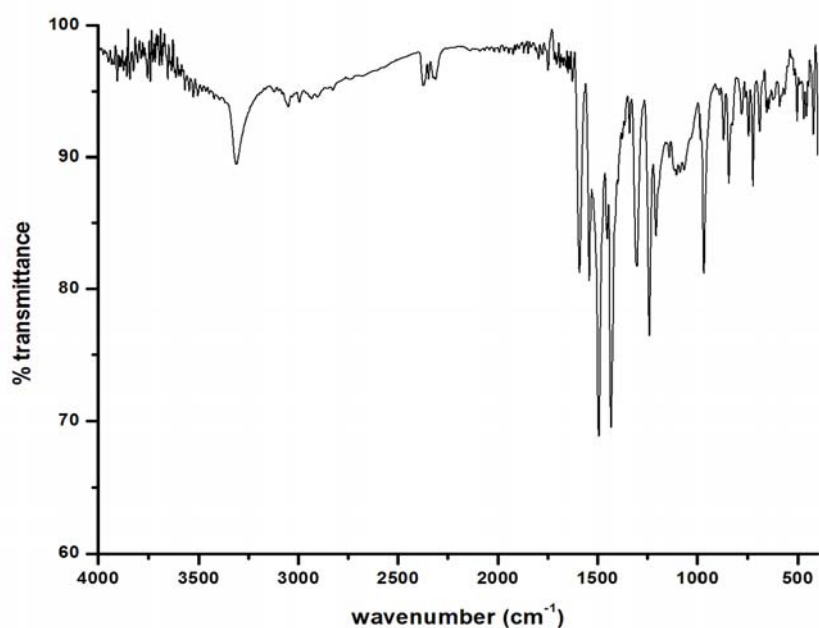


**Fig. 3.1. Infrared spectrum of [VOL<sup>1</sup>phen] (1).**

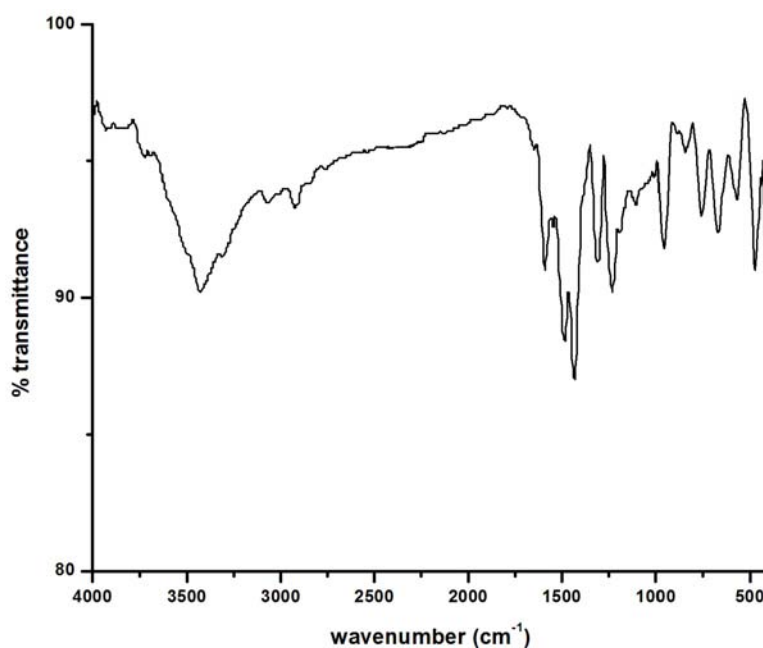


Fig. 3.2. Infrared spectrum of [VOL<sup>1</sup>bipy] (2).

### 3.3.4. Electronic spectra

The electronic spectra of both the complexes were taken in DMF. The significant electronic absorption bands in the spectra of H<sub>2</sub>L<sup>1</sup> and the oxidovanadium complexes are given in Table 3.3. The electronic transitions found in the free ligand due to imine function of thiosemicarbazone moiety were slightly shifted on complexation. The shift of the bands due to intraligand transitions is the result of the weakening of the C=S bond and the extension of conjugation upon complexation [25]. The shift occurs also due to coordination *via* phenolic oxygen and azomethine nitrogen [26] and is an indication of the enolization followed by the deprotonation of the thiosemicarbazone during complexation. The intraligand n→π\* and π→π\* transitions are assigned to bands in the range 28280-30200 cm<sup>-1</sup> for these complexes. In all the complexes, intense bands

in the 24810-26790  $\text{cm}^{-1}$  range are assigned to ligand to metal charge transfer transitions arising from the phenolate oxygen to an empty  $d$  orbital of the vanadium(IV) center [5]. Fig. 3.3 represents the electronic spectra of the complexes.

Ballhausen and Gray (BG scheme) have provided a convenient energy level scheme for VO(IV) type complexes [27]. In general, three absorptions are observed in the spectra of most of the oxidovanadium complexes, arising from the tetragonal compression caused by V=O bond, which results in further splitting of  $d$  orbitals and gives rise to three spin allowed transitions,  ${}^2E \leftarrow {}^2B_2$  ( $\nu_1$ ) ( $d_{xy} \rightarrow d_{xz}, d_{yz}$ ),  ${}^2B_1 \leftarrow {}^2B_2$  ( $\nu_2$ ) ( $d_{xy} \rightarrow d_{x^2-y^2}$ ),  ${}^2A_1 \leftarrow {}^2B_2$  ( $\nu_3$ ) ( $d_{xy} \rightarrow d_{z^2}$ ) [28]. Since the  ${}^2E$  and  ${}^2B_1$  levels are very close in energy, they may cross and result in a weak broad band. In complex **1**, the expected  $d-d$  bands are not observed and are probably obscured by the intense LMCT absorptions. We could locate only one band in [VOL<sup>1</sup>bipy] (**2**) due to the masking by high intensity charge transfer bands (Fig. 3.4).

**Table 3.3. Electronic spectral assignments ( $\text{cm}^{-1}$ ) of thiosemicarbazone and its V(IV) complexes**

Compound	$n \rightarrow \pi^* / \pi \rightarrow \pi^*$	LMCT	d-d
H <sub>2</sub> L <sup>1</sup>	28770, 30490	....	....
VOL <sup>1</sup> phen ( <b>1</b> )	28380, 30200	24810	....
VOL <sup>1</sup> bipy ( <b>2</b> )	28280, 30140	24790	14160

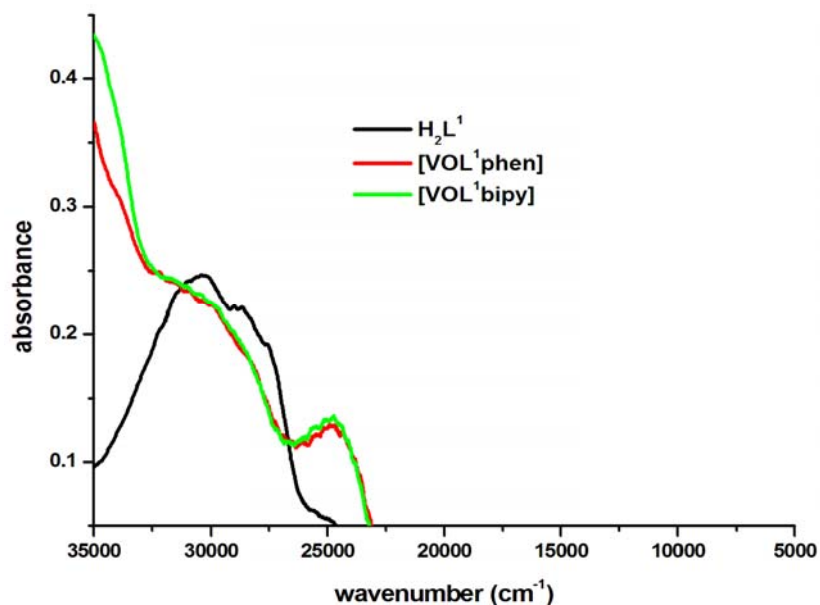


Fig. 3.3. Electronic spectra of  $H_2L^1$  and its oxidovanadium complexes.

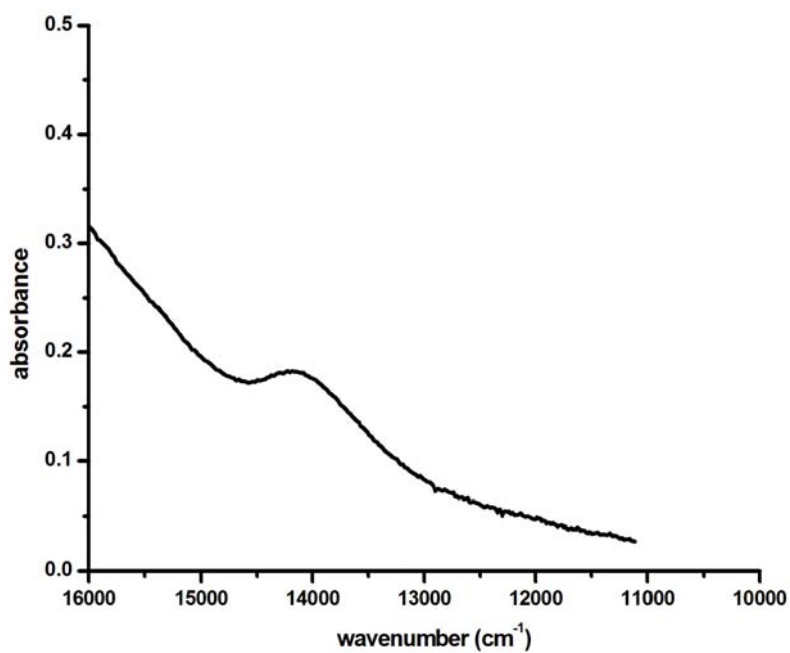


Fig. 3.4. Visible spectrum of  $[VOL^1bipy]$  (2).

### 3.3.5. EPR spectra

In Electron Paramagnetic Resonance spectroscopy, radiation of microwave frequency is absorbed by a molecule or ion having unpaired electron(s). Thus it is a convenient way to probe the electronic structure of paramagnetic compounds.

In vanadyl complexes, vanadium is in +4 oxidation state with  $d^1$  configuration and since the orbital angular momentum is quenched by the crystalline fields, the paramagnetism of the vanadyl ion arises from the single unpaired electron. In V(IV) complexes value of  $g$  is below the value for free electron. The spin of  $^{51}\text{V}$  nucleus is  $I = 7/2$ . In mononuclear V(IV) complexes, the EPR signals are split into eight and in binuclear complexes, fifteen hyperfine lines. Under the influence of magnetic field, the electronic ground state ( $S = 1/2$ ) is split into two ( $m_s = +1/2$  and  $-1/2$ ) and additional splitting occurs through the different magnetic orientations of the nuclear spin ( $m_I$ ).

$\text{VO}^{2+}$  is one of the most stable diatomic cation and its paramagnetism is almost due to spin angular momentum and EPR absorptions are obtained over a wide range of temperature including room temperature [29].

EPR spectra of all the oxidovanadium(IV) complexes were recorded in polycrystalline state at 298 K and in DMF at 77 K and the spectral parameters are summarized in Table 3.4. The EPR spectrum of complex **1** in DMF at 77 K is simulated and the experimental (red) and simulated (blue) best fit is included. Simulation was performed using Matlab 7.8.0 (R2009a) software and the EasySpin 4.0.0 package [30]. Figs. 3.5-3.8 depict the EPR spectra of the oxidovanadium complexes.

The EPR spectra of complexes **1** and **2** in the solid state at 298 K are isotropic in nature and hence only one  $g$  value, arising due to dipolar interactions and enhanced spin-lattice relaxation. In DMF at 77 K, both the complexes displayed well resolved axial anisotropy with two sets of eight line pattern which result from coupling of the electron spin with the spin of the  $^{51}\text{V}$  nucleus ( $I = 7/2$ ). They are found to exhibit  $g_{\parallel} < g_{\perp}$  and  $A_{\parallel} > A_{\perp}$  relationship, characteristic of an axially compressed  $d_{xy}^1$  configuration [31].

The absence of any superhyperfine lines in the spectrum is an explicit indication of the sole electron lying in the  $d_{xy}$  orbital ( $^2B_2$  ground state), localized on metal, thus excluding the possibility of its direct interaction with the azomethine nitrogen of the thiosemicarbazone [32,33].

The anisotropic parameters are related with isotropic parameters by the equations,  $A_{\text{iso}} = 1/3(A_{\parallel} + 2A_{\perp})$  and  $g_{\text{iso}} = 1/3(g_{\parallel} + 2g_{\perp})$  [34]. In both compounds, the  $g_{\text{iso}}$  values calculated are near to the value obtained from the polycrystalline spectra which suggests that the molecules retain their structural identity in solution.

The EPR parameters  $g_{\parallel}$ ,  $g_{\perp}$ ,  $A_{\parallel}$  and  $A_{\perp}$  and energies of  $d-d$  transitions were used to evaluate the molecular orbital coefficients  $\alpha^2$  and  $\beta^2$  for the complexes by using the following equations:

$$\alpha^2 = \frac{(2.00277 - g_{\parallel})E_{d-d}}{8\lambda\beta^2}$$

$$\beta^2 = \frac{7}{6} \left[ \left( \frac{-A_{\parallel}}{P} \right) + \left( \frac{A_{\perp}}{P} \right) + \left( g_{\parallel} - \frac{5}{14}g_{\perp} \right) - \frac{9}{14}g_e \right]$$

where  $P = 128 \times 10^4 \text{ cm}^{-1}$ ,  $\lambda = 135 \text{ cm}^{-1}$  and  $E_{d-d}$  is the energy of  $d-d$  transition.

**Table 3.4.** EPR spectral parameters of oxidovanadium(IV) complexes in the polycrystalline state at 298 K and in DMF at 77 K.

Compound	Polycrystalline state at 298 K		DMF (77 K)						
	$g_{iso}$	$g_{  }$	$g_{\perp}$	$g_{av}$	$A_{  }^a$	$A_{\perp}^a$	$A_{av}^a$	$\alpha^2$	$\beta^2$
[VOL <sup>1</sup> phen] (1)	1.983	1.955	1.970	1.965	175	54	95	---	0.979
[VOL <sup>1</sup> bipy] (2)	1.985	1.955	1.980	1.972	176	61	98	0.668	0.938

<sup>a</sup>Expressed in units of  $cm^{-1}$  multiplied by a factor of  $10^{-4}$ .

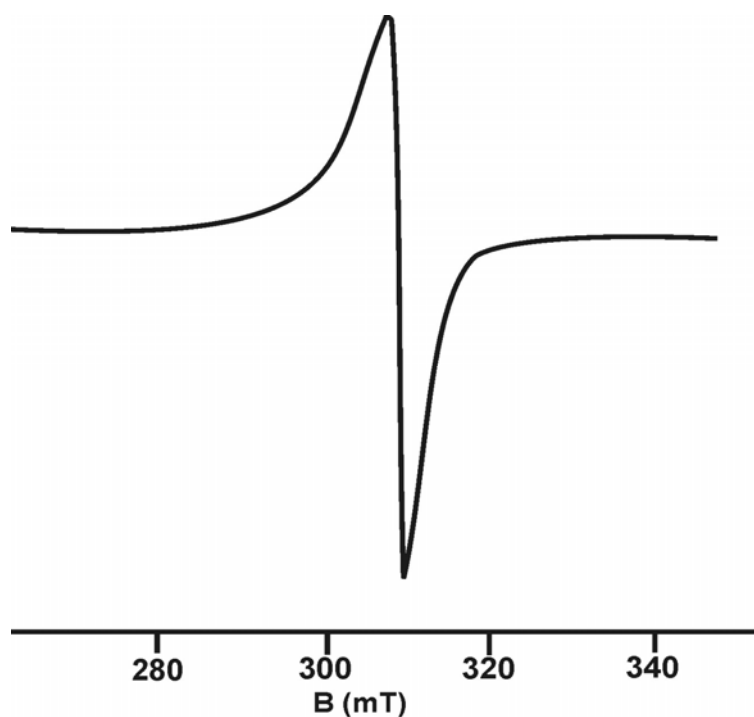


**Fig. 3.5.** EPR spectrum of [VOL<sup>1</sup>phen] (1) in polycrystalline state at 298 K.

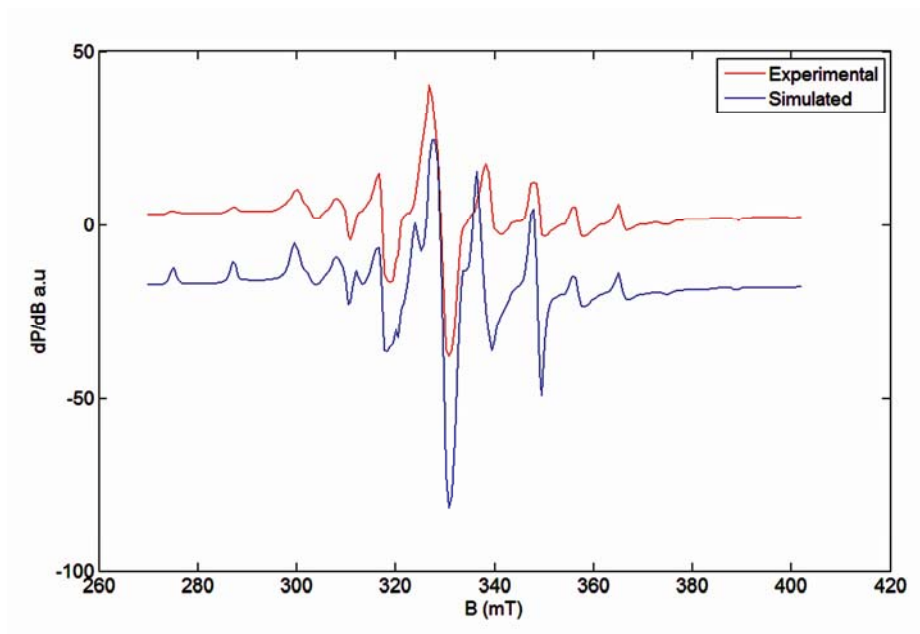


Fig. 3.6. EPR spectrum of [VOL<sup>1</sup>phen] (1) in DMF at 77 K.

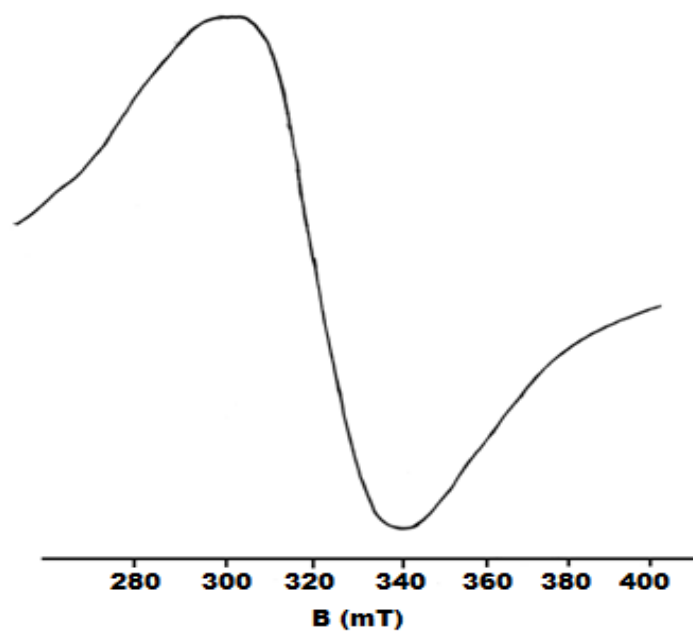


Fig. 3.7. EPR spectrum of [VOL<sup>1</sup>bipy] (2) in polycrystalline state at 298 K.

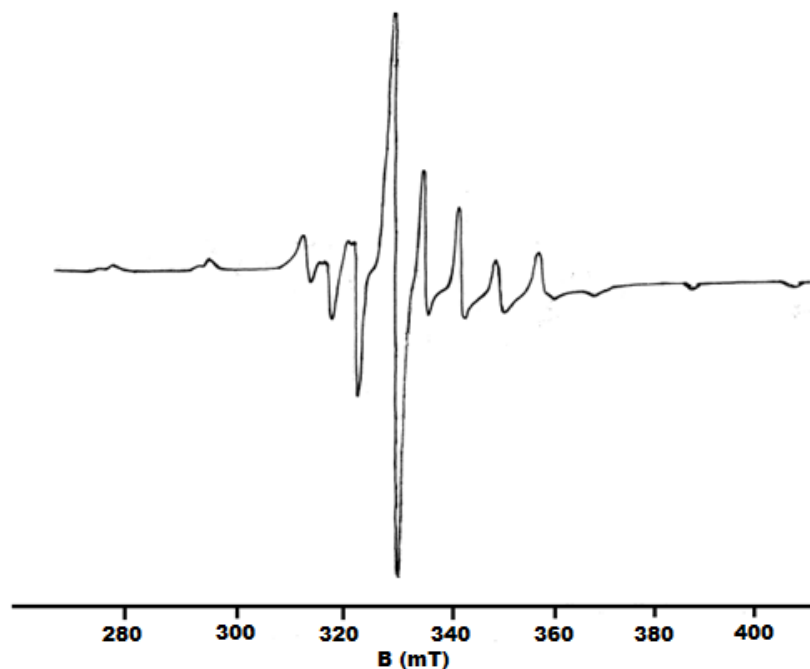


Fig. 3.8. EPR spectrum of [VOL<sup>1</sup>bipy] (2) in DMF at 77 K.

#### References

- [1] A. Papaioannon, M. Manos, S. Karkabanas, R. Liasko, A.M. Evangelon, I. Correia, V. Kalfakakou, J.C. Pessoa, T. Kabanos, *J. Inorg. Biochem.* 98 (2004) 959.
- [2] A. Buttler, V.J. Walker, *Chem. Rev.* 93 (1993) 1937.
- [3] H. Sakurai, Y. Kojima, Y. Yoshikawa, K. Kawabe, H. Yasui, *Coord. Chem. Rev.* 226 (2002) 187.
- [4] D. Rehder, *Inorg. Chem. Commun.* 6 (2003) 604.
- [5] M.R. Maurya, S. Khurana, Shailendra, A. Azam, W. Zhang, D. Rehder, *Eur. J. Inorg. Chem.* (2003) 1966.
- [6] S.K. Dutta, S.B. Kumar, S. Bhattacharyya, E.R.T. Tiekink, M. Chaudhury, *Inorg. Chem.* 36 (1997) 4954.

- [7] S. Samanta, D. Ghosh, S. Mukhopadhyay, A. Endo, T.J.R. Weakley, M. Chaudhury, *Inorg. Chem.* 42 (2003) 1508.
- [8] S.K. Dutta, E.R.T. Tiekink, M. Chaudhury, *Polyhedron* 16 (1997) 1863.
- [9] M.R. Maurya, A. Kumar, M. Abid, A. Azam, *Inorg. Chim. Acta* 359 (2006) 2439.
- [10] A.G.J. Ligtenbarg, R. Hage, B.L. Feringa, *Coord. Chem. Rev.* 237 (2003) 89.
- [11] C. Bohn, *Coord. Chem. Rev.* 237 (2003) 245.
- [12] E. Tsuchido, K. Oyaizu, *Coord. Chem. Rev.* 237 (2003) 213.
- [13] D. Rehder, J.C. Pessoa, C.F.G.C. Geraldes, M. Margida, C.A. Castro, T. Kabanos, T. Kiss, B. Meier, G. Micera, L. Pettersson, M. Rangel, A. Salifoglou, I. Turel, D. Wang, *J. Biol. Inorg. Chem.* 7 (2002) 384.
- [14] W.J. Geary, *Coord. Chem. Rev.* 7 (1971) 81.
- [15] R.I. Dutta, G.P. Sengupta, *J. Ind. Chem. Soc.* 49 (1972) 919.
- [16] M. Joseph, V. Suni, M.R.P. Kurup, M. Nethaji, A. Kishore, S.G. Bhat, *Polyhedron* 23 (2004) 3069.
- [17] M.A. Ali, M.T.H. Tarafdar, *J. Inorg. Nucl. Chem.* 39 (1977) 1785.
- [18] M.J.M. Campbell, *Coord. Chem. Rev.* 15 (1975) 279.
- [19] B.S. Garg, M.R.P. Kurup, S.K. Jain, Y.K. Bhoon, *Transit. Met. Chem.* 13 (1988) 247.
- [20] B.S. Garg, M.R.P. Kurup, S.K. Jain, Y.K. Bhoon, *Transit. Met. Chem.* 16 (1991) 111.
- [21] R. Mayer, *Organosulfur Chemistry*, M.J. Janssen, Ed.; Wiley-Interscience: New York (1967) 219.

*Syntheses and Spectral Aspects of Oxidovanadium(IV) Chelates Derived  
from ONS Donor Thiosemicarbazones*

---

- [22] B.S. Garg, M.R.P. Kurup, S.K. Jain, Y.K. Bhoon, *Transit. Met. Chem.* 13 (1988) 309.
- [23] P. Bindu, M.R.P. Kurup, T.R. Satyakeerty, *Polyhedron* 18 (1999) 321.
- [24] E. Manoj, M.R.P. Kurup, *Polyhedron* 27 (2008) 275.
- [25] I.-X. Li, H.-A. Tang, Y.-Z. Li, M. Wang, L.-F. Wang, C.-G. Xia, *J. Inorg. Biochem.* 78 (2000) 167.
- [26] R.P. John, A. Sreekanth, M.R.P. Kurup, A. Usman, I.A. Razak, H.-K. Fun, *Spectrochim. Acta* 59A (2003) 1349.
- [27] C.J. Ballhausen, H.B. Gray, *Inorg. Chem.* 1 (1962) 111.
- [28] E. Garriba, G. Micerra, A. Panzanelli, *Inorg. Chem.* 42 (2003) 3981.
- [29] D. Mustafi, M.W. Makinen, *Inorg. Chem.* 44 (2005) 5580.
- [30] S. Stoll, A.J. Schweiger, *J. Magn. Reson.* 42 (2006) 178.
- [31] S. Bhattacharya, T. Ghosh, *Indian J. Chem.* A38 (1999) 601.
- [32] H. Kon, E. Sharpless, *J. Chem. Phys.* 42 (1965) 906.
- [33] D. Kivelson, S.K. Lee, *J. Chem. Phys.* 41 (1964) 1896.
- [34] D. Rehder, *Bioinorganic Vanadium Chemistry*, Wiley, Chichester (2008).

\*\*\*RSC\*\*\*

**SYNTHESES AND SPECTRAL ASPECTS OF NICKEL(II)  
CHELATES DERIVED FROM ONS DONOR  
THIOSEMICARBAZONES**

3.1 Introduction  
3.2 Experimental  
3.3 Results and discussion  
**References**

#### 4.1. Introduction

Nickel is a silvery-white lustrous metal with a slight golden tinge and is hard and ductile. Pure nickel shows a significant chemical activity that can be observed when nickel is powdered to maximize the exposed surface area on which reactions can occur, but larger pieces of the metal are slow to react with air at ambient conditions due to the formation of a protective oxide surface. Because of nickel's slow rate of oxidation at room temperature, it is considered corrosion-resistant. Historically, this has led to its use for plating metals such as iron and brass, to its use for chemical apparatus and its use in certain alloys that retain a high silvery polish, such as German silver. An iron-nickel mixture is thought to compose earth's inner core [1]. Nickel is one of four elements that is ferromagnetic around room temperature. Alnico permanent magnets based partly on nickel are of intermediate strength between iron-based permanent magnets and rare-earth magnets. Its Curie temperature is 355 °C, meaning that bulk nickel is non-magnetic above this temperature [2]. Naturally occurring nickel is

composed of 5 stable isotopes;  $^{58}\text{Ni}$ ,  $^{60}\text{Ni}$ ,  $^{61}\text{Ni}$ ,  $^{62}\text{Ni}$  and  $^{64}\text{Ni}$  with  $^{58}\text{Ni}$  being the most abundant (68.077% natural abundance). On earth, nickel occurs most often in combination with sulfur and iron in pentlandite, with sulfur in millerite, with arsenic in the mineral nickeline and with arsenic and sulfur in nickel galena. Nickel is commonly found in iron meteorites as the alloys, kamacite and taenite.

Nickel plays important roles in the biology of microorganisms and plants. Enzymes of some microorganisms and plants contain nickel as an active site, which makes the metal an essential nutrient for them. The plant enzyme urease (an enzyme that assists in the hydrolysis of urea) contains nickel. The [NiFe] hydrogenases contain nickel in addition to iron-sulfur clusters. Such [NiFe] hydrogenases characteristically oxidise  $\text{H}_2$ . A nickel-tetrapyrrole coenzyme, Cofactor F430, is present in the methyl coenzyme M reductase, which powers methanogenic archaea. One of the carbon monoxide dehydrogenase enzymes consists of an Fe-Ni-S cluster. Other nickel-containing enzymes include a rare bacterial class of superoxide dismutase [3] and glyoxalase I enzymes in bacteria and several parasitic eukaryotic trypanosomal parasites [4-9].

One of the most remarkable facts about the stereochemistry of Ni(II) complexes is that equilibrium between different structural types exist in solution and these equilibria are temperature dependent also. Nickel atom is present in the active sites of several dehydrogenases and the chemistry of divalent and trivalent nickel complexes with nitrogen-sulfur donor ligands has received much attention [10,11]. There is currently intense interest in dinickel thiolate-bridged complexes as first generation models for the active site in [NiFe] hydrogenases [12].

## 4.2. Experimental

### 4.2.1. Materials

Nickel(II) acetate tetrahydrate (C.D.H. Chemicals), 1,10-phenanthroline (phen), 2,2'-bipyridine (bipy) and 5,5'-dimethylbipyridine (5,5'-dmbipy) were used as received. Solvents used are methanol and DMF.

### 4.2.2. Syntheses of the thiosemicarbazones

The syntheses of thiosemicarbazones  $H_2L^1$  and  $H_2L^2$  are discussed already in Chapter 2.

### 4.2.3. Syntheses of the complexes

#### 4.2.3.1. $[NiL^1]_2$ (3)

This complex was synthesized by refluxing a solution of  $H_2L^1$  (0.190 g, 0.5 mmol) in 1:1 (v/v) mixture of DMF and methanol with a methanolic solution of  $Ni(OAc)_2 \cdot 4H_2O$  (0.124 g, 0.5 mmol) for 3 hours. The complex formed was filtered, washed with methanol and dried *in vacuo*.

Elemental Anal. Found (Calcd.) (%): C, 40.83 (41.23); H, 2.67 (2.77); N, 9.59 (9.62); S, 7.20 (7.34). Yield: 73%

#### 4.2.3.2. $[NiL^1phen]$ (4)

Methanolic solution of nickel(II) acetate tetrahydrate (0.124 g, 0.5 mmol) was added to a stirred mixture of  $H_2L^1$  (0.190 g, 0.5 mmol) in DMF and methanol (1:1 v/v) and 1,10-phenanthroline (0.099 g, 0.5 mmol) in methanol. The resultant homogenous brown solution was refluxed for three hours. The brown product obtained was filtered, washed with methanol and dried *in vacuo*.

Elemental Anal. Found (Calcd.) (%): C, 52.70 (52.55); H, 2.69 (3.27); N, 11.42 (11.35); S, 5.72 (5.20). Yield: 75%

#### 4.2.3.3. [NiL<sup>1</sup>(5,5'-dmbipy)] (5)

Methanolic solution of nickel(II) acetate tetrahydrate (0.124 g, 0.5 mmol) was added to a stirred mixture of H<sub>2</sub>L<sup>1</sup> (0.190 g, 0.5 mmol) in DMF and methanol (1:1 v/v) and 5,5'-dimethylbipyridine (0.092 g, 0.5 mmol) in methanol. The resultant brown solution was refluxed for three hours. The brown product obtained was filtered, washed with methanol and dried *in vacuo*.

Elemental Anal. Found (Calcd.) (%): C, 52.65 (52.21); H, 3.65 (3.89); N, 10.84 (11.27); S, 4.86 (5.16). Yield: 69%

#### 4.2.3.4. [(NiL<sup>2</sup>)<sub>2</sub>] (6)

This complex was synthesized by refluxing a solution of H<sub>2</sub>L<sup>2</sup> (0.193 g, 0.5 mmol) in 1:1 (v/v) mixture of DMF and methanol with a methanolic solution of Ni(OAc)<sub>2</sub>·4H<sub>2</sub>O (0.124 g, 0.5 mmol) for 3 hours. The complex formed was filtered, washed with methanol and dried *in vacuo*.

Elemental Anal. Found (Calcd.) (%): C, 40.37 (40.67); H, 4.42 (4.10); N, 9.61 (9.49); S, 7.30 (7.24). Yield: 61%

#### 4.2.3.5. [NiL<sup>2</sup>bipy] (7)

To a stirred mixture of H<sub>2</sub>L<sup>2</sup> (0.193 g, 0.5 mmol) in DMF and methanol (1:1 v/v) and 2,2'-bipyridine (0.078 g, 0.5 mmol) in methanol, methanolic solution of nickel(II) acetate tetrahydrate (0.124 g, 0.5 mmol) was added. The resultant brown solution was refluxed for 3 hours and the product separated out was filtered, washed with methanol and dried *in vacuo*.

Elemental Anal. Found (Calcd.) (%): C, 49.98 (50.11); H, 4.71 (4.37); N, 11.30 (11.69); S, 5.17 (5.35). Yield: 61%

### 4.3. Results and discussion

Five nickel complexes of the thiosemicarbazones were synthesized. The compounds **3** and **6** were prepared by the reaction of equimolar mixture of the appropriate thiosemicarbazone and nickel acetate tetrahydrate. Complexes **4**, **5** and **7** were synthesized by refluxing metal salt, corresponding heterocyclic bases and thiosemicarbazones in 1:1:1 ratio. All the complexes are brown in colour and are soluble in solvents like DMF and DMSO. In all the complexes, thiosemicarbazones exist in the thioiminolate form and act as dideprotonated tridentate ligands coordinating through phenolic oxygen, thioiminolate sulfur and azomethine nitrogen. Compounds **3** and **6** are dimeric in nature while others are monomeric mixed ligand metal chelates. They are characterized by the following physico-chemical methods.

#### 4.3.1. Elemental analyses

The elemental analyses values showed that the found and calculated values are in close agreement with the proposed formula of the complexes. The analytical data are consistent with the general formula  $[(NiL)_2]$  for complexes **3** and **6** and  $[NiLB]$  for complexes **4**, **5** and **7** where L is the doubly deprotonated thiosemicarbazone ligand and B is the bidentate heterocyclic bases *viz.* phen, bipy and 5,5'-dmbipy. However we could not isolate single crystals of suitable quality for XRD studies for any of these complexes.

### 4.3.2. Molar conductivity and magnetic susceptibility measurements

The conductivity measurements were made in DMF ( $10^{-3}$  M) and it is observed that the values lie in the range  $4\text{-}6\text{ ohm}^{-1}\text{cm}^2\text{mol}^{-1}$ , which are well below the range ( $65\text{-}90\text{ ohm}^{-1}\text{cm}^2\text{mol}^{-1}$ ) for uni-univalent electrolytes in the same solvent, indicating the non-electrolytic nature of the complexes [13]. The effective magnetic moments of complexes **4** and **7** in the polycrystalline state are 2.87 and 2.51 B.M. respectively which is consistent with two unpaired electrons. Four coordinate complexes **3** and **6** show anomalous magnetic moments of 0.51 and 0.65 B.M. respectively which may be due to deviation from a perfect square planar geometry or the presence of impurity [14]. Square planar Ni(II) complexes are diamagnetic but weakly paramagnetic systems with low spin have also been reported [15].

**Table 4.1. Molar conductivity and magnetic moments of Ni(II) complexes**

Compound	$\lambda_m^a$	$\mu_{\text{eff}}$ (B.M.)
$[\text{NiL}^1]_2$ ( <b>3</b> )	5.4	0.51
$[\text{NiL}^1\text{phen}]$ ( <b>4</b> )	5.8	2.87
$[\text{NiL}^1(5,5'\text{-dmbipy})]$ ( <b>5</b> )	6.0	3.67
$[\text{NiL}^2]_2$ ( <b>6</b> )	4.0	0.65
$[\text{NiL}^2\text{bipy}]$ ( <b>7</b> )	4.4	2.51

<sup>a</sup> =  $\text{mho cm}^2 \text{mol}^{-1}$

### 4.3.3. Infrared spectra

The characteristic IR bands ( $4000\text{-}400\text{ cm}^{-1}$ ) of the Ni(II) complexes provide significant information regarding the bonding sites of the ligands. A comparison of the IR spectra of thiosemicarbazones and the Ni(II) complexes shows that significant variations have occurred in the

characteristic frequencies upon complexation. The tentative IR spectral assignments of the thiosemicarbazones and Ni(II) complexes are listed in Table 4.2. In all the complexes, the bands due to O-H and  $^2\text{N-H}$  stretching vibrations are absent which is a clear evidence for the coordination of the thiosemicarbazones in the dideprotonated form. The azomethine stretching vibrations are observed at  $\sim 1540\text{ cm}^{-1}$  in the thiosemicarbazones. However, in complexes these bands are shifted to higher wave numbers due to the combination of  $\nu(\text{C=N})$  with the newly formed C=N bond which results from the loss of the thioamide hydrogen from the thiosemicarbazone moiety [16-20]. It is learnt that the enolization is thermodynamically most favored due to the additional stability conferred on the resulting complex upon complexation. Further proof for the coordination of azomethine nitrogen to nickel is the appearance of new bands in the range  $429\text{-}445\text{ cm}^{-1}$  assignable to  $\nu(\text{Ni-N})$  for the complexes [21-23]. The enolization and the electron delocalization in the thiosemicarbazone moiety are supported by the increase in the stretching frequency of the N-N bond of the principal ligand [24]. The bands at  $1333$  and  $1342\text{ cm}^{-1}$  present in the thiosemicarbazones shift to lower wavenumbers in all the complexes and this can be assigned to the  $\nu(\text{C-S})$  vibration suggesting the change of bond order and strong electron delocalization upon chelation. This shows that the H-N-C=S in the ligands has transformed to N=C-S-H thereby coordinating to nickel in the thioiminolate form. Coordination *via* thioiminolate sulfur is also indicated by the negative shift of the band assigned to  $\delta(\text{C=S})$  vibration in the ligands [25]. The broad bands at  $3441$  and  $3454\text{ cm}^{-1}$  assigned to phenolic -OH of thiosemicarbazones have disappeared in the complexes which indicate the

coordination of the phenolic oxygen to the nickel atom [26]. The coordination of the heterocyclic bases to nickel is indicated by the presence of characteristic peaks of 1,10-phenanthroline, 2,2'-bipyridine and 5,5'-dimethyl-2,2'-bipyridine in the finger print region of 600-1400  $\text{cm}^{-1}$  in the complexes [27]. Figs. 4.1-4.3 depict the infrared spectra of some of the nickel complexes of thiosemicarbazones.

It is observed that in all the complexes, the thiosemicarbazones act as dianionic tridentate ligands coordinating to nickel through O, N and S atoms. In the case of mixed ligand nickel chelates, the two nitrogen atoms of heterocyclic bases occupy the fourth and fifth coordination positions of nickel.

**Table 4.2. IR spectral assignments ( $\text{cm}^{-1}$ ) of thiosemicarbazones and their Ni(II) complexes**

Compound	$\nu(\text{O-H})$	$\nu(\text{C=N})$	$\nu(\text{C=N})^a$	$\nu(\text{N-N})$	$\nu(\text{C=S})/\nu(\text{C-S}),$ $\delta(\text{C=S})/\delta(\text{C-S})$	$\nu(\text{C-O})$	$\nu(\text{Ni-O})$	$\nu(\text{Ni-N})$
$\text{H}_2\text{L}^1$	3441	1540	....	1071	1333, 857	1267	....	....
$[(\text{NiL}^1)_2]$ (3)	....	1642	1594	1115	1315, 750	1243	467	438
$[\text{NiL}^1\text{phen}]$ (4)	....	1634	1590	1176	1313, 753	1236	464	437
$[\text{NiL}^1(5,5'\text{-dmbipy})]$ (5)	....	1647	1588	1169	1305, 837	1227	471	440
$\text{H}_2\text{L}^2$	3454	1539	....	1067	1342, 851	1257	....	....
$[(\text{NiL}^2)_2]$ (6)	....	1592	1538	1126	1309, 813	1240	472	445
$[\text{NiL}^2\text{bipy}]$ (7)	....	1590	1538	1091	1318, 823	1240	465	429

<sup>a</sup> = newly formed C=N bond

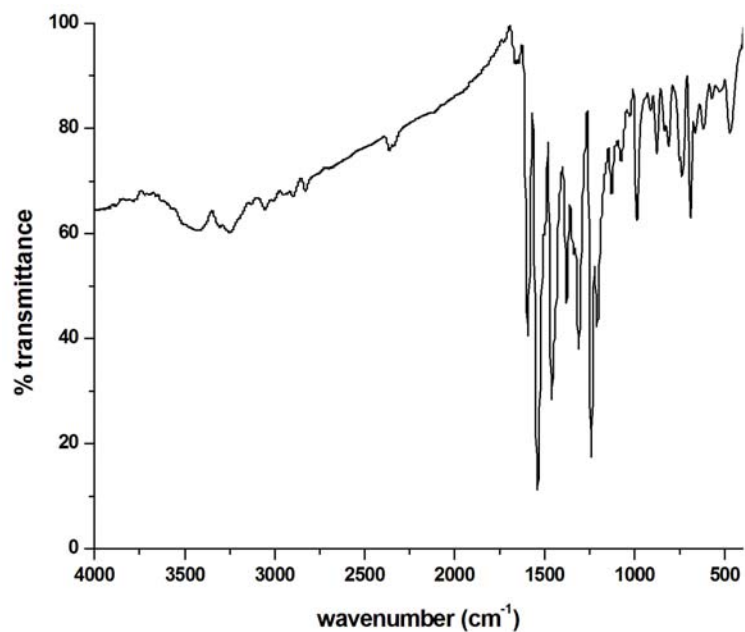


Fig. 4.1. Infrared spectrum of  $[(NiL^1)_2]$  (3).

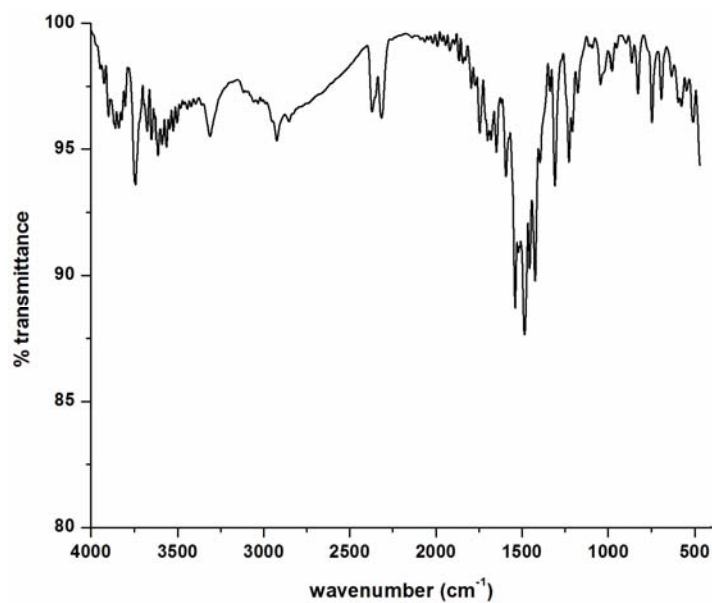


Fig. 4.2. Infrared spectrum of  $[NiL^1(5,5'-dmbipy)]$  (5).

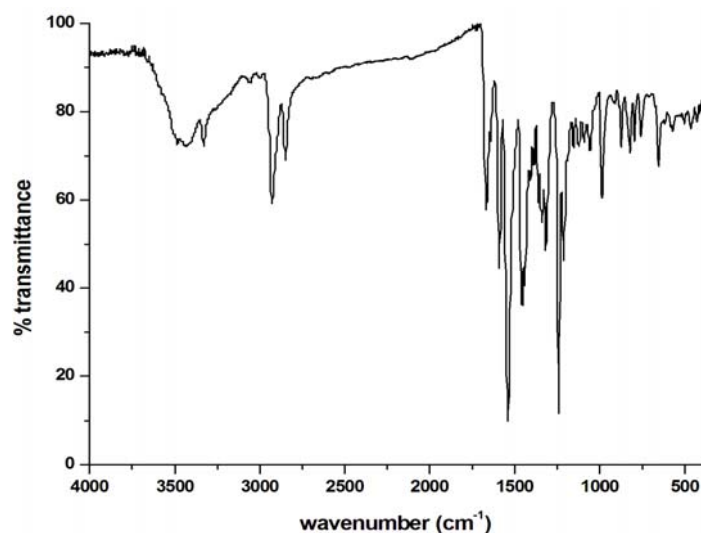


Fig. 4.3. Infrared spectrum of  $[(\text{NiL}^2)_2]$  (6).

#### 4.3.4. Electronic spectra

The UV-vis spectra give much insight into the coordination geometry around metal ion. The electronic spectra of all the Ni(II) complexes were taken in DMF. The electronic transitions found in thiosemicarbazones due to imine function were slightly shifted on complexation. The shift of the bands due to intraligand transitions is the result of the weakening of the C=S bond and the extension of conjugation upon complexation [28]. The shift occurs also due to coordination *via* phenolic oxygen and azomethine nitrogen [29] and is an indication of the enolization followed by the deprotonation of the ligands during complexation. The intraligand  $n \rightarrow \pi^*$  and  $\pi \rightarrow \pi^*$  transitions are assigned to bands in the range 26490-30210  $\text{cm}^{-1}$  for the nickel complexes of  $\text{H}_2\text{L}^1$  and 26570-30430  $\text{cm}^{-1}$  for the nickel complexes of  $\text{H}_2\text{L}^2$ . In all the complexes, intense bands in the 23100-24010  $\text{cm}^{-1}$  range are assigned to ligand to metal charge transfer transitions and

the broadness of these bands can be explained as due to the combination of  $O \rightarrow Ni^{II}$  and  $S \rightarrow Ni^{II}$  LMCT transitions [30,31]. Figs. 4.4-4.6 represent the electronic spectra of the Ni(II) complexes. The electronic spectral data of the thiosemicarbazones and their Ni(II) complexes are given in Table 4.3.

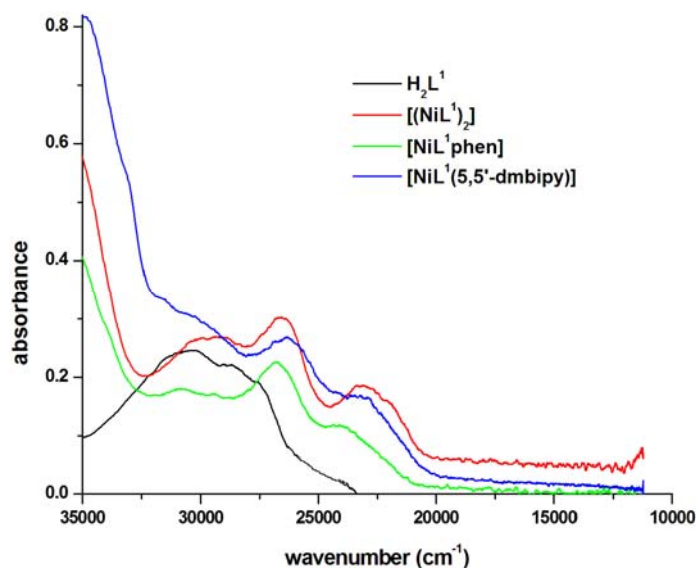


Fig. 4.4. Electronic spectra of  $H_2L^1$  and its nickel complexes.

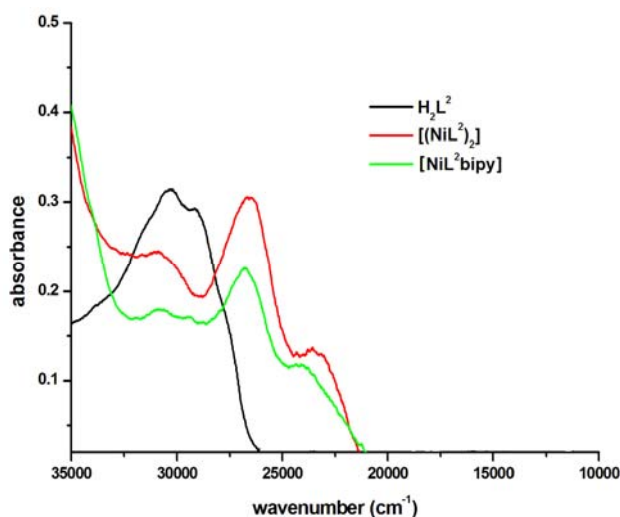


Fig. 4.5. Electronic spectra of  $H_2L^2$  and its nickel complexes.

For a diamagnetic Ni(II) complex, as a consequence of eight electrons being paired in the four low-lying  $d$  orbitals with the upper orbital being  $d_{x^2-y^2}$ , the four lower orbitals are often so close in energy that individual transitions from them to the upper  $d$  level cannot be distinguished, resulting in a single absorption band. The broad bands at  $14080\text{ cm}^{-1}$  for  $[(\text{NiL}^1)_2]$  (3) and  $16600\text{ cm}^{-1}$  for  $[(\text{NiL}^2)_2]$  (6) may be attributed to  $d-d$  bands of this type. However we could not locate any  $d-d$  bands for the other complexes, probably due to masking by the high intensity charge transfer bands.

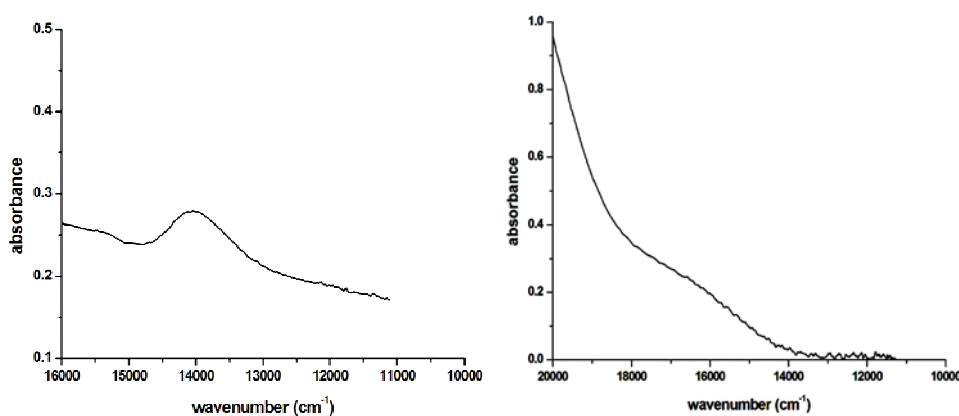


Fig. 4.6. Visible spectra of  $[(\text{NiL}^1)_2]$  (3) and  $[(\text{NiL}^2)_2]$  (6).

Table 4.3. Electronic spectral assignments ( $\text{cm}^{-1}$ ) of thiosemicarbazones and their Ni(II) complexes

Compound	$n \rightarrow \pi^*/\pi \rightarrow \pi^*$	LMCT	d-d
$\text{H}_2\text{L}^1$	28770, 30490	----	----
$[(\text{NiL}^1)_2]$ (3)	26500, 30070	23100	14080
$[\text{NiL}^1\text{phen}]$ (4)	26520, 30150	23210	----
$[\text{NiL}^1(5,5'\text{-dmbipy})]$ (5)	26490, 30210	23300	----
$\text{H}_2\text{L}^2$	29300, 30490	----	----
$[(\text{NiL}^2)_2]$ (6)	26570, 30430	23440	16600
$[\text{NiL}^2\text{bipy}]$ (7)	26780, 30210	24010	----

## References

- [1] L. Stixrude, E. Wasserman, R.E. Cohen, *Journal of Geophysical Research: Solid Earth* 102 (1997) 24729.
- [2] C. Kittel, *Introduction to Solid State Physics*, Wiley, 1996, 449.
- [3] R.K. Szilagyi, P.A. Bryngelson, M.J. Maroney, B.Hedman, K.O. Hodgson, E.I. Solomon, *J. Am. Chem. Soc.* 126 (2004) 3018.
- [4] N. Greig, S. Wyllie, T.J. Vickers, A.H. Fairlamb, *J. Biochem.* 400(2) (2006) 217.
- [5] A.C. Aronsson, E. Marmstal, B. Mannervik, *Biochem. Biophys. Res. Comm.* 81(4) (1978) 1235.
- [6] M. Ridderstrom, B. Mannervik, *J. Biochem.* 314 (1996) 463.
- [7] A.P. Saint-Jean, K.R. Philips, D.J. Creighton, M.J. Stone, *Biochemistry* 37 (1998) 10345.
- [8] P.J. Thornalley, *Biochemical Society Transactions* 31 (2003) 1343.
- [9] D.L. Vander Jagt, *Coenzymes and Cofactors VIII: Glutathione Part A*. New York: John Wiley and Sons.
- [10] E. Bermejo, A. Castineiras, L.M. Fostiak, I. Gareia, A.L. Llamas, J.K. Swearingen, D.K. West, *J. Braz. Chem. Soc.* 56 (2001) 1297.
- [11] H.J. Kruger, R.H. Holm, *Inorg. Chem.* 28 (1989) 1148.
- [12] S. Brooker, P.D. Croucher, *J. Chem. Soc., Chem. Commun.* (1997) 459.
- [13] W.J. Geary, *Coord. Chem. Rev.* 7 (1971) 81.
- [14] E. Manoj, M.R.P. Kurup, *Polyhedron* 27 (2008) 275.
- [15] M. Mathew, G.J. Palenik, G.R. Clark, *J. Inorg. Chem.* 12 (1973) 446.
- [16] M. Joseph, V. Suni, M.R.P. Kurup, M. Nethaji, A. Kishore, S.G. Bhat, *Polyhedron* 23 (2004) 3069.
- [17] M.A. Ali, M.T.H. Tarafdar, *J. Inorg. Nucl. Chem.* 39 (1977) 1785.

- [18] M.J.M. Campbell, *Coord. Chem. Rev.* 15 (1975) 279.
- [19] B.S. Garg, M.R.P. Kurup, S.K. Jain, Y.K. Bhoon, *Transit. Met. Chem.* 13 (1988) 247.
- [20] B.S. Garg, M.R.P. Kurup, S.K. Jain, Y.K. Bhoon, *Transit. Met. Chem.* 16 (1991) 111.
- [21] K. Nakamoto, *Infrared and Raman Spectra of Coordination Compounds*, 3<sup>rd</sup> edn, John Wiley and Sons, NY 1978.
- [22] V. Suni, M.R.P. Kurup, M. Nethaji, *Polyhedron* 26 (2007) 3097.
- [23] D.X. West, A.A. Nassar, F.A. El-Saied, M.I. Ayad, *Transit. Met. Chem.* 23 (1998) 423.
- [24] B.S. Garg, M.R.P. Kurup, S.K. Jain, Y.K. Bhoon, *Transit. Met. Chem.* 13 (1988) 309.
- [25] R. Mayer, *Organosulfur Chemistry*, M.J. Janssen, Ed.; Wiley-Interscience: New York (1967) 219.
- [26] P. Bindu, M.R.P. Kurup, *Ind. J. Chem.* 36A (1997) 1094.
- [27] P.B. Sreeja, M.R.P. Kurup, *Spectrochim. Acta* 61A (2005) 331.
- [28] I.-X. Li, H.-A. Tang, Y.-Z. Li, M. Wang, L.-F. Wang, C.-G. Xia, *J. Inorg. Biochem.* 78 (2000) 167.
- [29] R.P. John, A. Sreekanth, M.R.P. Kurup, A. Usman, I.A. Razak, H.-K. Fun, *Spectrochim. Acta.* 59A (2003) 1349.
- [30] V. Philip, V. Suni, M.R.P. Kurup, M. Nethaji, *Polyhedron* 23 (2004) 1225.
- [31] L. Latheef, M.R.P. Kurup, *Polyhedron* 27 (2008) 35.

\*\*\*RSC\*\*\*

**SYNTHESES, CRYSTAL STRUCTURES AND SPECTRAL ASPECTS OF COPPER(II) CHELATES DERIVED FROM ONS DONOR THIOSEMICARBAZONES**

5.1 Introduction  
5.2 Experimental  
5.3 Results and discussion  
**References**

**5.1. Introduction**

Copper exhibits considerable biochemical action either as an essential trace metal or as a constituent of various exogenously administered compounds in humans. In its former role it is bound to ceruloplasmin, albumin and other proteins, while in its latter it is bound to ligands of various types forming complexes that interact with biomolecules, mainly proteins and nucleic acids. The human body contains copper at a level of about 1.4 to 2.1 mg per kg of body mass. Copper(II) ions are water-soluble and they function as bacteriostatic substances, fungicides and wood preservatives at low concentration. It is a ductile metal with very high thermal and electrical conductivity. Copper is widely distributed in nature as metal, in sulphides, arsenides, chlorides, carbonates and so on [1]. More than a dozen of enzymes that depend on copper for their activity have been identified and the metabolic conversions catalyzed by all of these enzymes are oxidative. Many enzymes and proteins have copper at their active sites, which play a key role in biology [2]. Copper is essential to all living

organisms as a trace dietary mineral because it is a key constituent of the respiratory enzyme complex cytochrome c oxidase. The blue copper proteins are involved in outer-sphere long-range electron transfer, the hemocyanins reversibly bind dioxygen, the tyrosinases activate dioxygen for hydroxylation of monophenols and the multicopper oxidases couple four one-electron oxidations of substrate to the four-electron reduction of dioxygen to water [3]. Copper is effective against a wide range of bacteria, as well as influenza A virus, adenovirus and fungi. Due to their importance in biological processes, the synthesis of copper(II) complexes and their activity studies have been the focus from different perspectives.

The ability of NS donor ligands to stabilize reduced and oxidised forms of copper(II) has sparked interest in their bio-inorganic systems [4]. The copper complexes with thiosemicarbazones show potential anticancer, chemotherapeutic and superoxide dismutase-like activity [5]. They show enhanced biological activities compared to thiosemicarbazones and are potent cytotoxic agents as well as inhibitors of DNA synthesis [6]. It is thought that the antitumor activity of the copper complexes of thiosemicarbazones is due to their ability to inhibit DNA topoisomerase-II, an enzyme that regulates the topology of DNA [7]. Tridentate ONS donor thiosemicarbazones and their copper complexes have been studied owing to their pharmacological interest [8]. Copper(II) complexes are also attractive since Cu(II) is known to play a significant role in naturally occurring biological systems and can act as a pharmacological agent [9-11]. It is found that the copper(II) complex of thiosemicarbazone forms intermediate Cu(I) species after its reduction in the presence of thiols. The Cu(I) compounds activate the molecular oxygen present inside the cell to

form either hydroxyl radicals or superoxide anions [12]. These reactive species attack and break the DNA backbone, damage the cell membrane or interact with proteins.

Keeping all these facts in mind, we have synthesized ten copper(II) complexes of ONS donor thiosemicarbazones.

## 5.2. Experimental

### 5.2.1. Materials

Copper(II) acetate monohydrate (E-Merck), 1,10-phenanthroline (phen), 2,2'-bipyridine (bipy), 4,4'-dimethyl-2,2'-bipyridine (4,4'-dmbipy) and 5,5'-dimethyl-2,2'-bipyridine (5,5'-dmbipy) were used as received.

### 5.2.2. Syntheses of the thiosemicarbazones

The syntheses of thiosemicarbazones  $H_2L^1$  and  $H_2L^2$  are discussed already in Chapter 2.

### 5.2.3. Syntheses of the complexes

#### 5.2.3.1. $[(CuL^1)_2]$ (8)

This complex was synthesized by refluxing a solution of  $H_2L^1$  (0.190 g, 0.5 mmol) in 1:1 (v/v) mixture of DMF and methanol with a methanolic solution of  $Cu(OAc)_2 \cdot H_2O$  (0.099 g, 0.5 mmol) for 3 hours. The complex formed was filtered, washed with methanol and dried *in vacuo*.

Elemental Anal. Found (Calcd.) (%): C, 40.29 (40.78); H, 3.06 (2.74); N, 9.71 (9.51); S, 7.40 (7.26). Yield: 63%

#### 5.2.3.2. [CuL<sup>1</sup>phen] (9)

Methanolic solution of copper(II) acetate monohydrate (0.099 g, 0.5 mmol) was added to a stirred mixture of H<sub>2</sub>L<sup>1</sup> (0.190 g, 0.5 mmol) in DMF and methanol (1:1 v/v) and 1,10-phenanthroline (0.099 g, 0.5 mmol) in methanol. The resultant homogenous green solution was refluxed for three hours. The green product obtained was filtered, washed with methanol and dried *in vacuo*.

Elemental Anal. Found (Calcd.) (%): C, 52.73 (52.14); H, 2.73 (3.24); N, 11.40 (11.26); S, 5.32 (5.16). Yield: 75%

#### 5.2.3.3. [CuL<sup>1</sup>bipy] (10)

To a stirred mixture of H<sub>2</sub>L<sup>1</sup> (0.190 g, 0.5 mmol) in DMF and methanol (1:1 v/v) and 2,2'-bipyridine (0.078 g, 0.5 mmol) in methanol, methanolic solution of copper(II) acetate monohydrate (0.099 g, 0.5 mmol) was added. The resultant deep green solution was refluxed for 3 hours and the dark green product separated out was filtered, washed with methanol and dried *in vacuo*.

Elemental Anal. Found (Calcd.) (%): C, 50.17 (50.21); H, 3.80 (3.37); N, 11.15 (11.71); S, 5.48 (5.36). Yield: 76%

#### 5.2.3.4. [CuL<sup>1</sup>(4,4'-dmbipy)] (11)

To a stirred mixture of H<sub>2</sub>L<sup>1</sup> (0.190 g, 0.5 mmol) in DMF and methanol (1:1 v/v) and 4,4'-dimethylbipyridine (0.092 g, 0.5 mmol) in methanol, methanolic solution of copper(II) acetate monohydrate (0.099 g, 0.5 mmol) was added. The resultant deep green solution was refluxed for 3 hours and

the dark green product separated out was filtered, washed with methanol and dried *in vacuo*.

Elemental Anal. Found (Calcd.) (%) : C, 51.35 (51.80); H, 4.34 (3.86); N, 11.56 (11.19); S, 4.84 (5.12). Yield: 68%

#### 5.2.3.5. [CuL<sup>1</sup>(5,5'-dmbipy)]·DMF (12)

Methanolic solution of copper(II) acetate monohydrate (0.099 g, 0.5 mmol) was added to a stirred mixture of H<sub>2</sub>L<sup>1</sup> (0.190 g, 0.5 mmol) in DMF and methanol (1:1 v/v) and 5,5'-dimethylbipyridine (0.092 g, 0.5 mmol) in methanol. The resultant green solution was refluxed for three hours. The green product obtained was filtered, washed with methanol and dried *in vacuo*.

Elemental Anal. Found (Calcd.) (%) : C, 51.34 (51.54); H, 4.25 (4.47); N, 11.87 (12.02); S, 4.51 (4.59). Yield: 82%

#### 5.2.3.6. [(CuL<sup>2</sup>)<sub>2</sub>] (13)

This complex was synthesized by refluxing a solution of H<sub>2</sub>L<sup>2</sup> (0.193 g, 0.5 mmol) in 1:1 (v/v) mixture of DMF and methanol with a methanolic solution of Cu(OAc)<sub>2</sub>·H<sub>2</sub>O (0.099 g, 0.5 mmol) for 3 hours. The complex formed was filtered, washed with methanol and dried *in vacuo*.

Elemental Anal. Found (Calcd.) (%) : C, 40.02 (40.23); H, 4.21 (4.05); N, 8.89 (9.38); S, 7.25 (7.16). Yield: 74%

#### 5.2.3.7. [CuL<sup>2</sup>phen] (14)

Methanolic solution of copper(II) acetate monohydrate (0.099 g, 0.5 mmol) was added to a stirred mixture of H<sub>2</sub>L<sup>2</sup> (0.193 g, 0.5 mmol) in DMF

and methanol (1:1 v/v) and 1,10-phenanthroline (0.099 g, 0.5 mmol) in methanol. The resultant homogenous green solution was refluxed for three hours. The green product obtained was filtered, washed with methanol and dried *in vacuo*.

Elemental Anal. Found (Calcd.) (%): C, 52.23 (51.63); H, 3.71 (4.17); N, 11.30 (11.15); S, 5.17 (5.11). Yield: 80%

#### 5.2.3.8. [CuL<sup>2</sup>bipy] (15)

To a stirred mixture of H<sub>2</sub>L<sup>2</sup> (0.193 g, 0.5 mmol) in DMF and methanol (1:1 v/v) and 2,2'-bipyridine (0.078 g, 0.5 mmol) in methanol, methanolic solution of copper(II) acetate monohydrate (0.099 g, 0.5 mmol) was added. The resultant deep green solution was refluxed for 3 hours and the dark green product separated out was filtered, washed with methanol and dried *in vacuo*.

Elemental Anal. Found (Calcd.) (%): C, 49.58 (49.71); H, 4.11 (4.34); N, 11.30 (11.59); S, 5.17 (5.31). Yield: 68%

#### 5.2.3.9. [CuL<sup>2</sup>(4,4'-dmbipy)] (16)

To a stirred mixture of H<sub>2</sub>L<sup>2</sup> (0.193 g, 0.5 mmol) in DMF and methanol (1:1 v/v) and 4,4'-dimethylbipyridine (0.092 g, 0.5 mmol) in methanol, methanolic solution of copper(II) acetate monohydrate (0.099 g, 0.5 mmol) was added. The resultant deep green solution was refluxed for 3 hours and the dark green product separated out was filtered, washed with methanol and dried *in vacuo*.

Elemental Anal. Found (Calcd.) (%): C, 50.78 (51.31); H, 5.23 (4.78); N, 10.67 (11.08); S, 4.84 (5.07). Yield: 77%

#### 5.2.3.10. [CuL<sup>2</sup>(5,5'-dmbipy)] (17)

Methanolic solution of copper(II) acetate monohydrate (0.099 g, 0.5 mmol) was added to a stirred mixture of H<sub>2</sub>L<sup>2</sup> (0.193 g, 0.5 mmol) in DMF and methanol (1:1 v/v) and 5,5'-dimethylbipyridine (0.092 g, 0.5 mmol) in methanol. The resultant green solution was refluxed for three hours. The green product obtained was filtered, washed with methanol and dried *in vacuo*.

Elemental Anal. Found (Calcd.) (%) : C, 51.55 (51.31); H, 4.73 (4.78); N, 11.16 (11.08); S, 5.63 (5.07). Yield: 73%

### 5.3. Results and discussion

Ten copper complexes of the thiosemicarbazones were synthesized. The compounds **8** and **13** were prepared by the reaction of equimolar mixture of the appropriate thiosemicarbazone and copper acetate monohydrate. Complexes **9**, **10**, **11**, **12**, **14**, **15**, **16** and **17** were synthesized by refluxing metal salt, corresponding heterocyclic bases and thiosemicarbazones in 1:1:1 ratio. All the complexes are green in color which may be due to the sulfur to copper charge transfer bands dominating their visible spectra [13,14]. They are soluble in solvents like DMF and DMSO. In all the complexes, thiosemicarbazones exist in the thioiminolate form and act as dideprotonated tridentate ligands coordinating through phenolic oxygen, thioiminolate sulfur and azomethine nitrogen. Single crystals of compounds **10** and **12** could be isolated and the structures were established by single crystal XRD studies. Compounds **8** and **13** are dimeric in nature while others are monomeric mixed ligand metal chelates. They are characterized by the following physico-chemical methods.

### 5.3.1. Elemental analyses

The analytical data indicate that the compounds are analytically pure. The elemental analyses data are consistent with the general formula [CuLB], for complexes **9**, **10**, **11**, **12**, **14**, **15**, **16** and **17** and [(CuL)<sub>2</sub>] for complexes **8** and **13**, where L is the doubly deprotonated thiosemicarbazone and B is the bidentate heterocyclic base.

### 5.3.2. Molar conductivity and magnetic susceptibility measurements

The conductivity measurements were made in DMF (10<sup>-3</sup> M) and all the complexes were found to be non-electrolytes [15]. The room temperature magnetic moments of the complexes **9**, **10**, **11**, **12**, **14**, **15**, **16** and **17** in the polycrystalline state fall in the range 1.61-1.87 B.M., which are very close to the spin-only value of 1.73 B.M. for a *d*<sup>9</sup> copper system [16]. The magnetic moments of complexes **8** and **13** are found to be 1.35 and 1.45 B.M. respectively and this low magnetic moment may be attributed to considerable antiferromagnetic interaction between metal centres suggesting dimeric nature to these complexes [17].

**Table 5.1. Molar conductivity and magnetic moments of Cu(II) complexes**

Compound	$\lambda_m^a$	$\mu_{\text{eff}}$ (B.M.)
[(CuL <sup>1</sup> ) <sub>2</sub> ] ( <b>8</b> )	4.8	1.35
[CuL <sup>1</sup> phen] ( <b>9</b> )	5.2	1.63
[CuL <sup>1</sup> bipy] ( <b>10</b> )	4.5	1.72
[CuL <sup>1</sup> (4,4'-dmbipy)] ( <b>11</b> )	2.5	1.63
[CuL <sup>1</sup> (5,5'-dmbipy)]-DMF ( <b>12</b> )	4.5	1.61
[(CuL <sup>2</sup> ) <sub>2</sub> ] ( <b>13</b> )	4.3	1.45
[CuL <sup>2</sup> phen] ( <b>14</b> )	4.8	1.87
[CuL <sup>2</sup> bipy] ( <b>15</b> )	8.3	1.75
[CuL <sup>2</sup> (4,4'-dmbipy)] ( <b>16</b> )	6.5	1.76
[CuL <sup>2</sup> (5,5'-dmbipy)] ( <b>17</b> )	8.4	1.73

<sup>a</sup> = mho cm<sup>2</sup> mol<sup>-1</sup>

### 5.3.3. Infrared spectra

The IR spectra of the copper complexes were recorded in the range 4000-400  $\text{cm}^{-1}$  with KBr pellets. A comparison of the IR spectra of thiosemicarbazones and the metal complexes shows that significant variations have occurred in the characteristic frequencies upon complexation. The tentative assignments for the IR spectral bands useful for determining the ligand's mode of coordination are listed in Table 5.2. In all the complexes, the bands due to O-H and  $^2\text{N-H}$  stretching vibrations are absent which is a clear evidence for the coordination of the thiosemicarbazones in the dideprotonated form. The band corresponding to azomethine bond,  $\nu(\text{C=N})$ , shifts to higher energy on coordination due to the combination of  $\nu(\text{C=N})$  with the newly formed C=N bond which results from the loss of the thioamide hydrogen from the thiosemicarbazone moiety [18-22]. The bands at 1333 and 1342  $\text{cm}^{-1}$  present in the thiosemicarbazones shift to lower wavenumbers in all the complexes and this can be assigned to the  $\nu(\text{C-S})$  vibration suggesting the change of bond order and strong electron-delocalization upon chelation. This shows that the H-N-C=S in the ligands has transformed to N=C-S-H thereby coordinating to copper in the thioiminolate form. Coordination *via* thioiminolate sulfur is also indicated by the negative shift of the band assigned to  $\delta(\text{C=S})$  vibration in the thiosemicarbazones [23]. The bands in the range 460-483  $\text{cm}^{-1}$  indicate the coordination of azomethine nitrogen to copper centre. The increase in frequency of  $\nu(\text{N-N})$  bands in complexes, due to the increase in double bond character is another proof for the coordination of the ligands through the azomethine nitrogen [24]. The broad absorption bands at 3441 and 3454  $\text{cm}^{-1}$  assigned to phenolic -OH of

thiosemicarbazones have disappeared in the complexes which indicate the coordination of the phenolic oxygen to the copper atom. The IR spectra of complexes **9**, **10**, **11**, **12**, **14**, **15**, **16** and **17** display bands characteristic of coordinating heterocyclic bases [25]. Figs. 5.1-5.9 depict the infrared spectra of some of the copper complexes of thiosemicarbazones.

It is observed that in all the complexes the thiosemicarbazones act as dianionic tridentate ligands coordinating to copper through O, N and S atoms. In the case of mixed ligand copper chelates, the two nitrogen atoms of heterocyclic bases occupy the fourth and fifth coordination positions of copper.

**Table 5.2. IR spectral assignments ( $\text{cm}^{-1}$ ) of thiosemicarbazones and their Cu(II) complexes**

Compound	$\nu(\text{O-H})$	$\nu(\text{C=N})$	$\nu(\text{C=N})^a$	$\nu(\text{N-N})$	$\nu(\text{C=S})/\nu(\text{C-S}),$ $\delta(\text{C=S})/\delta(\text{C-S})$	$\nu(\text{C-O})$	$\nu(\text{Cu-O})$	$\nu(\text{Cu-N})$
$\text{H}_2\text{L}^1$	3441	1540	---	1071	1333, 857	1267	---	---
$[(\text{CuL}^1)_2]$ ( <b>8</b> )	---	1600	1504	1120	1315, 744	1237	463	437
$[\text{CuL}^1\text{phen}]$ ( <b>9</b> )	---	1594	1546	1082	1309, 726	1231	464	437
$[\text{CuL}^1\text{bipy}]$ ( <b>10</b> )	---	1589	1491	1090	1309, 752	1219	469	443
$[\text{CuL}^1(4,4'\text{-dmbipy})]$ ( <b>11</b> )	---	1597	1542	1094	1314, 831	1232	477	435
$[\text{CuL}^1(5,5'\text{-dmbipy})] \cdot \text{DMF}$ ( <b>12</b> )	---	1597	1542	1086	1314, 749	1232	483	435
$\text{H}_2\text{L}^2$	3454	1539	---	1067	1342, 851	1257	---	---
$[(\text{CuL}^2)_2]$ ( <b>13</b> )	---	1597	1556	1101	1328, 811	1225	460	422
$[\text{CuL}^2\text{phen}]$ ( <b>14</b> )	---	1585	1505	1098	1313, 831	1231	468	434
$[\text{CuL}^2\text{bipy}]$ ( <b>15</b> )	---	1586	1478	1094	1308, 764	1220	466	430
$[\text{CuL}^2(4,4'\text{-dmbipy})]$ ( <b>16</b> )	---	1597	1541	1121	1321, 797	1238	483	442
$[\text{CuL}^2(5,5'\text{-dmbipy})]$ ( <b>17</b> )	---	1590	1535	1093	1308, 831	1225	462	435

<sup>a</sup> = newly formed C=N bond

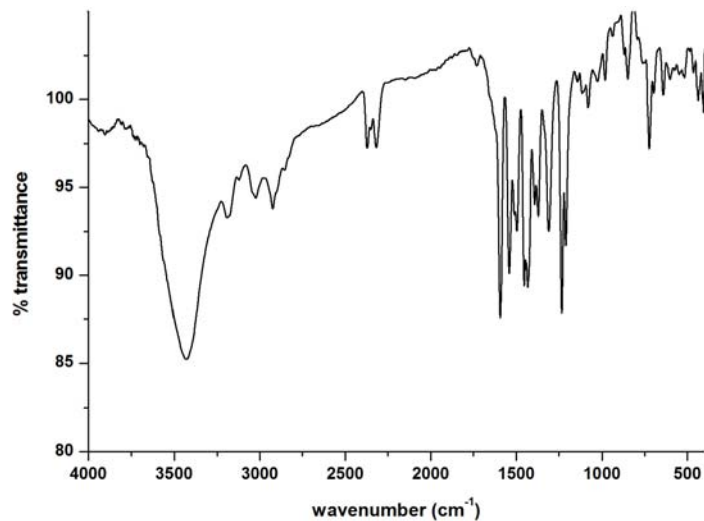


**Fig. 5.1.** Infrared spectrum of [CuL¹phen] (9).

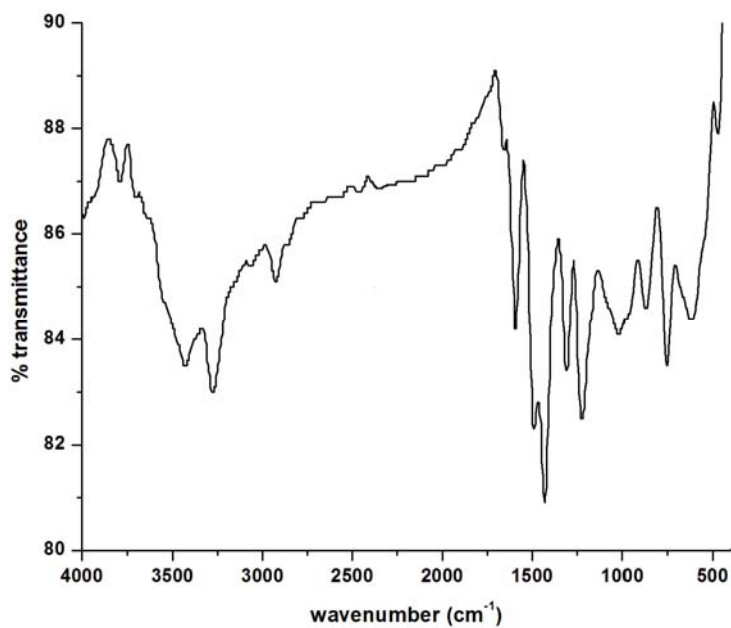


**Fig. 5.2.** Infrared spectrum of [CuL¹bipy] (10).

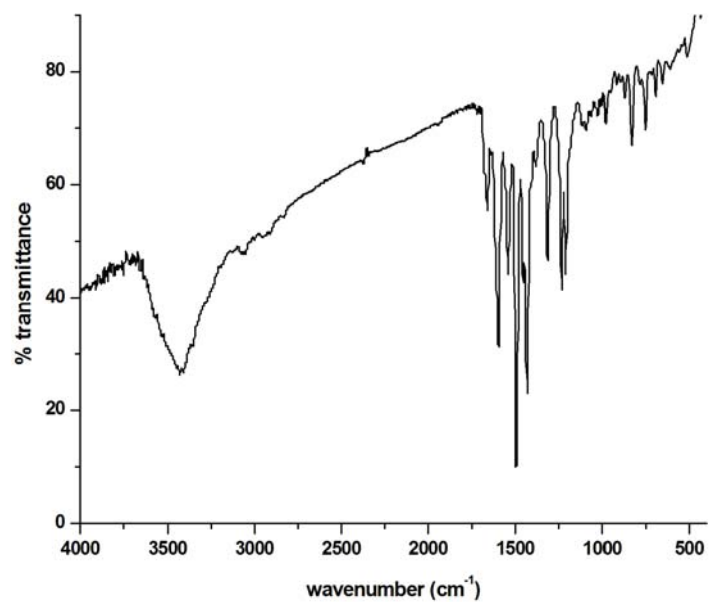


Fig. 5.3. Infrared spectrum of  $[\text{CuL}^1(4,4'\text{-dmbipy})]$  (11).

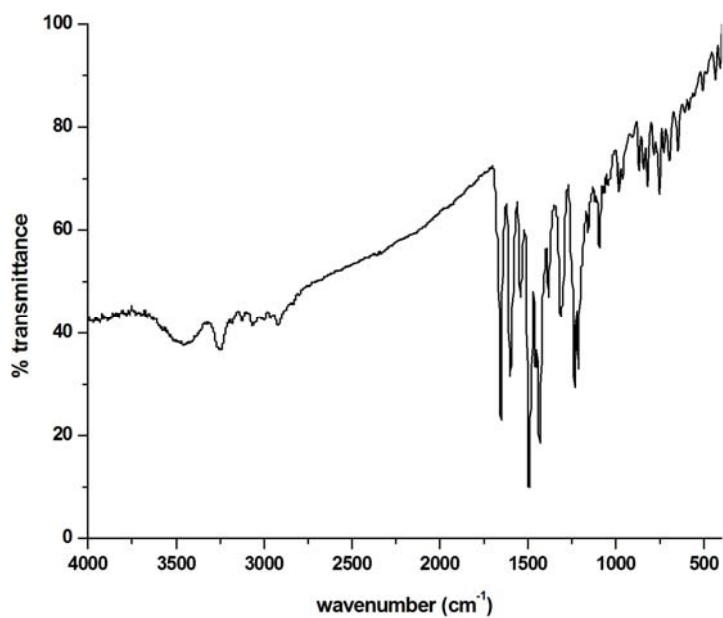
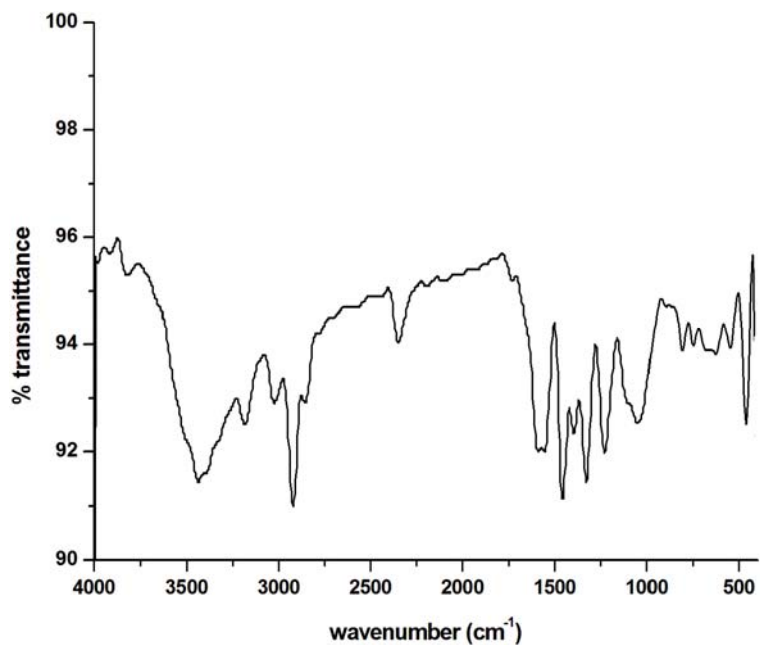
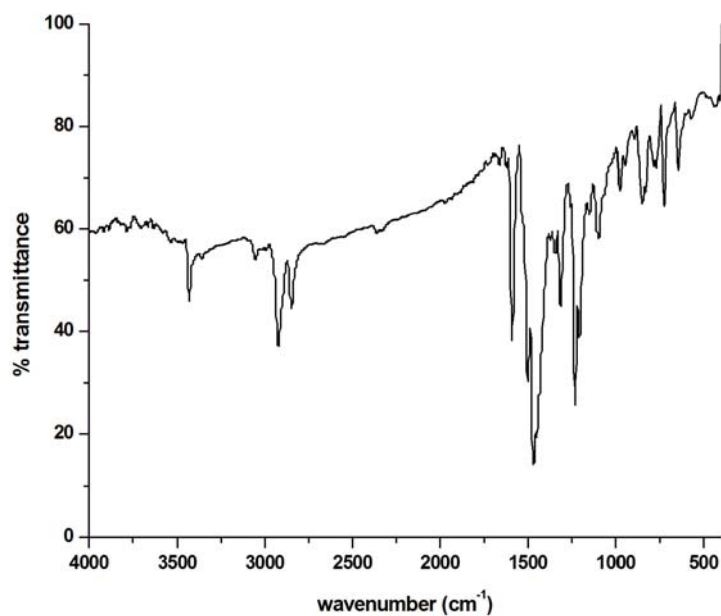


Fig. 5.4. Infrared spectrum of  $[\text{CuL}^1(5,5'\text{-dmbipy})]\cdot\text{DMF}$  (12).



**Fig. 5.5. Infrared spectrum of [(CuL<sup>2</sup>)<sub>2</sub>] (13).**



**Fig. 5.6. Infrared spectrum of [CuL<sup>2</sup>phen] (14).**

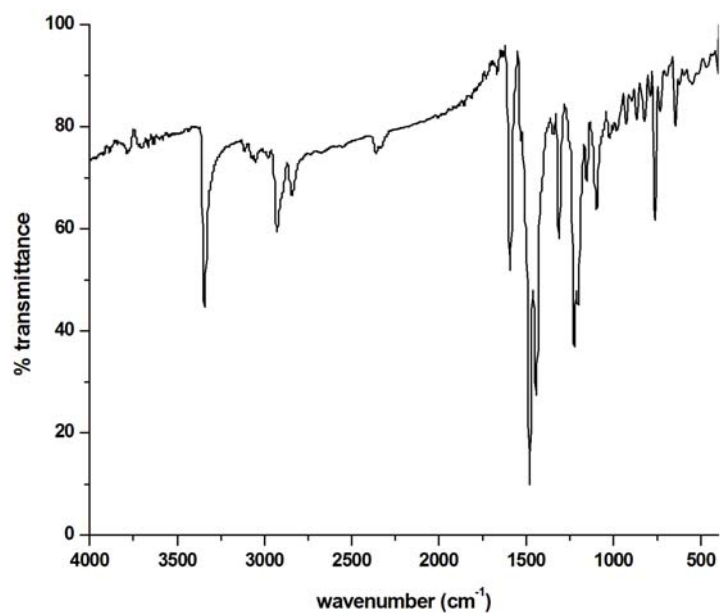


Fig. 5.7. Infrared spectrum of [CuL<sup>2</sup>bipy] (15).

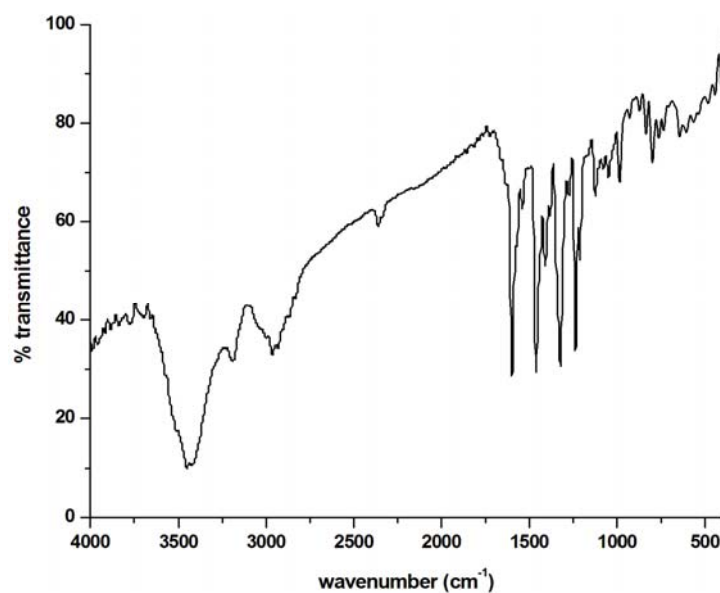


Fig. 5.8. Infrared spectrum of [CuL<sup>2</sup>(4,4'-dmbipy)] (16).

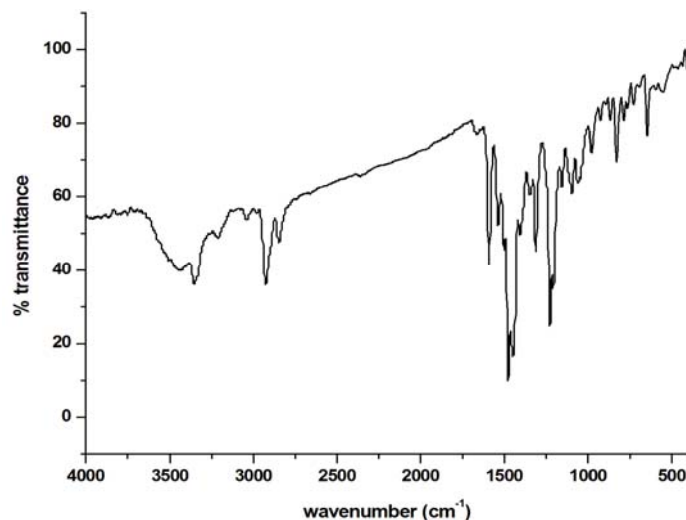


Fig. 5.9. Infrared spectrum of  $[\text{CuL}^2(5,5'\text{-dmbipy})]$  (17).

#### 5.3.4. Electronic spectra

The UV-vis spectra give much insight into the coordination geometry around copper(II) ion. The electronic spectra of all the complexes were taken in DMF. The electronic transitions found in free ligands due to imine function of thiosemicarbazone moiety were slightly shifted on complexation. The shift of the bands due to intraligand transitions is the result of the weakening of the C=S bond and the extension of conjugation upon complexation [26]. The shift occurs also due to coordination *via* phenolic oxygen and azomethine nitrogen [27] and is an indication of the enolization followed by the deprotonation of the ligands during complexation. The intraligand  $n \rightarrow \pi^*$  and  $\pi \rightarrow \pi^*$  transitions are assigned to bands in the range 28630-29960  $\text{cm}^{-1}$  for the copper complexes of  $\text{H}_2\text{L}^1$  and 29140-30330  $\text{cm}^{-1}$  for the copper complexes of  $\text{H}_2\text{L}^2$ . In all the complexes, intense bands in the 23940-24540  $\text{cm}^{-1}$  range are assigned to ligand to metal charge transfer transitions and the broadness of these bands can be explained as due to the combination of  $\text{O} \rightarrow \text{Cu}$ ,  $\text{N} \rightarrow \text{Cu}$  and  $\text{S} \rightarrow \text{Cu}$  LMCT

transitions [28,29]. Figs. 5.10 and 5.11 represent the electronic spectra of the complexes.

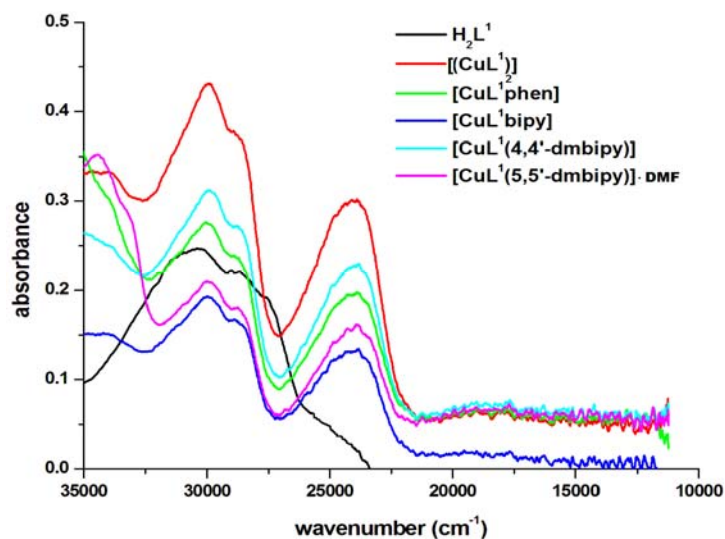


Fig. 5.10. Electronic spectra of  $H_2L^1$  and its copper complexes.

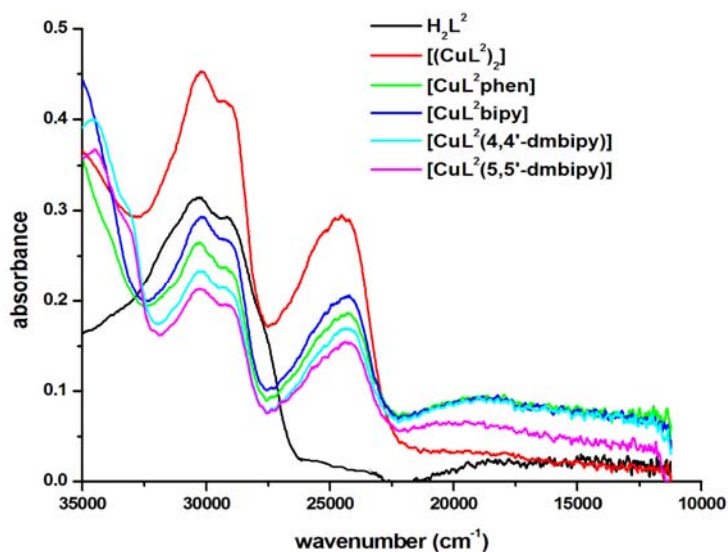


Fig. 5.11. Electronic spectra of  $H_2L^2$  and its copper complexes.

In an octahedral field, the ground state term  $^2D$  of copper(II) will be split into two levels,  $^2T_{2g}$  and  $^2E_g$ . However, the energy levels again split

resulting in more transitions if the geometry around copper(II) complex is of lower symmetry. For square planar complexes with a  $d_{x^2-y^2}$  ground state [30], three transitions are possible viz,  $d_{x^2-y^2} \rightarrow d_{xy}$ ,  $d_{x^2-y^2} \rightarrow d_{z^2}$  and  $d_{x^2-y^2} \rightarrow d_{xz}$ ,  $d_{yz}$  ( ${}^2B_{2g} \leftarrow {}^2B_{1g}$ ,  ${}^2A_{1g} \leftarrow {}^2B_{1g}$  and  ${}^2E_g \leftarrow {}^2B_{1g}$ ). Three transitions,  $d_{x^2-y^2} \rightarrow d_{z^2}$ ,  $d_{x^2-y^2} \rightarrow d_{xy}$  and  $d_{x^2-y^2} \rightarrow d_{xz}$ ,  $d_{yz}$  are possible for square pyramidal complexes with a  $d_{x^2-y^2}$  ground state [30,31]. Since the four  $d$  orbitals lie very close together, each transition cannot be distinguished by its energy and hence it is very difficult to resolve the three bands into separate components. The visible spectra of all the complexes were recorded in DMF and the  $d-d$  bands appeared as weak broad bands in the range 16940-17750  $\text{cm}^{-1}$  (Figs. 5.12 and 5.13) which can be assigned to  ${}^2E_g \rightarrow {}^2T_{2g}$  transitions [32]. The electronic spectral data of the copper(II) complexes are given in Table 5.3.

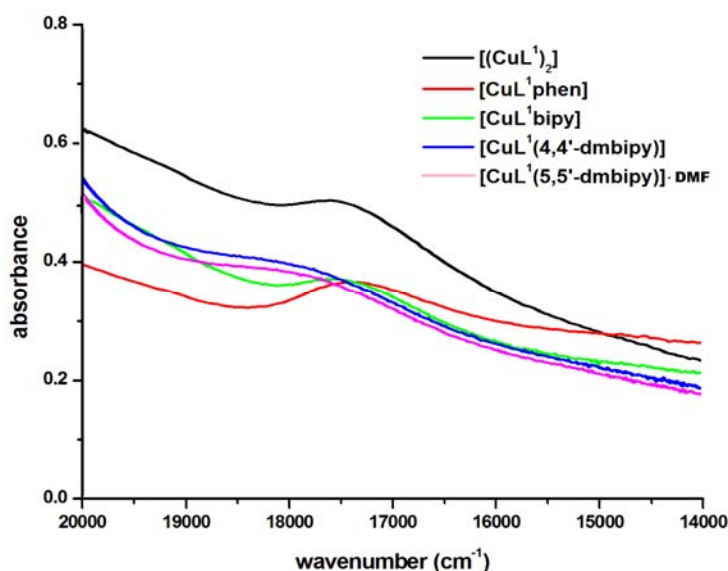
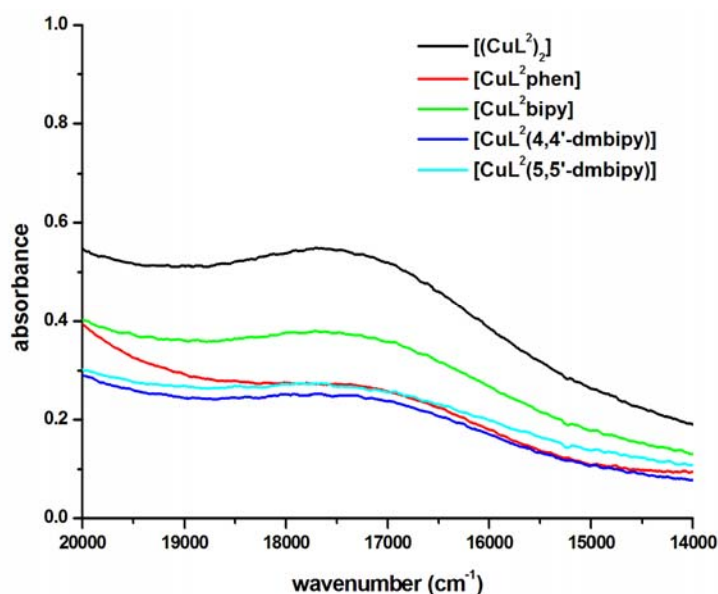


Fig. 5.12. Visible spectra of copper(II) complexes of  $H_2L^1$ .

Fig. 5.13. Visible spectra of copper(II) complexes of  $H_2L^2$ .Table 5.3. Electronic spectral assignments ( $cm^{-1}$ ) of thiosemicarbazones and their Cu(II) complexes

Compound	$n \rightarrow \pi^* / \pi \rightarrow \pi^*$	LMCT	$d-d$
$H_2L^1$	28770, 30490	----	----
$[(CuL^1)_2]$ (8)	28630, 29960	24110	17210
$[CuL^1phen]$ (9)	28630, 29960	24060	17240
$[CuL^1bipy]$ (10)	28660, 29960	24060	17330
$[CuL^1(4,4'-dmbipy)]$ (11)	28720, 29890	23940	17270
$[CuL^1(5,5'-dmbipy)] \cdot DMF$ (12)	28630, 29960	23940	17210
$H_2L^2$	29300, 30490	----	----
$[(CuL^2)_2]$ (13)	29140, 30160	24540	17450
$[CuL^2phen]$ (14)	29150, 30330	24380	16940
$[CuL^2bipy]$ (15)	29140, 30160	24380	17330
$[CuL^2(4,4'-dmbipy)]$ (16)	29230, 30240	24380	17330
$[CuL^2(5,5'-dmbipy)]$ (17)	29150, 30270	24250	17750

### 5.3.5. EPR spectra

The Electron Paramagnetic Resonance spectroscopy provides a wealth of information regarding the electronic structure of paramagnetic compounds. The magnetic parameters measured in EPR study are related to the structure of the paramagnetic complex, the number of ligands, nature of bonding and spatial arrangements of the ligands around the central metal ion.

The copper(II) ion, with a  $d^9$  configuration, has an effective spin of  $S = 1/2$  and associated spin angular momentum  $m_s = \pm 1/2$ , which leads to a doubly degenerate spin state in the absence of magnetic field. In a magnetic field, this degeneracy is removed and the energy difference between these two states is given by  $E = h\nu = g\beta B$ , where  $h$  is Planck's constant,  $\nu$  is the frequency,  $g$  is the Lande splitting factor,  $\beta$  is the electronic Bohr magneton and  $B$  is the magnetic field. In the case of a  $3d^9$  copper(II) ion, the appropriate spin Hamiltonian assuming a  $B_{1g}$  ground state is given by  $\hat{H} = \beta [g_{\parallel}B_zS_z + g_{\perp}(B_xS_x + B_yS_y)] + A_{\parallel}I_zS_z + A_{\perp}(I_xS_x + I_yS_y)$

The copper(II) ion having a  $d^9$  configuration with an effective spin of  $S = 1/2$  couples with nuclear spin of  $^{63}\text{Cu}$  ( $I = 3/2$ ) and gives rise to four ( $2nI+1=4$ ) hyperfine lines. The EPR spectra of all the complexes were recorded in polycrystalline state at 298 K and in DMF/DMSO at 77 K in the X band frequency using TCNE as standard ( $g = 2.00277$ ) with 100 kHz modulation frequency and 9.1 GHz microwave frequency. In polycrystalline state, since it is magnetically concentrated the anisotropy

may be lost. Dilution of the solid isolates the electron spin of the given complex from that of another paramagnetic molecule.

EPR spectra can be mainly of four types *viz.* isotropic, axial, rhombic and reverse axial. An isotropic spectrum with a single  $g$  value shows a cubic coordination environment. Sometimes broadening of signal can also occur which is attributable to enhanced spin lattice relaxation and dipolar interaction. For axial spectrum there will be atleast three fold axis of symmetry and  $g_{\parallel}$  is obtained when the magnetic field is aligned parallel to  $z$  axis. Signal due to  $g_{\perp}$  is obtained when the magnetic field is aligned perpendicular to  $z$  axis. A rhombic spectrum shows no axis of symmetry and hence three  $g$  values are obtained. Some of the EPR spectra are simulated using EasySpin 4.0.0 package [33] and the experimental (red) and simulated (blue) best fits are included.

The EPR parameters  $g_{\parallel}$ ,  $g_{\perp}$ ,  $A_{\parallel}$  and the energies of  $d-d$  transitions were used to evaluate the bonding parameters  $\alpha^2$ ,  $\beta^2$  and  $\gamma^2$  for the Cu(II) ion in various ligand field environments which may be regarded as measure of covalency in the in-plane  $\sigma$ -bonds ( $\alpha^2$ ), in-plane  $\pi$ -bonds ( $\beta^2$ ) and out-of-plane  $\pi$ -bonds ( $\gamma^2$ ) [34]. The orbital reduction factors  $K_{\parallel}$  and  $K_{\perp}$  were also calculated using these bonding parameters. The following expressions are used to calculate these parameters [35,36].

$$\alpha^2 = -(A_{\parallel} / 0.036) + (g_{\parallel} - 2.0023) + 3/7(g_{\perp} - 2.0023) + 0.04$$

$$K_{\parallel}^2 = (g_{\parallel} - 2.0023) E_{d-d} / 8\lambda_0$$

$$K_{\perp}^2 = (g_{\perp} - 2.0023) E_{d-d} / 2\lambda_0$$

$$K_{\parallel} = \alpha^2 \beta^2$$

$$K_{\perp} = \alpha^2 \gamma^2$$

where  $\lambda_0$  is the spin-orbit coupling constant and has a value  $-828 \text{ cm}^{-1}$  for Cu(II)  $d^9$  system. The value of  $\alpha^2$  indicates the extent of covalent nature, where the value of 1.0 corresponds to a purely ionic nature.

According to Hathaway [37], for pure  $\sigma$ -bonding  $K_{\parallel} \approx K_{\perp} \approx 0.77$  and for in-plane  $\pi$ -bonding  $K_{\parallel} < K_{\perp}$ , while for out-of-plane  $\pi$ -bonding  $K_{\perp} < K_{\parallel}$ . The values of bonding parameters  $\alpha^2$ ,  $\beta^2$  and  $\gamma^2 < 1$  confirm the covalent nature of complexes.

The EPR spectrum of complex **8** is isotropic in nature, which is attributable to enhanced spin lattice relaxation and extensive exchange coupling through misalignment of the local molecular axes between different molecules in the unit cell (dipolar broadening) (Fig. 5.14). This type of spectrum unfortunately gives no information on the electronic ground state of copper(II) ions present in the complex. It showed a well-resolved axial spectrum with four hyperfine lines in the parallel region and perpendicular region (due to coupling of the electron spin with the spin of the  $^{63}\text{Cu}$  nucleus where  $I = 3/2$ ) in DMF at 77 K (Fig. 5.15) with  $g_{\parallel} > g_{\perp} > 2.0023$  relationship, consistent with a  $d_{x^2-y^2}$  ground state in a square planar geometry [38,39].

In polynuclear Cu(II) complexes the most important application of EPR spectra is in the identification of Cu-Cu dipolar interaction. Additional transitions arise associated with the  $\Delta M_s = \pm 2$  values in the case of dinuclear complexes, compared with the  $\Delta M_s = \pm 1$  values in mononuclear

complexes. In the X-band spectra,  $\Delta M_s = \pm 1$  transitions are associated with fields of *ca.* 300 mT, while the  $\Delta M_s = \pm 2$  generate an absorption at the half field value of *ca.* 150 mT and the presence of this half field band is useful to identify a dinuclear or polynuclear complex [40]. The EPR spectrum of compound **8** in polycrystalline state suggests a dimeric structure as it exhibited a half field signal at 166 mT with *g* value of 4.01, which indicates that indeed a weak interaction between two Cu(II) ions is present.

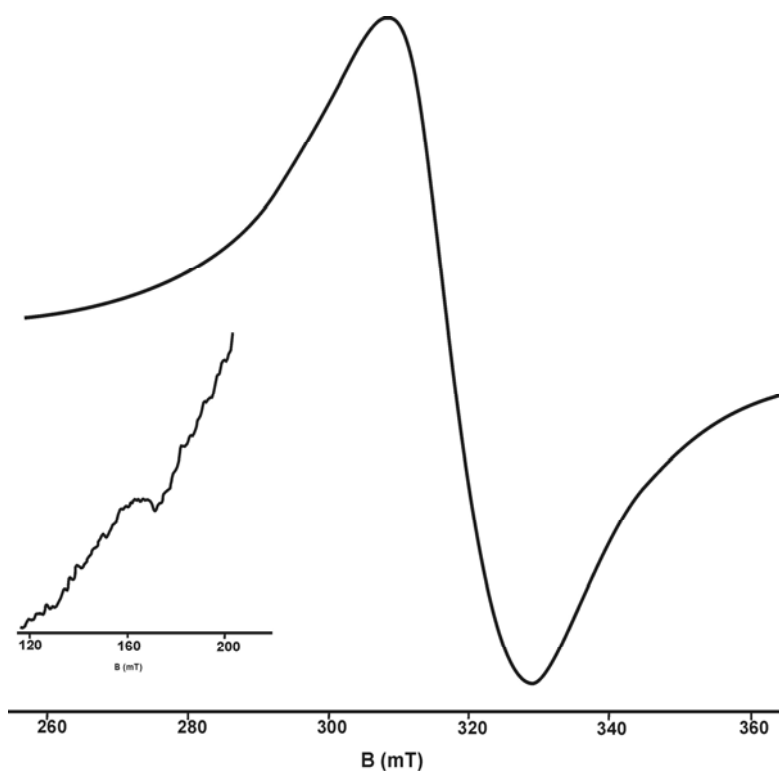
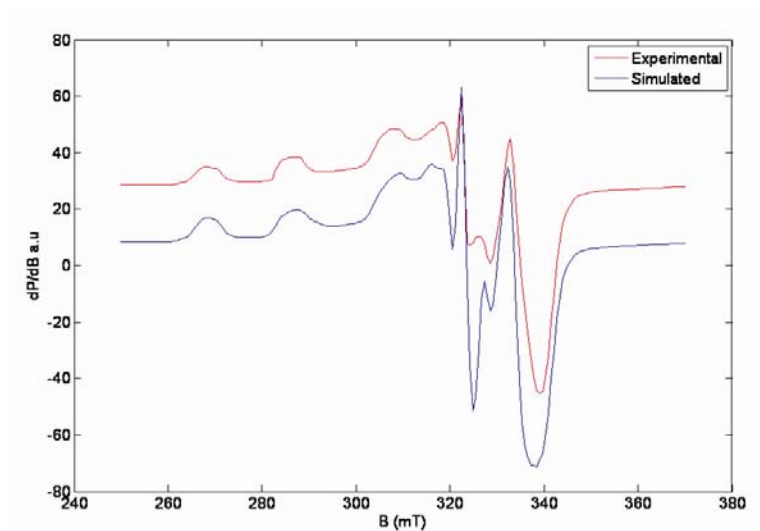
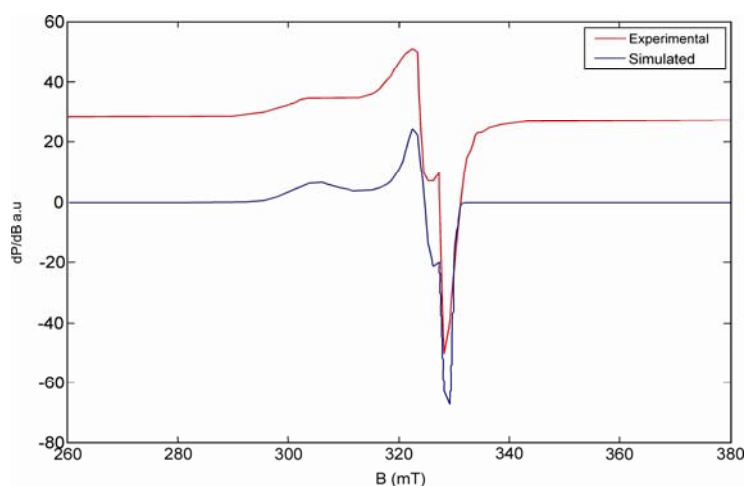


Fig. 5.14. EPR spectrum of  $[(\text{CuL}^1)_2]$  (**8**) in polycrystalline state at 298 K.



**Fig. 5.15.** EPR spectrum of  $[(\text{CuL}^1)_2]$  (8) in DMF at 77 K.

$[\text{CuL}^1\text{phen}]$  (9) displayed a typical rhombic spectrum (Fig. 5.16) with three  $g$  values which suggests that it has a distorted square pyramidal structure. But unfortunately it did not show any anisotropic feature and hyperfine splittings in frozen DMSO, which may be due to poor glass formation.



**Fig. 5.16.** EPR spectrum of  $[\text{CuL}^1\text{phen}]$  (9) in polycrystalline state at 298 K.

In polycrystalline state at 298 K, the EPR spectrum of  $[\text{CuL}^1\text{bipy}]$  (10) is found to be axial in nature (Fig. 5.17) with  $g_{\parallel} = 2.124$  and  $g_{\perp} = 2.017$ . In frozen DMF, it displayed well-resolved axial anisotropy with four hyperfine splittings (Fig. 5.18) resulting from coupling of the electron spin with the spin of the  $^{63}\text{Cu}$  nucleus ( $I = 3/2$ ).

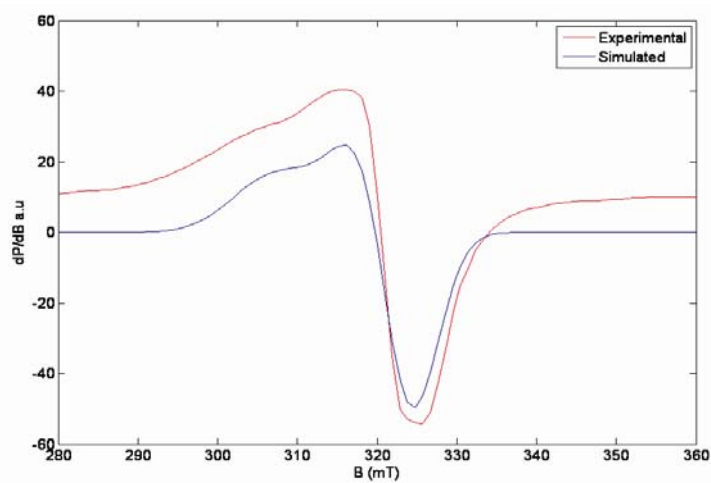


Fig. 5.17. EPR spectrum of  $[\text{CuL}^1\text{bipy}]$  (10) in polycrystalline state at 298 K.

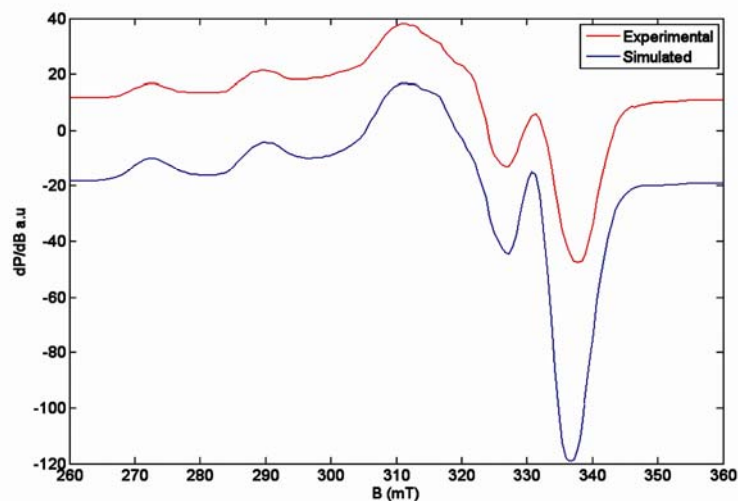


Fig. 5.18. EPR spectrum of  $[\text{CuL}^1\text{bipy}]$  (10) in DMF at 77 K.

The EPR spectrum of  $[\text{CuL}^1(4,4'\text{-dmbipy})]$  (**11**) in polycrystalline state at 298 K showed only one broad signal with  $g_{\text{iso}} = 2.071$  (Fig. 5.19). Unfortunately this complex gave isotropic spectrum in DMSO at 77 K also so that we could not furnish any details regarding the bonding nature of the complex.

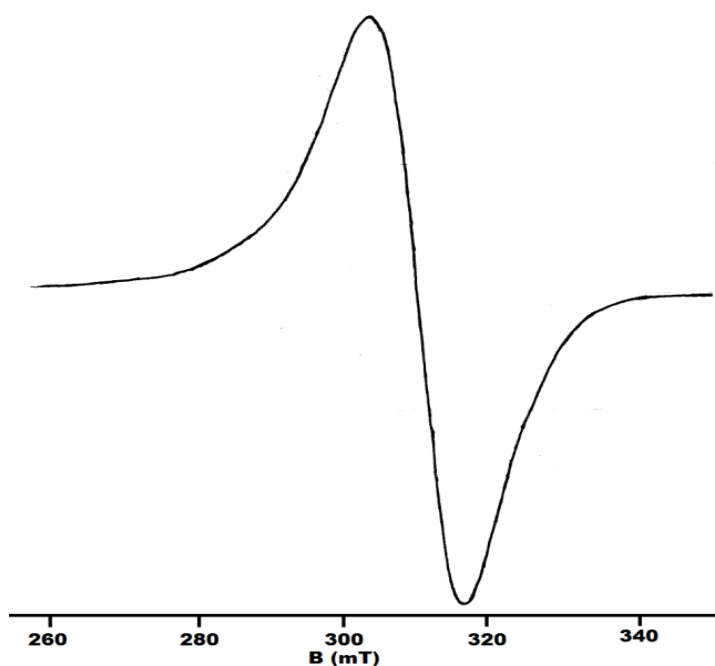


Fig. 5.19. EPR spectrum of  $[\text{CuL}^1(4,4'\text{-dmbipy})]$  (**11**) in polycrystalline state at 298 K.

Complex **12** gave an isotropic spectrum in polycrystalline state at 298 K (Fig. 5.20) with  $g_{\text{iso}} = 2.085$ . We did not get a good spectrum for this complex in DMSO at 77 K.

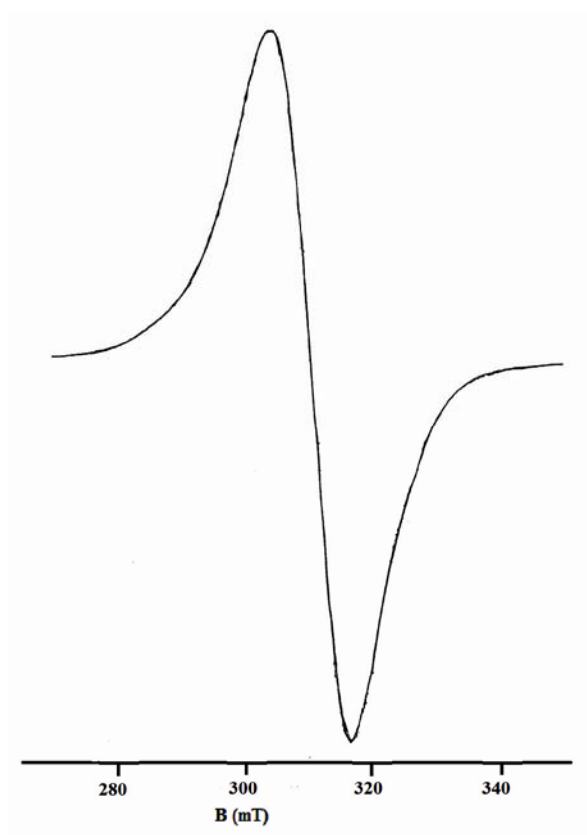


Fig. 5.20. EPR spectrum of  $[\text{CuL}^1(5,5'\text{-dmbipy})]\cdot\text{DMF}$  (**12**) in polycrystalline state at 298 K.

In polycrystalline state at 298 K, the EPR spectrum of compound **13** is found to be isotropic in nature (Fig. 5.21) with  $g_{\text{iso}} = 2.091$ . In DMF at 77 K, the compound  $[(\text{CuL}^2)_2]$  (**13**) showed four fairly resolved hyperfine lines [ $^{63,65}\text{Cu}$ ,  $I = 3/2$ ] corresponding to  $-3/2$ ,  $-1/2$ ,  $+1/2$  and  $+3/2$  transitions in parallel and perpendicular regions. In addition to this, three superhyperfine lines due to interaction with azomethine nitrogen are also observed (Fig. 5.22). A square pyramidal geometry can be assigned to this complex since  $g_{\parallel} > g_{\perp}$  and rules out the possibility of a trigonal bipyramidal structure which is expected to have  $g_{\parallel} < g_{\perp}$ .

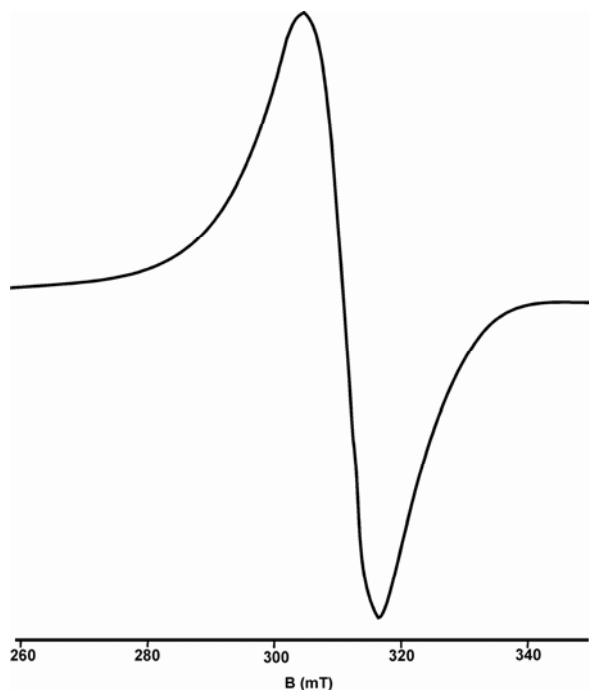


Fig. 5.21. EPR spectrum of  $[(\text{CuL}^2)_2]$  (13) in polycrystalline state at 298 K.

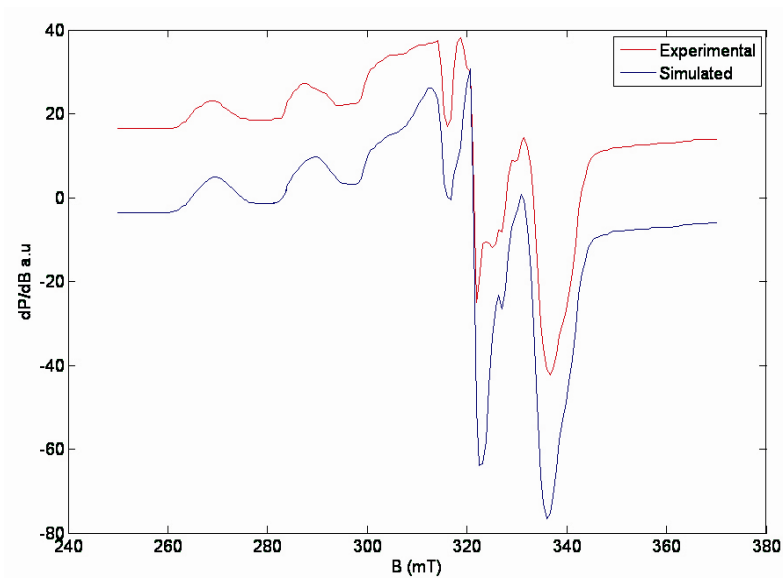


Fig. 5.22. EPR spectrum of  $[(\text{CuL}^2)_2]$  (13) in DMF at 77 K.

The spectrum of  $[\text{CuL}^2\text{phen}]$  (**14**) is axial in nature in polycrystalline state at 298 K (Fig. 5.23) with well defined  $g_{\parallel}$  and  $g_{\perp}$  features and  $g_{\parallel} > g_{\perp}$  ( $g_{\parallel} = 2.190$ ,  $g_{\perp} = 2.049$ ). In DMF at 77 K, it showed well resolved four hyperfine lines in the parallel region (Fig. 5.24). The expected superhyperfine lines are not observed in this complex. Since  $g_{\parallel} > g_{\perp}$ , a distorted square pyramidal geometry can be assigned to this complex.

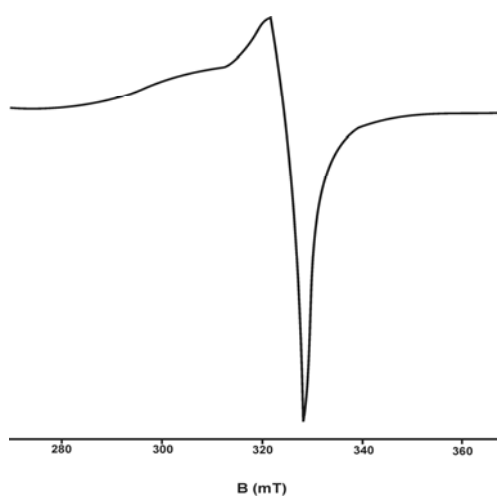


Fig. 5.23. EPR spectrum of  $[\text{CuL}^2\text{phen}]$  (**14**) in polycrystalline state at 298 K.

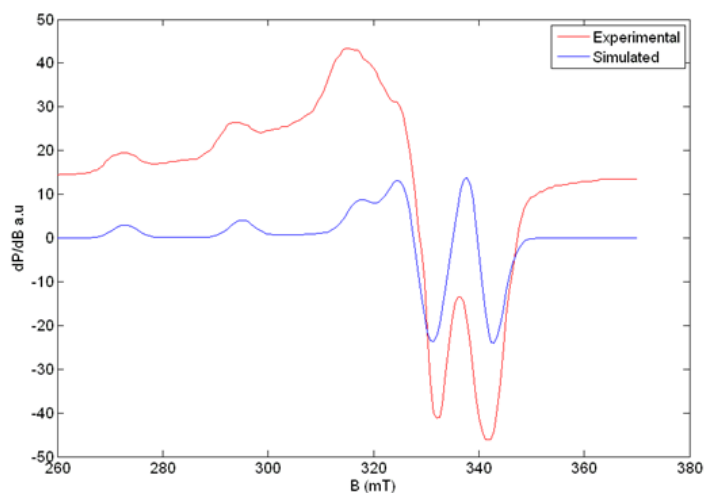
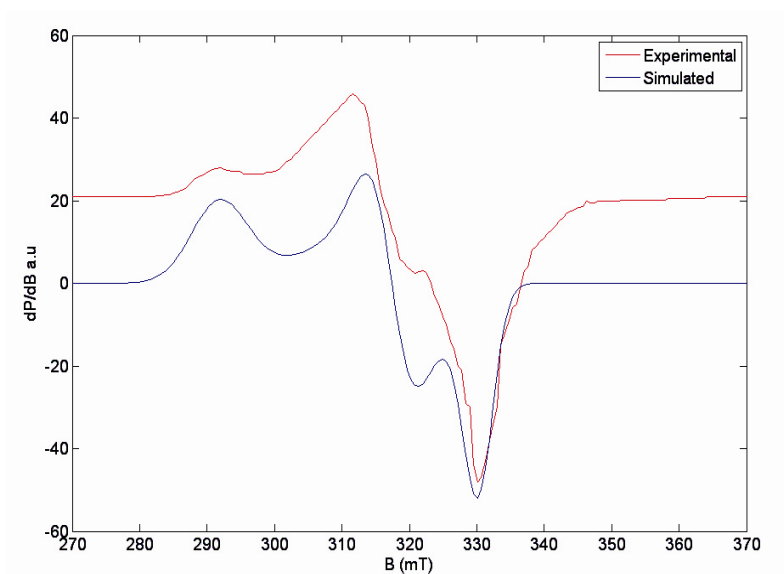


Fig. 5.24. EPR spectrum of  $[\text{CuL}^2\text{phen}]$  (**14**) in DMF at 77 K.

The EPR spectrum of [CuL<sup>2</sup>bipy] (**15**) in polycrystalline state at 298 K shows a rhombic spectrum with three g values suggesting a distorted square pyramidal geometry (Fig. 5.25). In DMSO at 77 K, it did not give good spectrum due to poor glass formation.



**Fig. 5.25.** EPR spectrum of [CuL<sup>2</sup>bipy] (**15**) in polycrystalline state at 298 K.

Complexes **16** and **17** gave isotropic spectra in polycrystalline state at 298 K and gave only poor quality spectra in DMSO at 77 K. So we could not furnish any details regarding the bonding nature of these complexes.

The  $\alpha^2$  values for the complexes were calculated and since the obtained values lie in between 0.5 and 1.0, it is inferred that the metal-ligand bonds in the complexes are partially ionic and partially covalent in nature. The EPR spectral parameters of the copper(II) complexes are presented in Table 5.4.

Table 5.4. EPR spectral parameters of copper(II) complexes in the polycrystalline state at 298 K and in DMF/DMSO at 77 K.

Compound	Polycrystalline state at 298 K			DMF/DMSO (77 K)								
	$g$	$g_{\parallel}$	$g_{\perp}$	$g_{av}$	$A_{\parallel}^a$	$A_{\perp}^a$	$A_{av}^a$	$\alpha^2$	$\beta^2$	$\gamma^2$	$K_{\parallel}$	$K_{\perp}$
[CuL <sup>1</sup> ] <sub>2</sub> (8)	2.087 ( $g_{av}$ )	2.165	2.012	2.063	227	31	96	0.8435	0.7708	0.3764	0.6502	0.3175
[CuL <sup>1</sup> phen] (9)	2.038, 2.055, 2.172 ( $g^1, g^2, g^3$ )	.	.	.	.	.	.	.	.	.	.	.
[CuL <sup>1</sup> bipy] (10)	2.124, 2.017 ( $g_{\parallel}, g_{\perp}$ )	2.170	2.058	2.095	195	40	92	0.7797	0.8496	0.9792	0.6624	0.7635
[CuL <sup>1</sup> (4,4'-dmbipy)] (11)	2.082 ( $g_{av}$ )	.	.	.	.	.	.	.	.	.	.	.
[CuL <sup>1</sup> (5,5'-dmbipy)]·DMF (12)	2.085 ( $g_{av}$ )	.	.	.	.	.	.	.	.	.	.	.
[CuL <sup>2</sup> ] <sub>2</sub> (13)	2.083 ( $g_{av}$ )	2.155	2.026	2.069	223	36	98	0.8254	0.7684	0.6054	0.6342	0.4997
[CuL <sup>2</sup> phen] (14)	2.190, 2.049 ( $g_{\parallel}, g_{\perp}$ )	2.174	2.060	2.098	235	.	.	0.8983	0.7376	0.8553	0.6626	0.7683
[CuL <sup>2</sup> bipy] (15)	2.038, 2.050, 2.230 ( $g^1, g^2, g^3$ )	.	.	.	.	.	.	.	.	.	.	.
[CuL <sup>2</sup> (4,4'-dmbipy)] (16)	2.084 ( $g_{av}$ )	.	.	.	.	.	.	.	.	.	.	.
[CuL <sup>2</sup> (5,5'-dmbipy)] (17)	2.089 ( $g_{av}$ )	.	.	.	.	.	.	.	.	.	.	.

<sup>a</sup>Expressed in units of  $\text{cm}^{-1}$  multiplied by a factor of  $10^{-4}$ .

The geometric parameter  $G$ , which is a measure of the exchange interaction between the copper centers in the polycrystalline state is calculated using the equation,

$$G = g_{\parallel} - 2.0023 / g_{\perp} - 2.0023 \text{ for axial spectra.}$$

For rhombic spectra,

$$G = g_3 - 2.0023 / g_{\perp} - 2.0023 \text{ where } g_{\perp} = (g_1 + g_2) / 2$$

If  $G > 4.4$ , exchange interaction is negligible and if  $G < 4.4$  considerable exchange interaction is indicated in the solid state [41,42]. Complexes **10** and **14** which gave axial spectra in solid state exhibited  $G$  values greater than 4.4 which indicate that exchange interaction between the metal centers is negligible.

From the EPR spectral data for these complexes it is clear that the  $g_{\parallel}$  values are nearly the same for all the complexes indicating that the bonding is dominated by the thiosemicarbazone moiety. Kivelson and Nieman have reported that  $g_{\parallel}$  values less than 2.3 indicate considerable covalent character to M-L bonds, while a value greater than 2.3 indicate ionic character. Here it is found that  $g_{\parallel} < 2.3$  showing significant covalent character to M-L bond [43,44]. The  $g_{av}$  values of all the complexes in the solution state are consistent with the  $g_{iso}$  values suggesting that they are not undergoing any kind of dissociation in the solution state.

The empirical factor,  $f = g_{\parallel} / A_{\parallel}$ , is an index of tetragonal distortion and it may vary from 105 to 135. In compound **10**,  $f$  falls in the range 105-135 which shows small to medium distortion from planarity [45].

### 5.3.6. X-ray crystallography

Single crystals of compounds  $[\text{CuL}^1\text{bipy}]$  (**10**) and  $[\text{CuL}^1(5,5'\text{-dmbipy})]\cdot\text{DMF}$  (**12**) suitable for X-ray diffraction studies were obtained by the slow evaporation of the mother liquors. Single crystals of dimensions  $0.35 \times 0.30 \times 0.25 \text{ mm}^3$  of the complex **10** and  $0.50 \times 0.40 \times 0.30 \text{ mm}^3$  of complex **12** were selected and mounted on a Bruker SMART APEXII CCD diffractometer, equipped with a graphite crystal, incident-beam monochromator and a fine focus sealed tube with Mo  $K\alpha$  ( $\lambda = 0.71073 \text{ \AA}$ ) radiation as the X-ray source. The crystallographic data and structure refinement parameters for compounds **10** and **12** are given in Table 5.5. The unit cell dimensions were measured and the data collection was performed at 296 K. Bruker SMART software was used for data acquisition and Bruker SAINT software for data integration [46]. Absorption corrections were carried out using SADABS based on Laue symmetry using equivalent reflections [47]. The structure was solved by direct methods using SHELXS97 [48] and refined by full-matrix least-squares calculations with SHELXL97 software package [49]. The molecular and crystal structures were plotted using DIAMOND version 3.2g [50].

In  $[\text{CuL}^1\text{bipy}]$  (**10**), all non-hydrogen atoms were refined anisotropically and all H atoms on C were placed in calculated positions, guided by difference maps, with C–H bond distances 0.93–0.96  $\text{\AA}$ . H atoms were assigned as  $U_{\text{iso}}=1.2U_{\text{eq}}$  (1.5 for Me). N3–H3' and N8–H8' H atoms were located from difference maps and their distances were restrained using DFIX instructions.

In  $[\text{CuL}^1(5,5'\text{-dmbipy})]\cdot\text{DMF}$  (**12**), all non-hydrogen atoms were refined anisotropically and all H atoms on C were placed in calculated positions, guided by difference maps, with C–H bond distances 0.93–0.96  $\text{\AA}$ . H atoms were assigned as  $U_{\text{iso}}=1.2U_{\text{eq}}$  (1.5 for Me). N3–H3' H atom was

located from difference maps and its distance was restrained using DFIX instruction.

**Table 5.5 Crystal data and structure refinement parameters for complexes 10 and 12**

Parameters	[CuL <sup>1</sup> bipy] (10)	[CuL <sup>1</sup> (5,5'-dmbipy)]-DMF (12)
Empirical formula	C <sub>25</sub> HBrCuN <sub>5</sub> O <sub>2</sub> S	C <sub>30</sub> H <sub>31</sub> BrCuN <sub>6</sub> O <sub>3</sub> S
Formula weight	578.82	699.12
Temperature	296 K	296 K
Wavelength	0.71073 Å	0.71073 Å
Crystal system	Triclinic	Monoclinic
Space group	$P\bar{1}$	$P2_1/c$
Unit cell dimensions	$a = 9.6577(6)$ Å $b = 14.2479(9)$ Å $c = 20.0690(13)$ Å $\alpha = 72.631(2)^\circ$ $\beta = 79.786(2)^\circ$ $\gamma = 82.073(2)^\circ$	$a = 12.5117(9)$ Å $b = 19.3540(13)$ Å $c = 13.0145(11)$ Å $\alpha = 90.00^\circ$ $\beta = 101.420(3)^\circ$ $\gamma = 90.00^\circ$
Volume	2583.2(3) Å <sup>3</sup>	3089.1(4) Å <sup>3</sup>
Z	4	4
Density (calculated)	1.488 Mg/m <sup>3</sup>	1.503 Mg/m <sup>3</sup>
Absorption coefficient	2.503 mm <sup>-1</sup>	2.110 mm <sup>-1</sup>
$F(000)$	1128	1428
Crystal size	0.35 x 0.30 x 0.25 mm <sup>3</sup>	0.50 x 0.40 x 0.30 mm <sup>3</sup>
$\theta$ range for data collection	1.07 to 22.00°	1.91 to 24.99°
Limiting indices	-10 ≤ h ≤ 10 -15 ≤ k ≤ 15 -21 ≤ l ≤ 21	-14 ≤ h ≤ 14 -22 ≤ k ≤ 23 -15 ≤ l ≤ 15
Reflections collected	39162	22763
Unique reflections	9066 [R(int) = 0.0457]	5414 [R(int) = 0.0353]
Refinement method	Full-matrix least-squares on F <sup>2</sup>	Full-matrix least-squares on F <sup>2</sup>
Data / restraints / parameters	9066 / 32 / 714	5414 / 1 / 388
Goodness-of-fit on F <sup>2</sup>	1.033	1.044
Final R indices [I > 2σ(I)]	R <sub>1</sub> = 0.0508, wR <sub>2</sub> = 0.1386	R <sub>1</sub> = 0.0327, wR <sub>2</sub> = 0.0823
R indices (all data)	R <sub>1</sub> = 0.0868, wR <sub>2</sub> = 0.1691	R <sub>1</sub> = 0.0488, wR <sub>2</sub> = 0.0914
Largest diff. peak and hole	1.265 and -0.683 e Å <sup>-3</sup>	0.755 and -0.462 e Å <sup>-3</sup>

$$R_1 = \frac{\sum ||F_o| - |F_c||}{\sum |F_o|}$$

$$wR_2 = [\frac{\sum w(F_o^2 - F_c^2)^2}{\sum w(F_o^2)^2}]^{1/2}$$

5.3.6a. Crystal structure of the compound [CuL<sup>1</sup>bipy] (10)

The compound [CuL<sup>1</sup>bipy] (10) crystallizes into a triclinic  $P\bar{1}$  space group with  $Z=4$ . In the asymmetric unit, two molecules are present and bond lengths and bond angles of these two are approximately the same. So the discussion is limited to one of the molecules. The copper atom in [CuL<sup>1</sup>bipy] (10) is coordinated by phenolato oxygen, O2, azomethine nitrogen, N1 and thioiminolato sulfur, S1 of the thiosemicarbazone and the pyridine nitrogens, N4 and N5 of bipyridine derivative and is having a distorted square pyramidal geometry. The asymmetric unit of the compound 10 along with atom numbering scheme is given in Fig. 5.26.

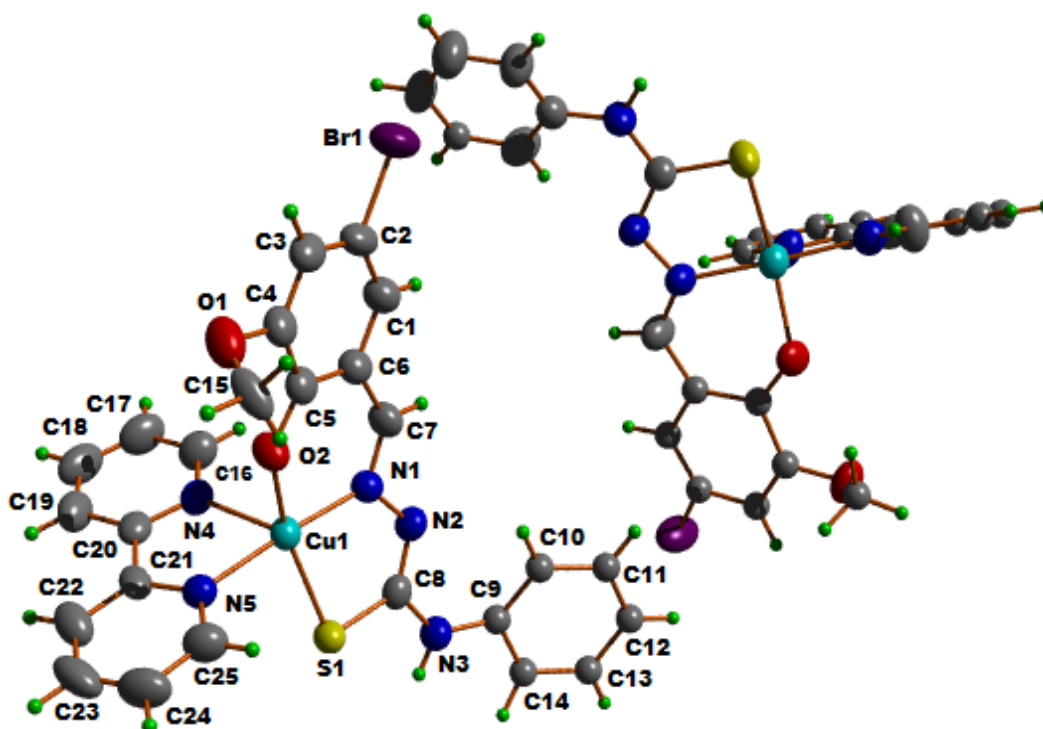


Fig. 5.26. Asymmetric unit of compound [CuL<sup>1</sup>bipy] (10).

In a five-coordinate system, the angular structural parameter ( $\tau$ ) is used to propose an index of trigonality. The value of  $\tau$  is defined by an equation represented by  $\tau = (\beta - \alpha)/60$ , where  $\beta$  is the greatest basal angle and  $\alpha$  is the second greatest basal angle;  $\tau$  is 0 for perfect square pyramidal forms and 1 for perfect trigonal bipyramidal forms [51,52]. However, in the case of five coordinate systems the structure varies from near regular trigonal bipyramidal (RTB) to near square based pyramidal (SBP). Since the value of  $\tau$  for the compound is 0.36, the coordination geometry around Cu(II) is best described as trigonal bipyramidal distorted square based pyramidal (TBDSBP) [53] with copper displaced 0.3109(6) Å above the N(1), N(5), S(1) and O(2) coordination plane and towards the elongated apical N(4) atom, at a larger distance of 2.198(5) Å. This value is larger than the normal Cu-N bond lengths reported [54,55]. One of the reasons for the deviation from an ideal stereochemistry is the restricted bite angle imposed by both the L<sup>2-</sup> and bipy ligands. The bite angle around the metal viz, N(4)-Cu(1)-N(5) of 77.94(19)° may be considered normal, when compared with an average value of 77° cited in the literature [56,57]. The O(2)-Cu(1)-N(4) bond angle, 99.14(18)°, and S(1)-Cu(1)-N(4) bond angle, 108.99(14), indicate a slight tilting of the apical Cu(1)-N(4) bond in the direction of the O(2)-Cu(1) bond and away from S(1)-Cu(1) bond. Some of the selected bond lengths and bond angles are given in Table 5.6.

**Table 5.6. Selected bond lengths (Å) and bond angles (°)**

Bond lengths		Bond angles		Bond angles	
Cu(1)–S(1)	2.2458(16)	N(1)–Cu(1)–O(2)	91.29(17)	C(25)–N(5)–C(21)	118.6(5)
Cu(1)–O(2)	1.940(4)	O(2)–Cu(1)–N(5)	91.82(17)	O(1)–C(4)–C(5)	120.8(5)
Cu(1)–N(1)	1.946(4)	N(1)–Cu(1)–N(5)	173.96(19)	N(3)–C(9)–C(14)	117.1(5)
Cu(1)–N(4)	2.198(5)	O(2)–Cu(1)–S(1)	151.86(13)	C(5)–O(2)–Cu(1)	121.3(3)
Cu(1)–N(5)	2.014(5)	O(2)–Cu(1)–N(4)	99.14(18)	C(8)–N(2)–N(1)	112.2(4)
S(1)–C(8)	1.731(5)	N(1)–Cu(1)–S(1)	85.01(13)	C(20)–N(4)–Cu(1)	111.8(4)
N(1)–N(2)	1.396(6)	N(1)–Cu(1)–N(4)	96.45(19)	O(2)–C(5)–C(6)	124.2(5)
N(4)–C(16)	1.331(8)	N(4)–Cu(1)–N(5)	77.94(19)	N(3)–C(8)–S(1)	115.7(4)
N(5)–C(25)	1.338(7)	N(5)–Cu(1)–S(1)	94.64(14)	C(8)–S(1)–Cu(1)	94.87(18)
N(2)–C(8)	1.301(7)	N(4)–Cu(1)–S(1)	108.99(14)	N(2)–N(1)–Cu(1)	121.8(3)
N(1)–C(7)	1.283(7)	C(8)–N(3)–C(9)	129.6(5)	C(16)–N(4)–Cu(1)	129.3(5)
N(3)–C(9)	1.399(7)	C(7)–N(1)–N(2)	114.7(5)		

The dihedral angle formed by the least square planes Cg(12) (comprising of atoms N4, C16, C17, C18, C19, C20) and Cg(13) (comprising of atoms N5, C21, C22, C23, C24, C25) is 7.9(4)° for the compound. Ring puckering analyses and least square plane calculations show that the Cg(3) ring comprising of atoms Cu(2), O(4), C(30), C(31), C(32) and N(6) adopts a screw boat conformation while Cg(11) ring comprising of atoms Cu(1), O(2), C(5), C(6), C(7) and N(1) and Cg(14) ring comprising of atoms C(1), C(2), C(3), C(4), C(5) and C(6) adopt a chair conformation. The unit cell packing diagram of this compound viewed along ‘a’ axis is shown in Fig. 5.27.

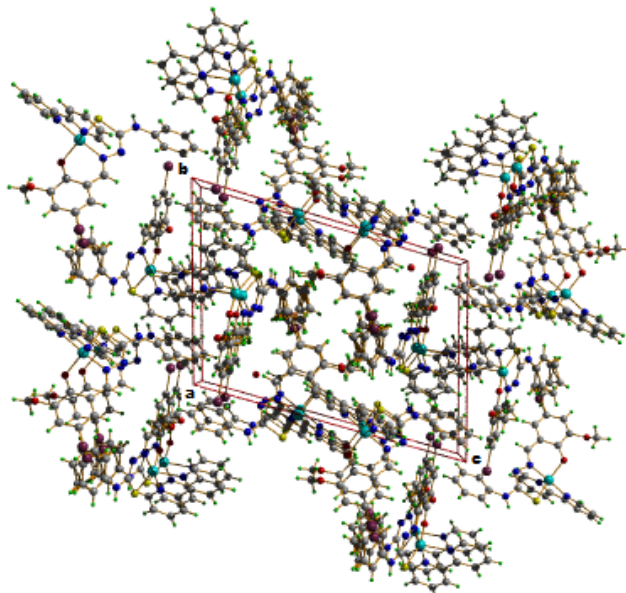


**Fig. 5.27. Packing diagram of compound [CuL<sup>1</sup>bipy] (10) along 'a' axis.**

The intermolecular hydrogen bonding interactions, N(3)–H(3')···S(2) and N(8)–H(8')···S(1) existing between the two molecules of the asymmetric unit give rise to centrosymmetric dimers in the crystal lattice (Fig 5.28). Non-classical hydrogen bonding interactions are also present. The  $\pi\cdots\pi$  interactions between Cg(4) (comprising of atoms N9, C41, C42, C43, C44, C45) and Cg(5) (comprising of atoms N10, C46, C47, C48, C49, C50) of neighboring molecules occur at a Cg···Cg distance of 3.685 Å.  $\pi\cdots\pi$  interactions are also present between rings Cg(12) and Cg(13) at a distance of 3.954(4) Å. C–H··· $\pi$  interactions also play an important role in the stabilization of the unit cell (Fig. 5.29). Additional non-covalent Y–X··· $\pi$  ring interaction is also found between C(2)–Br(1) and Cg(1) with  $d_{\text{Br}\cdots\text{Cg}} = 3.714(2)$  Å (Fig. 5.30). The various interaction parameters are shown in Table 5.7. The coordination polyhedra present in the unit cell is shown in Fig. 5.31.

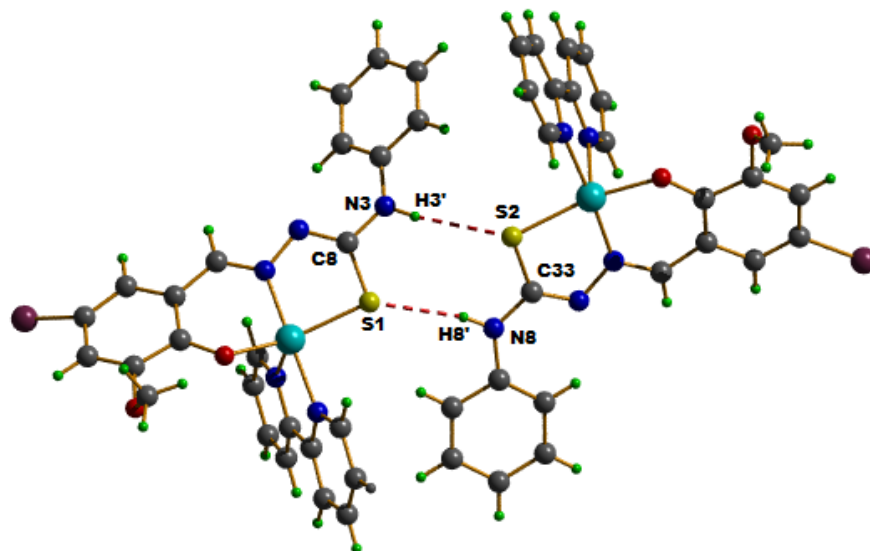


Fig. 5.28. Hydrogen bonds in [CuL<sup>1</sup>bipy] (10) shown as dotted lines.

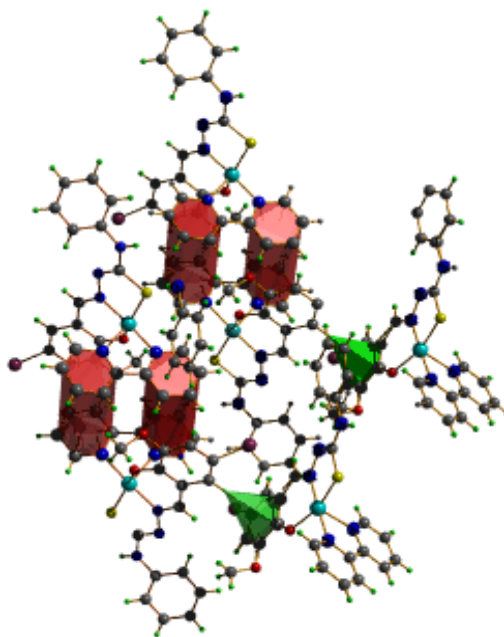


Fig 5.29. C-H $\cdots$  $\pi$  and  $\pi\cdots\pi$  interactions in [CuL<sup>1</sup>bipy] (10).

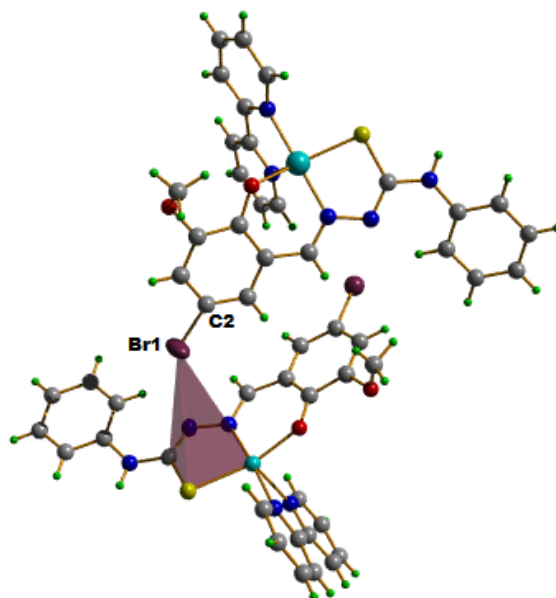


Fig. 5.30. C-Br... $\pi$  interaction in  $[\text{CuL}^1\text{bipy}]$  (10).

Table 5.7. Interaction parameters

H bonding				
D-H...A	D-H (Å)	H...A (Å)	D...A (Å)	D-H...A (°)
N(3)-H(3')...S(2) <sup>a</sup>	0.85(4)	2.63(4)	3.472(6)	173(5)
N(8)-H(8')...S(1) <sup>b</sup>	0.85(2)	2.57(3)	3.407(5)	167(5)
C(10)-H(10)...N(2)	0.93	2.41	2.905(7)	113
C(13)-H(13)...O(3) <sup>c</sup>	0.93	2.58	3.410(10)	149
C(18)-H(18)...S(1) <sup>d</sup>	0.93	2.81	3.719(8)	165
C(19)-H(19)...O(1) <sup>e</sup>	0.93	2.37	3.236(11)	154
C(44)-H(44)...O(3) <sup>f</sup>	0.93	2.48	3.296(8)	146
$\pi$ ... $\pi$ interactions				
Cg(I)...Cg(J)	Cg...Cg (Å)	$\alpha$ (°)	$\beta$ (°)	$\gamma$ (°)
Cg(4)...Cg(5) <sup>g</sup>	3.685	2.3(3)	25.91	23.65
Cg(12)...Cg(13) <sup>h</sup>	3.954(4)	7.9(4)	25.30	29.68
C-H... $\pi$ interactions				
C-H(I)...Cg(J)	H...Cg (Å)	C-H...Cg (°)	C...Cg (Å)	
C(1)-H(1)...Cg(6) <sup>i</sup>	2.97	163	3.865(8)	
C-Br... $\pi$ interactions				
Y-X(I)...Cg(J)	X...Cg (Å)	Y-X...Cg (°)	Y...Cg (Å)	
C(2)-Br(1)...Cg(1) <sup>j</sup>	3.714(2)	135.3(3)	5.241(9)	

Equivalent position codes : a = 1+x, -1+y, z, b = 1-x, 1-y, -z, c = -x, 2-y, -z, d = 1+x, y, z, e = 1-x, 2-y, 1-z, f = 1-x, 1-y, -z, g = 1-x, 1-y, -z, h = 1-x, 2-y, 1-z, i = x, y, z  
 Cg(4) = N(9), C(41), C(42), C(43), C(44), C(45); Cg(5) = N(10), C(46), C(47), C(48), C(49), C(50); Cg(12) = N(4), C(16), C(17), C(18), C(19), C(20); Cg(13) = N(5), C(21), C(22), C(23), C(24), C(25); Cg(6) = N(10), C(46), C(47), C(48), C(49), C(50); Cg(1) = Cu(2), S(2), C(33), N(7), N(6)  
 D = Donor, A = acceptor, Cg = Centroid  
 $\alpha$  ( $^\circ$ ) = Dihedral angle between planes I and J.  
 $\beta$  ( $^\circ$ ) = Angle between Cg(I)-Cg(J) vector and normal to plane I.  
 $\gamma$  ( $^\circ$ ) = Angle between Cg(I)-Cg(J) vector and normal to plane J.

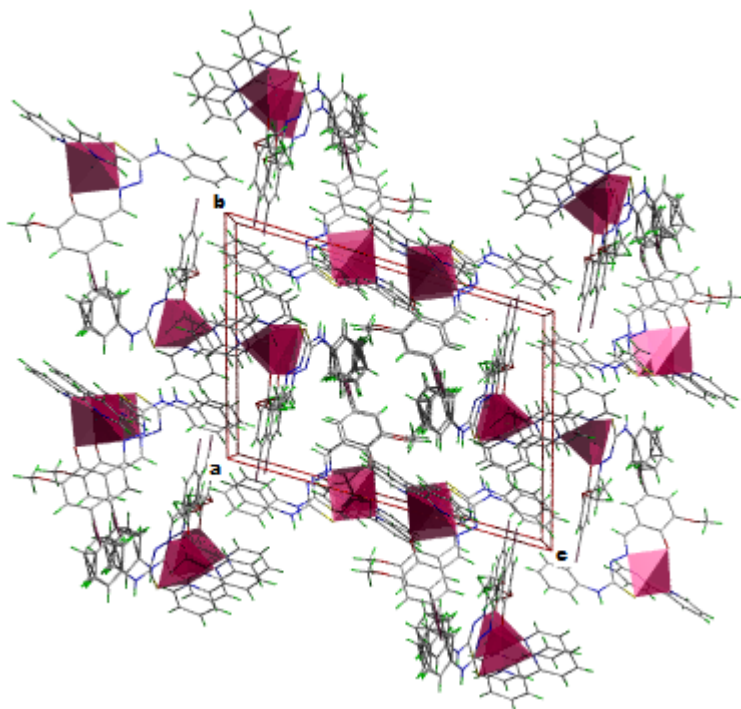


Fig. 5.31. Coordination polyhedra of [CuL<sup>1</sup>bipy] (10) in a unit cell.

### 5.3.6b. Crystal structure of the compound [CuL<sup>1</sup>(5,5'-dmbipy)]·DMF(12)

Dark green block like crystals of [CuL<sup>1</sup>(5,5'-dmbipy)]·DMF (12) suitable for X-ray diffraction studies were grown by slow evaporation of its mother liquor. The molecular structure of the compound along with atom numbering scheme is given in Fig. 5.32 and selected bond lengths and bond

angles are summarized in Table 5.8. The complex crystallizes into a monoclinic  $P2_1/c$  space group with  $Z=4$ . The copper in the mononuclear complex is five coordinated and is having a distorted square pyramidal geometry around copper(II) ion. The dianionic ligand, 5-bromo-3-methoxysalicylaldehyde-N(4)-phenylthiosemicarbazone is coordinated to copper centre through azomethine nitrogen N(1), phenolato oxygen O(2) and thioiminolato sulfur S(1) forming five and six membered rings.

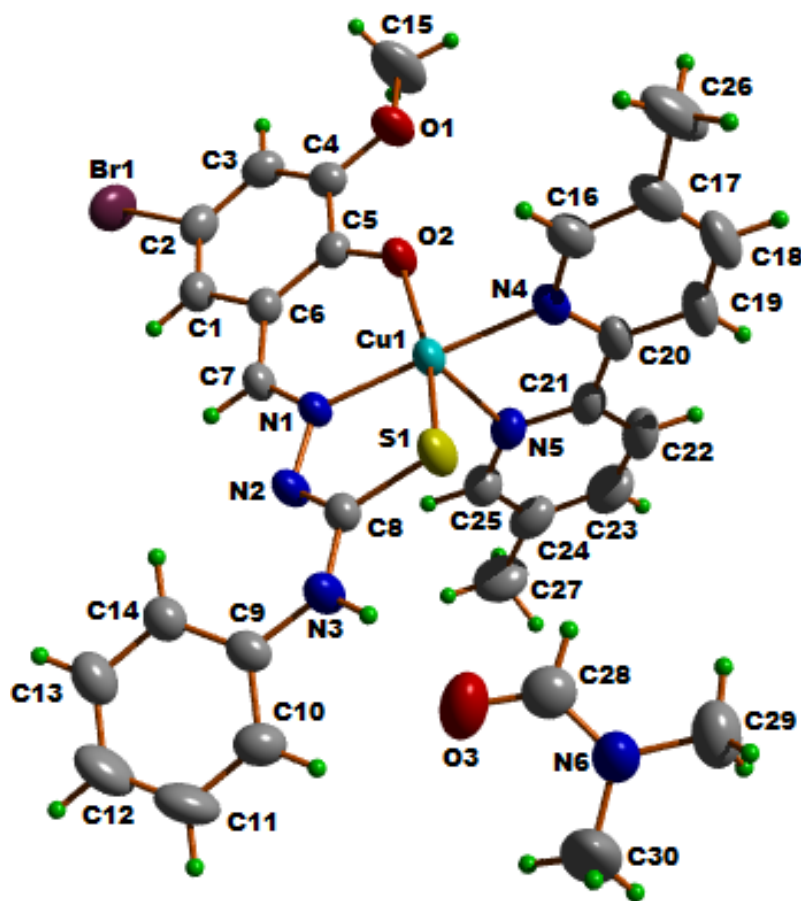


Fig. 5.32. Structure and labelling diagram for  $[\text{CuL}^1(5,5'\text{-dmbipy})]\cdot\text{DMF}$  (12).

Table 5.8. Selected bond lengths (Å) and bond angles (°)

Bond lengths		Bond angles		Bond angles	
Cu(1)–S(1)	2.2970(8)	N(1)–Cu(1)–O(2)	92.52(8)	C(25)–N(5)–C(21)	118.9(3)
Cu(1)–O(2)	1.946(2)	O(2)–Cu(1)–N(5)	99.98(9)	O(1)–C(4)–C(5)	114.2(2)
Cu(1)–N(1)	1.944(2)	N(1)–Cu(1)–N(5)	102.02(9)	N(3)–C(9)–C(14)	123.1(3)
Cu(1)–N(4)	2.038(2)	O(2)–Cu(1)–S(1)	159.47(7)	C(5)–O(2)–Cu(1)	126.82(17)
Cu(1)–N(5)	2.246(2)	O(2)–Cu(1)–N(4)	88.26(8)	C(8)–N(2)–N(1)	113.5(2)
S(1)–C(8)	1.737(3)	N(1)–Cu(1)–S(1)	84.29(6)	C(20)–N(4)–Cu(1)	118.4(2)
N(1)–N(2)	1.392(3)	N(1)–Cu(1)–N(4)	178.36(10)	O(1)–C(4)–C(3)	123.7(3)
N(4)–C(16)	1.334(4)	N(4)–Cu(1)–N(5)	76.43(10)	N(3)–C(8)–S(1)	116.2(2)
N(5)–C(25)	1.333(4)	N(5)–Cu(1)–S(1)	100.53(6)	C(8)–S(1)–Cu(1)	93.48(9)
N(2)–C(8)	1.294(3)	C(7)–N(1)–N(2)	113.4(2)	N(2)–N(1)–Cu(1)	120.83(16)
N(1)–C(7)	1.289(3)	C(8)–N(3)–C(9)	127.3(2)	C(16)–N(4)–Cu(1)	122.6(2)
N(3)–C(9)	1.412(4)				

The bond length of C(8)–S(1), 1.737(3) Å agrees with the coordinating pattern of thiosemicarbazone *via* thioiminolate form. The heterocyclic base 5,5'-dimethylbipyridine which acts as the coligand binds asymmetrically to Cu(II) as there is a longer Cu(1)–N(5) bond (axial) when compared with strongly bound Cu(1)–N(4) bond (equatorial) and forms a five membered chelate ring consisting of atoms Cu(1), N(4), C(20), C(21) and N(5). The Cu(1)–N(1) and Cu(1)–O(2) bond lengths are less than 2 Å and that of Cu(1)–S(1) and Cu(1)–N(4) are 2.2970(8) and 2.038(2) Å respectively indicating a strong coordination of 5,5'-dimethylbipyridine and the thiosemicarbazone to the metal center.

The five coordinated complex adopts a square pyramidal structure but deviates from a regular square pyramidal geometry as evidenced from the following observations. The apical and the basal coordination positions of the square pyramid are occupied by N(5), O(2), N(1), S(1) and N(4) atoms. The apical Cu(1)-N(5) bond is not exactly perpendicular to the basal plane as seen from the bond angles, N(5)-Cu(1)-N(1) (102.02°), N(5)-Cu(1)-O(2) (99.98°) etc. The equatorial bond angles deviate slightly from the expected value of 90.0° as given in Table 5.8. When these bond angles are summed it comes below 360° which illustrates that the basal portion has a little distortion from planarity and copper atom slightly shifted from the square plane. Also the two trans N atoms are at an angle of 178.36(10)° and the two trans S and O atoms are not completely linear, O(2)-Cu(1)-S(1) bond angle being 159.47(7)°.

The angular structural parameter  $\tau = 0.31 \{(\beta - \alpha)/60\}$ , shows that there is a small distortion from square pyramidal towards trigonal bipyramidal geometry of the complex. The Cu(II) center is shared by two fused five and six membered chelate rings Cg(1) {Cu1, N1, N2, C8, S1} and Cg(3) {Cu1, N1, C7, C6, C5, O2} with a dihedral angle of 13.01(9)° between them and another five membered chelate ring Cg(2) {Cu1, N4, C20, C21, N5} making dihedral angles of 84.08(10)° and 83.31(10)° with the above said five and six membered chelate rings respectively. From ring puckering analysis it is clear that the five membered ring Cg(1) {Cu1, N1, N2, C8, S1} is puckered and forms an envelope on Cu, the central metal atom [Q = 0.1976(16) Å,  $\phi = 180^\circ$ ]. The six membered chelate ring Cg(3) {Cu1, N1, C7, C6, C5, O2} exhibits an envelope conformation [Q = 0.1073(17),  $\phi = 2.3(16)^\circ$ ]. Thus the five coordinated complex exhibits a distorted square

pyramidal geometry and the significant deviation from regular square pyramidal geometry is evident from the values of bond lengths and bond angles (Table 5.8).

A strong classical intermolecular hydrogen bond, N(3)-H(3') $\cdots$ O(3) is present in the crystal structure in which the oxygen atom of the solvent dimethyl formamide acts as the acceptor (Fig. 5.33). Non classical hydrogen bonds are also present in the crystal structure. Rings Cg(3) and Cg(4) of neighboring molecules are involved in  $\pi\cdots\pi$  stacking with a distance of 3.880(13) Å,  $\beta = 20.52$  (Fig. 5.34). The unit cell packing diagram of the compound along 'c' axis is shown in Fig. 5.35. The coordination polyhedra present in the unit cell is shown in Fig. 5.36. The interaction parameters are listed in Table 5.9.

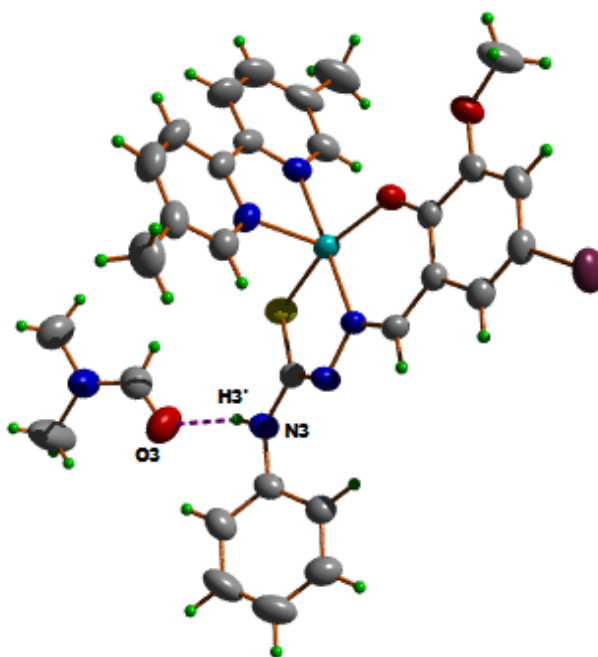


Fig. 5.33. Hydrogen bond shown as dotted line.

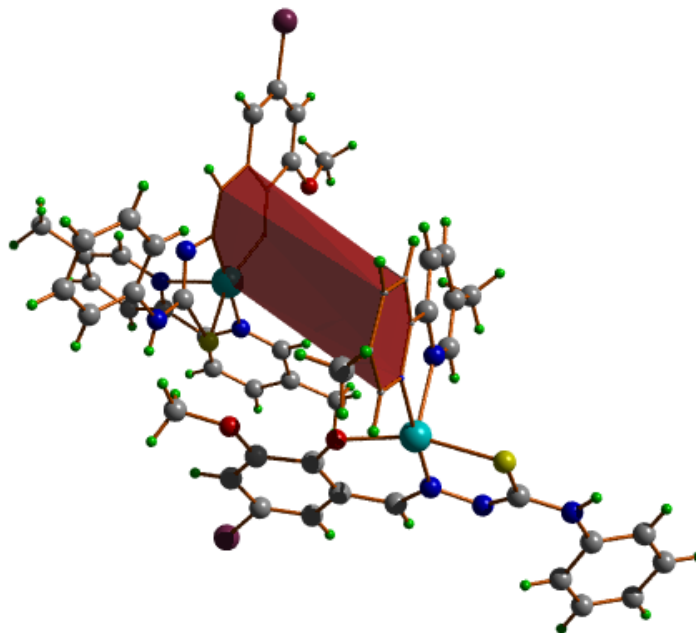


Fig 5.34.  $\pi \cdots \pi$  interactions in  $[\text{CuL}^1(5,5'\text{-dmbipy})]\cdot\text{DMF}$  (12).

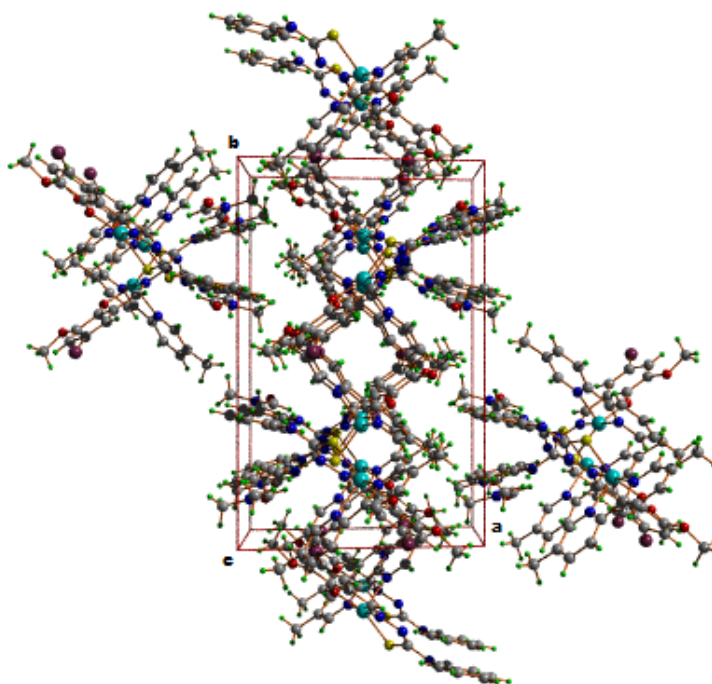


Fig. 5.35. Packing diagram of the compound along 'c' axis.

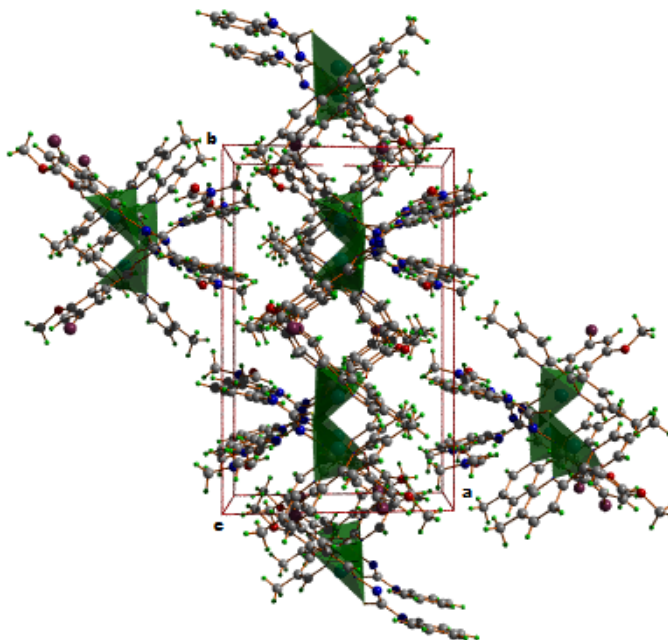
Fig 5.36. Coordination polyhedra of  $[\text{CuL}^1(5,5'\text{-dmbipy})]\cdot\text{DMF}$  (12) in a unit cell.

Table 5.9. Interaction parameters

H-bonding				
D-H...A	D-H (Å)	H...A (Å)	D...A (Å)	D-H...A (°)
N(3)-H(3')...O(3)	0.84(4)	2.11(2)	2.927(4)	165(2)
C(7)-H(7)...S(1) <sup>a</sup>	0.93	2.76	3.577(3)	148
C(10)-H(10)...O(3)	0.93	2.60	3.327(5)	136
C(14)-H(14)...N(2)	0.93	2.39	2.862(4)	111
C(23)-H(23)...O(1) <sup>b</sup>	0.93	2.42	3.119(4)	132
C(30)-H(30A)...O(3)	0.96	2.40	2.748(7)	101
π...π interactions				
Cg(I)...Cg(J)	Cg...Cg (Å)	α (°)	β (°)	γ (°)
Cg(3)...Cg(4) <sup>a</sup>	3.8800(13)	3.88	20.52	27.28

Equivalent position codes : a =  $x, \frac{1}{2}-y, -\frac{1}{2}+z$ , b =  $1-x, -y, 1-z$ ,

Cg(3) = Cu(1), O(2), C(5), C(6), C(7), N(1); Cg(4) = N(4), C(16), C(17), C(18), C(19), C(20)

D = Donor, A = acceptor, Cg = Centroid

α (°) = Dihedral angle between planes I and J.

β (°) = Angle between Cg(I)-Cg(J) vector and normal to plane I.

γ (°) = Angle between Cg(I)-Cg(J) vector and normal to plane J.

## References

- [1] F.A. Cotton, G. Wilkinson, C.A. Murillo, M. Bochmann, *Advanced Inorganic Chemistry*, 6<sup>th</sup> ed., Wiley, New York, 1999.
- [2] R.N. Mukherjee, *Indian J. Chem.* 42A (2003) 2175.
- [3] E.I. Solomon, M.J. Baldwin, M.D. Lowery, *Chem. Rev.* 92 (1992) 521.
- [4] S.P.J. Albracht, *Biochim. Biophys. Acta* 111 (1993) 317.
- [5] G.Z. Bahr, *Allg. Chem.* 268 (1952) 351A.
- [6] D.X. West, A.E. Liberta, S.B. Padhye, R.C. Chikate, P.B. Sonawane, A.S. Kumbhar, R.G. Yerande, *Coord. Chem. Rev.* 123 (1993) 49.
- [7] J. Easmon, G. Pürstinger, G. Heinisch, T. Roth, H.H. Fiebig, W. Holzer, W. Jäger, M. Jenny, J. Hofmann, *J. Med. Chem.* 44 (2001) 2164.
- [8] D.X. West, S.B. Padhye, P.S. Sonawane, *Struct Bonding* 76 (1991) 1.
- [9] H. Sigel (Ed.), *Metal ions in Biological Systems*, vol. 13, Marcel Dekker, New York. 1981.
- [10] T. Miura, A. Hori-I, H. Mototani, H. Takeuchi, *Biochemistry* 38 (1999) 11560.
- [11] V. Uma, M. Kanthimathi, T. Weyhermuller, B.U. Nair, *J. Inorg. Biochem.* 99 (2005) 2299.
- [12] R.W. Byrnes, M. Mohan, W.E. Antholine, R.X. Xu, D.H. Petering, *Biochemistry* 29 (1990) 7046.
- [13] H. Beraldo, L.P. Boyd, D.X. West, *Transit. Met. Chem.* 23 (1998) 67.

- [14] H. Beraldo, S.B. Kaisner, J.D. Turner, I.S. Billeh, J.S. Ives, D.X. West, *Transit. Met. Chem.* 22 (1997) 459.
- [15] W.J. Geary, *Coord. Chem. Rev.* 7 (1971) 81.
- [16] P.R. Athappan, G. Rajagopal, *Polyhedron* 15 (1996) 527.
- [17] G. Plesch, C. Friebel, *Polyhedron* 14 (1995) 1185.
- [18] M. Joseph, V. Suni, M.R.P. Kurup, M. Nethaji, A. Kishore, S.G. Bhat, *Polyhedron* 23 (2004) 3069.
- [19] A. Ali, M.T.H. Tarafdar, *J. Inorg. Nucl. Chem.* 39 (1977) 1785.
- [20] M.J.M. Campbell, *Coord. Chem. Rev.* 15 (1975) 279.
- [21] B.S. Garg, M.R.P. Kurup, S.K. Jain, Y.K. Bhoon, *Transit. Met. Chem.* 13 (1988) 247.
- [22] B.S. Garg, M.R.P. Kurup, S.K. Jain, Y.K. Bhoon, *Transit. Met. Chem.* 16 (1991) 111.
- [23] R. Mayer, *Organosulfur Chemistry*, M.J. Janssen, Ed.; Wiley-Interscience: Newyork, (1967) 219.
- [24] B.S. Garg, M.R.P. Kurup, S.K. Jain, Y.K. Bhoon, *Transit. Met. Chem.* 13 (1988) 309.
- [25] P. Bindu, M.R.P. Kurup, T.R. Satyakeerty, *Polyhedron* 18 (1999) 321.
- [26] I.-X. Li, H.-A. Tang, Yi-Zhi Li, M. Wang, L.-F. Wang, C.-G. Xia, J. *Inorg. Biochem.* 78 (2000) 167.
- [27] R.P. John, A. Sreekanth, M.R.P. Kurup, A. Usman, I.A. Razak, H.-K. Fun, *Spectrochim. Acta* 59A (2003) 1349.

- [28] M.A. Ali, D.A. Chowdhary, M. Nazimuddin, *Polyhedron* 3 (1984) 595.
- [29] V. Philip, V. Suni, M.R.P. Kurup, M. Nethaji, *Polyhedron* 24 (2005) 1133.
- [30] A.B.P. Lever, *Inorganic Electronic Spectroscopy*, 2<sup>nd</sup> ed., Elsevier, Amsterdam, 1984.
- [31] B.J. Hathaway, A.A.G. Tomlinson, *Coord. Chem. Rev.* 5 (1970) 24.
- [32] M.J.M. Campbell, *Coord. Chem. Rev.* 15 (1975) 279.
- [33] S. Stoll, *Spectral Simulations in Solid-State Electron Paramagnetic Resonance*, Ph.D. thesis, ETH, Zurich, 2003.
- [34] U.L. Kala, S. Suma, S. Krishnan, M.R.P. Kurup, R.P. John, *Polyhedron* 26 (2007) 1427.
- [35] A.W. Addison, T.N. Rao, J. Reedijk, J. Van Rijn, G.C. Verschoor, *J. Chem. Soc., Dalton Trans.* (1984) 1349.
- [36] M. Antosik, N.M.D. Brown, A.A. McConnell, A.L. Porte, *J. Chem. Soc. A* (1969) 545.
- [37]. B.J. Hathaway, *J. Chem. Soc., Dalton Trans.* (1972) 1196.
- [38] S. Thakurta, P. Roy, G. Rosair, C.J.G. -Garcia, E. Garriba, S. Mitra, *Polyhedron* 28 (2009) 695.
- [39] V.P. Singh, *Spectrochim. Acta Part A* 71 (2008) 17.

- [40] B.J. Hathaway, G. Wilkinson, R.D. Gillard, J.A. McCleverty (Eds.), *Comprehensive Coordination Chemistry*, Pergamon, Oxford, 5 (1987) 533.
- [41] A.H. Maki, B.R. McGarvey, *J. Chem. Phys.* 29 (1958) 35.
- [42] B.J. Hathaway, D.E. Billing, *Coord. Chem. Rev.* 5 (1970) 1949.
- [43] D. Kivelson, R. Nieman, *J. Chem. Soc., Dalton Trans.* 35 (1961) 149.
- [44] J.R. Wasson, C. Trapp, *J. Phys. Chem.* 73 (1969) 3763.
- [45] S.I. Findone, K.W.H. Stevens, *Proc. Phys. Soc.* 73 (1959) 116.
- [46] SMART and SAINT, Area Detector Software Package and SAX Area Detector Integration Program, Bruker Analytical X-ray; Madison, WI, USA, 1997.
- [47] SADABS, Area Detector Absorption Correction Program; Bruker Analytical X-ray; Madison, WI, USA, 1997.
- [48] G.M. Sheldrick, *Acta Crystallogr., Sect. A* 46 (1990) 467.
- [49] G.M. Sheldrick, SHELXL97 and SHELXS97, University of Göttingen, Germany, 1997.
- [50] K. Brandenburg, Diamond Version 3.2g, Crystal Impact GbR, Bonn, Germany, 2010.
- [51] A.W. Addison, T.N. Rao, J. Reedijk, J. Van Rijn, G.C. Verschoor, *J. Chem. Soc., Dalton Trans.* (1984) 1349.
- [52] G. Murphy, C.O. Sullivan, B. Murphy, B. Hathaway, *Inorg. Chem.* 37 (1998) 240.

*Syntheses, Crystal Structures and Spectral Aspects of Copper(II) Chelates  
Derived from ONS Donor Thiosemicarbazones*

---

- [53] M. Vaidyanathan, R. Balamurugan, U. Sivagnanam, M. Palaniandavar, *J. Chem. Soc., Dalton Trans.* (2001) 3498.
- [54] P.C. Chieh, G.J. Palenik, *Inorg. Chem.* 11 (1972) 816.
- [55] F. Clifford, E. Counihan, W. Fitzgerald, K. Seff, C. Simmons, S. Tyagi, B. Hathaway, *J. Chem. Soc., Chem. Commun.* (1982) 196.
- [56] N.J. Ray, B.J. Hathaway, *Acta Cryst. B*34 (1978) 3224.
- [57] G. Druhan, B.J. Hathaway, *Acta. Cryst. B*35 (1979) 344.

\*\*\*\*\*\*

**SYNTHESES, CRYSTAL STRUCTURES AND SPECTRAL ASPECTS OF ZINC(II) CHELATES DERIVED FROM ONS DONOR THIOSEMICARBAZONES**

6.1 Introduction  
6.2 Experimental  
6.3 Results and discussions  
**References**

**6.1. Introduction**

Zinc is a bluish-white, lustrous, diamagnetic metal [1]. It is somewhat less dense than iron and has a hexagonal crystal structure [2]. The metal is hard and brittle at most temperatures but becomes malleable between 100 and 150 °C [1,3]. Zinc is a fair conductor of electricity [1]. Its melting point is the lowest of all the transition metals aside from mercury and cadmium [4]. Many alloys contain zinc, including brass, an alloy of zinc and copper. Zinc makes up about 75 ppm (0.0075%) of the earth's crust, making it the 24<sup>th</sup> most abundant element and has five stable isotopes. The most common zinc ore is sphalerite (zinc blende), a zinc sulfide mineral. Zinc production includes froth floatation of the ore, roasting and final extraction using electricity (electrowinning). Alchemists burned zinc in air to form what they called "philosopher's wool" or "white snow". The element was probably named by the alchemist Paracelsus after

the German word *Zinke*. German chemist Andreas Sigismund Marggraf is normally given credit for discovering pure metallic zinc in 1746.

Zinc is an essential mineral of exceptional biologic and public health importance [5]. In children it causes growth retardation, delayed sexual maturation, infection susceptibility and diarrhea. Enzymes with a zinc atom in the reactive center are widespread in biochemistry, such as alcohol dehydrogenase in humans. Consumption of excess zinc can cause ataxia, lethargy and copper deficiency.

The biological activity of Zn(II) complexes of thiosemicarbazones mainly 2-pyridyl ketone thiosemicarbazone and *p*-isopropylbenzaldehyde thiosemicarbazone were reported earlier [6,7]. Zinc atom has either a structural or analytical role in several proteins. It has been recognized as an important cofactor in biological molecules, either as a structural template in protein folding or as a Lewis acid catalyst that can readily adopt 4-, 5- or 6-coordination [8]. Zinc is able to play a catalytic role in the activation of thiols as nucleophiles at physiological pH. Mononuclear zinc complexes may serve as model compounds for zinc enzymes such as phospholipase C, bovine lens leucine aminopeptidase, ATPases, carbonic anhydrases and peptide deformylase. Binuclear cores are versatile at active sites of many metalloenzymes and play essential role in biological systems.

The zinc(II) ion is known to have a high affinity towards nitrogen and sulfur donor ligands. Dowling and Perkin investigated Zn(II) complexes with mixed N, O and S coordination to understand the reactivity of the pseudotetrahedral zinc center in proteins [9]. The zinc(II) ion has been found to be of catalytic importance in enzymatic reactions [10]. The

enhancement of antitumor activity of some thiosemicarbazones in the presence of zinc(II) ions has been reported [11].

## 6.2. Experimental

### 6.2.1. Materials

Zinc(II) acetate dihydrate (E-Merck), 1,10-phenanthroline (phen), 2,2'-bipyridine (bipy), 4,4'-dimethyl-2,2'-bipyridine (4,4'-dmbipy), 5,5'-dimethyl-2,2'-bipyridine (5,5'-dmbipy) were used as received.

### 6.2.2. Syntheses of the thiosemicarbazones

The syntheses of thiosemicarbazones  $H_2L^1$  and  $H_2L^2$  are discussed already in Chapter 2.

### 6.2.3. Syntheses of the complexes

#### 6.2.3.1. $[ZnL^1]_2$ (18)

This complex was synthesized by refluxing a solution of  $H_2L^1$  (0.190 g, 0.5 mmol) in 1:1 (v/v) mixture of DMF and methanol with a methanolic solution of  $Zn(OAc)_2 \cdot 2H_2O$  (0.109 g, 0.5 mmol) for 3 hours. The complex formed was filtered, washed with methanol and dried *in vacuo*.

Elemental Anal. Found (Calcd.) (%): C, 40.83 (40.61); H, 3.06 (2.73); N, 9.66 (9.47); S, 7.46 (7.23). Yield: 70%

#### 6.2.3.2. $[ZnL^1phen]$ (19)

Methanolic solution of zinc(II) acetate dihydrate (0.109 g, 0.5 mmol) was added to a stirred mixture of  $H_2L^1$  (0.190 g, 0.5 mmol) in DMF and methanol (1:1 v/v) and 1,10-phenanthroline (0.099 g, 0.5 mmol) in methanol. The resultant homogenous yellow solution was refluxed for

three hours. The yellow product obtained was filtered, washed with methanol and dried *in vacuo*.

Elemental Anal. Found (Calcd.) (%) : C, 52.14 (51.98); H, 3.41 (3.23); N, 11.34 (11.23); S, 5.35 (5.14). Yield: 75%

#### 6.2.3.3. [ZnL<sup>1</sup>bipy] (20)

To a stirred mixture of H<sub>2</sub>L<sup>1</sup> (0.190 g, 0.5 mmol) in DMF and methanol (1:1 v/v) and 2,2'-bipyridine (0.078 g, 0.5 mmol) in methanol, zinc(II) acetate dihydrate (0.109 g, 0.5 mmol) was added. The resultant yellow solution was refluxed for 3 hours and the yellow product separated out was filtered, washed with methanol and dried *in vacuo*.

Elemental Anal. Found (Calcd.) (%) : C, 50.35 (50.06); H, 3.64 (3.36); N, 11.73 (11.68); S, 5.35 (5.35). Yield: 77%

#### 6.2.3.4. [ZnL<sup>1</sup>(4,4'-dmbipy)]·DMF (21)

To a stirred mixture of H<sub>2</sub>L<sup>1</sup> (0.190 g, 0.5 mmol) in DMF and methanol (1:1 v/v) and 4,4'-dimethyl-2,2'-bipyridine (0.092 g, 0.5 mmol) in methanol, methanolic solution of zinc(II) acetate dihydrate (0.109 g, 0.5 mmol) was added. The resultant yellow solution was refluxed for 3 hours and single crystals suitable for X-ray diffraction studies were obtained from mother liquor after three days.

Elemental Anal. Found (Calcd.) (%) : C, 51.30 (51.40); H, 4.54 (4.46); N, 11.56 (11.99); S, 4.84 (4.57). Yield: 83%

#### 6.2.3.5. [ZnL<sup>1</sup>(5,5'-dmbipy)] (22)

Methanolic solution of zinc(II) acetate dihydrate (0.109 g, 0.5 mmol) was added to a stirred mixture of H<sub>2</sub>L<sup>1</sup> (0.190 g, 0.5 mmol) in DMF and methanol (1:1 v/v) and 5,5'-dimethyl-2,2'-bipyridine (0.092 g, 0.5 mmol) in methanol. The resultant yellow solution was refluxed for three hours. The yellow product obtained was filtered, washed with methanol and dried *in vacuo*.

Elemental Anal. Found (Calcd.) (%): C, 51.45 (51.65); H, 3.57 (3.85); N, 11.31 (11.15); S, 4.97 (5.11). Yield: 78%

#### 6.2.3.6. [(ZnL<sup>2</sup>)<sub>2</sub>] (23)

This complex was synthesized by refluxing a solution of H<sub>2</sub>L<sup>2</sup> (0.193 g, 0.5 mmol) in 1:1 (v/v) mixture of DMF and methanol with a methanolic solution of Zn(OAc)<sub>2</sub>·2H<sub>2</sub>O (0.109 g, 0.5 mmol) for 3 hours. The complex formed was filtered, washed with methanol and dried *in vacuo*.

Elemental Anal. Found (Calcd.) (%): C, 40.25 (40.06); H, 3.88 (4.03); N, 9.68 (9.34); S, 6.86 (7.13). Yield: 72%

#### 6.2.3.7. [ZnL<sup>2</sup>phen] (24)

Methanolic solution of zinc(II) acetate dihydrate (0.109 g, 0.5 mmol) was added to a stirred mixture of H<sub>2</sub>L<sup>2</sup> (0.193 g, 0.5 mmol) in DMF and methanol (1:1 v/v) and 1,10-phenanthroline (0.099 g, 0.5 mmol) in methanol. The resultant homogenous yellow solution was refluxed for three hours. The yellow product obtained was filtered, washed with methanol and dried *in vacuo*.

Elemental Anal. Found (Calcd.) (%): C, 51.14 (51.48); H, 4.36 (4.16); N, 11.55 (11.12); S, 5.36 (5.09). Yield: 77%

#### 6.2.3.8. [ZnL<sup>2</sup>bipy] (25)

To a stirred mixture of H<sub>2</sub>L<sup>2</sup> (0.193 g, 0.5 mmol) in DMF and methanol (1:1 v/v) and 2,2'-bipyridine (0.078 g, 0.5 mmol) in methanol, zinc(II) acetate dihydrate (0.109 g, 0.5 mmol) was added. The resultant yellow solution was refluxed for 3 hours and the yellow product separated out was filtered, washed with methanol and dried *in vacuo*.

Elemental Anal. Found (Calcd.) (%): C, 49.69 (49.56); H, 4.66 (4.33); N, 11.87 (11.56); S, 5.51 (5.29). Yield: 69%

### 6.3. Results and discussion

Equimolar ratios of the thiosemicarbazones and the metal acetate yielded the light yellow colored complexes [(ZnL<sup>1</sup>)<sub>2</sub>] (**18**) and [(ZnL<sup>2</sup>)<sub>2</sub>] (**23**). The other compounds were prepared by using the heterocyclic bases like 1,10-phenanthroline, 2,2'-bipyridine, 4,4'-dimethylbipyridine and 5,5'-dimethylbipyridine. Single crystals of compound **21** could be isolated and the structure was established by single crystal XRD studies. The complexes were characterized by the following physico-chemical methods.

#### 6.3.1. Elemental analyses

From the observed C, H, N and S values, the above stoichiometry of the complexes were proposed.

### 6.3.2. Molar conductivity

The molar conductivities of the complexes in DMF ( $10^{-3}$  M) was measured at 298 K with a Systronic model 303 direct reading conductivity bridge. The molar conductivity measurements showed that all the complexes are non-electrolytic in nature since the observed values are less than  $10 \text{ ohm}^{-1}\text{cm}^2\text{mol}^{-1}$  which are very much less than the value of 65-90  $\text{ohm}^{-1}\text{cm}^2\text{mol}^{-1}$  reported for a 1:1 electrolyte in the same solvent [12].

**Table 6.1. Molar conductivity of Zn(II) complexes**

Compound	$\lambda_m^a$
$[(\text{ZnL}^1)_2]$ ( <b>18</b> )	2.0
$[\text{ZnL}^1\text{phen}]$ ( <b>19</b> )	4.0
$[\text{ZnL}^1\text{bipy}]$ ( <b>20</b> )	2.5
$[\text{ZnL}^1(4,4'\text{-dmbipy})]\cdot\text{DMF}$ ( <b>21</b> )	4.0
$[\text{ZnL}^1(5,5'\text{-dmbipy})]$ ( <b>22</b> )	3.5
$[(\text{ZnL}^2)_2]$ ( <b>23</b> )	2.0
$[\text{ZnL}^2\text{phen}]$ ( <b>24</b> )	4.3
$[\text{ZnL}^2\text{bipy}]$ ( <b>25</b> )	3.0

<sup>a</sup> =  $\text{mho cm}^2 \text{mol}^{-1}$

### 6.3.3. Infrared spectra

To clarify the mode of bonding, the IR spectra of the thiosemicarbazones and their Zn(II) complexes were studied and assigned on the basis of a careful comparison of the latter with the thiosemicarbazones. The tentative IR spectral assignments are listed in Table 6.2. The IR spectra of the thiosemicarbazones exhibit a medium band

at  $\sim 3305\text{ cm}^{-1}$  which is assigned to  $^2\text{NH}$  vibration. It disappears in the spectra of complexes providing strong evidence for ligand coordination to the metal in the deprotonated thioiminolate form [13]. The band corresponding to azomethine bond,  $\nu(\text{C}=\text{N})$ , shifts to higher energy on coordination due to the combination of  $\nu(\text{C}=\text{N})$  with the newly formed  $\text{C}=\text{N}$  bond which results from the loss of the thioamide hydrogen from the thiosemicarbazone moiety [14-18]. The involvement of this nitrogen in bonding is also supported by a shift in  $\nu(\text{N}-\text{N})$  to higher frequencies. Coordination *via* the thioiminolate sulfur is indicated by the negative shift of the two bands assigned to  $\nu(\text{C}=\text{S})$  and  $\delta(\text{C}=\text{S})$  vibrations. Some of the IR spectra of the Zn(II) complexes are depicted in Figs. 6.1-6.6.

**Table 6.2. IR spectral assignments ( $\text{cm}^{-1}$ ) of thiosemicarbazones and their Zn(II) complexes**

Compound	$\nu(\text{O}-\text{H})$	$\nu(\text{C}=\text{N})$	$\nu(\text{C}=\text{N})^a$	$\nu(\text{N}-\text{N})$	$\nu(\text{C}=\text{S})/\nu(\text{C}-\text{S}),$ $\delta(\text{C}=\text{S})/\delta(\text{C}-\text{S})$	$\nu(\text{C}-\text{O})$	$\nu(\text{Zn}-\text{O})$	$\nu(\text{Zn}-\text{N})$
$\text{H}_2\text{L}^1$	3441	1540	---	1071	1333, 857	1267	---	---
$[\text{ZnL}^1]_2$ (18)	---	1603	1523	1112	1318, 833	1237	498	435
$[\text{ZnL}^1\text{phen}]$ (19)	---	1595	1535	1102	1306, 766	1232	502	458
$[\text{ZnL}^1\text{bipy}]$ (20)	---	1599	1481	1100	1306, 766	1228	502	454
$[\text{ZnL}^1(4,4'\text{-dmbipy})]\cdot\text{DMF}$ (21)	---	1608	1539	1093	1316, 832	1228	502	460
$[\text{ZnL}^1(5,5'\text{-dmbipy})]$ (22)	---	1608	1539	1096	1316, 834	1237	504	470
$\text{H}_2\text{L}^2$	3454	1539	---	1067	1342, 851	1257	---	---
$[\text{ZnL}^2]_2$ (23)	---	1597	1556	1101	1328, 811	1225	500	459
$[\text{ZnL}^2\text{phen}]$ (24)	---	1589	1535	1110	1315, 806	1232	482	441
$[\text{ZnL}^2\text{bipy}]$ (25)	---	1590	1542	1097	1322, 821	1233	480	436

<sup>a</sup> = newly formed  $\text{C}=\text{N}$  bond

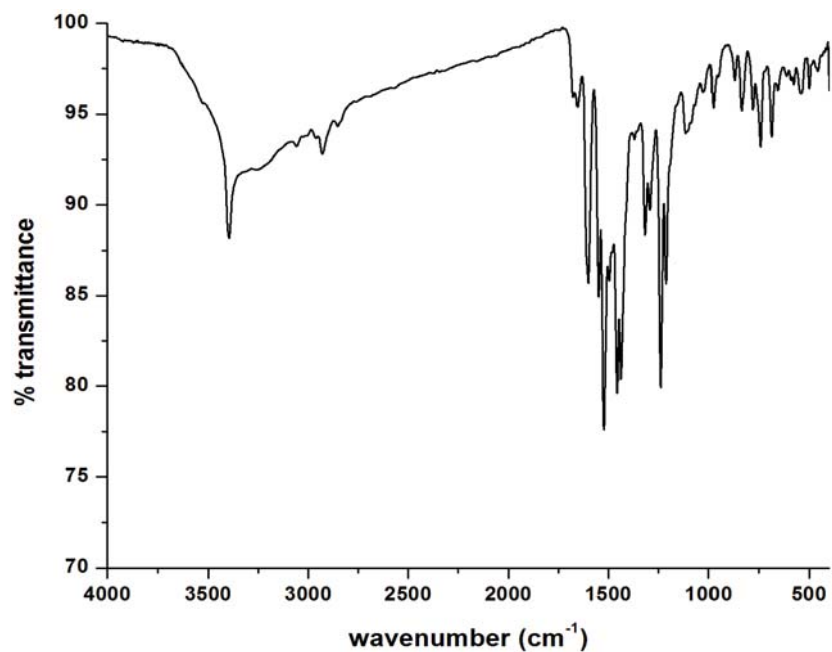


Fig. 6.1. Infrared spectrum of  $[(ZnL^1)_2]$  (18).

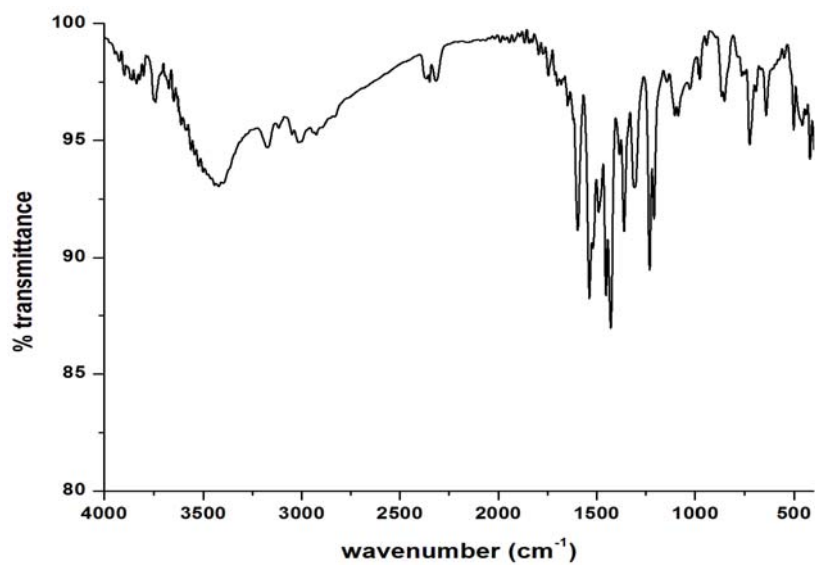


Fig. 6.2. Infrared spectrum of  $[ZnL^1phen]$  (19).

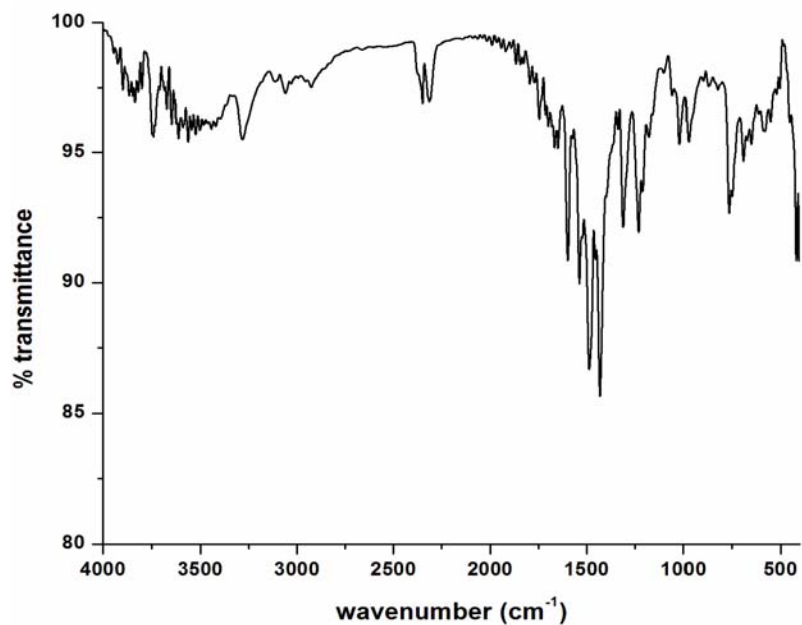


Fig. 6.3. Infrared spectrum of  $[ZnL^1bipy]$  (20).

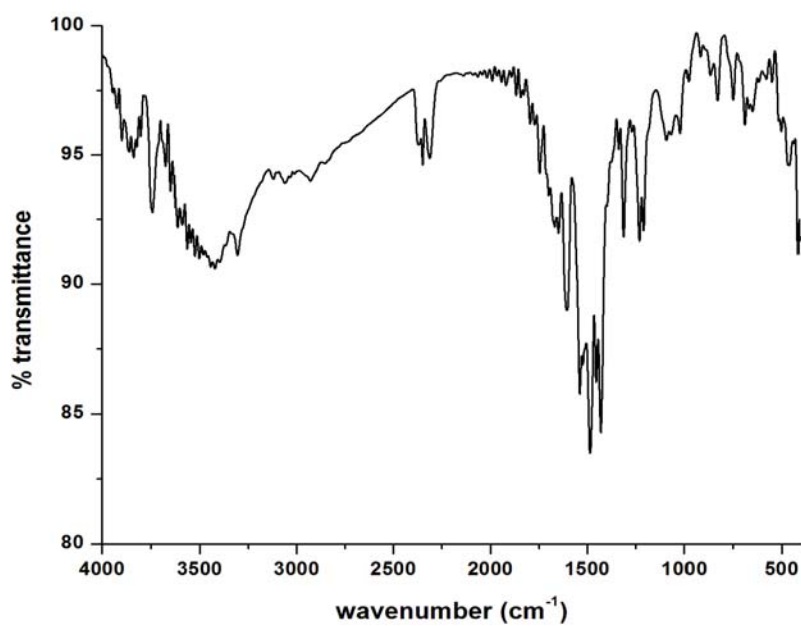


Fig. 6.4. Infrared spectrum of  $[ZnL^1(4,4'-dmbipy)] \cdot DMF$  (21).

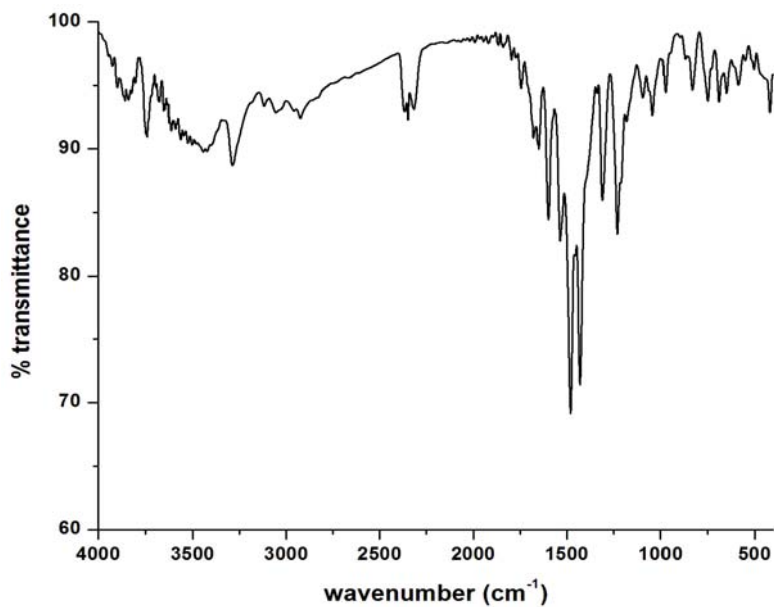


Fig. 6.5. Infrared spectrum of  $[\text{ZnL}^1(5,5'\text{-dmbipy})]$  (22).

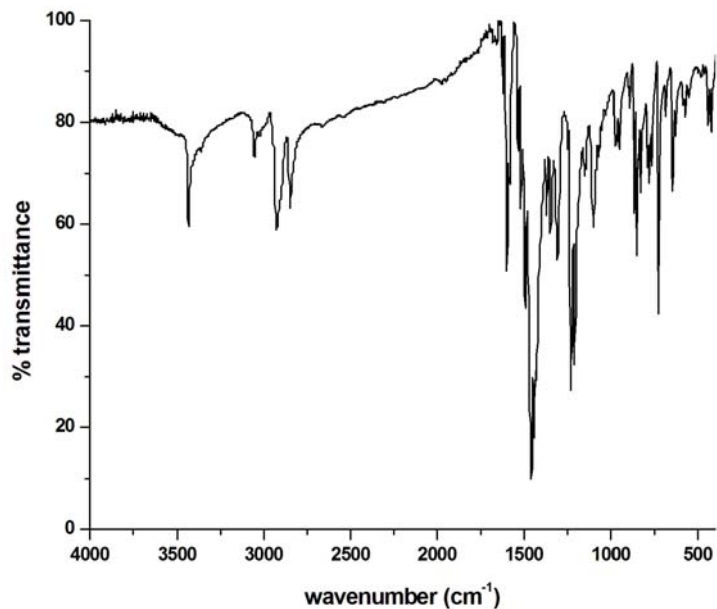


Fig. 6.6. Infrared spectrum of  $[\text{ZnL}^2\text{phen}]$  (24).

### 6.3.4. Electronic spectra

Electronic spectroscopy is an important and valuable tool for chemists to draw important information about the structural aspects of complexes. The UV-vis spectra of the Zn(II) complexes were studied in DMF. The bands in the range 28700-30590  $\text{cm}^{-1}$  in the electronic spectra of thiosemicarbazones due to  $\pi \rightarrow \pi^*$  and  $n \rightarrow \pi^*$  transitions suffered marginal shifts upon complexation. This may be due to the weakening of the C=S bond and the extension of conjugation upon complexation [19]. The shift occurs also due to coordination *via* phenolic oxygen and azomethine nitrogen [20] and is an indication of the enolization followed by the deprotonation of the ligands during complexation. In addition to this, a new band in the range 24300-25170  $\text{cm}^{-1}$  is observed in the spectra of complexes and this can be assigned to the  $\text{O}_{\text{phenolate}} \rightarrow \text{Zn}$ ,  $\text{N}_{\text{azomethine}} \rightarrow \text{Zn}$  and  $\text{S} \rightarrow \text{Zn}$  LMCT transitions [21,22]. The electronic spectral data of the Zn(II) complexes are given in Table 6.3. Figs. 6.7 and 6.8 represent the electronic spectra of the complexes.

**Table 6.3. Electronic spectral assignments ( $\text{cm}^{-1}$ ) of thiosemicarbazones and their Zn(II) complexes**

Compound	$n \rightarrow \pi^* / \pi \rightarrow \pi^*$	LMCT
$\text{H}_2\text{L}^1$	28770, 30490	----
$[(\text{ZnL}^1)_2]$ (18)	29160, 30590	24600
$[\text{ZnL}^1\text{phen}]$ (19)	29160, 30530	24480
$[\text{ZnL}^1\text{bipy}]$ (20)	29100, 30590	24650
$[\text{ZnL}^1(4,4'\text{-dmbipy})] \cdot \text{DMF}$ (21)	29100, 30590	24650
$[\text{ZnL}^1(5,5'\text{-dmbipy})]$ (22)	28700, 29960	24300
$\text{H}_2\text{L}^2$	29300, 30490	----
$[(\text{ZnL}^2)_2]$ (23)	29620, 30980	25170
$[\text{ZnL}^2\text{phen}]$ (24)	29670, 31040	25170
$[\text{ZnL}^2\text{bipy}]$ (25)	29670, 30990	25170

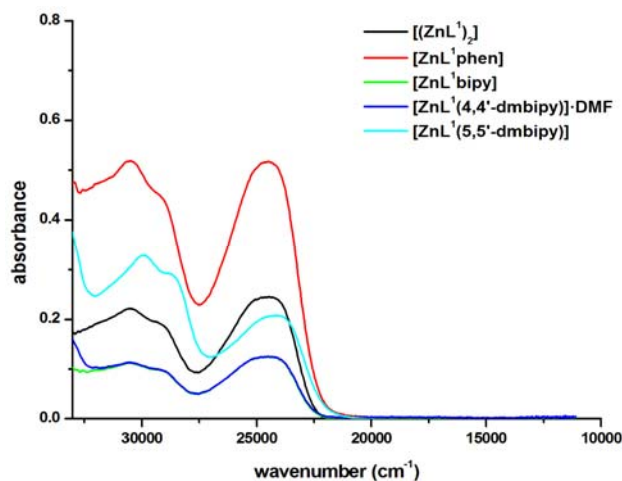


Fig. 6.7. Electronic spectra of Zn(II) complexes of  $H_2L^1$ .

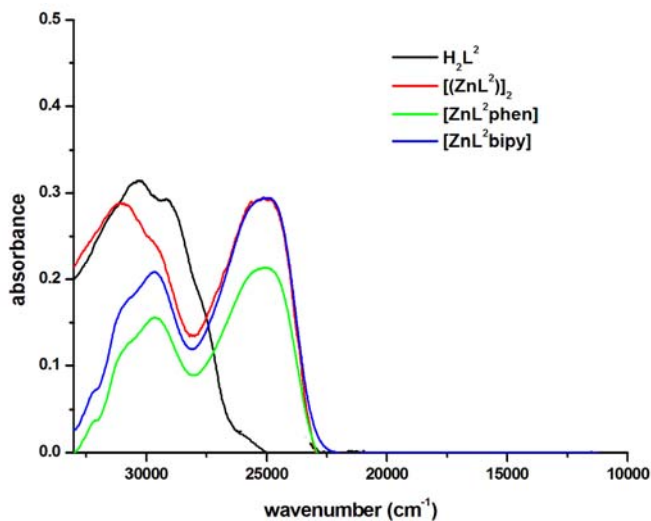


Fig. 6.8. Electronic spectra of Zn(II) complexes of  $H_2L^2$ .

### 6.3.5. X-ray crystallography

#### 6.3.5a. Crystal structure of the compound $[ZnL^1(4,4'-dmbipy)] \cdot DMF$ (21)

Single crystals of the complex **21** suitable for X-ray diffraction studies were obtained by slow evaporation of the mother liquor over 3 days. The

crystallographic data and structure refinement parameters for the complex are given in Table 6.4.

**Table 6.4 Crystal data and structure refinement parameters for complex 21**

Parameters	[ZnL <sup>1</sup> (4,4'-dmbipy)]-DMF (21)
Empirical formula	C <sub>30</sub> H <sub>31</sub> BrN <sub>6</sub> O <sub>3</sub> SZn
Formula weight	700.95
Temperature	293 K
Wavelength	0.71073 Å
Crystal system	Monoclinic
Space group	<i>P</i> 2 <sub>1</sub>
Unit cell dimensions	<i>a</i> = 15.2674(3) Å <i>b</i> = 12.2422(3) Å <i>c</i> = 22.3402(5) Å $\alpha$ = 90° $\beta$ = 131.425(10)° $\gamma$ = 90°
Volume	3130.90(12) Å <sup>3</sup>
Z	4
Density (calculated)	1.487 Mg/m <sup>3</sup>
Absorption coefficient	2.168 mm <sup>-1</sup>
<i>F</i> (000)	1432
Crystal size	0.40 x 0.30 x 0.25 mm <sup>3</sup>
$\theta$ range for data collection	2.47 to 26.31°
Limiting indices	-19 ≤ <i>h</i> ≤ 19, -15 ≤ <i>k</i> ≤ 15, -29 ≤ <i>l</i> ≤ 28
Reflections collected	52133
Independent reflections	14238 [R(int) = 0.0505]
Refinement method	Full-matrix least-squares on <i>F</i> <sup>2</sup>
Data / restraints / parameters	14238 / 66 / 676
Goodness-of-fit on <i>F</i> <sup>2</sup>	1.011
Final R indices [ <i>I</i> > 2 $\sigma$ ( <i>I</i> )]	R <sub>1</sub> = 0.0697, wR <sub>2</sub> = 0.1751
R indices (all data)	R <sub>1</sub> = 0.1204, wR <sub>2</sub> = 0.2105
Largest diff. peak and hole	1.22 and -1.64 e Å <sup>-3</sup>

$$R_1 = \frac{\sum ||F_o| - |F_c||}{\sum |F_o|}$$

$$wR_2 = [\sum w(F_o^2 - F_c^2)^2 / \sum w(F_o^2)^2]^{1/2}$$

A yellow prism like crystal of the compound having approximate dimensions of  $0.40 \times 0.30 \times 0.25 \text{ mm}^3$  was selected. The unit cell parameters were determined and the data collections were performed on a Bruker SMART APEXII CCD diffractometer with graphite-monochromated Mo K $\alpha$  ( $\lambda = 0.71073 \text{ \AA}$ ) radiation at the Sophisticated Analytical Instruments facility (SAIF), Cochin University of Science and Technology, Kochi-22, Kerala, India. The programs SAINT and XPREP were used for data reduction and APEX2 and SAINT were used for cell refinement [23]. The structure was solved by direct methods using SHELXS97 [24] and refined by full-matrix least-squares refinement on  $F^2$  using SHELXL97 [25]. The molecular and crystal structures were plotted using DIAMOND version 3.2g [26] and X-SEED [27].

Carbon and nitrogen bound H-atoms were placed in calculated positions (C-H 0.93 to 0.96  $\text{\AA}$ , N-H 0.88  $\text{\AA}$ ) and were included in the refinement in the riding model approximation, with  $U(\text{H})$  set to 1.2 to 1.5  $U(\text{C,N})$ . Omitted owing to bad disagreement was (0 1 1). All aromatic and pyridine rings were refined as rigid hexagons of 1.39  $\text{\AA}$  sides. One of the phenyl rings of the thiosemicarbazone is disordered over two positions in a 1:1 ratio. The temperature factors of the primed atoms were set to those of the unprimed ones but in the reverse order (*i.e.*, those of C11 to those of C15), and the pair of N-C<sub>phenyl</sub> distances were restrained to within 0.01  $\text{\AA}$  of each other. The molecules of DMF were each restrained to lie on a plane. The anisotropic temperature factors were restrained to be nearly isotropic. The final difference Fourier map had a peak at 0.91  $\text{\AA}$  from Br1 and a hole at 0.96  $\text{\AA}$  from Br2. The base scale factor was explicitly refined.

The zinc homolog has been isolated as a 2,2'-bipyridine adduct [28]. The compound crystallizes as a DMF solvate. The asymmetric unit of the compound,  $[\text{Zn}(\text{C}_{15}\text{H}_{12}\text{BrN}_3\text{O}_2\text{S})(\text{C}_{12}\text{H}_{12}\text{N}_2)]\text{C}_3\text{H}_7\text{NO}$  (**21**) contains two independent molecules with a similar structure. In one molecule, Zn is displaced by 0.305(3) Å in the direction of the apical occupant (Fig. 6.9) whereas in the other, the displacement is 0.103(6) Å in the opposite direction (Fig. 6.10).

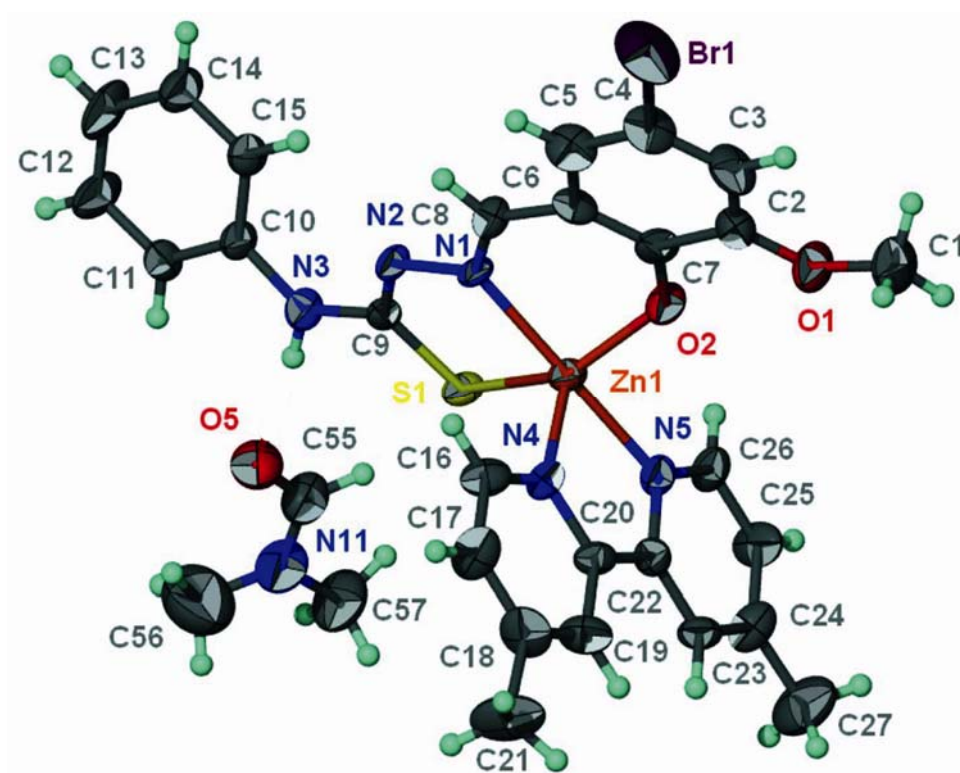


Fig. 6.9. Thermal ellipsoid plot of one  $[\text{ZnL}^1(4,4'\text{-dmbipy})]\cdot\text{DMF}$  molecule at the 50% probability level; hydrogen atoms are drawn as spheres of arbitrary radius. The disorder in one of the phenyl rings is not shown.

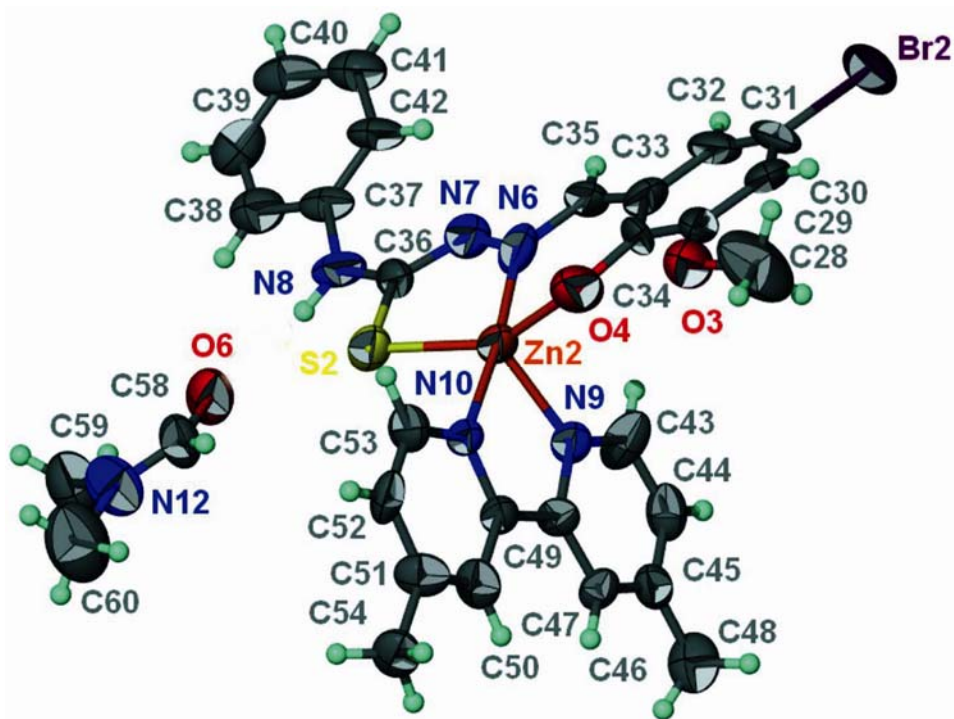


Fig. 6.10. Thermal ellipsoid plot of second  $[\text{ZnL}^1(4,4'\text{-dmbipy})]\cdot\text{DMF}$  molecule at the 50% probability level; hydrogen atoms are drawn as spheres of arbitrary radius. The disorder in one of the phenyl rings is not shown.

The metal center shows square pyramidal coordination. Substituents in the thiosemicarbazone as well as 2,2'-bipyridine do not perturb the square pyramidal coordination geometry in  $[\text{Zn}(\text{C}_{12}\text{H}_{12}\text{N}_2)(\text{C}_{15}\text{H}_{12}\text{BrN}_3\text{O}_2\text{S})]\cdot\text{DMF}$ . The doubly deprotonated Schiff base ligand O,N,S-chelates to the metal atom and the three coordinating atoms along with one N atom of the substituted 2,2'-bipyridine constitute the square plane of the distorted square pyramid surrounding the metal atom. The apical site is occupied by the second N atom of the substituted 2,2'-bipyridine. The secondary amine group of the Schiff base dianion forms a hydrogen bond to the O atom of the dimethylformamide solvent (Fig. 6.11). In the crystal, the phenyl ring

of one of the two thiosemicarbazones is disordered over two positions in a 1:1 ratio. The crystal is found to be a racemic twin. The packing diagram of the compound is shown in Fig. 6.12. The coordination polyhedra present in the unit cell is shown in Fig. 6.13. Selected bond distances and bond angles are given in Table 6.5 and interaction parameters are given in Table 6.6.

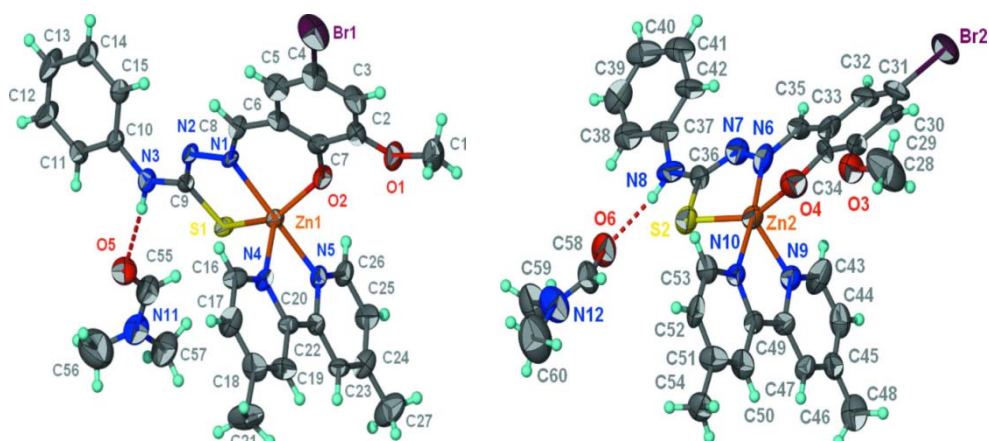


Fig. 6.11. Hydrogen bonding interactions shown as dotted lines.

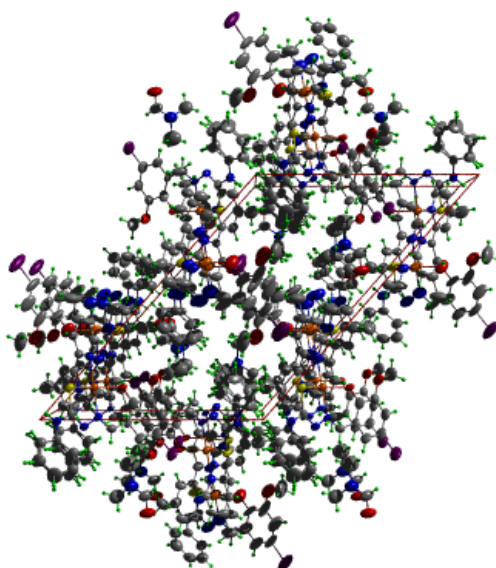


Fig. 6.12. Packing diagram along 'b' axis.

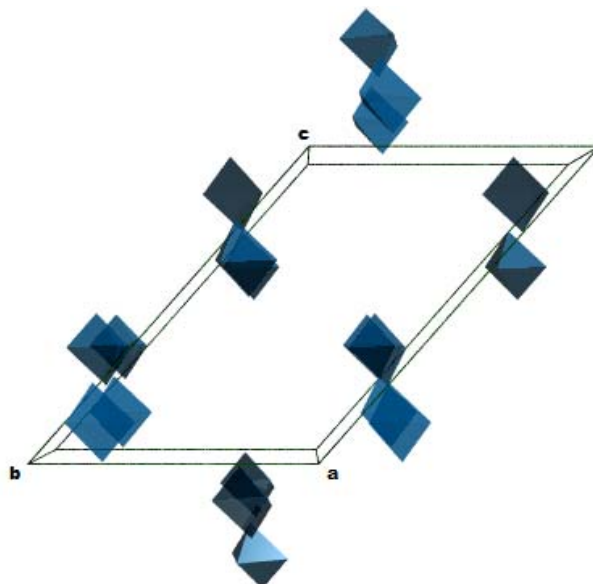


Fig. 6.13. Coordination polyhedra in a unit cell.

**Table 6.5 Selected bond lengths and angles for complex 21**

Bond lengths (Å)		Bond angles (°)		Bond angles (°)	
Zn(1)–S(1)	2.353(2)	N(1)–Zn(1)–O(2)	87.7(2)	C(22)–N(5)–C(26)	120.0
Zn(1)–O(2)	1.987(6)	O(2)–Zn(1)–N(5)	93.9(2)	O(1)–C(2)–C(3)	124.2(5)
Zn(1)–N(1)	2.124(6)	N(1)–Zn(1)–N(5)	176.3(3)	N(1)–C(8)–C(6)	128.3(8)
Zn(1)–N(5)	2.134(4)	O(2)–Zn(1)–S(1)	148.2(2)	C(7)–O(2)–Zn(1)	126.8(4)
S(1)–C(9)	1.765(10)	O(2)–Zn(1)–N(4)	103.2(3)	C(9)–N(2)–N(1)	114.2(6)
N(1)–N(2)	1.388(9)	N(1)–Zn(1)–S(1)	82.0(2)	C(20)–N(4)–Zn(1)	114.9(3)
N(4)–C(16)	1.390	N(1)–Zn(1)–N(4)	104.9(3)	O(1)–C(2)–C(3)	124.2(5)
N(5)–C(26)	1.390	N(4)–Zn(1)–N(5)	78.0(2)	N(3)–C(9)–S(1)	111.4(7)
N(2)–C(9)	1.251(11)	N(5)–Zn(1)–S(1)	94.97(17)	C(9)–S(1)–Zn(1)	93.8(3)
N(1)–C(8)	1.246(11)	C(8)–N(1)–N(2)	117.1(7)	N(2)–N(1)–Zn(1)	119.5(5)
N(3)–C(9)	1.401(11)	C(9)–N(3)–C(10)	130.1(11)	C(16)–N(4)–Zn(1)	125.1(3)
Zn(1)–N(4)	2.088(4)				

Table 6.6. Interaction parameters

H bonding				
D-H...A	D-H (Å)	H...A (Å)	D...A (Å)	D-H...A (°)
N(3)-H(3)...O(5)	0.88	2.07	2.950(10)	175
N(8)-H(8)...O(6)	0.88	2.07	2.950(10)	172
C(15)-H(15)...N(2)	0.93	2.39	2.954(17)	119
C(17)-H(17)...O(5)	0.93	2.52	3.089(10)	120
C(19)-H(19)...O(3)	0.93	2.35	3.168(14)	146
C(42)-H(42)...N(7)	0.93	2.31	2.917(15)	123
C(46)-H(46)...O(1)	0.93	2.34	3.204(11)	154

D = Donor, A = acceptor, Cg = Centroid

### References

- [1] D.R. Lide, Handbook of Chemistry and Physics, 87<sup>th</sup> ed. CRC Press, Taylor & Francis, Boca Raton, Florida, 2006.
- [2] R.S. Lehto, Zinc, In Clifford A. Hampel, The Encyclopedia of the Chemical Elements, New York: Reinhold Book Corporation (1968) 822.
- [3] D.L. Heiserman, Element 30: Zinc, Exploring Chemical Elements and their Compounds. New York: TAB Books, 1992.
- [4] "Zinc Metal Properties", American Galvanizers Association, 2008.
- [5] K.M. Hambidge, N.F. Krebs, J. Nutr. 137 (2007) 1101.
- [6] Q. Li, H. Tang, Y. Li, M. Wang, L. Wang, C. Xia, J. Inorg. Biochem. 78 (2000) 167.
- [7] J.M. Perez, A.I. Matesanz, A. Martine-Ambite, P. Navaro, C. Alonso, P. Souza, J. Inorg. Biochem. 75 (1999) 255.

- [8] K. Peariso, C.W. Goulding, S. Huang, R.G. Mathews, J.E. Penner-Hahn, *J. Am. Chem. Soc.* 120 (1998) 8410.
- [9] C. Dowling, G. Perkin, *Polyhedron* 15 (1996) 2463.
- [10] M.B. Ferrari, G.G. Fava, C. Pelizzic, P. Tarasconi, *J. Chem. Soc., Dalton Trans.* (1992) 2153.
- [11] D. Solaiman, L. Saryan, D.H. Petering, *J. Inorg. Biochem.* 10 (1979) 135.
- [12] W.J. Geary, *Coord. Chem. Rev.* 7 (1971) 81.
- [13] V. Philip, V. Suni, M.R.P. Kurup, M. Nethaji, *Spectrochim. Acta Part A* 64 (2006) 171.
- [14] G. Plesch, C. Friebel, *Polyhedron* 14 (1995) 1185.
- [15] M. Joseph, V. Suni, M.R.P. Kurup, M. Nethaji, A. Kishore, S.G. Bhat, *Polyhedron* 23 (2004) 3069.
- [16] M.A. Ali, M.T.H. Tarafdar, *J. Inorg. Nucl. Chem.* 39 (1977) 1785.
- [17] M.J.M. Campbell, *Coord. Chem. Rev.* 15 (1975) 279.
- [18] B.S. Garg, M.R.P. Kurup, S.K. Jain, Y.K. Bhoon, *Transit. Met. Chem.* 13 (1988) 247.
- [19] I.-X. Li, H.-A. Tang, Y.-Z. Li, M. Wang, L.-F. Wang, C.-G. Xia, *J. Inorg. Biochem.* 78 (2000) 167.
- [20] R.P. John, A. Sreekanth, M.R.P. Kurup, A. Usman, I.A. Razak, H.K. Fun, *Spectrochim. Acta.* 59A (2003) 1349.
- [21] M.A. Ali, D.A. Chowdhary, M. Nazimuddin, *Polyhedron* 3 (1984) 595.
- [22] V. Philip, V. Suni, M.R.P. Kurup, M. Nethaji, *Polyhedron* 24 (2005) 1133.
- [24] G.M. Sheldrick, *Acta Crystallogr., Sect. A* 46 (1990) 467.

- [25] G.M. Sheldrick, SHELXL97 and SHELXS97, University of Göttingen, Germany, 1997.
- [26] K. Brandenburg, Diamond Version 3.2g, Crystal Impact GbR, Bonn, Germany, 2010.
- [27] L.J. Barbour, J. Supramol. Chem. 1 (2001) 189.
- [28] E.B. Seená, M.R.P. Kurup, Spectrochim. Acta Part A 69 (2008) 726.

\*\*\*RSC\*\*\*

**SYNTHESES AND SPECTRAL ASPECTS OF CADMIUM(II)  
CHELATES DERIVED FROM ONS DONOR  
THIOSEMICARBAZONES**

7.1 Introduction  
7.2 Experimental  
7.3 Results and discussions  
**References**

### 7.1. Introduction

Cadmium is a soft, malleable, ductile, bluish-white divalent metal and it prefers +2 oxidation state in most of its compounds. The average concentration of cadmium in the earth's crust is between 0.1 and 0.5 parts per million (ppm). Although cadmium has no known biological function in higher organisms, a cadmium-dependent carbonic anhydrase has been found in marine diatoms. Cadmium is used as a barrier to control neutrons in nuclear fission [1]. In molecular biology, cadmium is used to block voltage-dependent calcium channels from fluxing calcium ions, as well as in hypoxia research to stimulate proteasome-dependent degradation of Hif-1 $\alpha$  [2].

Cadmium is an extremely toxic element that is naturally present in the environment and also as a result of human activities. There is substantial interest in the coordination chemistry of cadmium complexes because of the toxic environmental impact of cadmium. The mobilization and immobilization of cadmium in the environment, in organisms and in

some technical processes (such as in ligand exchange chromatography) have been shown to depend significantly on the complexation of the metal center by chelating nitrogen donor ligands [3]. Complexes of Cd(II) with different molecular architectures with the same trimesate ligands showing strong fluorescence have been reported [4]. Though cadmium has been known as a toxic metal and is often associated with mercury and lead as one of the biologically harmful metal ions, the cadmium(II) ion has recently been found to serve as the catalytic center in a newly discovered carbonic anhydrase [5].

Thiosemicarbazones and their complexes have been subject of interest in numerous studies because of their chemical and biological activities and they possess a wide range of beneficial medicinal properties that are often attributed to their chelating ability with metal ions. Complexes of Group 12 metals, zinc and cadmium, can provide an interesting range of stoichiometries depending on the preparative salts [6]. Here we discuss the syntheses and spectral characterization of cadmium(II) complexes of the aldehyde based ONS donor thiosemicarbazones.

## 7.2. Experimental

### 7.2.1. Materials

Cadmium(II) acetate dihydrate (E-Merck), 1,10-phenanthroline (phen), 2,2'-bipyridine (bipy), 4,4'-dimethyl-2,2'-bipyridine (4,4'-dmbipy), 5,5'-dimethyl-2,2'-bipyridine (5,5'-dmbipy) were used as received.

## 7.2.2. Syntheses of the thiosemicarbazones

The syntheses of thiosemicarbazones  $H_2L^1$  and  $H_2L^2$  are discussed already in Chapter 2.

## 7.2.3. Syntheses of the complexes

### 7.2.3.1. $[CdL^1]_2$ (26)

This complex was synthesized by refluxing a solution of  $H_2L^1$  (0.190 g, 0.5 mmol) in 1:1 (v/v) mixture of DMF and methanol with a methanolic solution of  $Cd(OAc)_2 \cdot 2H_2O$  (0.133 g, 0.5 mmol) for 3 hours. The complex formed was filtered, washed with methanol and dried *in vacuo*.

Elemental Anal. Found (Calcd.) (%) : C, 37.15 (36.72); H, 2.66 (2.47); N, 8.67 (8.56); S, 5.99 (6.54). Yield: 63%

### 7.2.3.2. $[CdL^1phen]$ (27)

Methanolic solution of cadmium(II) acetate dihydrate (0.133 g, 0.5 mmol) was added to a stirred mixture of  $H_2L^1$  (0.190 g, 0.5 mmol) in DMF and methanol (1:1 v/v) and 1,10-phenanthroline (0.099 g, 0.5 mmol) in methanol. The resultant homogenous yellow solution was refluxed for three hours. The yellow product obtained was filtered, washed with methanol and dried *in vacuo*.

Elemental Anal. Found (Calcd.) (%) : C, 48.37 (48.34); H, 2.75 (3.00); N, 10.80 (10.44); S, 4.51 (4.78). Yield: 68%

### 7.2.3.3. [CdL<sup>1</sup>bipy] (28)

To a stirred mixture of H<sub>2</sub>L<sup>1</sup> (0.190 g, 0.5 mmol) in DMF and methanol (1:1 v/v) and 2,2'-bipyridine (0.078 g, 0.5 mmol) in methanol, cadmium(II) acetate dihydrate (0.133 g, 0.5 mmol) was added. The resultant yellow solution was refluxed for 3 hours and the yellow product separated out was filtered, washed with methanol and dried *in vacuo*.

Elemental Anal. Found (Calcd.) (%) : C, 46.35 (46.42); H, 3.24 (3.12); N, 10.70 (10.83); S, 4.75 (4.96). Yield: 74%

### 7.2.3.4. [CdL<sup>1</sup>(4,4'-dmbipy)] (29)

To a stirred mixture of H<sub>2</sub>L<sup>1</sup> (0.190 g, 0.5 mmol) in DMF and methanol (1:1 v/v) and 4,4'-dimethyl-2,2'-bipyridine (0.092 g, 0.5 mmol) in methanol, methanolic solution of cadmium(II) acetate dihydrate (0.133 g, 0.5 mmol) was added. The resultant yellow solution was refluxed for 3 hours and the yellow product separated out was filtered, washed with methanol and dried *in vacuo*.

Elemental Anal. Found (Calcd.) (%) : C, 48.30 (48.05); H, 3.89 (3.58); N, 10.26 (10.38); S, 4.84 (4.75). Yield: 60%

### 7.2.3.5. [CdL<sup>1</sup>(5,5'-dmbipy)] (30)

Methanolic solution of cadmium(II) acetate dihydrate (0.133 g, 0.5 mmol) was added to a stirred mixture of H<sub>2</sub>L<sup>1</sup> (0.190 g, 0.5 mmol) in DMF and methanol (1:1 v/v) and 5,5'-dimethyl-2,2'-bipyridine (0.092 g, 0.5 mmol) in methanol. The resultant yellow solution was refluxed for three hours. The yellow product obtained was filtered, washed with methanol and dried *in vacuo*.

Elemental Anal. Found (Calcd.) (%) : C, 48.34 (48.05); H, 3.25 (3.58); N, 10.87 (10.38); S, 4.51 (4.75). Yield: 62%

#### 7.2.3.6. [(CdL<sup>2</sup>)<sub>2</sub>] (31)

This complex was synthesized by refluxing a solution of H<sub>2</sub>L<sup>2</sup> (0.193 g, 0.5 mmol) in 1:1 (v/v) mixture of DMF and methanol with a methanolic solution of Cd(OAc)<sub>2</sub>·2H<sub>2</sub>O (0.133 g, 0.5 mmol) for 3 hours. The complex formed was filtered, washed with methanol and dried *in vacuo*.

Elemental Anal. Found (Calcd.) (%) : C, 36.59 (36.27); H, 3.82 (3.65); N, 8.55 (8.46); S, 6.47 (6.46). Yield: 60%

#### 7.2.3.7. [CdL<sup>2</sup>phen] (32)

Methanolic solution of cadmium(II) acetate dihydrate (0.133 g, 0.5 mmol) was added to a stirred mixture of H<sub>2</sub>L<sup>2</sup> (0.193 g, 0.5 mmol) in DMF and methanol (1:1 v/v) and 1,10-phenanthroline (0.099 g, 0.5 mmol) in methanol. The resultant homogenous yellow solution was refluxed for three hours. The yellow product obtained was filtered, washed with methanol and dried *in vacuo*.

Elemental Anal. Found (Calcd.) (%) : C, 47.64 (47.91); H, 3.61 (3.87); N, 10.44 (10.35); S, 4.56 (4.74). Yield: 67%

#### 7.2.3.8. [CdL<sup>2</sup>bipy] (33)

To a stirred mixture of H<sub>2</sub>L<sup>2</sup> (0.193 g, 0.5 mmol) in DMF and methanol (1:1 v/v) and 2,2'-bipyridine (0.078 g, 0.5 mmol) in methanol, cadmium(II) acetate dihydrate (0.133 g, 0.5 mmol) was added. The resultant yellow

solution was refluxed for 3 hours and the yellow product separated out was filtered, washed with methanol and dried *in vacuo*.

Elemental Anal. Found (Calcd.) (%) : C, 45.78 (45.99); H, 4.14 (4.01); N, 10.58 (10.73); S, 4.78 (4.91). Yield: 69%

### 7.3. Results and discussion

We synthesized and characterized eight cadmium complexes which are found to be stable. The complexes are soluble in organic solvents like DMF and DMSO. The thiosemicarbazones coordinate to the central metal ion in the thioiminolate form in all the complexes as evidenced by the IR spectral data. Compounds  $[(CdL^1)_2]$  (**26**) and  $[(CdL^2)_2]$  (**31**) are dimeric in nature while others are monomeric mixed ligand metal chelates. The isolation of X-ray quality single crystals of the Cd(II) complexes had not been successful. The synthesized complexes are characterized by the following physico-chemical methods.

#### 7.3.1. Elemental analyses

Elemental analyses data of complexes **26** and **31** reveal that metal and thiosemicarbazone are in the ratio 1:1 and in all other complexes the metal, thiosemicarbazone and the respective heterocyclic bases are in the ratio 1:1:1.

#### 7.3.2. Molar conductivity

The molar conductivity of the complexes in DMF ( $10^{-3}$  M) were measured at 298 K with a Systronic model 303 direct reading conductivity bridge, which suggest that these complexes are non-electrolytic in nature [7].

**Table 7.1. Molar conductivity of Cd(II) complexes**

Compound	$\lambda_m^a$
[(CdL <sup>1</sup> ) <sub>2</sub> ] ( <b>26</b> )	3.4
[CdL <sup>1</sup> phen] ( <b>27</b> )	2.0
[CdL <sup>1</sup> bipy] ( <b>28</b> )	2.5
[CdL <sup>1</sup> (4,4'-dmbipy)] ( <b>29</b> )	3.6
[CdL <sup>1</sup> (5,5'-dmbipy)] ( <b>30</b> )	2.6
[(CdL <sup>2</sup> ) <sub>2</sub> ] ( <b>31</b> )	3.5
[CdL <sup>2</sup> phen] ( <b>32</b> )	4.0
[CdL <sup>2</sup> bipy] ( <b>33</b> )	3.3

<sup>a</sup> = mho cm<sup>2</sup> mol<sup>-1</sup>

### 7.3.3. Infrared spectra

The IR spectra of the thiosemicarbazones when compared with the Cd(II) complexes confirm the coordination of the thiosemicarbazone to the metal. The significant bands observed in the IR spectra of the thiosemicarbazones and their complexes are summarized in Table 7.2.

The band corresponding to azomethine bond,  $\nu(\text{C}=\text{N})$ , shifts to higher energy on complexation due to the combination of  $\nu(\text{C}=\text{N})$  with the newly formed C=N bond which results from the loss of the thioamide hydrogen from the thiosemicarbazone moiety [8-12]. Strong bands found at 1071 and 1067 cm<sup>-1</sup> in the thiosemicarbazones are assigned to the  $\nu(\text{N}-\text{N})$  band. The increase in frequency of this band in the spectra of complexes is due to the increase in the bond strength, again confirming the coordination *via* the azomethine nitrogen. Coordination *via* thioiminolate sulfur is indicated by the downward shift of frequencies of  $\delta/\nu$  CS bands in the

complexes [13]. Some of the IR spectra of complexes are given in Figs. 7.1-7.6.

**Table 7.2. IR spectral assignments ( $\text{cm}^{-1}$ ) of thiosemicarbazones and their Cd(II) complexes**

Compound	$\nu(\text{O-H})$	$\nu(\text{C=N})$	$\nu(\text{N=C})^a$	$\nu(\text{N-N})$	$\nu(\text{C=S})/\nu(\text{C-S}),$ $\delta(\text{C=S})/\delta(\text{C-S})$	$\nu(\text{C-O})$	$\nu(\text{Cd-O})$	$\nu(\text{Cd-N})$
$\text{H}_2\text{L}^1$	3441	1540	....	1071	1333, 857	1267	....	....
$[(\text{CdL}^1)_2]$ (26)	....	1596	1546	1098	1288, 839	1228	464	431
$[\text{CdL}^1\text{phen}]$ (27)	....	1595	1550	1102	1309, 842	1228	465	422
$[\text{CdL}^1\text{bipy}]$ (28)	....	1599	1550	1100	1306, 844	1228	470	443
$[\text{CdL}^1(4,4'\text{-dmbipy})]$ (29)	....	1599	1550	1098	1316, 835	1237	463	427
$[\text{CdL}^1(5,5'\text{-dmbipy})]$ (30)	....	1598	1550	1100	1316, 840	1237	463	435
$\text{H}_2\text{L}^2$	3454	1539	....	1067	1342, 851	1257	....	....
$[(\text{CdL}^2)_2]$ (31)	....	1597	1556	1101	1328, 811	1225	472	459
$[\text{CdL}^2\text{phen}]$ (32)	....	1590	1560	1090	1330, 840	1230	466	446
$[\text{CdL}^2\text{bipy}]$ (33)	....	1586	1558	1092	1325, 833	1228	475	442

<sup>a</sup> = newly formed C=N bond

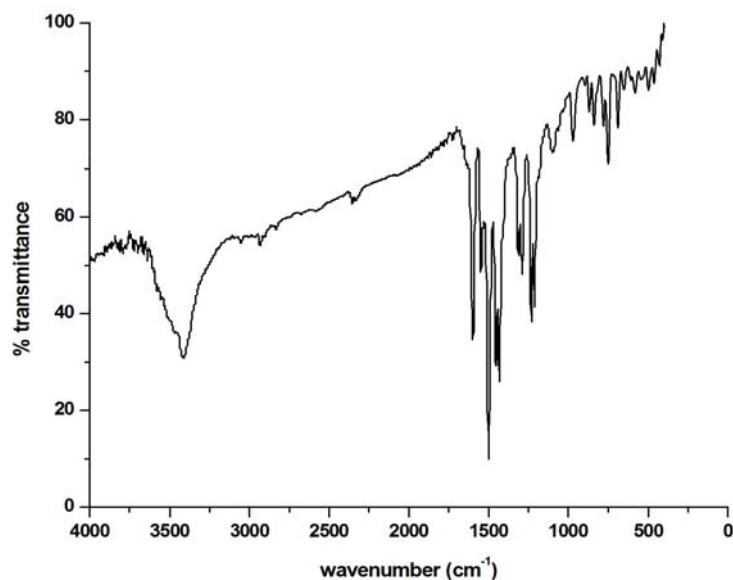


**Fig. 7.1. Infrared spectrum of  $[(\text{CdL}^1)_2]$  (26).**

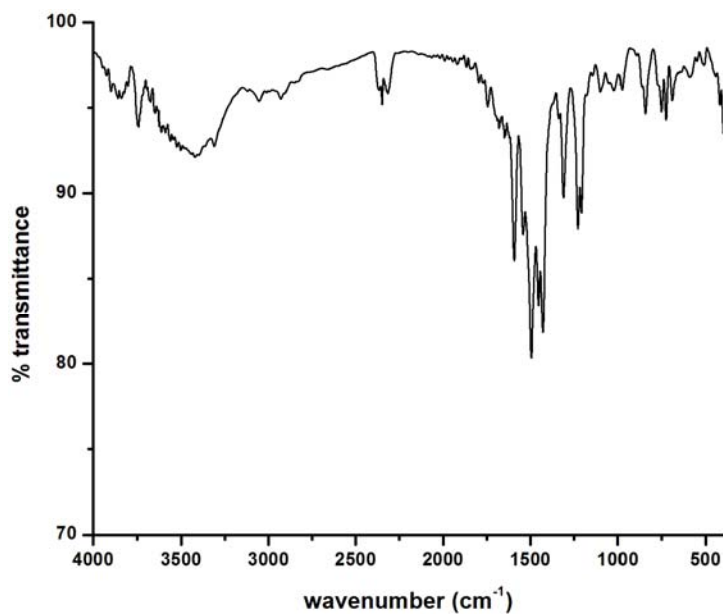


Fig. 7.2. Infrared spectrum of [CdL¹bipy] (28).

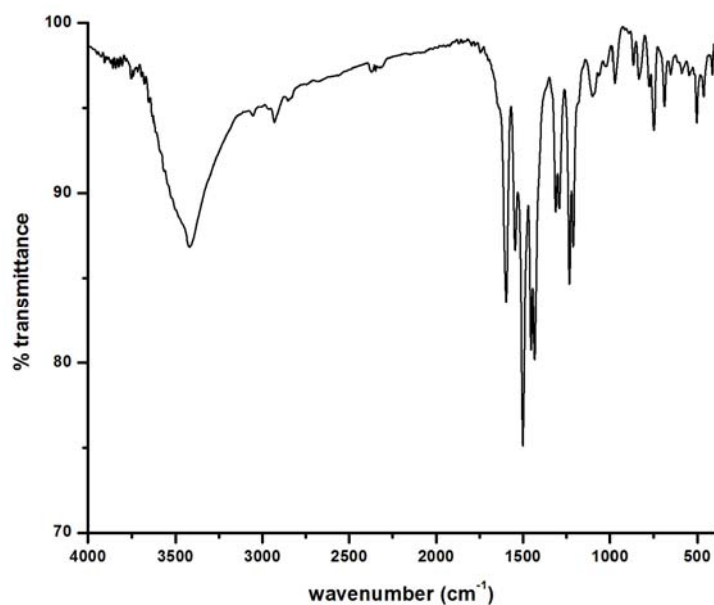


Fig. 7.3. Infrared spectrum of [CdL¹(4,4'-dmbipy)] (29).

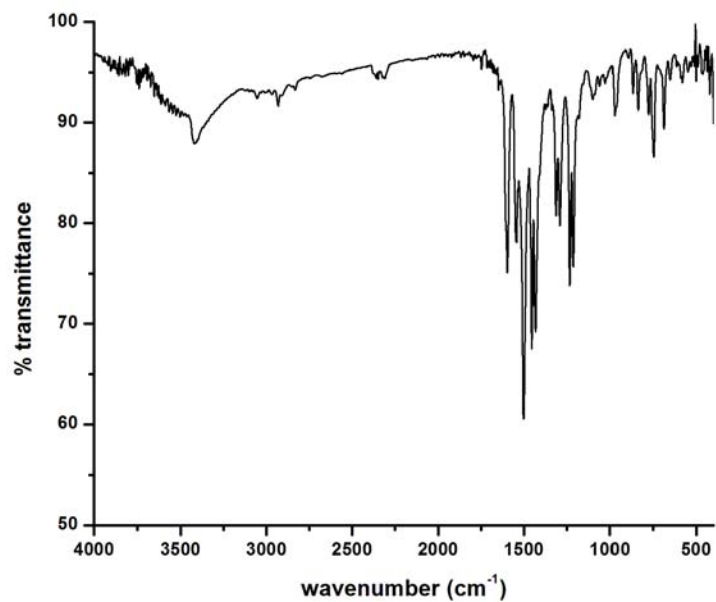


Fig. 7.4. Infrared spectrum of  $[\text{CdL}^1(5,5'\text{-dmbipy})]$  (30).

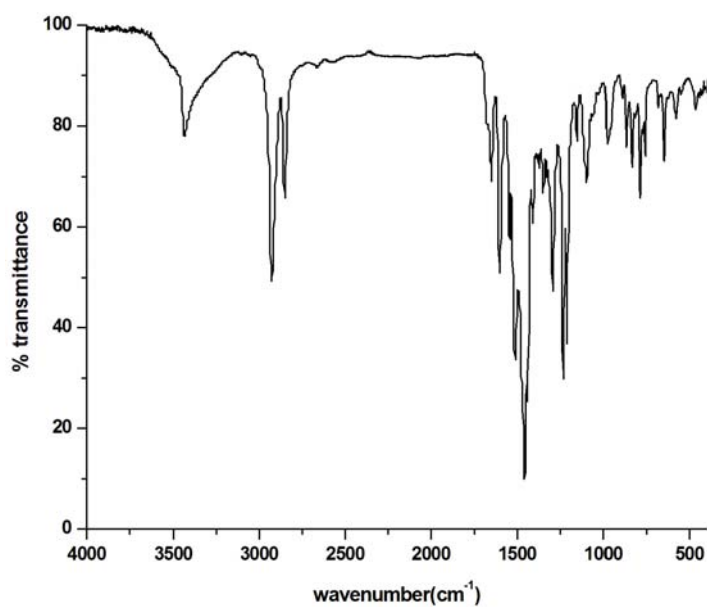


Fig. 7.5. Infrared spectrum of  $[\text{CdL}^2\text{phen}]$  (32).

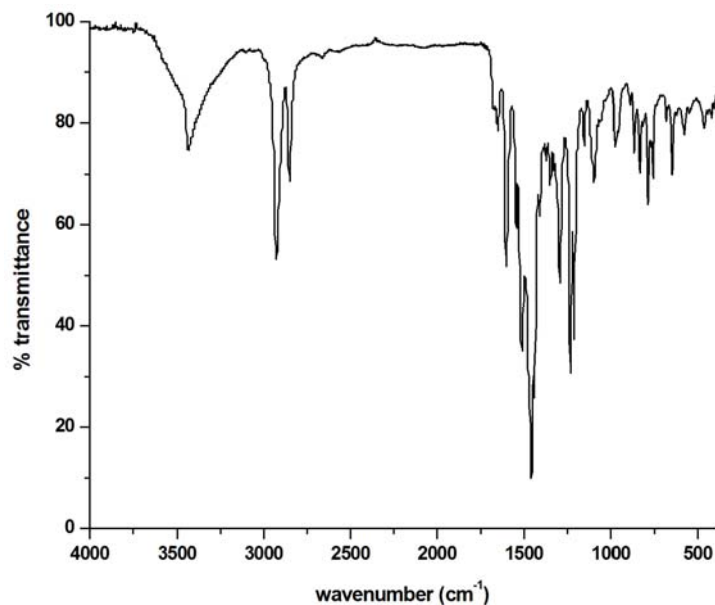
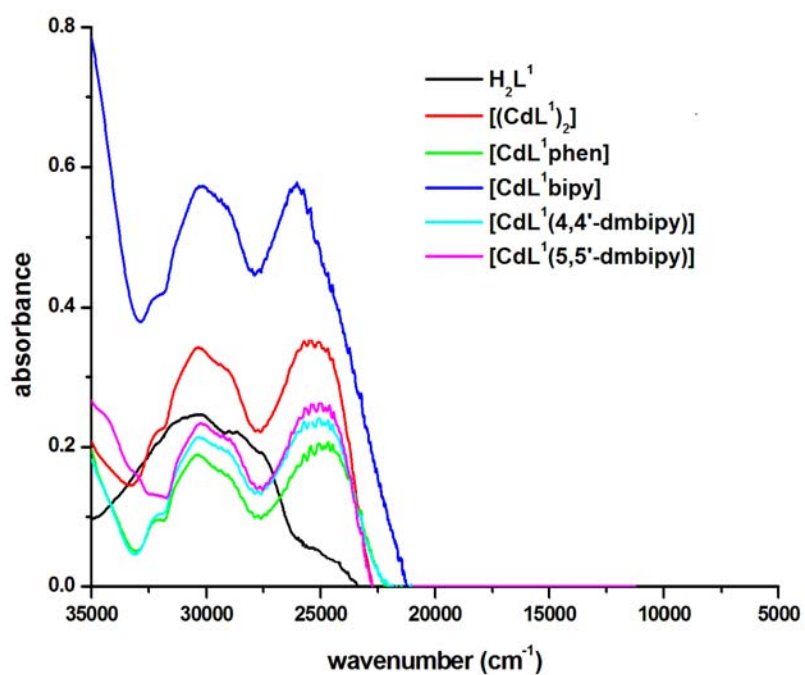
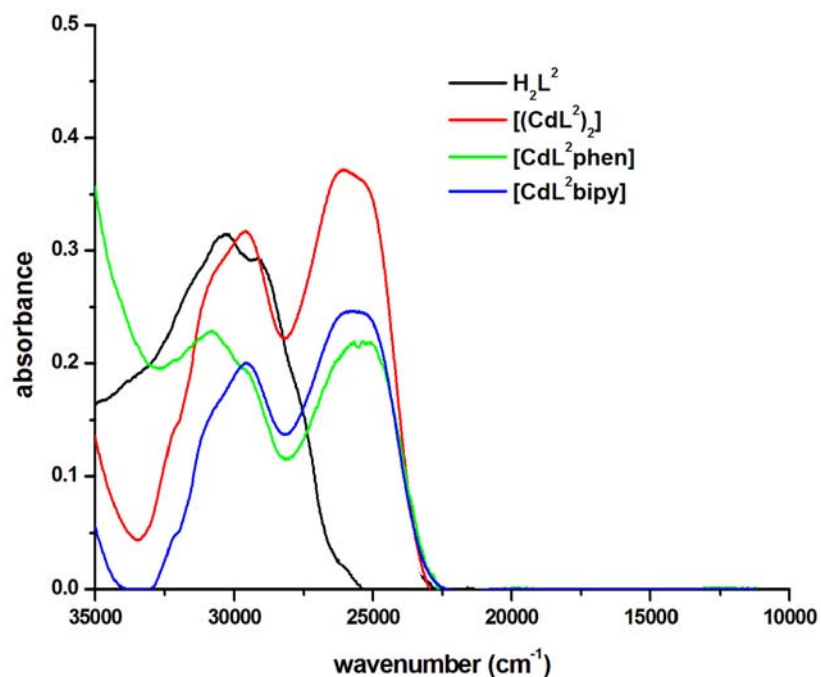


Fig. 7.6. Infrared spectrum of [CdL<sup>2</sup>bipy] (33).

#### 7.3.4. Electronic spectra

The electronic spectral assignments for the thiosemicarbazones and their Cd(II) complexes recorded in DMF are summarized in Table 7.3. The electronic spectra of the thiosemicarbazones showed bands in the range 28770-30490 cm<sup>-1</sup> which are assignable to azomethine bond and the thiosemicarbazone moiety [14]. These bands are slightly shifted on complexation. In addition to these bands due to intraligand transitions, new bands around 24990-26110 cm<sup>-1</sup> range are observed in the spectra of complexes. These bands can be assigned to metal to ligand charge transfer transitions. No appreciable absorptions occurred below 20000 cm<sup>-1</sup>, indicating the absence of *d-d* bands, which is in accordance with the *d*<sup>10</sup> configuration of Cd(II) ion [15]. The electronic spectra of complexes are given in Figs. 7.7 and 7.8.

Fig. 7.7. Electronic spectra of  $H_2L^1$  and its Cd(II) complexes.Fig. 7.8. Electronic spectra of  $H_2L^2$  and its Cd(II) complexes.

**Table 7.3. Electronic spectral assignments (cm<sup>-1</sup>) of thiosemicarbazones  
and their Cd(II) complexes**

Compound	n→π*/π→π*	LMCT
H <sub>2</sub> L <sup>1</sup>	28770, 30490	----
[(CdL <sup>1</sup> ) <sub>2</sub> ] (26)	29210, 30380	25430
[CdL <sup>1</sup> phen] (27)	29030, 30450	24990
[CdL <sup>1</sup> bipy] (28)	29090, 30210	26110
[CdL <sup>1</sup> (4,4'-dmbipy)] (29)	29250, 30330	25230
[CdL <sup>1</sup> (5,5'-dmbipy)] (30)	29020, 30290	25160
H <sub>2</sub> L <sup>2</sup>	29300, 30490	----
[(CdL <sup>2</sup> ) <sub>2</sub> ] (31)	29590, 30890	26050
[CdL <sup>2</sup> phen] (32)	29520, 30820	25550
[CdL <sup>2</sup> bipy] (33)	29520, 30700	25740

## References

- [1] G. Buxbaum, G. Pfaff, "Cadmium Pigments", Industrial inorganic pigments, Wiley-VCH, pp.121, 2005.
- [2] K.R. Nambiar, "Helium-cadmium Laser", Lasers: Principles, Types and Applications, 2006.
- [3] L. Pag, J.N. Lindner, G. Davies, D.E. Seitz, B.L. Karger, Anal. Chem. 51 (1979) 433.
- [4] J.-C. Dai, X.-T. Wu, Z.-Y. Fu, C.-P. Cui, S.-M. Hu, W.-X. Du, L.-M. Wu, H.-H. Zhang, R.-Q. Sun, Inorg. Chem. 41 (2002) 1391.
- [5] T.W. Lane, F.M.M. Morel, Proc. Natl. Acad. Sci. USA 97 (2000) 4627.
- [6] E. Bermejo, A. Castineiras, L.M. Fostiak, I.G. Santos, J.K. Swearingen, D.X. West, Polyhedron 23 (2004) 2303.
- [7] W.J. Geary, Coord. Chem. Rev. 7 (1971) 81.

- [8] M. Joseph, V. Suni, M.R.P. Kurup, M. Nethaji, A. Kishore, S.G. Bhat, *Polyhedron* 23 (2004) 3069.
- [9] M.A. Ali, M.T.H. Tarafdar, *J. Inorg. Nucl. Chem.* 39 (1977) 1785.
- [10] M.J.M. Campbell, *Coord. Chem. Rev.* 15 (1975) 279.
- [11] B.S. Garg, M.R.P. Kurup, S.K. Jain, Y.K. Bhoon, *Transit. Met. Chem.* 13 (1988) 247.
- [12] B.S. Garg, M.R.P. Kurup, S.K. Jain, Y.K. Bhoon, *Transit. Met. Chem.* 16 (1991) 111.
- [13] P.F. Rapheal, E. Manoj, M.R.P. Kurup, E. Suresh, *Polyhedron* 26 (2007) 607.
- [14] A. Castineiras, E. Bermejo, D.X. West, L.J. Ackerman, J.V. Martinez, S.H. Ortega, *Polyhedron* 18 (1999) 1469.
- [15] V. Philip, V. Suni, M.R.P. Kurup, *Polyhedron* 25 (2006) 1931.

\*\*\*RSC\*\*\*

**SYNTHESIS, CRYSTAL STRUCTURE AND SPECTRAL ASPECTS OF A DIOXIDOMOLYBDENUM(VI) CHELATE DERIVED FROM ONS DONOR THIOSEMICARBAZONE**

8.1 Introduction  
8.2 Experimental  
8.3 Results and discussions  
**References**

### 8.1. Introduction

Molybdenum is a biologically important trace element which is of essential importance. It is required by enzymes catalyzing diverse key reactions in the global carbon, sulfur and nitrogen metabolism. It occurs in the redox-active sites of molybdoenzymes involved in nitrogen, sulfur or carbon metabolism [1]. The ‘oxo-type’ molybdoenzymes, which possess a common molybdenum cofactor, catalyze biological two electron reactions that involve a change in the number of oxygen atoms in the substrate [2]. The mononuclear molybdoenzymes contain terminal oxo group(s), believed to be obligatory for the oxotransferase activity of these enzymes. It occurs in a wide range of metalloenzymes in bacteria, fungi, algae, plants and animals where it forms part of the active sites of these enzymes. The active site includes the metal atom coordinated to one or two pyranopterin molecules and to a variable number of ligands such as oxygen, sulfur and selenium atoms [3,4].

Diverse class of molybdenum complexes were prepared, tested and developed for various pharmaceutical purposes, whereby their anticancer activities gained special attention. For example, tetrathiomolybdate (TM) is an anticopper drug under development for treating Wilson's disease. Its mechanism of action involves forming a tight tripartite complex in the blood with serum albumin and available copper. In addition, it has been shown that lowering copper levels with TM produces an antiangiogenic, anticancer effect, probably due to inhibition of many copper-dependent proangiogenic cytokines. Therefore, it has shown a promising role in suppressing tumor angiogenesis, retinal neovascularization and pathologic inflammatory conditions [5,6].

Additionally, polyoxometalates, negatively charged inorganic substances which contain early transition metal ions and make a cluster with the surrounding oxygen atoms are a large class of inorganic compounds with great molecular diversity and significant potential applications in chemistry and medicine [7]. Yamase had reported that significant antitumoral effect of polyoxomolybdates, especially  $[\text{NH}_3\text{Pr}^+ ]_6[\text{Mo}_7\text{O}_{24}] \cdot 3\text{H}_2\text{O}$  (PM-8) was found against MX-1 murine mammary cancer cell line, Meth A sarcoma and MM46 adenocarcinoma [8].  $\sqrt{3}$ -octamolybdates containing aminoacids and peptides showed differential cell-growth inhibition in a close dependent manner selectively on hepatocellular carcinoma cell line (HepG2) and breast cancer cell line (MCF-7) [9]. Furthermore, metallocene diacido complexes containing molybdenum exhibit antitumor activity for a wide spectrum of murine and human tumors with reduced toxicity when compared with cisplatin [10].

Molybdenum is a versatile transition element because it possesses a large number of stable and accessible oxidation states as well as coordination numbers. The formal oxidation state of molybdenum fluctuates between +6 and +4 *via* a +5 intermediate during turnover [11]. Complexes containing the molybdenum-oxo group dominate the higher oxidation state of molybdenum. Most simple dioxidomolybdenum(VI) coordination complexes contain the *cis*-MoO<sub>2</sub><sup>2+</sup> cation. The chemistry of nitrogen-sulfur chelating ligands bound to Mo with higher oxidation states is a field of great interest. Thiosemicarbazones obtained by condensing ring substituted aromatic thiosemicarbazides with *o*-hydroxy carbonyl compounds have rarely been used in molybdenum chemistry. These ligands are of particular interest because their complexes of the type MoO<sub>2</sub>L or MoOL possess one or two “open” coordination sites that can be utilized for substrate binding.

## **8.2. Experimental**

### **8.2.1. Materials**

The reagents used for the synthesis of the ligand H<sub>2</sub>L<sup>1</sup> are discussed in Chapter 2. MoO<sub>2</sub>(acac)<sub>2</sub> (Sigma-Aldrich) was used as received. Solvents used are methanol and dimethylformamide.

### **8.2.2. Synthesis of the thiosemicarbazone H<sub>2</sub>L<sup>1</sup>**

The synthesis of thiosemicarbazone H<sub>2</sub>L<sup>1</sup> is discussed already in Chapter 2.

### 8.2.3. Synthesis of the complex $[\text{MoO}_2\text{L}^1\text{DMF}]\cdot\text{DMF}$ (**34**)

This complex was synthesized by mixing a solution of  $\text{H}_2\text{L}^1$  (0.190 g, 0.5 mmol) in a mixture of DMF and methanol (1:1 v/v) with a hot methanolic solution of  $\text{MoO}_2(\text{acac})_2$  (0.163 g, 0.5 mmol) and refluxing for 3 hours. This was cooled and the orange colored crystalline complex formed was filtered, washed with methanol and dried *in vacuo*.

Elemental Anal. Found (Calcd.) (%): C, 38.20 (38.66); H, 4.16 (4.02); N, 10.81 (10.74); S, 5.40 (4.92). Yield: 57%

## 8.3. Results and discussion

The stoichiometric reaction of bis(acetylacetonato)dioxido molybdenum(VI) with  $\text{H}_2\text{L}^1$  in a N,N-dimethylformamide-methanol binary mixture afforded the orange six coordinate complex  $[\text{MoO}_2\text{L}^1\text{DMF}]\cdot\text{DMF}$  (**34**) even though the expected product was  $[(\text{MoO}_2\text{L}^1)_2]$ . The thiosemicarbazone  $\text{H}_2\text{L}^2$  did not give any complex with molybdenum. We tried to prepare Mo(VI) complexes using heterocyclic bases like pyridine and  $\gamma$ -picoline with both the thiosemicarbazones  $\text{H}_2\text{L}^1$  and  $\text{H}_2\text{L}^2$ . Unfortunately these bases are not getting coordinated to  $\text{MoO}_2^{2+}$ . Instead, the solvent DMF is found to coordinate to the metal in all the cases. The complex **34** is soluble in DMF and DMSO. It is characterized by the following physicochemical methods.

### 8.3.1. Elemental analysis

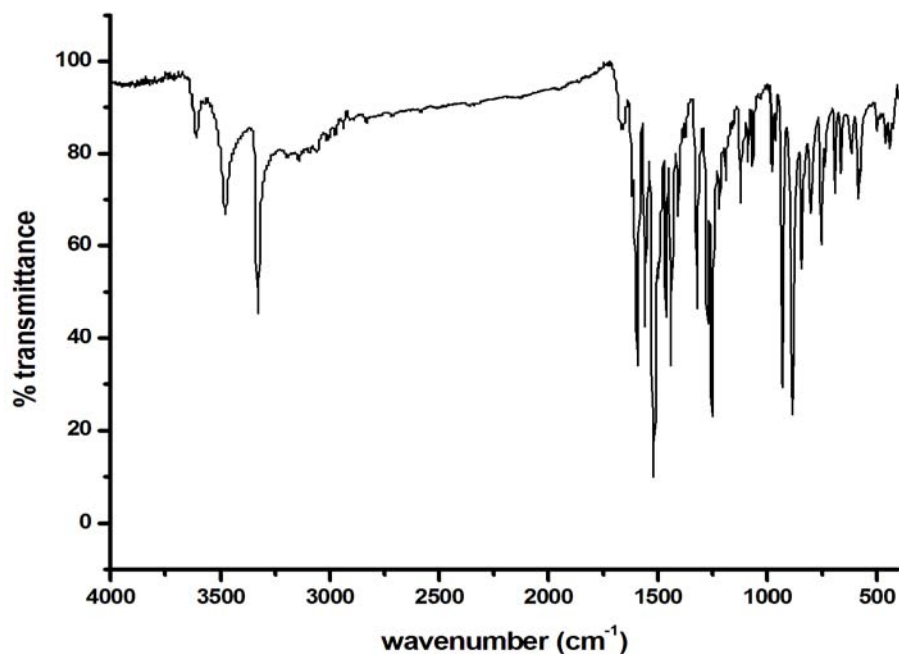
The analytical data indicate that the observed C, H, N and S values are in close agreement with that of the proposed formula  $[\text{MoO}_2\text{L}^1\text{DMF}]\cdot\text{DMF}$ .

### 8.3.2. Molar conductivity and magnetic susceptibility measurements

The conductivity measurement was made in DMF ( $10^{-3}$  M) and the complex was found to be electrically non-conducting in solution [12]. Magnetic susceptibility data indicate that the complex is diamagnetic.  $\lambda_m = 10.2 \text{ ohm}^{-1}\text{cm}^2\text{mol}^{-1}$ ,  $\mu_{\text{eff}} = 0.21 \text{ B.M.}$

### 8.3.3. Infrared spectrum

Table 8.1. lists the tentative assignments of the main IR bands of the dioxidomolybdenum(VI) complex in  $4000\text{-}400 \text{ cm}^{-1}$  region. The ligand  $\text{H}_2\text{L}^1$  shows bands at  $3441$  and  $3305 \text{ cm}^{-1}$ , which are due to the stretching modes of the  $-\text{OH}$  and  $-\text{NH}$  groups respectively. These bands are absent in the complexes which suggests deprotonation of the phenolic group, indicating coordination through the phenolic oxygen and enolization of the thioamido sulfur followed by deprotonation. The ligand has a band at  $1267 \text{ cm}^{-1}$  which is due to  $\nu(\text{C}-\text{O})$ . This band is shifted to  $1253 \text{ cm}^{-1}$  in the complex which also indicates the coordination of  $\text{O}^-$  [13]. The band corresponding to azomethine bond,  $\nu(\text{C}=\text{N})$ , shifts to higher energy on coordination due to the combination of  $\nu(\text{C}=\text{N})$  with the newly formed  $\text{C}=\text{N}$  bond which results from the loss of the thioamide hydrogen from the thiosemicarbazone moiety [14-18]. The increase in frequency of  $\nu(\text{N}-\text{N})$  band in the complex, due to an increase in the bond strength, again confirms coordination *via* the azomethine nitrogen [19,20]. The decrease in frequency of the  $\nu(\text{CS})$  band from  $1333 \text{ cm}^{-1}$  in the thiosemicarbazone by  $12 \text{ cm}^{-1}$  upon complexation indicates coordination *via* the thioiminolato sulfur [21,22]. The complex exhibits two bands at  $845$  and  $916 \text{ cm}^{-1}$  assigned to symmetric and antisymmetric vibrations, respectively, of the *cis*- $\text{MoO}_2^{2+}$  core [23,24].

Fig. 8.1. Infrared spectrum of  $[\text{MoO}_2\text{L}^1\text{DMF}]\cdot\text{DMF}$  (**34**).Table 8.1. IR spectral assignments ( $\text{cm}^{-1}$ ) of  $\text{H}_2\text{L}^1$  and its dioxidomolybdenum(VI) complex

Compound	$\nu(\text{O-H})$	$\nu(\text{C=N})$	$\nu(\text{C=N})^a$	$\nu(\text{N-N})$	$\nu(\text{C=S})/\nu(\text{C-S}),$ $\delta(\text{C=S})/\delta(\text{C-S})$	$\nu(\text{C-O})$	$\nu(\text{Mo=O})$
$\text{H}_2\text{L}^1$	3441	1540	----	1071	1333, 857	1267	----
$[\text{MoO}_2\text{L}^1\text{DMF}]\cdot\text{DMF}$ ( <b>34</b> )	----	1590	1558	1122	1320, 804	1253	887, 935

<sup>a</sup> = newly formed C=N bond

### 8.3.4. Electronic spectrum

The electronic spectrum of the dioxidomolybdenum(VI) complex was recorded in DMF ( $10^{-3}$  M) and the electronic spectral assignments are given in Table 8.2. The thiosemicarbazone  $\text{H}_2\text{L}^1$  shows bands at 30490 and 28770  $\text{cm}^{-1}$  corresponding to intraligand transitions. These bands suffer marginal shifts upon complexation. The complex displays a broad band at 24330

$\text{cm}^{-1}$  which is assignable to  $\text{L} \rightarrow \text{Mo} (\text{d}\pi)$  LMCT transition [25-27]. The electronic spectrum of the complex is given in Fig. 8.2.

**Table 8.2. Electronic spectral assignments ( $\text{cm}^{-1}$ ) of thiosemicarbazone and the Mo(VI) complex**

Compound	$n \rightarrow \pi^* / \pi \rightarrow \pi^*$	LMCT	d-d
$\text{H}_2\text{L}^1$	28770, 30490	----	----
$[\text{MoO}_2\text{L}^1\text{DMF}]\cdot\text{DMF}$ (34)	28500, 30070	24330	----

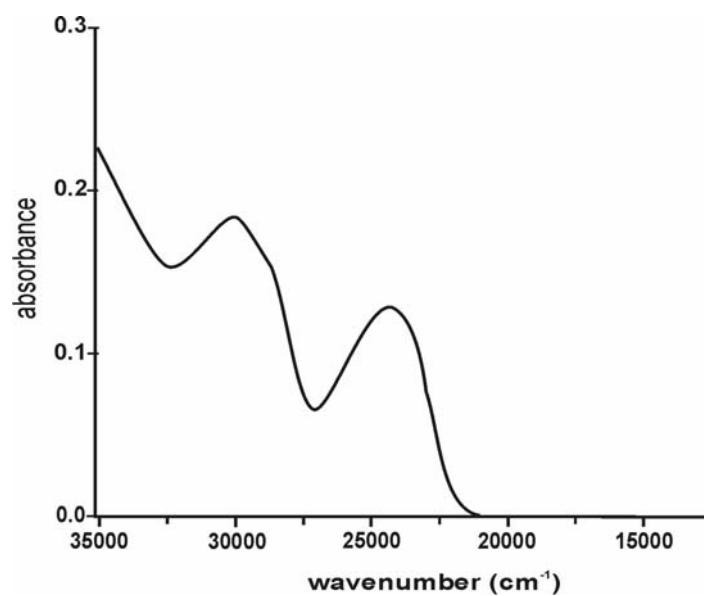


**Fig. 8.2. Electronic spectrum of  $[\text{MoO}_2\text{L}^1\text{DMF}]\cdot\text{DMF}$  (34).**

### 8.3.5. X-ray crystallography

Single crystals of  $[\text{MoO}_2\text{L}^1\text{DMF}]\cdot\text{DMF}$  (**34**) was obtained by slow evaporation of its mother liquor over a week. The crystallographic data and structure refinement parameters for the complex at 296 K are given in Table 8.3. An orange block shaped crystal with approximate dimensions of  $0.30 \times 0.25 \times 0.20 \text{ mm}^3$  was selected for collecting the data. It was mounted on a Bruker SMART APEXII CCD diffractometer, equipped with a graphite crystal, incident-beam monochromator and a fine focus sealed tube with Mo  $K\alpha$  radiation ( $\lambda = 0.71073 \text{ \AA}$ ) as the X-ray source. The unit cell dimensions were measured and the data collection was performed at 296 K. Bruker SMART software was used for data acquisition and Bruker SAINT software for data integration [28]. Absorption corrections were carried out using SADABS based on Laue symmetry using equivalent reflections [29]. The structure was solved by direct methods using SHELXS97 [30] and refined by full-matrix least-squares calculations with SHELXL97 software package [31]. The molecular and crystal structures were plotted using DIAMOND version 3.2g [32].

All non-hydrogen atoms were refined anisotropically and all H atoms on C were placed in calculated positions, guided by difference maps, with C-H bond distances 0.93–0.96 Å. H atoms were assigned as  $U_{\text{iso}}=1.2U_{\text{eq}}$  (1.5 for Me). The N3-H' hydrogen atom was located from difference Fourier maps and the distance was restrained using DFIX instruction. The final refinement cycle was based on all 6488 independent reflections and 326 variables with  $R_1 = 0.0341$ ,  $wR_2 = 0.0778$ .

*Synthesis, Crystal Structure and Spectral Aspects of a Dioxidomolybdenum(VI)  
Chelate Derived from ONS Donor Thiosemicarbazone*

**Table 8.3 Crystal data and structure refinement parameters for complex 34**

Parameters	[MoO <sub>2</sub> L <sup>1</sup> DMF]·DMF (34)
Empirical formula	C <sub>21</sub> H <sub>26</sub> BrMoN <sub>5</sub> O <sub>6</sub> S
Formula weight	652.38
Temperature	296 K
Wavelength	0.71073 Å
Crystal system	Monoclinic
Space group	<i>P</i> 2 <sub>1</sub> / <i>n</i>
Unit cell dimensions	<i>a</i> = 15.4646(6) Å <i>b</i> = 11.0191(4) Å <i>c</i> = 15.4756(6) Å $\alpha$ = 90° $\beta$ = 98.761(2)° $\gamma$ = 90°
Volume	2606.37(17) Å <sup>3</sup>
Z	4
Density (calculated)	1.663 Mg/m <sup>3</sup>
Absorption coefficient	2.161 mm <sup>-1</sup>
<i>F</i> (000)	1312
Crystal size	0.30 x 0.25 x 0.20 mm <sup>3</sup>
$\theta$ range for data collection	2.28 to 28.31°
Limiting indices	-20 ≤ <i>h</i> ≤ 20 -14 ≤ <i>k</i> ≤ 14 -20 ≤ <i>l</i> ≤ 20
Reflections collected	44354
Independent reflections	6488 [R(int) = 0.0441]
Refinement method	Full-matrix least-squares on <i>F</i> <sup>2</sup>
Data / restraints / parameters	6488 / 1 / 326
Goodness-of-fit on <i>F</i> <sup>2</sup>	1.015
Final R indices [ <i>I</i> > 2 $\sigma$ ( <i>I</i> )]	R <sub>1</sub> = 0.0341, wR <sub>2</sub> = 0.0778
R indices (all data)	R <sub>1</sub> = 0.0540, wR <sub>2</sub> = 0.0862
Largest diff. peak and hole	1.485 and -1.308 e Å <sup>-3</sup>

$$R_1 = \sum ||F_o| - |F_c|| / \sum |F_o|$$

$$wR_2 = [\sum w(F_o^2 - F_c^2)^2 / \sum w(F_o^2)^2]^{1/2}$$



**Table 8.4 Selected bond lengths and angles for complex 34**

Bond lengths (Å)		Bond angles (°)	
Mo(1)–S(1)	2.4549(8)	S(1)–Mo(1)–O(2)	152.66(6)
Mo(1)–O(2)	1.939(1)	S(1)–Mo(1)–O(3)	89.23(7)
Mo(1)–O(3)	1.699(1)	S(1)–Mo(1)–O(4)	97.86(8)
Mo(1)–O(4)	1.690(2)	S(1)–Mo(1)–O(5)	81.68(5)
Mo(1)–N(1)	2.250(2)	S(1)–Mo(1)–N(1)	75.39(6)
Mo(1)–O(5)	2.370(2)	O(2)–Mo(1)–O(3)	106.43(9)
S(1)–C(8)	1.755(3)	O(2)–Mo(1)–O(4)	99.52(10)
N(1)–N(2)	1.385(3)	O(2)–Mo(1)–O(5)	78.12(8)
N(4)–C(16)	1.440(6)	O(2)–Mo(1)–N(1)	82.78(8)
C(7)–N(1)	1.295(3)	N(1)–N(2)–C(8)	114.5(2)
C(8)–N(2)	1.291(3)		

By comparing the bond distances and angles of thiosemicarbazone with the complex, it is clear that the ligand coordinates to the MoO<sub>2</sub><sup>2+</sup> core in the deprotonated thioiminolate form because in the complex, the C(8)–S(1) bond distance is 1.755(3) Å and is nearer to C–S single bond distance [1.81 Å] than to C–S double bond distance [1.60 Å] [33]. However, it falls short of the pure C–S single bond distance. The reason for such shortening may be attributed to electron delocalization in the coordinated ligand [34]. The adjacent C(8)–N(2) bond displays a typical double bond distance [1.291(3) Å] whereas in the ligand, C(8)–N(2) bond distance is 1.342(3) Å. The C(7)–N(1) bond distance is close to the usual C=N bond length [C(7)–N(1), 1.295(3) Å]. The N–N–C bond angle of the ligand [N(1)–N(2)–C(8), 122.0(2)°] is reduced by few degrees [N(1)–N(2)–C(8), 114.5(2)°] on complex formation.

The rings Cg(3) and Cg(4) make a dihedral angle of 16.36(5)° with each other. Ring puckering analysis and least square plane calculations

show that the ring Cg(2) comprising of atoms Mo(1), O(2), C(5), C(6), C(7) and N(1) is puckered with puckering amplitude  $Q = 0.321(2) \text{ \AA}$  and  $\phi = 190.3(6)^\circ$ . Fig. 8.4. shows the unit cell packing diagram of the complex viewed along 'c' axis.

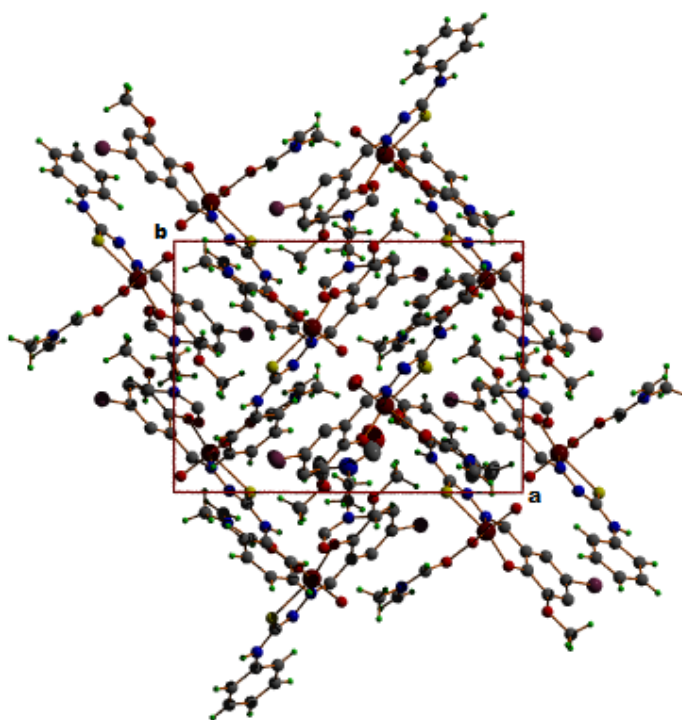


Fig. 8.4. Packing diagram of complex viewed along 'c' axis.

A strong classical hydrogen bond  $N(3)-H(\prime)\cdots O(6)$  is present in the crystal structure in which the oxygen atom of the solvent dimethylformamide acts as the acceptor (Fig. 8.5). Intramolecular and intermolecular nonclassical hydrogen bonds are also present in the crystal structure. The  $\pi\cdots\pi$  interactions are absent while  $C-H\cdots\pi$  interaction exists between H(15B) and Cg(4) comprising of atoms C(9), C(10), C(11), C(12), C(13) and C(14) (Fig. 8.6). The interaction parameters are shown in Table 8.5. The coordination polyhedra present in a super cell is shown in Fig. 8.7.

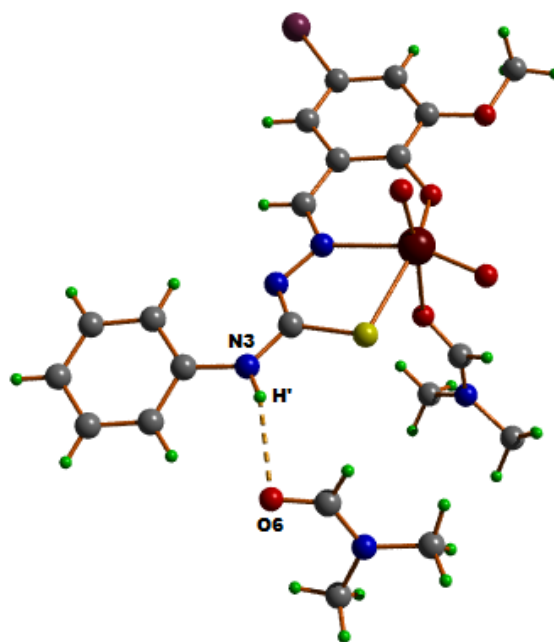


Fig. 8.5. Hydrogen bonding interaction shown as dotted line.

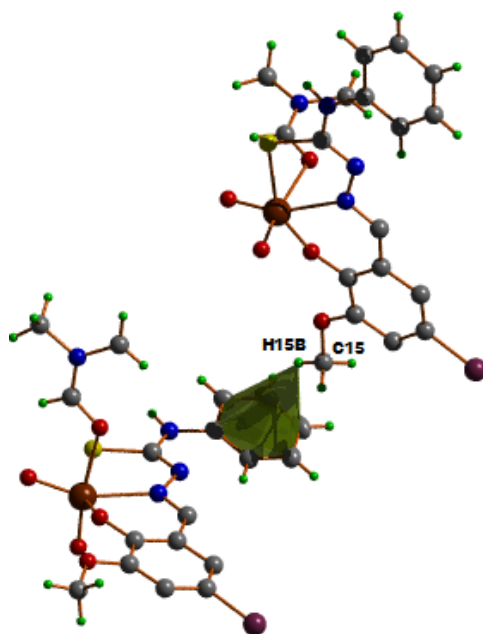
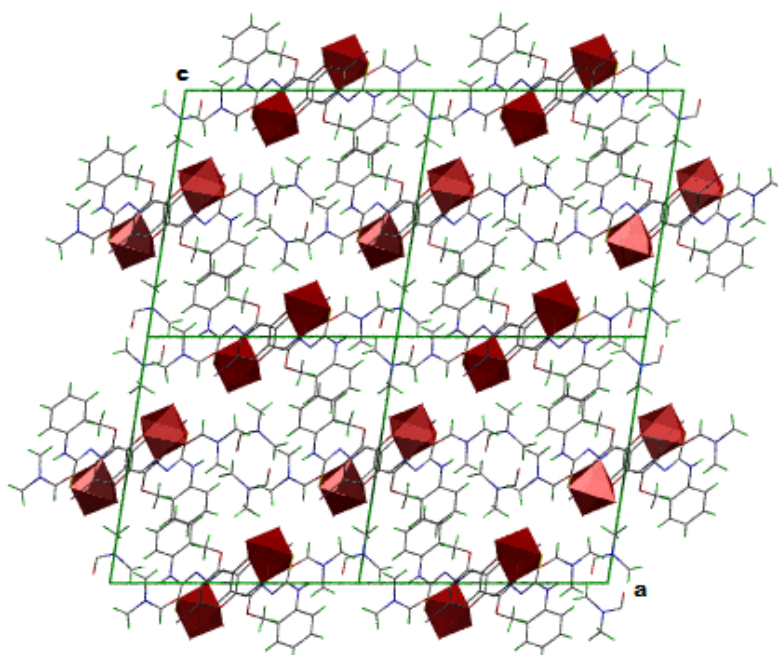


Fig. 8.6. C-H... $\pi$  interactions in  $[\text{MoO}_2\text{L}^1\text{DMF}]\cdot\text{DMF}$  (34).

Table 8.5. Interaction parameters

H-bonding				
D-H...A	D-H (Å)	H...A (Å)	D...A (Å)	D-H...A (°)
N(3)-H'...O(6) <sup>a</sup>	0.85(4)	2.23(3)	3.053(6)	164(4)
C(14)-H(12)...O(6) <sup>a</sup>	0.93	2.42	3.238(7)	147
C(12)-H(14)...N(2) <sup>a</sup>	0.93	2.58	3.485(5)	163
C(10)-H(16)...N(2)	0.93	2.26	2.839(4)	120
C(18)-H(21)...O(3)	0.93	2.35	2.896(5)	117
C(20)-H(30C)...O(1) <sup>b</sup>	0.96	2.42	3.154(9)	133
C-H...π interactions				
C-H(I)...Cg(J)	H...Cg (Å)	C-H...Cg (°)	C...Cg (Å)	
C(15)-H(15B)...Cg(4) <sup>c</sup>	2.83	136	3.579(4)	

Equivalent position codes : a =  $\frac{1}{2}-x, \frac{1}{2}+y, \frac{1}{2}-z$ , b =  $x, y, 1+z$ , c =  $-\frac{1}{2}+x, \frac{1}{2}-y, -\frac{1}{2}+z$   
Cg(4) = C(9), C(10), C(11), C(12), C(13), C(14)  
D = Donor, A = acceptor, Cg = Centroid

Fig. 8.7. Coordination polyhedra of  $[\text{MoO}_2\text{L}^1\text{DMF}]\cdot\text{DMF}$  (34) in a super cell.

## References

- [1] I.K. Dhavan, J.H. Enemark, *Inorg. Chem.* 35 (1996) 4873.
- [2] S.J.N. Burgmayer, E.I. Stiefel, *J. Chem. Educ.* 62 (1985) 943.
- [3] R.R. Mendel, F. Bittner, *Biochim. Biophys. Acta Mol. Cell Res.* 1763 (2006) 621.
- [4] C.D. Brondino, M.J. Romão, I. Moura, J.J.G. Moura, *Curr. Opin. Chem. Biol.* 10 (2006) 109.
- [5] G. Hou, R. Dick, C. Zeng, G.J. Brewer, *Transl. Res.* 149 (2007) 260.
- [6] B. Hassouneh, M. Islam, T. Nagel, Q. Pan, S.D. Merajver, T.N. Teknos, *Mol. Cancer Ther.* 6 (2007) 1039.
- [7] H. Yanagiea, A. Ogatab, S. Mitsuib, T. Hisaa, T. Yamaseb, M. Eriguchia, *Biomed. Pharmacother.* 60 (2006) 349.
- [8] T. Yamase, *Mol. Eng.* 3 (1993) 241.
- [9] M. Cindrić, T. Kajfez Novak, S. Kraljević, M. Kralj, B. Kamenar, *Inorg. Chim. Acta* 359 (2006) 1673.
- [10] P. Ghosh, O.J. D'Cruz, R.K. Narla, F.M. Uckun, *Clin. Cancer Res.* 6 (2000) 1536.
- [11] S.B. Kumar, M. Chaudhury, *J. Chem. Soc., Dalton Trans.* (1992) 269.
- [12] W.J. Geary, *Coord. Chem. Rev.* 7 (1971) 81.
- [13] O.A. Rajan, A. Chakravarthy, *Inorg. Chem.* 20 (1981) 660.
- [14] M. Joseph, V. Suni, M.R.P. Kurup, M. Nethaji, A. Kishore, S.G. Bhat, *Polyhedron* 23 (2004) 3069.
- [15] M.A. Ali, M.T.H. Tarafdar, *J. Inorg. Nucl. Chem.* 39 (1977) 1785.
- [16] M.J.M. Campbell, *Coord. Chem. Rev.* 15 (1975) 279.

- [17] B.S. Garg, M.R.P. Kurup, S.K. Jain, Y.K. Bhoon, *Transit. Met. Chem.* 13 (1988) 247.
- [18] B.S. Garg, M.R.P. Kurup, S.K. Jain, Y.K. Bhoon, *Transit. Met. Chem.* 16 (1991) 111.
- [19] A. Syamal, K.S. Kale, *Inorg. Chem.* 4 (1965) 867.
- [20] B.S. Garg, M.R.P. Kurup, S.K. Jain, Y.K. Bhoon, *Transit. Met. Chem.* 13 (1988) 309.
- [21] L.J. Willis, J.M. Loehr, K.F. Miller, A.E. Bruce, E.I. Stiefel, *Inorg. Chem.* 25 (1986) 4289.
- [22] M. Joseph, M. Kuriakose, M.R.P. Kurup, E. Suresh, A. Kishore, S.G. Bhat, *Polyhedron* 25 (2006) 61.
- [23] F.J. Arnaiz, R. Aguado, M.R. Podrosa, A.D. Cian, J. Fischer, *Polyhedron* 19 (2000) 2141.
- [24] A. Rana, R. Dinda, P. Sengupta, L.R. Falvello, S. Ghosh, *Polyhedron* 21 (2002) 1023.
- [25] S. Purohit, A.P. Koley, L.S. Prasad, P.T. Manoharan, S. Ghosh, *Inorg. Chem.* 28 (1989) 3735.
- [26] C.S.J. Chang, J.H. Enemark, *Inorg. Chem.* 30 (1991) 683.
- [27] S. Gupta, A.K. Barik, S. Pal, A. Hazra, S. Roy, R.J. Butcher, S.K. Kar, *Polyhedron* 26 (2007) 133.
- [28] SMART and SAINT, Area Detector Software Package and SAX Area Detector Integration Program, Bruker Analytical X-ray; Madison, WI, USA, 1997.
- [29] SADABS, Area Detector Absorption Correction Program; Bruker Analytical X-ray; Madison, WI, USA, 1997.

*Synthesis, Crystal Structure and Spectral Aspects of a Dioxidomolybdenum(VI)  
Chelate Derived from ONS Donor Thiosemicarbazone*

---

- [30] G.M. Sheldrick, Acta. Cryst. A64 (2008) 112.
- [31] G.M. Sheldrick, SHELXL97 and SHELXS97, University of Göttingen, Germany, 1997.
- [32] K. Brandenburg, Diamond Version 3.2g, Crystal Impact GbR, Bonn, Germany, 2010.
- [33] E.B. Seena, B.N. Bessy Raj, M.R.P. Kurup, E. Suresh, J. Chem. Cryst. 36 (2006) 189.
- [34] M.W. Bishop, J. Chatt, J.R. Dilworth, M.B. Hursthouse, M. Motevalli, J. Chem. Soc., Dalton Trans. (1979) 1603.

\*\*\*RSC\*\*\*

## SUMMARY AND CONCLUSION

---

The increasing interest in thiosemicarbazones that has arisen in recent decades has to a large extent been prompted by their broad therapeutic activity. The thiosemicarbazones of aromatic aldehydes and ketones have been shown to possess a diverse range of biological activities including anticancer, antitumor, antibacterial, antiviral, antimalarial and antifungal properties owing to their property to diffuse through the semipermeable membrane of the cell lines. Metal complexes of thiosemicarbazones often display enhanced activities when compared to the uncomplexed thiosemicarbazones. The enhanced effect may be attributed to the increased lipophilicity of the metal complexes compared to the ligand alone. The presence of coordination sites in the complexes enhances their activity. It is observed that biological activity depends on the parent aldehyde or ketone and increases remarkably when bulky groups are present at N<sup>4</sup> position.

Thiosemicarbazones are thiourea derivatives and are prepared by the condensation of thiosemicarbazides with aldehydes or ketones in acidic medium. They are represented by the general formula  $R^1R^2C=N-NH-C(S)-NH_2$ . They generally exist in the thioamido form in the solid state but in solution, they tend to exist as an equilibrium mixture of thioamido and thioiminol forms. The thioamido-thioiminol equilibrium depends on the pH of the medium used for reaction. Thiosemicarbazones can bind to a metal center in the neutral or the anionic forms.

Thiosemicarbazones have emerged as an important class of ligands over a period of time, for a variety of reasons, such as variable donor properties, structural diversity and biological applications. In order to pursue the interesting coordinating properties of thiosemicarbazones, complexes with different types of ligand environments are essential. So in the present work we chose two different ONS donor thiosemicarbazones as principal ligands. Introduction of heterocyclic bases like 1,10-phenanthroline, 2,2'-bipyridine, 4,4'-dimethyl-2,2'-bipyridine and 5,5'-dimethyl-2,2'-bipyridine, the classical N,N donor ligands leads to the syntheses of mixed ligand complexes which can cause different bonding, spectral properties and geometries in coordination compounds.

We have synthesized the following two new ligands using 5-bromo-3-methoxysalicylaldehyde, N(4)-phenylthiosemicarbazide and N(4)-cyclohexylthiosemicarbazide.

- 5-Bromo-3-methoxysalicylaldehyde-N(4)-phenylthiosemicarbazone
- 5-Bromo-3-methoxysalicylaldehyde-N(4)-cyclohexylthiosemicarbazone

The thesis is divided into eight chapters.

### *Chapter 1*

Chapter 1 involves a brief prologue to thiosemicarbazones and their metal complexes, bonding and coordination strategy of thiosemicarbazones and their various applications. The objectives of the present work and the various physicochemical methods adopted for the characterization of the thiosemicarbazones and their complexes are also discussed in this chapter.

## Chapter 2

Chapter 2 describes the syntheses of two new aldehyde based ONS donor thiosemicarbazones and their characterization by elemental analyses, mass, FTIR, UV-vis and <sup>1</sup>H NMR spectral studies. X-ray quality single crystals of these two ligands were grown and their molecular structures were established by single crystal X-ray diffraction studies.

The thiosemicarbazones synthesized are

- 5-Bromo-3-methoxysalicylaldehyde-N(4)-phenylthiosemicarbazone
- 5-Bromo-3-methoxysalicylaldehyde-N(4)-cyclohexylthiosemicarbazone

## Chapter 3

This chapter discusses the syntheses and characterization of two oxidovanadium(IV) complexes with one of the thiosemicarbazones. They are mononuclear complexes with heterocyclic bases 1,10-phenanthroline and 2,2'-bipyridine as coligands. Both the complexes are characterized by various techniques such as elemental analyses, molar conductivity studies, magnetic susceptibility measurements, FTIR, UV-vis and EPR spectral studies. The observed molar conductivity values in 10<sup>-3</sup> M DMF solution confirm that both the complexes are non-electrolytic in nature. Magnetic susceptibility measurements clearly indicate that the two complexes are paramagnetic in nature with vanadium in +4 oxidation state. In both the complexes, thiosemicarbazones are coordinated to the metal centre in the thioiminolate form and act as dideprotonated tridentate ligands. In the EPR spectra, *g* values are found to be less than the free electron value and in DMF at 77 K, they displayed well resolved axial anisotropy with two sets

of eight line pattern with  $g_{\parallel} < g_{\perp}$  and  $A_{\parallel} > A_{\perp}$  relationship characteristic of an axially compressed  $d_{xy}^1$  configuration.

#### *Chapter 4*

Chapter 4 deals with the syntheses and characterization of five nickel complexes of the thiosemicarbazones by CHNS analyses, conductivity and magnetic susceptibility measurements, infrared and electronic spectral studies. All the complexes are found to be non-electrolytic in nature. The five-coordinate complexes are found to be paramagnetic with two unpaired electrons. In all of them, thiosemicarbazone moiety coordinates to the metal in the thioiminolate form as evidenced from the infrared spectra.

#### *Chapter 5*

This chapter describes the syntheses and characterization of ten copper(II) complexes. The characterization techniques include elemental analyses, molar conductivity studies, magnetic susceptibility measurements, FTIR, UV-vis and EPR spectral studies and single crystal X-ray diffraction studies. Heterocyclic bases like 1,10-phenanthroline, 2,2'-bipyridine, 4,4'-dimethyl-2,2'-bipyridine and 5,5'-dimethyl-2,2'-bipyridine were used as coligands. In all the complexes, thiosemicarbazone exists in thioiminolate form and coordinates to the metal through azomethine nitrogen, thioiminolate sulfur and phenolate oxygen. The molar conductivity values obtained for all the complexes confirmed their non-electrolytic nature. The magnetic susceptibility measurements reveal that all the complexes are paramagnetic and for mononuclear complexes the effective magnetic moment values are found to be close to the spin only

value which corresponds to a single unpaired electron. The low magnetic moment values for two complexes may be due to considerable antiferromagnetic interaction between the metal centers. EPR spectra in polycrystalline state at 298 K show that some of the compounds are isotropic, some are axial and others are rhombic in nature. In DMF at 77 K, some complexes are found to be axial with hyperfine lines in the parallel and perpendicular regions. Superhyperfine splittings give clear evidence for the coordination of azomethine nitrogen and that of heterocyclic bases to the metal. The  $g$  values calculated indicate that in most of the complexes the unpaired electron in Cu(II) resides in the  $d_{x^2-y^2}$  orbital. The complexes in which  $g_{\parallel} > g_{\perp} > 2.0023$  suggest a distorted square pyramidal structure and rules out the possibility of a trigonal bipyramidal structure which would be expected to have  $g_{\parallel} < g_{\perp}$ . We could isolate X-ray quality single crystals for two of the complexes by the slow evaporation of their mother liquors. They exhibit distorted square pyramidal geometry with O, N and S atoms of the principal ligand and one of the N atoms from the heterocyclic base occupying the square plane and the other N atom of base occupying the axial position. Intra and intermolecular hydrogen bonds facilitate packing in the crystal lattice. C-H $\cdots$  $\pi$  and  $\pi\cdots\pi$  interactions are also present.

### Chapter 6

Chapter 6 explains the syntheses and characterization of eight zinc complexes of the thiosemicarbazones by CHNS analyses, conductivity and magnetic susceptibility measurements, infrared and electronic spectral studies. The observed molar conductivity values in  $10^{-3}$  M DMF solution confirm that all the complexes are non-electrolytes. The tridentate

character of the thiosemicarbazones is inferred from IR spectra. The structure of one of the complexes has been resolved using single crystal X-ray diffraction studies. The crystal structure revealed a monoclinic space group  $P2_1$ . The compound adopts a distorted square pyramidal geometry with an  $N_2OS$  core as the base. The secondary amine group of the Schiff base dianion forms a hydrogen bond to the O atom of the dimethylformamide solvent. In the crystal, the phenyl ring of one of the two Schiff base anions is disordered over two positions in a 1:1 ratio. The crystal is found to be a racemic twin.

### *Chapter 7*

Eight cadmium complexes have been synthesized and physico-chemically characterized by CHNS analyses, conductivity and magnetic susceptibility measurements, infrared and electronic spectral studies. Heterocyclic bases like 1,10-phenanthroline, 2,2'-bipyridine, 4,4'-dimethyl-2,2'-bipyridine and 5,5'-dimethyl-2,2'-bipyridine act as coligands. The molar conductivity measurements in DMF ( $10^{-3}$  M) indicate that all the complexes are non-electrolytes. The IR spectral studies show that the thiosemicarbazones coordinate in thioiminolate form in all the complexes and act as dideprotonated tridentate ligands.

### *Chapter 8*

Chapter 8 includes the synthesis, crystal structure and spectral characterization of a dioxidomolybdenum(VI) complex of 5-bromo-3-methoxysalicylaldehyde-N(4)-phenylthiosemicarbazone. The characterization techniques include elemental analyses, magnetic susceptibility measurements, FTIR and UV-vis spectral studies. The compound is

diamagnetic in nature. The molecular structure of this complex was established by single crystal X-ray diffraction study. The coordination geometry around molybdenum is distorted octahedral in which the ligand coordinates to the metal in a tridentate manner forming five membered and six membered metallocycles involving the  $\text{MoO}_2^{2+}$  moiety. Oxygen, nitrogen and sulfur atoms of the ligand and one of the terminal oxo atom occupy the equatorial positions of the complex. The axial positions are occupied by the other terminal oxygen and oxygen atom of the solvent N,N-dimethylformamide.

\*\*\*RSC\*\*\*

## *Curriculum vitae*

**Jinsa Mary Jacob**  
Kanjikamundakathil  
Erumathala P.O.  
Choondy  
Aluva-683112  
KERALA, INDIA



Email: jinsamaryjacob@gmail.com  
jinsamary@cusat.ac.in

**Areas of Interest:** Teaching and Research

### Academic Profile

Pursuing Ph.D. (Inorganic Chemistry)  
(2009-present)  
Area of research - Coordination Chemistry  
Supervising guide - Prof. M.R. Prathapachandra Kurup  
Department of Applied Chemistry  
Cochin University of Science & Technology, Kochi

M.Sc. Chemistry (2006-2008)  
Union Christian College, Aluva  
University - Mahatma Gandhi University, Kerala  
Percentage of marks - 79.13%

B.Sc. Chemistry (2003-2006)  
Union Christian College, Aluva  
University - Mahatma Gandhi University, Kerala  
Percentage of marks - 96.0%

Plus-Two (2001-2003)  
St. Clare's School, Thrissur, Kerala  
Percentage of marks - 85.16%

S.S.L.C (2001)  
Nirmala High School, Aluva, Ernakulam, Kerala  
Percentage of marks - 95.16%

## Achievements

1. Qualified CSIR-JRF - 2008 December

## Research Experience

- Four years of research experience in the field of coordination chemistry

## Professional Skills

- Familiar with MS Office
- Familiar with chemistry software packages like Chems sketch, Origin, EPR simulation packages
- Familiar with crystallographic softwares
- Experienced in using instruments like UV-vis spectrometer, FTIR spectrometer, Thermogravimetric analyzer, Gouy balance etc.

## Personal Profile

Father's name	: K.J. Jacob
Date of birth	: 25 <sup>th</sup> January 1985
Nationality	: Indian
Gender	: Female
Marital status	: Single

## Papers published

1. (2*E*)-2-(5-Bromo-2-hydroxy-3-methoxybenzylidene)-*N*-cyclohexylhydrazine carbothioamide, **Jinsa Mary Jacob** and M.R.P. Kurup, Acta Cryst. (2012) E68, o836–o837.
2. (2*E*)-2-[(2-Hydroxy-4-methoxyphenyl)(phenyl)methylidene]-*N*-phenyl hydrazinecarboxamide dimethylformamide monosolvate, C.F. Annie, **Jinsa Mary Jacob**, M. Sithambaresan and M.R.P. Kurup, Acta Cryst. (2012) E68, o1519–o1520.

3. (2*E*)-2-(5-Bromo-2-hydroxy-3-methoxybenzylidene)-*N*-phenylhydrazine carbothioamide, **Jinsa Mary Jacob**, M. Sithambaresan and M.R.P. Kurup, Acta Cryst. (2012) E68, o1871–o1872.
4. Bis(1-phenyl-3-((*Z*)-[phenyl(pyridin-2-yl)-methylidene]amino- $\kappa^2N,N'$ )urea- $\kappa O$ )-nickel(II) dinitrate, N. Aiswarya, **Jinsa Mary Jacob**, M.R.P. Kurup and Seik Weng Ng, Acta Cryst. (2012), E68, m918.
5. Di- $\mu$ -acetato- $\kappa^4O:O$ -bis({*N'*-[(*E*)-phenyl(pyridin-2-yl- $\kappa N$ ) methylidene]benzohydrazidato- $\kappa^2N',O$ })copper(II), M.C. Vineetha, M. Sithambaresan, **Jinsa Mary Jacob** and M.R.P. Kurup, Acta Cryst. (2012), E68, m1086–m1087.
6. 2-Ethoxy-6-((2-[(3-ethoxy-2-hydroxybenzylidene)amino]-benzyl)iminomethyl) phenol, K.U. Ambili, S.S. Sreejith, **Jinsa Mary Jacob**, M. Sithambaresan and M.R.P. Kurup, Acta Cryst. (2012), E68, o2482.
7. (Anilino{(Z)-2-[(*E*)-5-bromo-3-methoxy-2-oxidobenzylidene]hydrazin-1-ylidene- $\kappa^2O^2,N^2$ })methanethiolato- $\kappa S$ (4,4'-dimethyl-2,2'-bipyridine- $\kappa^2N,N'$ ) zinc*N,N*-dimethylformamide monosolvate, **Jinsa Mary Jacob**, M.R.P. Kurup and Seik Weng Ng, Acta Cryst. (2012), E68, m1089.
8. (2*E*)-2-[1-(2-Hydroxy-4-methoxyphenyl)-ethylidene]-*N*-phenylhydrazine carboxamide monohydrate, C.F. Annie, **Jinsa Mary Jacob**, M. Sithambaresan and M.R.P. Kurup, Acta Cryst. (2012), E68, o2985–o2986.

#### Papers presented in symposia

1. Participated in the International Conference on Materials for the New Millennium (MATCON-2010), held at Department of Applied Chemistry, Cochin University of Science and Technology, Kochi-22 during 10-13 January 2010.
2. Participated and presented a paper in the National Seminar “Recent Trends and the Sequels in Chemistry” (RTSC-2011) held at the Department of Chemistry, Sacred Heart College, Thevara, Kochi during 7-8 December 2011.

3. Participated and presented a poster in the National Conference “Current Trends in Chemistry” (CTriC-2012) held at the Department of Applied Chemistry, Cochin University of Science and Technology, Kochi during 20-21 January 2012.
4. Participated and presented a paper in the National Conference “Advances in Materials Science: Macro to Nano Scales” (NCAMS-2012) held at the Department of Chemistry, Union Christian College, Aluva during 16-17 March 2012.
5. Participated and presented a poster in the National Conference “Current Trends in Chemistry” (CTriC-2013) held at the Department of Applied Chemistry, Cochin University of Science and Technology, Kochi during 22-23 March 2013.